U.S. DEPARTMENT OF ENERGY

PNNL-21798

Prepared for the U.S. Department of Energy
under Contract DE-AC05-76RL01830

Intrinsic Dosimetry: Properties and Mechanisms of Thermoluminescence in Commercial Borosilicate Glass

RA Clark

October 2012

Pacific Northwest
NATIONAL LABORATORY

Proudly Operated by Battelle *Since 1965*

DISCLAIMER

PACIFIC NORTHWEST NATIONAL LABORATORY
operated by
BATTELLE
for the
UNITED STATES DEPARTMENT OF ENERGY
under Contract DE-AC05-76RL01830

Printed in the United States of America

Available to DOE and DOE contractors from the
Office of Scientific and Technical Information,
P.O. Box 62, Oak Ridge, TN 37831-0062;
ph: (865) 576-8401
fax: (865) 576-5728
email: reports@adonis.osti.gov

Available to the public from the National Technical Information Service,
U.S. Department of Commerce, 5285 Port Royal Rd., Springfield, VA 22161
ph: (800) 553-6847
fax: (703) 605-6900
email: orders@ntis.fedworld.gov
online ordering: http://www.ntis.gov/ordering.htm

This document was printed on recycled paper.
(9/2003)

PNNL-21798

Intrinsic Dosimetry: Properties and Mechanisms of Thermoluminescence in Commercial Borosilicate Glass

RA Clark

October 2012

Prepared for the U.S. Department of Energy
under Contract DE-AC05-76RL01830

Pacific Northwest National Laboratory
Richland, Washington 99352

INTRINSIC DOSIMETRY: PROPERTIES AND MECHANISMS OF THERMOLUMINESCENCE IN COMMERCIAL BOROSILICATE GLASS

A Dissertation

Presented to

The Faculty of the Graduate School

At the University of Missouri

In Partial Fulfillment

Of the Requirements for the Degree

Doctor of Philosophy

By

Richard A. Clark

Dr. J. David Robertson, Dissertation Supervisor

December 2012

PNNL-21798

The undersigned, appointed by the dean of the Graduate School, have examined the Dissertation entitled

INTRINSIC DOSIMETRY: PROPERTIES AND MECHANISMS OF THERMOLUMINESCENCE IN COMMERCIAL BOROSILICATE GLASS

presented by Richard A. Clark,

a candidate for the degree of Doctor of Philosophy,

and hereby certify that, in their opinion, it is worthy of acceptance.

Dr. J. David Robertson

Dr. C. Michael Greenlief

Dr. Silvia S. Jurisson

Dr. William H. Miller

Dr. Jon M. Schwantes

ACKNOWLEDEGMENTS

This research was sponsored by the National Technical Nuclear Forensics Center within the Department of Homeland Security and conducted at the U.S. Department of Energy's Pacific Northwest National Laboratory (PNNL), which is operated for DOE by Battelle under Contract DE-AC05-76RL1830. This research was performed under the Nuclear Forensics Graduate Fellowship Program, which is sponsored by the U.S. Department of Homeland Security, Domestic Nuclear Detection Office and the U.S. Department of Defense, Defense Threat Reduction Agency. A portion of the research was performed using Environmental Molecular Sciences Laboratory (EMSL), a national scientific user facility sponsored by the Department of Energy's Office of Biological and Environmental Research and located at PNNL.

This research could not have been completed without the direction and advice of Dr. J. David Robertson, my advisor at the University of Missouri–Columbia, and Dr. Jon M. Schwantes and Dr. Steve D. Miller from Pacific Northwest National Laboratory (PNNL). The rest of my graduate committee members (Dr. C. Michael Greenlief, Dr. Silvia S. Jurisson, and Dr. William H. Miller) were always available to give advice when needed.

Other individuals were instrumental in performing this research. Roger A. Gregg performed the bulk of the irradiations at the High Exposure Facility (HEF) at PNNL, sometimes at short notice. Doug Conner and Anthony Guzmán cut hundreds of discs

from the borosilicate rods for samples. The electron paramagnetic resonance (EPR) work could not have been accomplished without Dr. Eric D. Walter and Dr. Jim E. Amonette at EMSL. The understanding needed to perform principal component analysis (PCA) and partial least squares (PLS) regression analyses was aided by Dr. Christopher R. Orton and Dr. Jamie B. Coble. None of the documents of this work could have been released without the aid of Nadia Yearout and Christine Bauman.

On a personal level, I would like to acknowledge the constant support and encouragement of my immediate and extended family. In addition to the monumental amount of support and encouragement, my wife (Alisha) and son (Caleb) made enormous sacrifices during this time.

TABLE OF CONTENTS

Chapter 4

Chapter 5

LIST OF FIGURES

LIST OF TABLES

LIST OF ABBREVIATIONS

AEC	Alkali electron center
AEEC	Alkaline earth electron center
Al E′	Aluminum E′-defect center
AlOHC	Aluminum oxygen hole center
B E′	Boron E′-defect center
BEC	Boron electron center
BO	Bridging oxygen
BOHC	Boron oxygen hole center
CRN	Continuous random network
EIC	Extrapolation ionization chamber
EMSL	Environmental Molecular Sciences Laboratory
EPR	Electron paramagnetic resonance
ESR	Electron spin resonance
EXAFS	Extended X-ray absorption fine structure
FOM	Figure-of-merit
GA	General approximation or generalized approach
HC	Hole center
ICP-AES	Inductively coupled plasma-atomic emission spectroscopy
ICP-MS	Inductively coupled plasma-mass spectroscopy
ILS	Inverse least squares
LET	Linear energy transfer
LOQ	Limit of quantification
LV	Latent variable
MMD	Minimum measurable dose
MRN	Modified random network

MVA	Multivariate analysis
NBO	Non-bridging oxygen
NBOHC	Non-bridging oxygen hole center
NIST	National Institute of Standards and Technology
NMR	Nuclear magnetic resonance
OHC	Oxygen hole center
OSL	Optically stimulated luminescence
PC	Principal component
PCA	Principal component analysis
PLS	Partial least squares
PMT	Photomultiplier tube
PNNL	Pacific Northwest National Laboratory
RDD	Radioactive dispersal devices
SHC	Silicon hole center
Si E’	Silicon E’-defect center
SWRI	Southwest Research Institute
TL	Thermoluminescence
TSL	Thermally stimulated luminescence
U	Undetected or not detected above the method reporting limit
UV	Ultraviolet
VIP	Variable importance in projection

NOMENCLATURE

Electron Paramagnetic Resonance

Symbol	Description	Units
B_o	External magnetic field	G
ΔE	The separation of the parallel and antiparallel electron energy states	eV
g	Electron's g-factor	
h	Planck's constant	4.136×10^{-15} eV s
m_s	Magnetic moment of an electron	$\pm\frac{1}{2}$
μ_B	Bohr magneton	5.788×10^{-9} eV G^{-1}
ν	Frequency	Hz

Exposure

α	Activity of the source	mCi
d	Concentration of BO_4 units	cm
Γ_δ	Exposure rate constant for a specific isotope of interest	R cm^2 h^{-1} mCi^{-1}
$\dot{X}$	Exposure accumulated over time from a specific source	R hr^{-1}

Glass Structure

K	Ratio of glass formers (SiO_2 : B_2O_3)
N^4	Concentration of BO_4 units
Q^n	Silicon environment with n denoting the number of bridging oxygens the silicon is bonded to
R	Molar ratio of alkali oxide to B_2O_3
x	Alkali concentration

Multivariate Analysis

Symbol	Description	Units
$\mathbf{b}$	Regression vector	
$\mathbf{C}$	Collection of measurements or calibration matrix	
$\mathbf{C}^+$	Pseudo-inverse of $\mathbf{C}$	
$\mathbf{E}$	Residual matrix	
k	Number of meaningful scores and loadings	
$\mathbf{p}_i$	Loadings vector (contains information on how the variables relate to each other)	
$\mathbf{P}$	Loadings matrix for PLS (similar to $\mathbf{p}_i$)	
r	Mathematical rank of the data matrix	
R^2	Coefficient of determination	
$\mathbf{t}_i$	Scores vector (contains information on how the samples relate to each other)	
T	Superscript that denotes transpose	
$\mathbf{T}$	Scores matrix for PLS (similar to $\mathbf{t}_i$)	
$\mathbf{W}$	Weights matrix	
$\mathbf{x}$	Measured variables (input)	
$\mathbf{X}$	Data matrix with m rows and n columns	
y	Property of the system (output)	
$\mathbf{y}$	Vector containing the respective values of the quantity of interest for each measurement in $\mathbf{C}$	

Thermoluminescence Peak Parameters

A_m	Rate of recombination	$m^3\ s^{-1}$
A_n	Rate of retrapping	$m^3\ s^{-1}$
β	Heating rate	$K\ s^{-1}$
b	General-order parameter	
Ec	Conduction band	

Symbol	Description	Units
Ev	Valence band	
E	Energy difference between the trap and the edge of the delocalized band	eV
I	Intensity of a glow peak	
k	Boltzmann's constant	8.617×10^{-5} eV K^{-1}
n	Number of trapped electrons	m^{-3}
n_c	Concentration of electrons in the conduction band	m^{-3}
n_i	Intrinsic free carrier density	m^{-2}
n_o	Initial value of n at time $t = 0$	m^{-3}
N	Total trap concentration	m^{-3}
R_d	Temperature-dependent rate of direct recombination	m^{-2} s^{-1}
s	Frequency factor or "attempt-to-escape" frequency	s^{-1}
τ	Mean time an electron and hole spend in a trap	s
τ_r	Lifetime of a free carrier for direct recombination (the mean time an electron spends in the conduction band before direct recombination with a free hole in the valence band)	s
T	Absolute temperature	K
T_f	End point temperature of the glow peak	K
T_o	Initial temperature at time $t = 0$	K
T_{max} or T_m	Temperature of the glow peak maximum	K
T_{stop}	Temperature the sample is heated to before rapid cooling during the T_m-T_{stop} analysis	K
T'	Dummy variable used for integration that represents temperature	K

ABSTRACT

Intrinsic dosimetry is the method of measuring total absorbed dose received by the walls of a container holding radioactive material. By considering the total absorbed dose received by a container in tandem with the physical characteristics of the radioactive material housed within that container, this method has the potential to provide enhanced pathway information regarding the history of the container and its radioactive contents. The latest in a series of experiments designed to validate and demonstrate this newly developed tool are reported.

Thermoluminescence (TL) dosimetry was used to measure dose effects on raw stock borosilicate container glass up to 70 days after gamma ray, x-ray, beta particle or ultraviolet irradiations at doses from 0.15 to 20 Gy. The TL glow curve when irradiated with ^{60}Co was separated into five peaks: two relatively unstable peaks centered near 120 and 165°C, and three relatively stable peaks centered near 225, 285, and 360°C. Depending on the borosilicate glass source, the minimum measurable dose using this technique is 0.15-0.5 Gy, which is roughly equivalent to a 24 hr irradiation at 1 cm from a 48-160 ng source of ^{60}Co. Differences in TL glow curve shape and intensity were observed for the glasses from different geographical origins. These differences can be explained by changes in the intensities of the five peaks. Electron paramagnetic resonance (EPR) and multivariate statistical methods were used to relate the TL intensity and peaks to electron/hole traps and compositional variations.

Chapter 1

Overview

1.1 Introduction

Glass containers have been used for the storage of nuclear materials by waste management sites and traffickers of illicit materials.[1-4] When a sample of nuclear material is interdicted or a sample of unknown history is discovered at a waste depository, examiners attempt to gather as much information as possible about the sample for the purpose of forensics investigations or sample history.[2-3] In a container, all of the emitted radiation from the nuclear material will either be self-attenuated or incident on the walls of that container. In the latter case, the total dose to the container wall will be a function of the residence time of the material within the container – a key piece of information when investigating the history of an unknown sample. By applying dosimetry techniques to the walls of a container, information relating to the residence time of the nuclear material could become available to investigators.

1.2 Intrinsic Dosimetry

Ionizing radiation has a wide range of effects on materials. Some materials are highly sensitive to ionizing radiation while others are resistant to damage from high radiation fields.[5] Radiation damage is generally connected to the creation of disorder in the irradiated material through the formation of vacancies and interstitial atoms within the material's crystal structure.[6] Due to its non-crystalline (amorphous) structure, glass

is relatively resistant to radiation damage. For this reason, glass has been used as the storage matrix of choice for highly radioactive material, ranging from samples in laboratories to waste forms at long term disposal sites.[1] It has also been documented that traffickers of nuclear materials have used glass vials for storage and transport.[2]

Though relatively resistant to radiation damage, glass is still affected by ionizing radiation. For instance, radiation can create electron-hole pairs, sometimes referred to as defects, which can become trapped within the glass.[7-10] Through heating, or other forms of stimulation, the electron-hole pairs are released, recombine, and emit light. The amount of light released is typically proportional to the radiation dose received by that material, so quantifying this light output provides a means for measuring the exposed dose. This process forms the basis of thermoluminescence (TL) dosimetry.[8, 11-12] Other dosimetry techniques have also been developed such as optically stimulated luminescence (OSL)[13] and electron paramagnetic resonance (EPR)[14] that are nondestructive and sometimes provide greater sensitivity; however, these techniques only apply to select materials and defect types.

Dosimetry has previously been used to measure the dose delivered to materials with applications to post-detonation nuclear forensics and emergency response following an accident or nuclear attack.[15-25] In these instances dosimetry was used to measure delivered dose independent of information regarding the radiation source, and usually to material surfaces open to the environment. However, in instances where the dose is delivered to the walls of glass containers holding radioactive material, both the

measured dose and the attributes (amount and type) of the radioactive material may be considered together in order to acquire further details about the sample's history. This situation defines intrinsic dosimetry–the measurement of the total absorbed dose received by the walls of a container holding radioactive material.[26] Intrinsic dosimetry is intended to be used as an interrogation tool for interdicted or newly discovered waste containers of unknown origin or history, for the purpose of acquiring pathway information between loss of control of the radioactive material and discovery of the container. The types of information that may be available to investigators using intrinsic dosimetric techniques include:[26-28]

- the residence time of an unadulterated sample of a radioactive material;
- evidence of sample splitting during transit of the radioactive sample;
- the amount of radioactive material that once resided in an "empty" container.

1.3 Objectives and Scope of the Study

In order to apply intrinsic dosimetry to glasses of varied composition, additional research was performed to understand the properties and mechanisms behind thermoluminescence of glass. A review of the structure of glass and the effects that various additives and impurities have on the structure is presented in Chapter 2. An overview of our current understanding of the common electron/hole traps generated from ionizing radiation interacting with glass is presented in Chapter 3. In Chapter 4, the main experimental techniques which were used are laid out (TL and EPR) along with

a description of the materials and irradiation procedures used. Chapter 5 and Chapter 6 discuss the TL properties of the studied glass and the modeling of the TL glow peaks. Evidence is presented in these chapters that the glasses have the same basic TL glow peaks regardless of the glass source, irradiation source, and time post-irradiation and that the differences between the observed TL glow curves are due to the relative ratios of the individual TL peak intensities. The results of EPR experiments are given in Chapter 7, and a relationship between a specific hole center and a TL peak is established. Chapter 8 presents results of a multivariate statistical analysis, namely principal component analysis (PCA) and partial least squares (PLS) regression, of the correlations between the composition of the glass and the TL glow curve shape, overall TL intensity, and the relative intensities of the individual TL glow peaks. Conclusions of our studies of TL of borosilicate glasses and suggestions for future work are given in Chapter 9.

Chapter 2

Structure of Glass

2.1 Definition of Glass

The term glass does not necessarily define a material with a particular chemical composition; but rather, it refers to a state of matter.[29] Because of this, there are many definitions of glass. Within materials science, however, glass can be defined as an inorganic product of fusion which has been cooled to a rigid condition without crystallizing.[9, 30-33] In this definition lies one of the most defining characteristics of glasses; they are non-crystalline or amorphous materials. As many materials of vastly different chemical composition may fit this rather broad definition, it is necessary to limit studies to a particular type of glass. For the purposes of this volume of research, the term glass will refer specifically to sodium aluminoborosilicate glass with low (<5%) sodium oxide and aluminum oxide content.

2.2 General Structure of Glass

Glass is one of the most ancient materials known to mankind. Prehistorically, the naturally occurring glass *obsidian* was used to make weapons and tools.[34] The most ancient man-made glass objects were discovered in Egypt and date to approximately 3000 BC. However, there is evidence that glass manufacturing methods had already been discovered in Mesopotamia by approximately 4500 BC.[9, 35] Despite its long history, there is much that is not well understood beyond the basic structures of most glasses.[30, 36]

Glass is formed when a liquid is cooled in a way that on dropping below the melting temperature, “freezing” occurs rather than crystallization; the final temperature is low enough that atoms move too slowly to rearrange to the more stable form.[37] Whereas a material allowed to crystallize would have long-range order (Figure 2-1), this “freezing” creates an amorphous glass of the same chemical composition that only has short-range order (Figure 2-2).[38] One of the earliest and most influential structural theories of oxide glass known as the Continuous Random Network (CRN) was based on this concept of short-range order.[39-41]

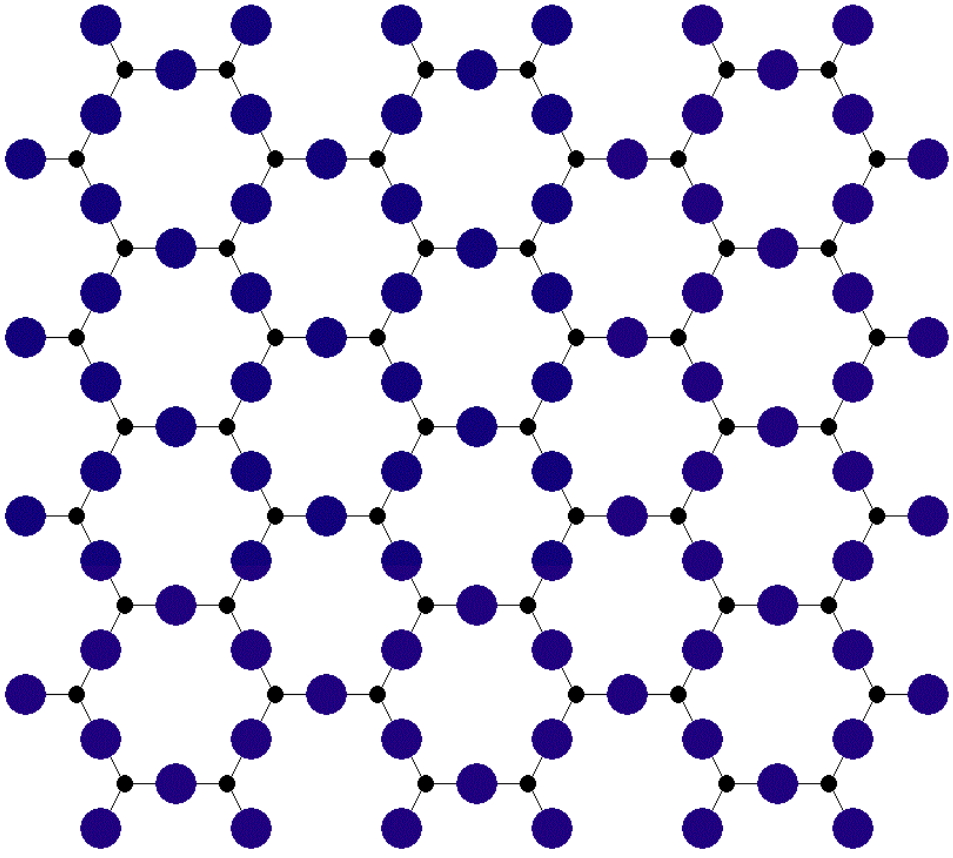

Figure 2-1: Two-dimensional representation using CRN of crystalline A_2O_3 with long-range order; also representative of crystalline SiO_2 (quartz) with large blue circles representing O and small black circles representing Si. Adapted from [41].

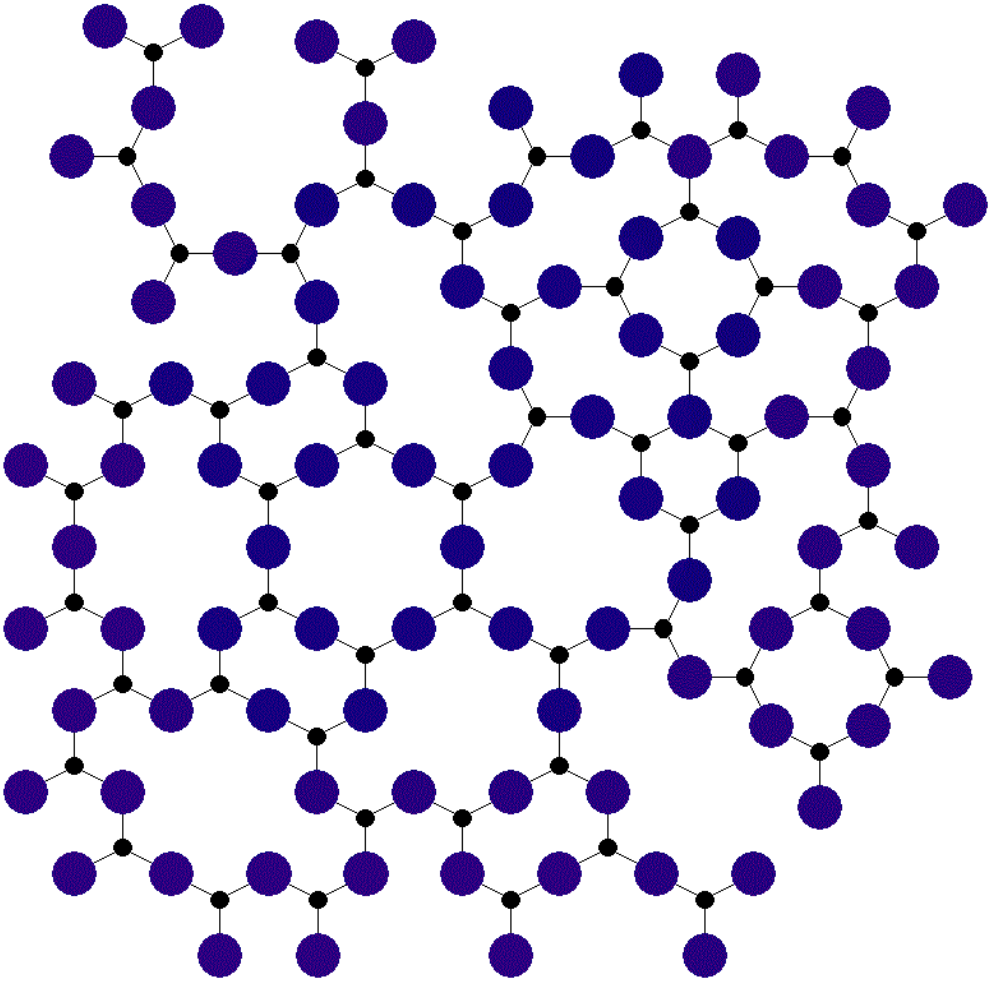

Figure 2-2: Two-dimensional representation using CRN of amorphous (glassy) A_2O_3 with short-range order; also representative of silicate glass with large blue circles representing O and small black circles representing Si. Adapted from [41].

2.2.1 Continuous Random Network (CRN) Model

In the early 1930's, Zachariasen used x-ray diffraction to compare the structure of crystalline and amorphous materials. In the study, he observed that the mechanical properties of glasses are similar to those of crystals of the same composition. He then showed that the structure of these amorphous materials

are not entirely random and have similar structural elements as their crystalline counterparts, but the amorphous materials lack a large periodic and symmetrical network. Zachariasen went on to propose that glasses consist of an extended three-dimensional network made up of well-defined small structural units. These structural units are the same or similar as the structural units found in crystalline materials and are what is linked together in a random way.[41] Zachariasen proposed four rules for glass formation in an oxide A_mO_n in order to obtain a random network:[9, 31-33, 40-41]

1. Each oxygen atom is linked to no more than two atoms A (cations).
2. The oxygen coordination number of the network cation is small (i.e. less than 4).
3. The oxygen polyhedra share only corners with each other and not edges or faces.
4. At least three corners in each oxygen polyhedron must be shared in order to form a 3-dimensional network.

From his work, Zachariasen concluded that only a handful of oxides were capable of forming a glass: B_2O_3, SiO_2, GeO_2, P_2O_5, P_2O_3, As_2O_5, As_2O_3, Sb_2O_3, Sb_2O_5, V_2O_5, Nb_2O_5, and Ta_2O_5. At the time, only B_2O_3, SiO_2, GeO_2, P_2O_5, As_2O_5, and As_2O_3 had been vitrified. The addition of other oxides (alkali metal, alkaline earth, transition metal, etc.) to any one of these materials would form a more

complex oxide glass (Figure 2-3). To form a complex oxide glass it is necessary that:[9, 41-42]

1. The sample contains a high percentage of cations which are surrounded by oxygen tetrahedra or by oxygen triangles.
2. The tetrahedra or triangles share only corners with each other.
3. Some oxygen atoms are linked to only two such cations and do not form further bonds with any other cations.

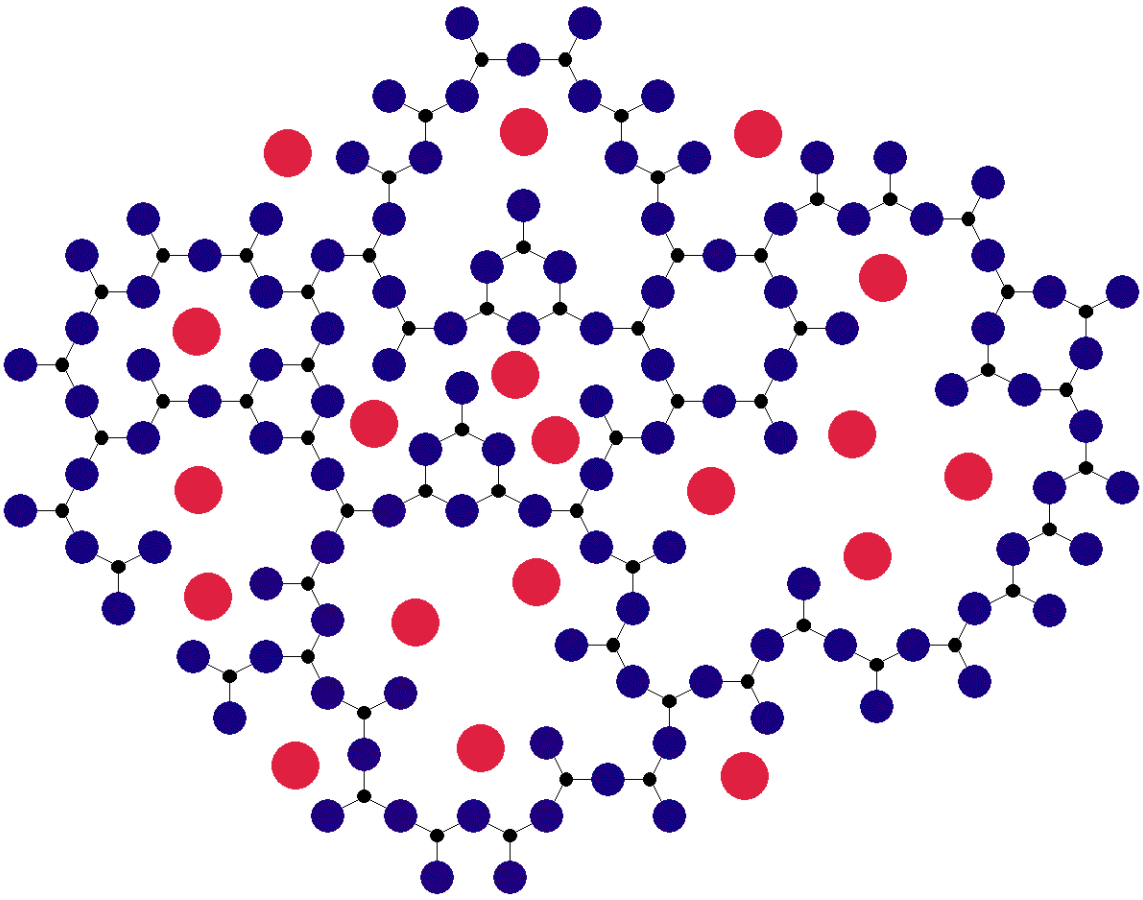

Figure 2-3: Two-dimensional representation using CRN of a complex (disordered) network; also representative of sodium silicate glass with large red circles representing Na, medium blue circles representing O, and small black circles representing Si. Adapted from [9].

This means that oxide glasses must contain a significant amount of cations that can form vitreous oxides or of other cations which are able to replace them in an isomorphic manner. Zachariasen added the Al^{3+} cation to the list of glass-forming cations (B^{3+}, Si^{4+}, Ge^{4+}, P^{3+}, P^{5+}, As^{3+}, As^{5+}, Sb^{3+}, Sb^{5+}, V^{5+}, Nb^{5+}, and Ta^{5+}). The Al^{3+} cation can replace Si^{4+} isomorphically, but Al_2O_3 cannot form a glass by itself. Zachariasen gave the term *network-forming cations* to these ions which, according to his rules of association with oxygen, form the random network or "vitreous network" of the glass.[41] The term *network former* is now generally adopted for oxides in the vitreous network. Glasses also may contain oxides known as *network modifiers*. These are oxides that do not participate in forming the network structure. With the addition of *network modifiers*, it becomes important to distinguish between two types of oxygen in the glass structure: bridging and non-bridging. A bridging oxygen (BO) is bonded to and connects two *network-forming cations* (acting like a bridge), while a non-bridging oxygen (NBO) is only bonded to one *network-forming cations*.

When a network modifying oxide, such as Na_2O, is added to the glass, the additional oxygens are incorporated into the glass network. The addition of this modifying oxide can affect the glass in three ways (Figure 2-4):[43]

(a) A bond between a *network former* and oxygen is ruptured creating NBO's.

(b) The coordination number of a *network former* is increased.

(c) A combination of (a) and (b) where the coordination number of a *network former* is increased, and a NBO is created.

In each of these cases, charge is compensated by the *network modifier*. These same mechanisms apply when an oxide of a divalent cation is added, such as CaO. In these cases, a single cation can compensate for the two negative charges.

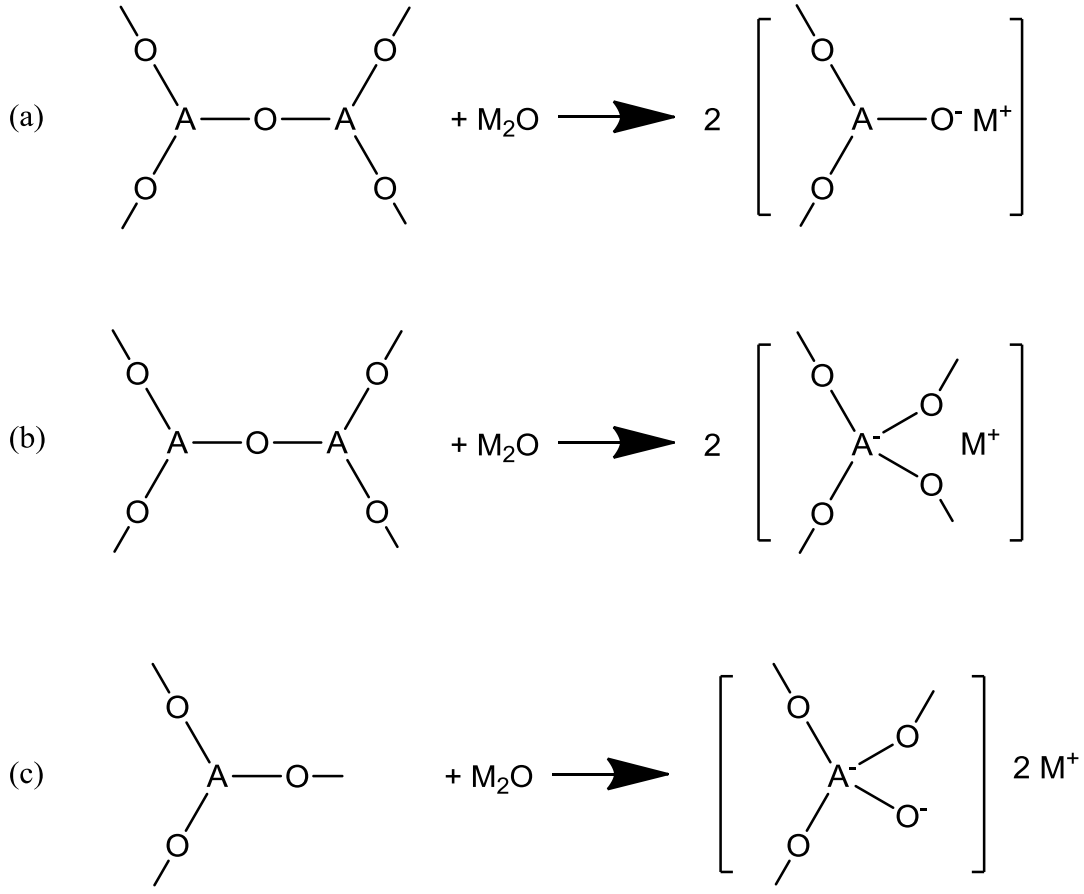

Figure 2-4: Mechanisms for the possible results of adding a network modifier in oxide glasses: (a) formation of non-bridging oxygen atoms; (b) increase of the coordination number of network forming cations; (c) combination of (a) and (b) . Adapted from [43].

Other than the listed *network formers* and the alkali metal and alkaline earth oxides that tend to be *network modifiers*, certain oxides can function either as glass-formers or as modifiers. These oxides are known as *intermediate oxides* or *network intermediates*. Some *network intermediates* often found in glass that can be important to the glass structure include the elements aluminum,[9, 44-46] iron,[44, 47-48] lead,[49-50] tin,[51-52] titanium,[45, 53-54] zinc,[45, 55] and zirconium.[53, 56-57]

2.2.2 Modified Random Network (MRN) Model

Controversy about the reliability of the CRN model arose with the development of X-ray diffraction,[58] extended X-ray absorption fine structure (EXAFS),[59] and neutron diffraction.[60] These techniques allowed the environment around particular *network formers* and *network modifiers* to be analyzed. Experiments using these methods revealed three important results. First, the environment around the network modifying cations was much more explicit than the CRN model predicted. Second, the *network modifiers* were not homogenously distributed throughout the glass, but the glass had rich regions of modifier inhomogeneously distributed throughout the glass. These rich regions of *network modifier* also separated rich regions of *network formers*. Third, the coordination number around cations and the distance between ions only changed slightly with changes in concentration.[61-62] From these results, the structure of glass was proposed to have disorder in the long distance of the

material, order in the middle distance around the cations of the *network modifiers*, and order in the short distance around the *network formers*.[62-64]

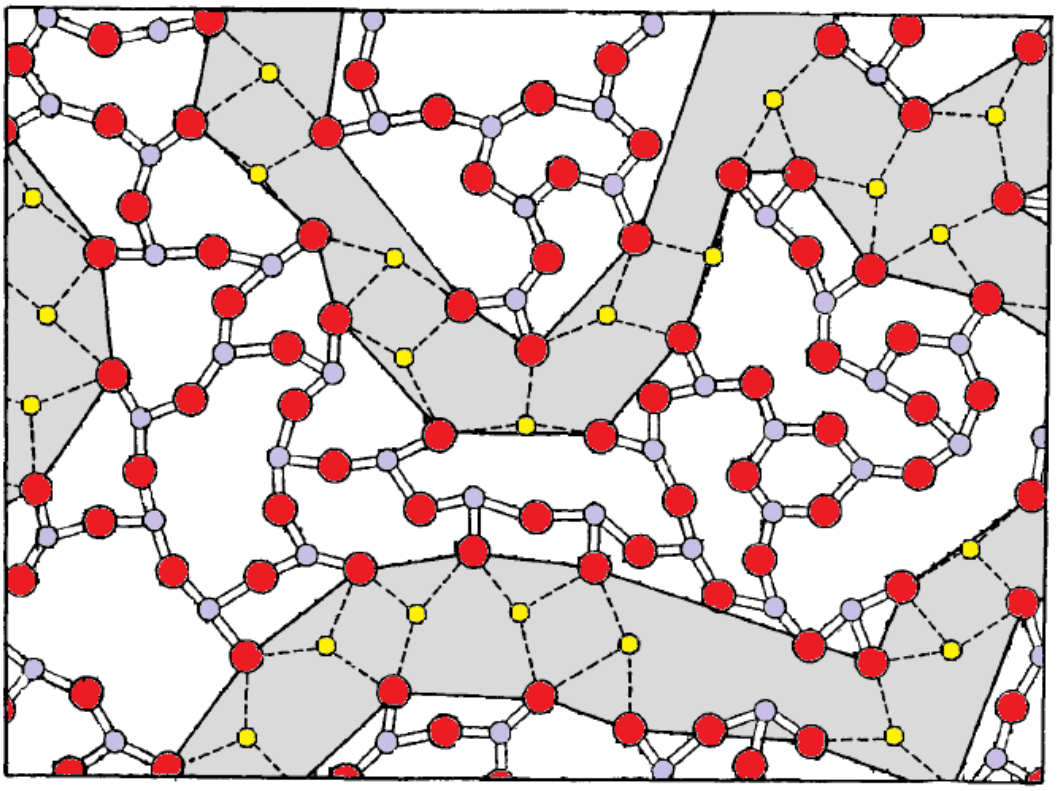

Figure 2-5: Two-dimensional representation using MRN of a complex (disordered) network; also representative of sodium silicate glass with red circles representing O, purple circles representing Si, and yellow circles representing Na. The highlighted grey region shows the modifier rich channel separating the former rich zones. Adapted from [65].

From these observations, Greaves introduced the Modified Random Network (MRN) Model.[65] In this model, *network modifiers* form zones that connect the *network former* rich zones through mostly NBO's. The coordination number around the cations and the distance between ions has order. Molecular

dynamics calculations support the hypothesis of the MRN model.[66-69] Figure 2-5 shows a two-dimensional representation of sodium silicate glass using the MRN Model.[38] Currently, the MRN is the most accepted model for glass structure, but the CRN is still widely used due to its simplicity.[70]

2.3 Structure of Silica Glass

Though one of the most expensive and difficult glasses to fabricate,[29] silica glass (SiO_2) has the simplest of all glass structures.[71-76] The basic structural units in silica glass are very similar to the structural units found in crystalline silica (quartz). Quartz consists of corner-sharing silica tetrahedra (Figure 2-6)[38] arranged in orderly 6-member rings at specified bond and torsion angles with long-range order (Figure 2-7).[73] Figure 2-1 shows a two-dimensional representation of quartz using the CRN Model.

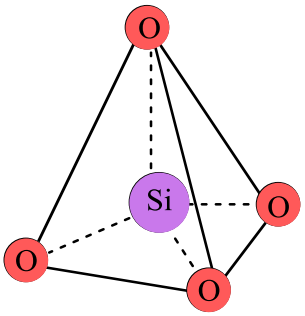

Figure 2-6: Silica tetrahedron. Adapted from [38].

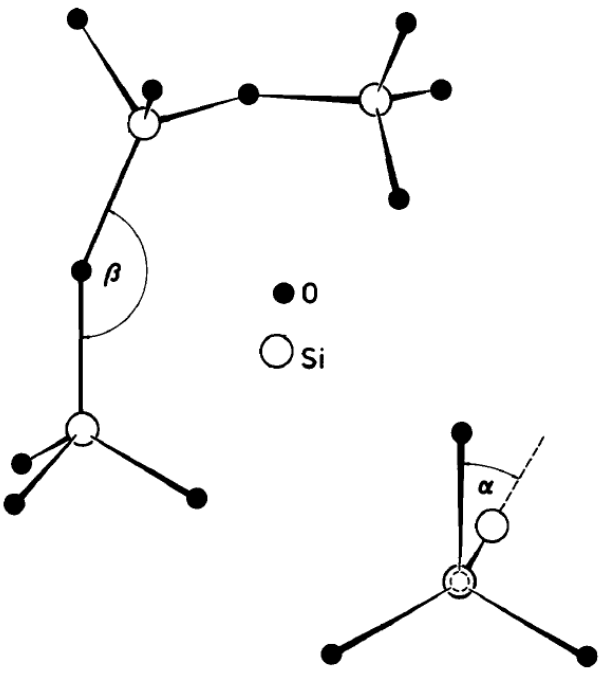

Figure 2-7: Definition of torsion angle α and bond angle β. Adapted from [73].

In pure silica glass, the structure again consists of corner-

sharing silica tetrahedra with virtually all BO's. However, disorder is introduced into the network structure through variations in the bond angles and torsion angles and to a minor extent by distortions in the silica tetrahedron.[73, 77] Though the glass does not have long-range order, short-range and intermediate-range order exists. Short-range order is exhibited in the form of the tetrahedra mentioned, while intermediate-range order is seen in the existence of ring and ring-like structures. This network of ring and ring-like structures can exist on the order of 1.0 nm (or 10 Å).[74, 78-79] Under normal conditions, these structures also favor 6-member ring structures.[80-81] Figure 2-2 shows a two-dimensional representation of silica glass using the CRN Model with intermediate-range order represented by ring structures.

2.4 Structure of Modified Silicate Glass (Alkali Silicate)

The most common modification to silicate glass is the introduction of *network modifiers* in the form of alkali and/or alkaline earth oxides with the most common being Na_2O.[82-85] The addition of these cations breaks up the connectivity of BO's corner linking the SiO_4 tetrahedra with the creation of NBO's that are linked to only one Si atom. Each alkali cation introduces one NBO, while each alkaline earth cation introduces two NBO's.[33, 86-89] Figure 2-4 and Figure 2-8 show the creation of NBO's in glass. Modifying cations in general and alkali cations in particular are mobile in silicate glasses, but ionic diffusion is reduced if more than one type of alkali is present in the glass. This effect on diffusion is known as the Mixed Alkali Effect.[90-91]

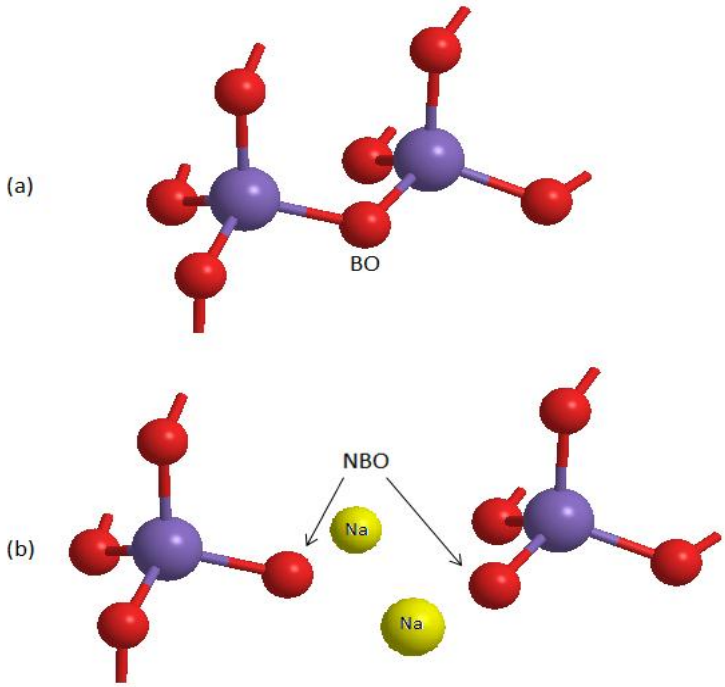

Figure 2-8: (a) Silica glass with only bridging oxygens (BO); (b) Creation of non-bridging oxygens (NBO) through the addition of Na_2O. Adapted from [89].

Depending on the concentration of *network modifier*, the Si atoms present in the glass can have zero, one, two, three, or four NBO's as nearest neighbors. The local order of the glass can be characterized by the Si environment. This is expressed as Q^n species where n denotes the number of BO's to which the Si is bonded. Figure 2-9 illustrates the expected fractions of Q^n using two model distributions as the mole percent (mol %) of alkali oxide changes.[92] In the binary distribution model, only one Q^n species is allowed to exist at any stoichiometric composition, and only two species are allowed to exist at other compositions. In the random distribution model, Q^n species are allowed to cover a much broader composition range with three or four species present even at stoichiometric compositions. Detailed studies have shown that the Q-

species distribution is neither binary nor random, but falls in between these two extreme models.[70, 92-93]

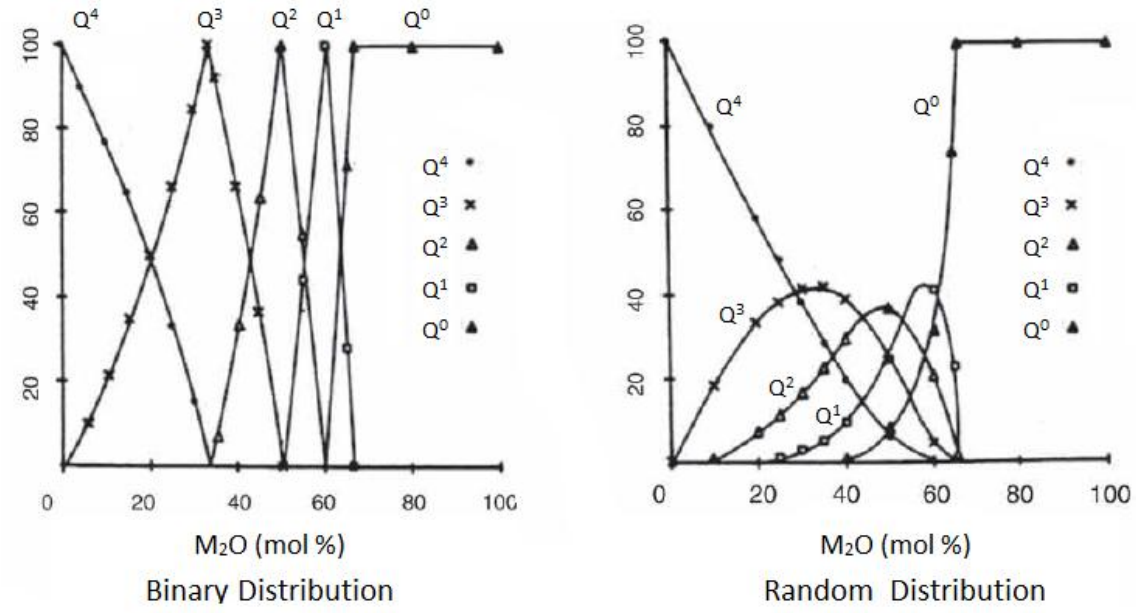

Figure 2-9: Theoretical Q^n species distribution using a binary distribution model (left) and a random distribution model (right) for a binary alkali silicate glass. Adapted from [92].

2.5 Structure of Alkali Borosilicate (Addition of Boron)

Borosilicate glass is one of the oldest types of glass to have considerable resistance to sudden changes in temperature.[29] Although not as easy to fabricate and more expensive than some other glasses, borosilicate's cost is moderate when considering the broad range of applications in which it can be used due to its high temperature resistance, high chemical resistance, and low coefficient of linear expansion. These properties have made borosilicate glass common in areas such as cookware and laboratory glassware.[29, 94]

2.5.1 Borate Glass

The structures of borate glasses are much more complicated than silicate glasses. Though the structure and physical properties of borate glasses have been studied extensively,[95-96] there is some controversy of the structural groups of these materials with alterations arising from composition variations and manufacturing process.[97]

The structure of the most basic borate glass, vitreous B_2O_3, has been studied by Raman scattering, neutron scattering, and ^{10}B, ^{11}B, and ^{17}O Nuclear Magnetic Resonance (NMR) spectroscopy.[97-103] These studies showed that the basic structural unit of borate glasses is a BO_3 triangle, and B_2O_3 consists mainly of three corner-shared BO_3 triangles forming a B_3O_6 boroxol ring, Figure 2-11(1). These rings are connected to one another by a small non-ring population of BO_3 triangles (Figure 2-10)[70] with approximately 75-80% of B atoms belonging to these boroxol rings, indicating the presence of substantial intermediate-range order in B_2O_3 glass.[70, 103-104]

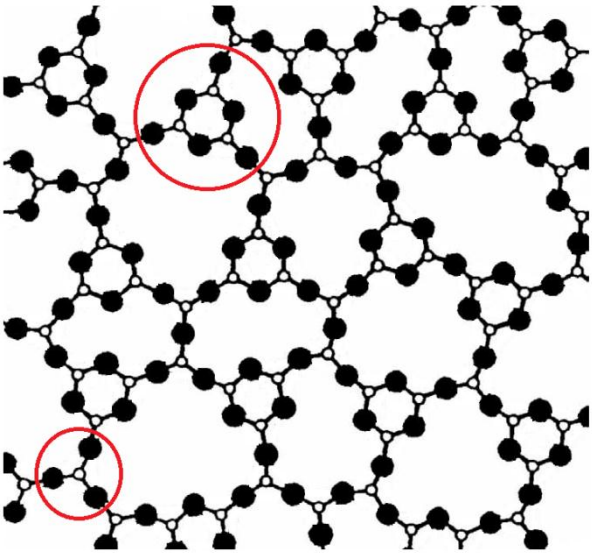

Figure 2-10: Two-dimensional representation using CRN of B_2O_3 glass consisting of B_3O_6 boroxol rings and BO_3 triangles. B is represented as open circles and O as filled circles. Adapted from [70].

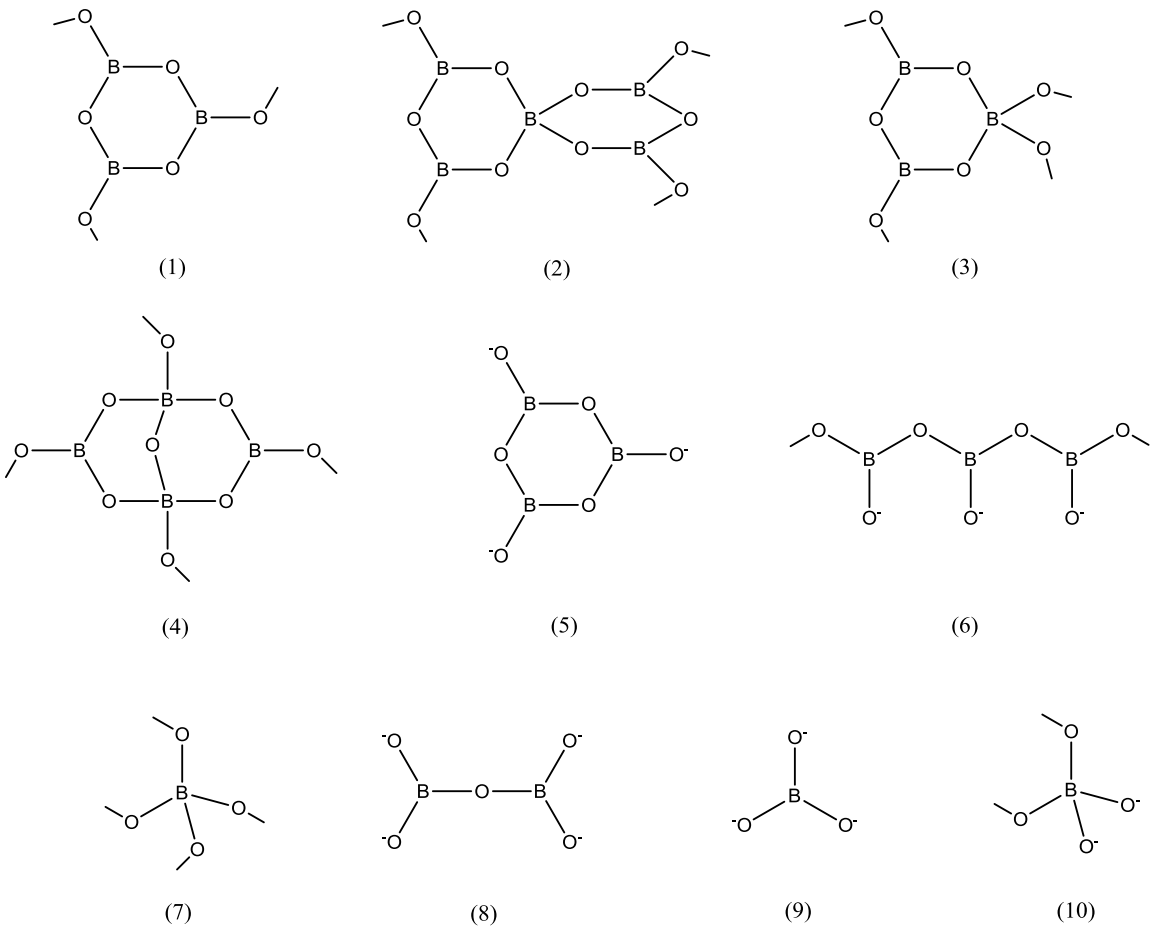

Figure 2-11: Structural groups for borate glasses: (1) boroxol ring; (2) pentaborate unit; (3) triborate unit; (4) diborate unit; (5) metaborate unit; (6) metaborate chain; (7) "loose" BO_4 tetrahedron; (8) pyroborate unit; (9) orthoborate unit; (10) boron–oxygen tetrahedron with two bridging and two non-bridging oxygen atoms. An oxygen atom with a dangling bond represents a bridging oxygen. Adapted from [112].

2.5.2 Modified Borate Glass (Alkali Borate)

The effect of adding *network modifiers* such as alkali and alkaline earth cations to borate glasses is more complex than when these are added to silicate glasses.[105] In silicate glasses, the addition of *network modifiers* leads to the creation of non-BO's with the NBO concentration increasing linearly with the

alkali content.[86-87] In borate glasses, however, all three mechanisms illustrated in Figure 2-4 can take place.[43]

The initial addition of modifier cations to B_2O_3 glass results in the conversion of BO_3 units into BO_4 units without the creation of NBO's, Figure 2-4(b).[70, 106-110] In borate glasses, the concentration of BO_4 units, N_4, increases with alkali concentration, x, reaching a maximum at $x \sim 1/3$ or $R \sim 0.5$, where $R = x/(1-x)$ is the molar ratio of alkali oxide to B_2O_3. When R exceeds 0.5, the BO_4 concentration begins to decrease with the formation of BO_3 units incorporating NBO's.[70, 111] As the *network modifier* concentration changes, any of the structural groups shown in Figure 2-11 can exist.[112]

2.5.3 Alkali Borosilicate Glass

When B_2O_3 is combined with SiO_2, a borosilicate glass can be formed. The atomic structures of these glasses have a systematic variation in boron coordination and the distributing of NBO's between B and Si as the alkali/alkaline earth oxide : B_2O_3 ratio (R) and the SiO_2 : B_2O_3 ratio (K) change.[70, 113-118] Similar to the modified borate glasses, the concentration of BO_4 units in borosilicate glasses initially increases linearly with increasing *network modifier*. Again, the modifier concentration will reach a point that the BO_4 units are replaced by BO_3 units with NBO's. The point at which this takes place is dependent on the ratio of glass formers (K).[119-120] These trends are summarized in the Bray Model (Figure 2-12).[121]

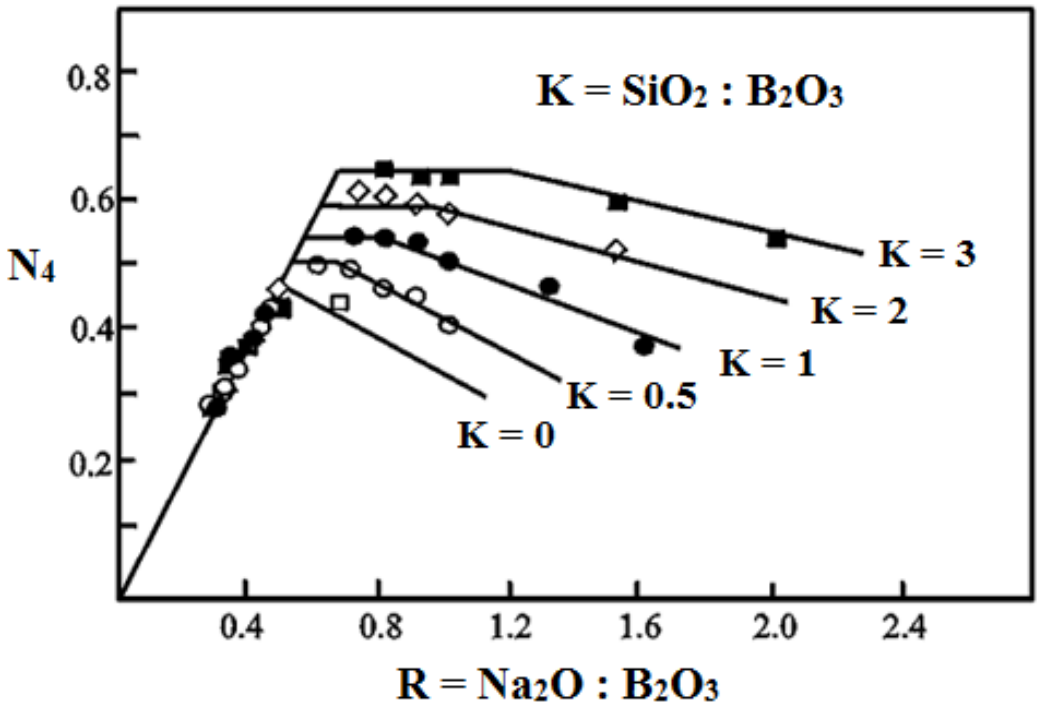

Figure 2-12: The fraction of tetrahedrally coordinated boron (N_4) as a function of the R and K ratios in sodium borosilicate glasses. Adapted from [121].

In borosilicate glasses, the intermediate-range order also has some variations with changing modifier content. At low alkali content or R value, alkali/alkaline earth cations preferentially associate with borate-type structural units in the glass. At higher R values, there is a more homogeneous distribution of the alkali/alkaline earth cations as well as NBO's between the borate and silicate network structures.[118]

Another important aspect of borosilicate glass (and other glasses with multiple *network formers*) is that *network intermediates* often coordinate differently in borates than they do in silicates, and their coordination changes

with alkali content. With both borate and silicate components of the glass, it becomes difficult to predict and observe what the ideal coordination of intermediates is.[122]

2.6 Structure of Alkali Aluminoborosilicate (Addition of Aluminum)

Aluminosilicate glass is a type of glass similar to borosilicate with high resistance to heat shock, but it has the ability to withstand higher operating temperatures than borosilicate glass. Aluminosilicate, however, is approximately three times as expensive as borosilicate and more difficult to fabricate. The addition of some aluminum to form an aluminoborosilicate glass creates a glass with enhanced properties of borosilicate without substantial additional cost.[29] Most laboratory glassware and glass cookware is a borosilicate glass with a small amount of Al_2O_3 added, or an aluminoborosilicate, even though these wares are still commonly referred to as borosilicate.[123]

2.6.1 Aluminosilicate Glass (Alkali Aluminosilicate)

Unlike B_2O_3 which can form a glass on its own, Al_2O_3 is a *network intermediate* and must be used with a *network former*. The simplest form of glass containing aluminum comes from adding Al_2O_3 to SiO_2 to form an aluminosilicate glass. When added to a silicate glass, Al is found exclusively in a tetrahedral coordination with respect to oxygen, effectively substituting for Si. As a result, the Al carries a net negative charge, and therefore, a *network modifier* is required for charge compensation.[70, 124-127] Since the Al tetrahedra

require charge compensation, the addition of Al_2O_3 effectively lowers the number of NBO's associated with Si in the vitreous framework.[70, 127]

Though aluminosilicate glasses generally have tetrahedrally coordinated Al, deviations from this standard occur. When glasses are modified by high field strength cations, five- and six-coordinated Al species may be formed.[128] When the alkali/alkaline earth : Al_2O_3 ratio approaches stoichiometric levels, a lack of enough charge-balancing modifier is created. This can also drive the formation of high-coordinated Al species.[128-130] Analysis have also shown the possibility of the formation of oxygen 'triclusters', one oxygen atom is shared by three (Si, Al)O_4 tetrahedra, in order to maintain charge balance.[127, 131-132]

2.6.2 Alkali Aluminoborosilicate Glass

The structure of aluminoborosilicate is more complicated and less understood than silica or borosilicate glasses due to the mixing of three network-forming cations (Si, B, and Al). While the extent and nature of the mixing of theses oxides is still not well defined, some of the basic structural characteristics of silica and borate glasses are present in aluminoborosilicates.[133]

When Al_2O_3 is added to a modified borosilicate glass, there is a drop in the concentration of BO_4 units and an increase in the Si bridging oxygen. This results in the creation of BO_3 units, and subsequently a net loss of NBO's associated with both the B and Si throughout the vitreous framework. The Al in these glasses is also generally four-coordinated, although there is a greater

tendency to form five- and six-coordinated Al ions as well.[134-139] Like aluminosilicate glasses, the amount of highly-coordinated Al ions increases with the increasing field strength of the *network modifiers*. This indicates a possible competition for oxygen between the Al and B ions.[136]

As the concentration of Na_2O, or other *network modifier*, increases, O^{2-} ions are introduced into the glass network. In the vitreous network, three reactions are expected to take place with respect to the coordination of Al and B: (a) conversion of octahedral aluminum to tetrahedral aluminum; (b) conversion of three-coordinate boron to tetrahedral units; and (c) formation of three coordinate boron having one or two NBO's.[36, 139-141] These reactions are closely dependent on the composition of the glass. For a glass with low aluminum and alkali contents, Table 8-1, reaction (a) is expected to go to completion; therefore, aluminum is expected to be in tetrahedral environments. For a glass of this composition, reaction (b) is expected to dominate over reaction (c), though some of reaction (c) will still occur.[36]

2.6.3 Intermediate Oxide Coordination in Aluminoborosilicate

Early glass fabrication methods tended to introduce a variety of unintended impurities. These impurities often imparted color to the glass. Early glasses were rarely colorless, primarily due to impurities of iron in the sand, which imparts a light blue-green color to the glass.[142] As glassmaking developed, glassmakers developed a number of additives, particularly transition metal

oxides, to impart a variety of colors to the glass, or remove the natural color.[143] As techniques improved and purer materials were found, color became more controlled. Since all sands contain a certain amount of Fe_2O_3, iron remains a relatively large impurity in basic glass.[142, 144-145]

The coordination of transition metals, which are normally *intermediate oxides* or *network intermediates*, is often difficult to predict. Their coordination is influenced by the amount of alkali content, and the ratio of *network formers*.[122] Many of these transition metals also have multivalent states that can exist simultaneously in the glass.[146-147] For instance, iron exists as both Fe(II) and Fe(III) in glasses. The ratio of multivalent states is controlled by the manufacturing procedure (reductive vs. oxidative environment).[148-152] The oxidation state of these *network intermediates* often influence how they are incorporated into a glass. For instance, in aluminoborosilicate glass, Fe(II) is usually octahedrally coordintaed with oxygen and incorporated as a *network modifier*, while Fe(III) is usually tetrahedrally coordinated with oxygen and incorporated as a *network former*.[153-158]

Chapter 3

Radiation Effects in Glass

3.1 Introduction

Ionizing radiation interacts with matter in a number of ways. Figure 3-1 depicts the complexity of the damage creation processes taking place during irradiation.[159] In general, energetic particles or photons passing through a material lose energy through a variety of interactions and scattering mechanisms. The final result of the radiation can

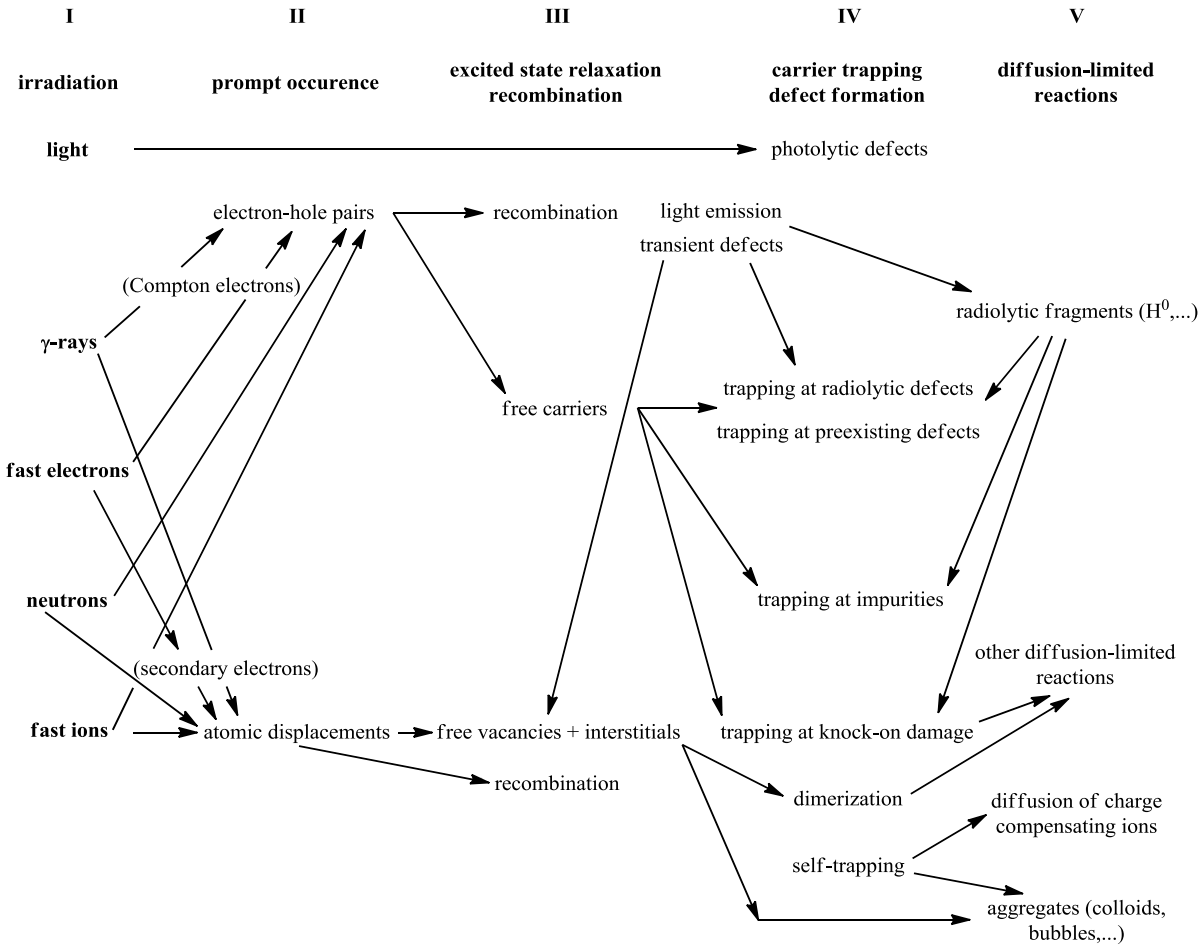

Figure 3-1: Schematic diagram of some of the most relevant radiation damage processes in glasses. Adapted from [159].

depend on a number of factors including: the type of radiation, the dose rate of the irradiation, the total dose absorbed by the material, and the type of material being irradiated.[160] The two main types of interaction with materials important to this study are ionization and atomic displacement.[161-164]

3.2 Radiation Type

The way radiation interacts with matter is dependent on the irradiating material.[165-166] The basic radiation types (β-particles, α-particles, recoil nuclei, and γ-rays) that would come from the storage of radioactive material interact in two basic ways: (a) transfer of energy to electrons through ionization and electronic excitations; and (b) transfer of energy to atomic nuclei through collisions resulting in atomic displacement.[161-164, 167] For electronic excitations, this transfer of energy is usually just a few eV (3.62 eV in silicon at room temperature),[163] whereas atomic displacement typically requires a transfer of 25 eV of kinetic energy.[168]

In general, ionization/electronic processes dominate the energy transfer for β-particles and γ-rays with little atomic displacement. For ions (α-particles and recoil nuclei), however, more of the energy transferred is partitioned between electronic excitations and nuclear collisions. A useful relation is that ionization processes dominate if the energy of the ion, expressed in keV, is greater than its atomic weight, and nuclear collisions dominate if the energy of the ion falls below this limiting approximation.[167] An α-particle, with an atomic weight of 4 and initial decay energy in the MeV range will predominately deposit its energy by ionization processes, but as it

loses energy, it will have a significant amount of nuclear collisions.[161-164] However, a recoil ion will generally lose most of its energy through collisions as its atomic weight is generally larger than its energy (expressed in keV).[167]

The linear energy transfer (LET) of the particle also affects the trapping (Section 3.5), with high LET radiation resulting in less trapping per dose than low LET. The type of traps that are filled are also different between high and low LET, with high LET radiation filling a greater ratio of deep (more stable) traps when compared to low LET.[169]

3.3 Atomic Displacement

Radiation damage to materials is generally linked to the creation of disorder within the material's lattice structure through atomic displacement which often creates an interstitial atom and vacancy (Figure 3-2).[6, 170] This disorder can change the physical and chemical properties of the material.[171-174] The changes can degrade the performance of the material in a manner that may or may not recover over a period of time.[160] Since glass is a non-crystalline (amorphous) material, its structure lacks long-range order. Therefore, many of the physical and chemical properties of glass are less affected by atomic displacements making glass more resistant to radiation damage.[175-177]

Though atomic displacement does not alter the physical and chemical properties of glass to the same extent as crystalline structures, the radiation creates defects in glass similar in structure and quantity to those created in crystalline materials.[178-182] However, due to their disordered structure, amorphous materials typically contain significantly more defects prior to irradiation.[183]

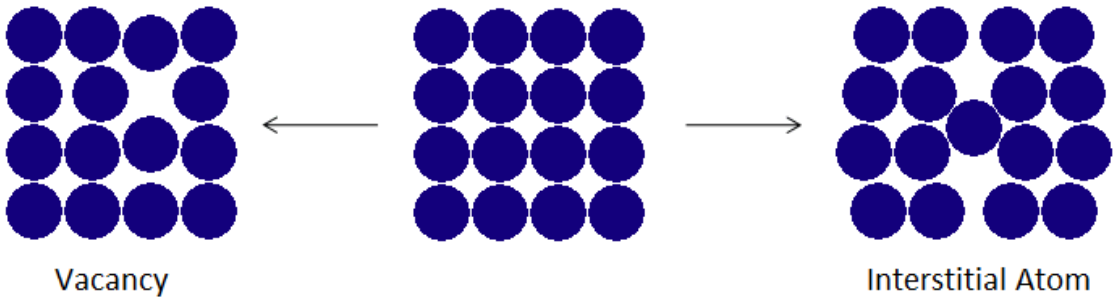

Figure 3-2: Atomic displacement in a crystalline structure with representation of the creation of a vacancy (left) and an interstitial atom (right). Adapted from [170].

3.4 Ionization (Electron-Hole Pair Production)

The primary interactions between radiation and the electronic structure of atoms are more complex and varied than atomic displacement (transfer of momentum to the nuclei of atoms).[184] Though there is initial variety in interaction, much of the loss of energy to the electrons in glasses is eventually converted to the formation of electron-hole pairs or ionization.[184-185] Once formed, these electron-hole pairs can occasionally become trapped within the glass.

Band theory, which was originally developed using a semi-infinite periodic lattice model to describe electron-hole pair formation for crystalline materials, can also be applied to non-crystalline materials due to the short- and intermediate-range order that many of these non-crystalline materials, including glass, possess.[7-10] Some modifications to band-theory are required in order to apply it to non-crystalline materials. These modifications include modeling the localized energy levels as being distributed in energy, rather than discrete bands.[7] This results in conduction and valence bands with an energy gap, or mobility gap, that contains localized states which can trap both

electrons and holes at defects (inherent to the material or created through processes such as atomic dislocation) or impurities within the material,[8, 186] as shown in Figure 3-3.

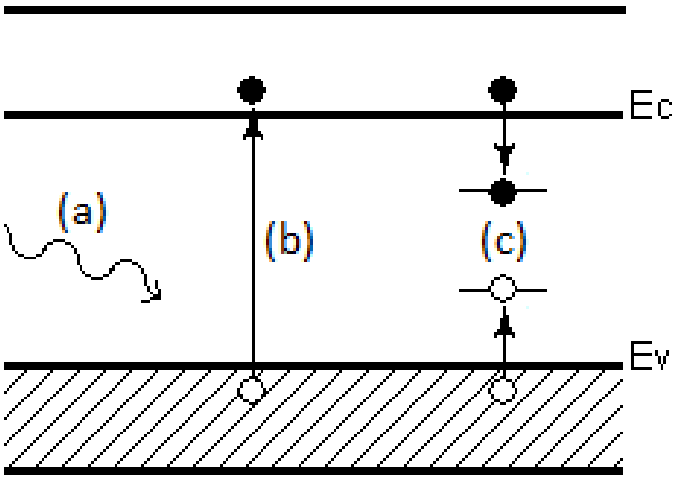

Figure 3-3: Electron-hole pair formation and trapping: (a) radiation interacts with the electronic structure of the material; (b) and electron-hole pair is generated with the electron (solid circle) being excited to the conduction band (Ec), leaving the hole (open circle) in the valence band (Ev); (c) both the electron and hole free to move through the material until they become trapped at defects centers. Adapted from [8].

3.5 Electron/Hole Traps

As has been established, glass does not contain long-range order in its vitreous network. This makes the concept of an extended network defect, such as a dislocation, meaningless. Instead the idea of a point defect, a departure from an atom's ideal short-range order,[187-188] is utilized. Point defects can be classified into four basic categories (Figure 3-4):[9]

1. *Vacancies*-the absence of certain atoms from their normal positions.

2. *Interstitials*-additional atoms in positions different from those normally expected. A non-bridging oxygen accompanied by a *network modifier* could be considered an interstitial relative to a pure network.
3. *Substitutional*-atoms of a nature different from those generally present in the network. In silicate glasses, this refers to species replacing Si^{4+} sites, such as Ge^{4+} and Al^{3+} even if the substituting species are a major part of the network.
4. *Impurities*-species present that include *network formers*, *network modifiers*, and *network intermediates* incorporated into the glass, but were not intentionally added, such as transition metals. These can also act like interstitial and substitutional point defects.

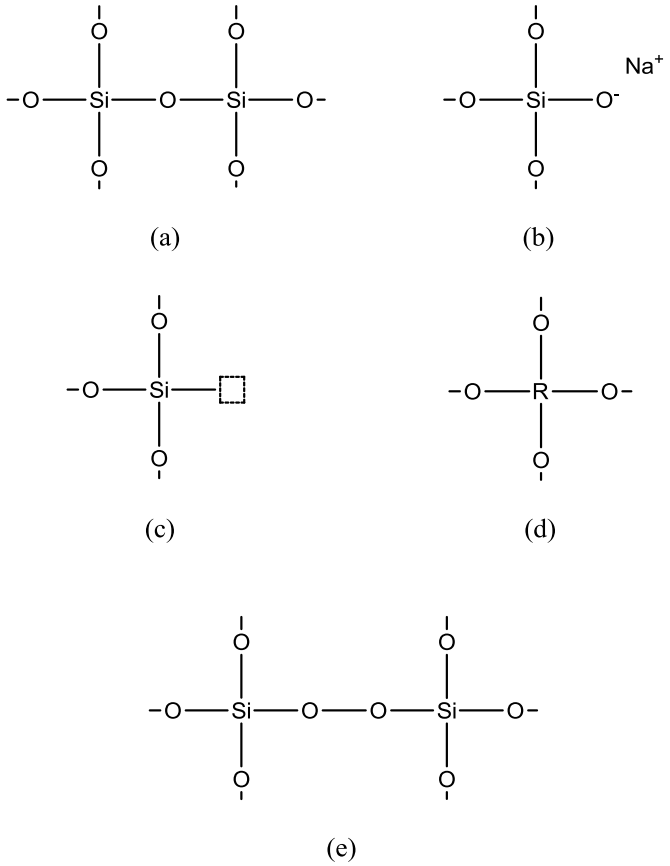

Figure 3-4: Examples of point defects in glasses; (a) reference network; (b) non-bridging oxygen; (c) oxygen vacancy; (d) substitutional impurity; (e) interstitial oxygen. Adapted from [9].

Depending on the point defect, these imperfections can trap electrons or holes, or in some circumstances, assist in the recombination of electrons and holes. Some of the more common and important traps for alkali aluminoborosilicate glasses are described below.

3.5.1 E'-Defect Center (Network Defect)

The most famous and studied defect trap in oxide glasses is the E'-center.[189-198] The E'-center is associated with an oxygen vacancy defect in the vitreous network (Figure 3-4c). In the simplest description, an E'-center is an unpaired electron trapped in a dangling sp^3 hybrid orbital of an atom A bonded to three oxygens, where A = Si, Ge, B, P, or Al.[189-191] A related defect (not discussed in further detail) is an E"-center which is formed when two electrons are trapped in an oxygen vacancy (Figure 3-5).[198-199]

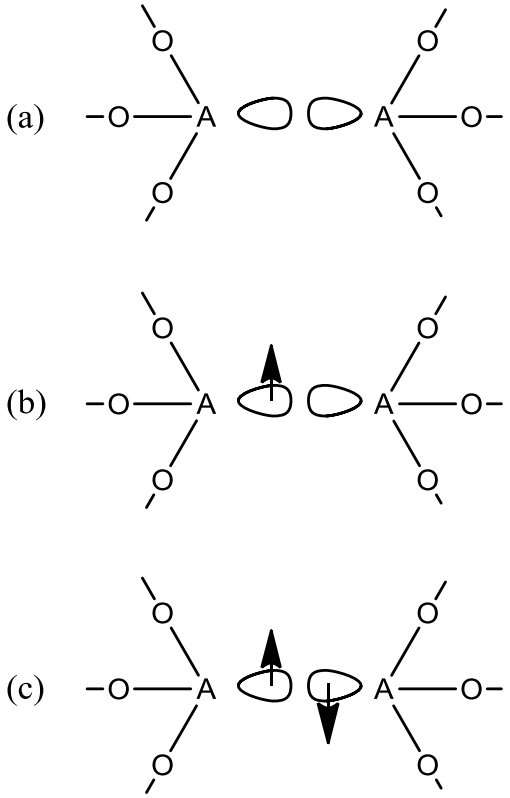

Figure 3-5: Schematic diagram of (a) an oxygen vacancy; (b) E'-center; and (c) E"-center. Adapted from [198].

3.5.1.1 Silicon E'-Defect Center

Many forms of the E'-center exist and have been observed in quartz and silicate glasses.[198-202] The nomenclature used to distinguish these defects is based on their EPR signal. The E indicates that the oxygen vacancy is an electron trapping site, and the number of primes indicates the number of electrons trapped at the site. A subscript is added to indicate the number of EPR lines observed for the defect.[198] The most common silicon E'-center is the E_1' which is an electron trapped in an oxygen vacancy between two silicon atoms (Figure 3-6a), though there is disagreement of its formation mechanism.[188-207]

When hydrogen, a common impurity in silicate glasses,[208] is in the vicinity of an E'-center it interacts with the hyperfine EPR structure and introduces two or four additional EPR lines for the E_2' and E_4' species

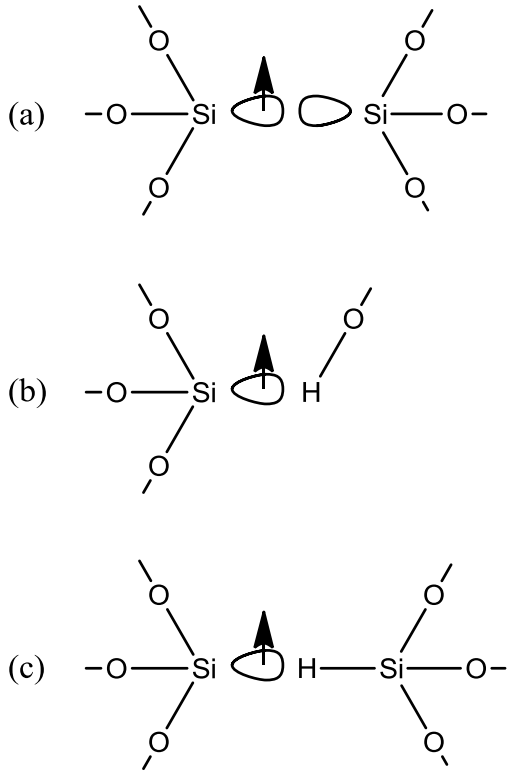

Figure 3-6: Schematic diagram of different E'-centers found in silicate glass (a) E_1'; (b) E_2'; and (c) E_4'. Adapted from [198].

respectively. In the E_2' species, a hydrogen atom from a hydroxyl group replaces one of the Si atoms, while in the E_4' species, the hydrogen is associated with a silica tetrahedron (Figure 3-6).[198]

3.5.1.2 Boron E'-Center

The boron E'- center (B E') is virtually identical to the silicon E'-center (Si E'). It again is an electron trapped in a dangling sp^3 hybrid orbital;[189-190, 209] however, two distinctions should be made between the B E' and the Si E' centers. Because silicon is normally tetrahedrally coordinated in silicate glasses (and the first studies of the E'-center were of silica), the E'-center is normally associated with an oxygen vacancy. In the case of boron, the three-coordinate state is normal and, therefore, can be created without any additional defect formation.[189] The Si E' "half unit" is electrostatically neutral while the B E' "half unit" has a -1 charge. Because of this, the Si E'-center is more stable than the B E'-center.[209] Depending on the glass, the B E'-center begins to decay at temperatures from 400-500 K, while the Si E'-center begins to decay at temperatures from 450-550 K.[209-210]

Related to the Si E' and B E'-centers and potentially present in aluminoborosilicate glass is an aluminum E'-center (Al E'). However, studies have shown that the number of Al E' centers is extremely low even when the aluminum content of the glass is large.[211] For this reason,

Al E’ centers should contribute very little to the signals observed in the glass of this study.

3.5.2 Boron Electron Center (BEC)

The boron electron center (BEC) is structurally very similar to the B E’-center. Like the B E’-center and the Si E’-center, this center is formed when an electron is trapped on a dangling sp^3 hybrid orbital. Unlike the B E’-center, this trapped electron is shared between the boron atom and an alkali or alkaline earth cation.[191, 212] The electron is mainly localized on the boron, but it is influenced by the *network modifier*.[191, 210]

The stability of the BEC is much lower than the E’-centers with decay beginning around 80 K.[212-214] Decay of this trap continues from 80-320 K with the BEC almost completely bleached (recombined–Section 4.2.1) at room temperature.[215-219] A BEC that traps two electrons (BEC^{2-} center) has been theorized and predicted to be more stable than the BEC with one electron.[218-219] These BEC’s account for ~15% of the total number of trapped electrons generated from ionizing radiation in many borate related glasses at temperatures less than 77 K.[213]

3.5.3 Alkali/Alkaline Earth Electron Center (AEC/AEEC)

The alkali electron center (AEC) and alkaline earth electron center (AEEC) are common electron traps in silicate type glasses that are very similar to one another with only slight differences, which will be discussed. The AEC and AEEC

are also often created along with non-bridging oxygen hole centers (NBOHC's) which are discussed below (Section 3.5.5).

As described earlier (Section 2.4), an effect of adding *network modifiers* such as alkali or alkali earth oxides to a glass is the creation of NBO's with the alkali/alkali earth cation charge compensating (Figure 2-8). Each alkali cation introduces and compensates for one NBO, while each alkaline earth cation introduces and compensates two NBO's.[33, 86-88] This situation creates electrical dipoles within the glass composed of a negatively charged NBO and a positively charged cation.[218] The extra electron of the NBO can be excited during irradiation. If this electron is then trapped by the network modifying cation, an AEC or AEEC is formed (Figure 3-7).[218, 220-223] This also, in effect, neutralizes a dipole, or in the case of the AEEC, reduces a quadrupole to a dipole.[218]

Due to the loss of the dipole, these electron traps are able to migrate through the glass and form clusters with other modifiers.[213, 221-222] Though the other modifiers brought into the clusters have not necessarily trapped an electron of their own, in general, the trapped electrons become spin-paired in the large conglomerations.[210, 213] This clustering proceeds more rapidly at higher temperatures.[222]

Unlike alkali cations, an alkaline earth cation compensates two NBO's which results in a quadrupole instead of a dipole. Therefore, when an electron is trapped to form an AEEC, the quadrupole is reduced to a dipole (Figure 3-7).

This hinders the ability of the AEEC to migrate and keeps it near the neutralized NBO.[221]

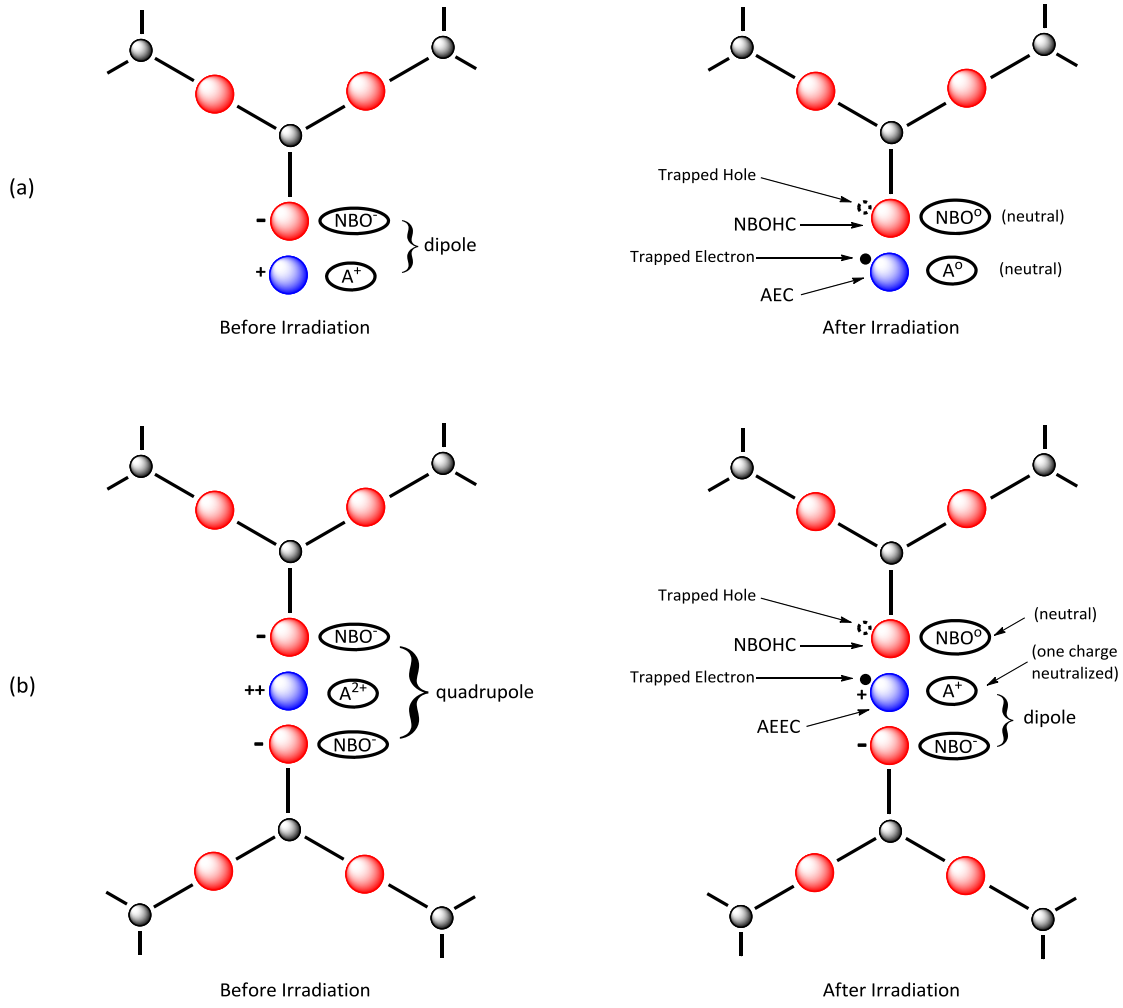

Figure 3-7: Schematic representation of the formation of an alkali electron center (AEC), an alkaline earth electron center (AEEC), and a non-bridging oxygen hole center (NBOHC). (a) Before irradiation, an alkali cation (A^+) and a non-bridging oxygen (NBO) form a dipole. Following irradiation, an electron from the NBO is excited and captured on the A^+ to form A^o or an AEC leaving the NBO in a metastable state, or a captured hole to form a NBOHC. The AEC is able to migrate and form clusters in the material. (b) Before irradiation, an alkali earth cation (A^{2+}) is associated with two NBO's forming a quadrupole. An electron-hole pair is trapped to form an AEEC and NBOHC. Since there are two NBO's, a dipole remains, and the AEEC is less mobile than an AEC. Adapted from [218].

3.5.4 Multivalent Ion Center

Impurity ions and additive ions (elements other than Si, B, Al, alkali, and alkaline earth species in aluminoborosilicate glasses) can be incorporated into the glass. These can act as *network formers*, *network modifiers*, or both (*network intermediates*). How these ions are incorporated into the glass depends upon the element and the oxidation state of that element, determined by the manufacturing conditions.[148-152] Some impurities are able to exist in multiple oxidation states simultaneously within the glass.[146-147] These impurity ions can act as traps for either electrons or holes, and in some cases both (Figure 3-8).[146-147, 223-230] In most cases, a metastable state of the impurity ion is formed when an electron or hole is captured.[227]

(1)

(a) $\equiv Si-O^- + Fe^{3+} \longrightarrow \equiv Si-O^{\bullet} + (Fe^{3+})^-$

(b) $\equiv Si-O^{\bullet} + Fe^{2+} \longrightarrow \equiv Si-O^- + (Fe^{2+})^+$

(2)

(a) $\equiv Si-O^- + Zn^{2+} \longrightarrow \equiv Si-O^{\bullet} + (Zn^{2+})^-$

(b) $\equiv Si-O^{\bullet} + Zn^{2+} \longrightarrow \equiv Si-O^- + (Zn^{2+})^+$

Figure 3-8: Example equations of multivalent ion centers: (1a) Fe^{3+} captures an electron to form $(Fe^{3+})^-$; (1b) Fe^{2+} captures a hole to form $(Fe^{2+})^+$; (2) Zn^{2+} captures an electron or hole to form $(Zn^{2+})^-$ and $(Zn^{2+})^+$ respectively. Adapted from [229].

Iron, which is one of the most abundant impurities in the glass used in this study (Table 8-2), coexists in glass as iron(II), Fe^{2+}, and iron(III), Fe^{3+}.[146-158] In aluminoborosilicate glass, Fe^{2+} acts as a *network modifier* and is typically octahedrally coordinated with oxygen, while Fe^{3+} acts as a *network former* and is typically tetrahedrally coordinated with oxygen.[44, 47-48, 153-158, 215, 231] The Fe^{2+} ion can become oxidized by trapping a hole and forming the metastable $(Fe^{2+})^{+}$ ion (Figure 3-8). Due to its initial environment, the $(Fe^{2+})^{+}$ remains octahedrally coordinated with oxygen, distinguishing it from the tetrahedral Fe^{3+}. Likewise, the Fe^{3+} ion can be reduced by trapping an electron and forming the metastable $(Fe^{3+})^{-}$ ion which is distinguished from the Fe^{2+} by its coordination environment.[155-157, 222, 232]

Zirconium, like iron, is an abundant impurity in the glasses of this study (Table 8-2). Unlike iron, zirconium is only incorporated into glasses as Zr^{4+} and will only trap electrons during irradiation.[233] Other impurities, such as zinc, that are often found in only one oxidation state, can also act as electron/hole traps. As shown in Figure 3-8, these impurities can be oxidized (trap a hole), reduced (trap an electron), or both (impurity center can trap either an electron or a hole) to form metastable defect centers.[229] Additional impurities, such as vanadium, coexist in multiple oxidation states but with each oxidation state possessing identical coordination. Though these centers can still trap electrons and/or holes, they are indistiguishable from one another.[9]

3.5.5 Non-Bridging Oxygen Hole Centers (NBOHC)

The most abundant hole trap in silicate glasses is the non-bridging oxygen hole center (NBOHC).[8-9, 165, 167, 186-190, 233-237] An intrinsic defect of all glass is the non-bridging oxygen (NBO), an oxygen that is only associated with one *network former* (typically Si, B, or Al for aluminoborosilicate glasses). NBO's tend to be associated with hydrogen, alkali, or alkaline earth ions for charge compensation.[86-88] These oxygens are susceptible to the loss of an electron by ionization which corresponds to the capture of a hole.[9]

3.5.5.1 Oxygen Hole Center (OHC)

In simple silicate glasses, the most commonly observed NBOHC is associated with a NBO of silicon. The literature distinguishes between NBOHC's of silicon by the charge compensator (*network modifier*). When a NBO of a silicon associated with a hydrogen or an alkali ion captures a hole, it is referred to as simply a hole center (HC) or an oxygen hole center (OHC).[192, 228, 238-242]

The OHC has been further subdivided into two hole centers: OHC_1 and OHC_2. If an electron from an NBO of a Q^3-silicon (Section 2.4) is excited during irradiation and trapped at an electron center, the OHC_1 is formed (Figure 3-7). The degree to which the OHC_1 involves *network modifying* cations is unknown. There are two views that: (i) following the hole trapping, the compensating alkali cation (or hydrogen) migrates

away from the Q^3 unit leaving an uncompensated complex,[189, 197, 238-239] represented in Figure 3-9a, and (ii) the compensating cation remains near the OHC_1 and remains strongly coupled to the NBO.[192, 197] There is also a possibility that the compensating cation is missing from the NBO complex prior to trapping.[197, 210, 236]

The OHC_2 is not as well characterized as the OHC_1. The OHC_2 is believed to be a hole trapped on a NBO of a Q^2-silicon with one of the charge compensating cations missing.[189-190, 197, 238-239] The remaining *network modifier* either couples to a single NBO (yielding an OHC_1-like defect) or migrates away (yielding the OHC_2). Following migration, the two NBO's are equivalent, and the hole is shared between them,[197] represented in Figure 3-9b.

When a NBO of a silicon associated with an alkaline earth ion captures a hole, the silicon hole center (SHC) is formed.[233, 241] The SHC, like the OHC, can form a SHC_1 and SHC_2 in a similar fashion as described above. Since the SHC is associated with an alkaline earth cation, the *network modifier* is charge compensating two NBO's. Therefore, when the hole is trapped, the alkaline earth ion will not migrate,[241] as represented in Figure 3-9c.

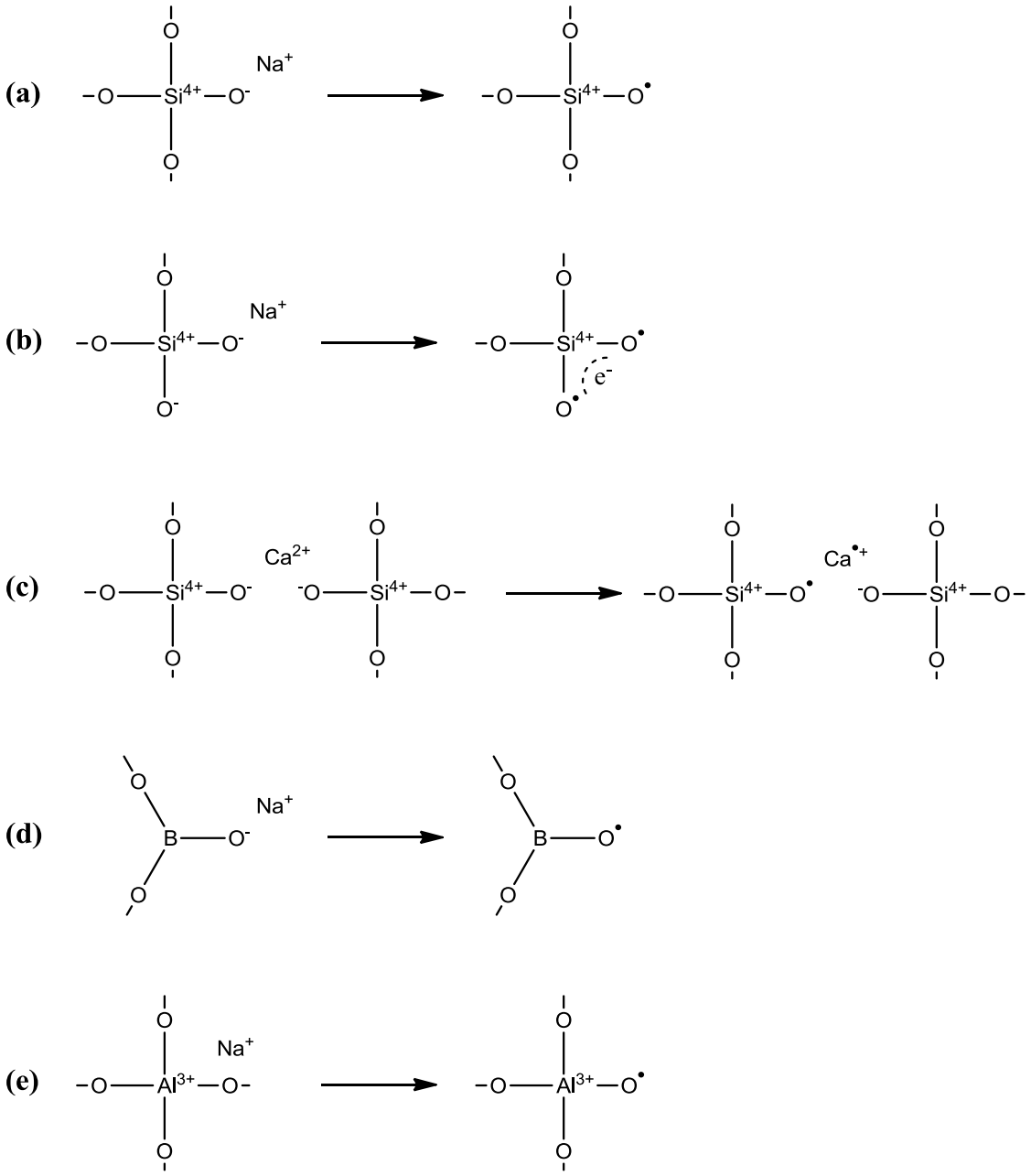

Figure 3-9: Possible mechanisms for the formation of the most common non-bridging oxygen hole centers (NBOHC): (a) oxygen hole center (OHC_1); (b) OHC_2; (c) silicon hole center (SHC_1) (d) boron oxygen hole center ($BOHC_1$); and (e) aluminum oxygen hole center (AlOHC). Adapted from [9].

3.5.5.2 Boron Oxygen Hole Center (BOHC)

In the majority of borosilicate glasses, the most abundant defect is the boron oxygen hole center (BOHC).[209, 236] Like the OHC and SHC, there are different varieties of the BOHC, the most prevalent of which is the $BOHC_1$.[243-244] The structure of the $BOHC_1$ has been disputed for many years. Presently, it is widely believed that the $BOHC_1$ originates from a NBO bonded to a trigonal boron.[244-247] As with the OHC and SHC, an electron from the NBO can be excited during irradiation and trapped at an electron center leaving a trapped hole on the NBO, specifically known as a BOHC.[210, 236, 248-249] As before, the charge compensator can migrate through the material (Figure 3-9d). In general, the BOHC is considered more stable than the B E', but slightly less stable than the Si E'.[209]

As with the OHC and SHC, a hole can also be trapped on a NBO of a trigonal boron with two NBO's to form the $BOHC_2$.[210] In addition to these, a $BOHC_3$ has been observed. This hole center is formed when a hole is captured on a BO between two tetrahedral boron units.[210, 243] Both the $BOHC_2$ and $BOHC_3$ are more stable than the $BOHC_1$. However, due to the precursor structure, they are less prevalent in aluminoborosilicate glasses.[210]

3.5.5.3 Aluminum Oxygen Hole Center (AlOHC)

Though it has been observed, the aluminum oxygen hole center (AlOHC) is the least characterized of any of the hole centers. It is theorized to be formed from a tetrahedrally coordinated aluminum precursor. The hole is trapped on a NBO of the aluminum, but it is not known if the oxygen was non-bridging prior to capture or if it was formed during trapping.[9, 225, 250-253] Though present in aluminosilicate glasses,[254] the AlOHC is rarely seen in aluminoborosilicate glass as most of the holes are trapped on NBO's of boron to form $BOHC_1$ species.[210, 255]

Chapter 4

Experimental Techniques

4.1 Introduction

The primary interaction between ionizing radiation and the electronic structure of atoms is the formation of electron-hole pairs.[184-185] Once formed, these electron-hole pairs can become trapped within the glass. A measurement of the occupied traps could then be used to determine the amount of energy, or radiation, that the material initially absorbed.[256] This dosimetry measurement can be accomplished through direct measurement of the electron/hole centers or through forced migration of the trapped electrons/holes.

4.2 Thermoluminescence (TL)

When radiation is incident on a material, some of its energy may be absorbed and re-emitted as light of a longer wavelength. This process is known as luminescence. The wavelength of the emitted light is dependent on the characteristics of the luminescent material and not of the incident radiation.[8] The various luminescence processes are given names which reflect the method used to stimulate the light emission, such as cathodoluminescence[257] (stimulated by an electron beam) and photoluminescence (stimulated by optical or ultra-violet light).[258]

Thermoluminescence (TL), also known as Thermally Stimulated Luminescence (TSL), is the emission of light from an insulator or semiconductor which is observed

when the metastable solid is thermally stimulated.[8, 11-12, 259-260] This phenomenon should not be confused with black body radiation, the light spontaneously emitted from a substance when it is heated to incandescence where the solid emits radiation of which the intensity increases with increasing temperature.[260] Unlike black body radiation, TL is the thermally stimulated emission of light following the previous absorption of energy from radiation. Three essential conditions are necessary for the production of TL. First, the material must be an insulator or a semiconductor – conductors, such as metals, do not exhibit luminescent properties since they lack a band gap (Section 3.4).[8, 162, 260-262] Second, the material must have at some time absorbed energy during exposure to ionizing radiation. Third, the luminescence emission is stimulated by heating the material.[8, 260] In addition, an important property of TL is that once heated to stimulate the light emission, the material cannot be made to emit TL again by simply cooling the sample and reheating. In order to re-exhibit this type of luminescence, the material must be re-exposed to ionizing radiation.[8]

As stated previously, the primary interaction between ionizing radiation and the electronic structure of atoms is the eventual formation of electron-hole pairs (transition (a) in Figure 4-1) which can occasionally become trapped (transitions (b) and (e) in Figure 4-1). Through heating, these electrons and holes can be stimulated into migration (transitions (c) and (f) in Figure 4-1) which can lead to electron-hole recombination. If light is emitted during the recombination process, thermoluminescence occurs.[8]

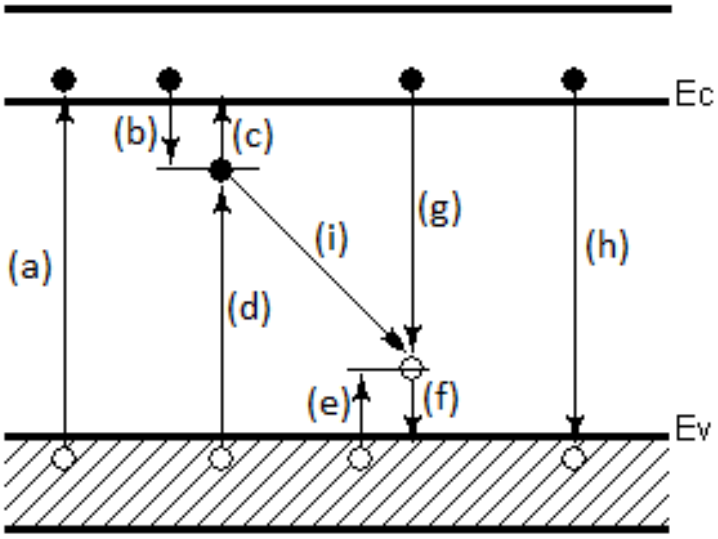

Figure 4-1: Common electronic transitions involving the conduction band (Ec) and valence band (Ev): (a) ionization; (b) and (e) electron (solid circle) and hole (open circle) trapping respectively; (c) and (f) electron and hole release; (d) and (g) band-to-center recombination; (h) band-to-band recombination; and (i) center-to-center recombination. Adapted from [8].

4.2.1 Recombination

Thermoluminescence is governed by the process of electron-hole recombination. Three distinct types of recombination processes are possible: band-to-band (transition (h) in Figure 4-1), band-to-center (transitions (d) and (g) in Figure 4-1), and center-to-center (transitions (i) in Figure 4-1). The band-to-band recombination is termed 'direct' due to an electron in the conduction band recombining with a hole in the valence band (an excited electron relaxing to the ground state). The band-to-center and center-to-center recombination processes are termed 'indirect' due to recombination involving localized levels

(transitions from or to a trap center).[8] For luminescence to occur, the recombination must be accompanied by the emission of a photon (i.e. radiative).

4.2.1.1 Direct Transition

In a direct transition (Figure 4-2), the excited electron must lose an amount of energy corresponding to the band gap. As this would require the simultaneous creation of many phonons, or phonon-like excitations in the case of non-crystalline materials like glass,[263-266] to dissipate the electron's energy, it is unlikely that this energy could be totally dissipated by phonon interaction alone which would be required for a non-radiative transition. Therefore, photons are emitted during band-to-band transitions, and the transitions are radiative.[8]

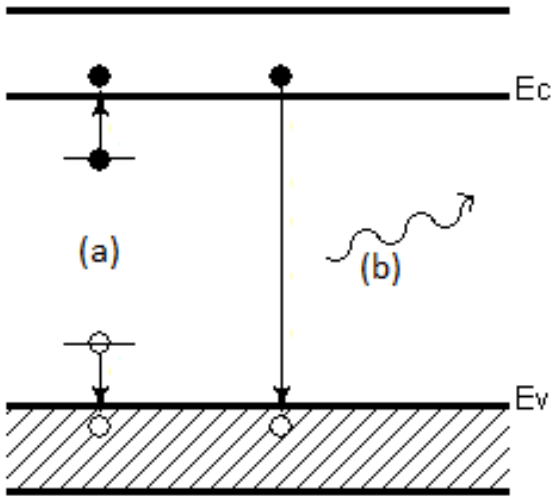

Figure 4-2: Direct recombination transition (band-to-band): (a) the electron (solid circle) and hole (open circle) are stimulated back to the conduction (Ec) and valence (Ev) bands; (b) the electron and hole recombine and a photon is emitted. Adapted from [8].

4.2.1.2 Indirect Transition

In an indirect transition (Figure 4-3 and Figure 4-4), the energy dissipated is much less than the band-gap. The energy, therefore, may be

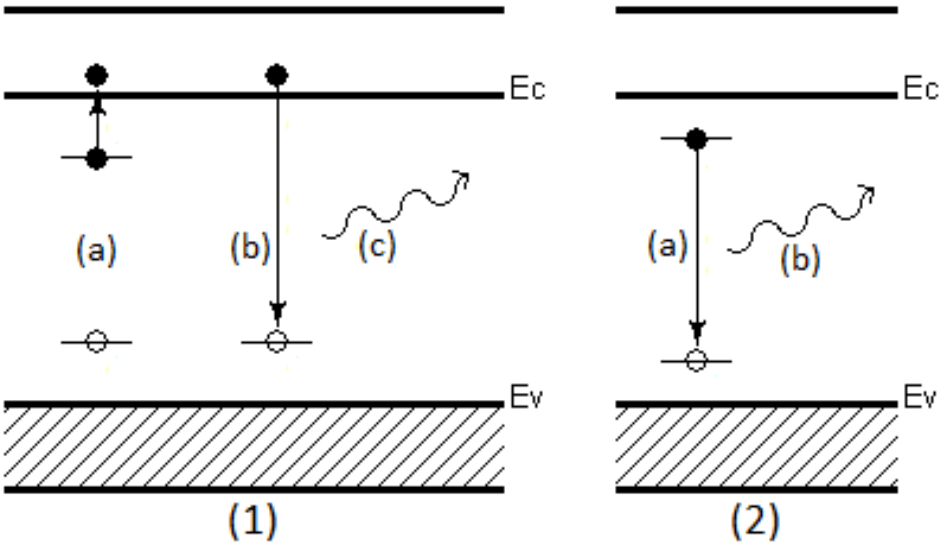

Figure 4-3: Indirect recombination transitions: (1) band-to-center transition – (a) the electron (solid circle) is stimulated to the conduction band (Ec); (b) the electron recombines with a trapped hole (open circle); (c) if required, a photon is emitted. Though not shown, band-to-center with hole transition can also occur. (2) center-to-center transition – (a) the electron and hole recombine without movement to the conduction or valence band; (b) if required, a photon is emitted. Adapted from [8].

dissipated either radiatively (via photons) or non-radiatively (via phonons).[8] A material's relative probability of direct vs. indirect transitions and radiative vs. non-radiative processes for indirect transitions, therefore, has a strong influence on the amount of luminescence the material will exhibit.

As all direct recombination transitions are radiative and stimulation to the conduction and valence band for the electron and hole is necessary for a direct recombination, the probability for an electron and hole to be stimulated to their respective band is important. It has

been shown that the mean time an electron and hole spend in a trap (τ) at temperature T is given by

$$\tau = s^{-1}\exp(E/kT) \tag{4.1}$$

where s is a constant (also known as the frequency factor or the "attempt-to-escape" frequency), k is Boltzmann's constant, and E is the energy difference between the trap and the edge of the corresponding delocalized band (i.e. trap depth).[8, 10, 12, 260, 267-270] For a given temperature, those centers with a small trap depth are more likely to release their electron/hole to its respective band, whereas those centers with a large trap depth are more likely to remain trapped and act as recombination centers. Therefore, as the trap depth of a center increases, the probability of indirect recombination also increases. It can also be seen that at higher temperatures electrons/holes in recombination centers are more likely to escape to the conduction/valence band than at lower temperatures which results in more direct recombination transitions as the temperature increases.[8]

Once stimulated, the lifetime, τ_r, of a free carrier for direct recombination (the mean time an electron spends in the conduction band before direct recombination with a free hole in the valence band) was determined by van Roosbroeck & Shockley and was found to be temperature dependent.[271-273] The lifetime is given by

$$\tau_r = n_i/2R_d \quad (4.2)$$

where n_i is the intrinsic free carrier density and R_d is the temperature-dependent rate of direct recombination. Though values of τ_r have been experimentally determined that are consistent with equation (4.2),[274-275] many recombination lifetimes have been observed which are much less than the lifetimes expected for band-to-band recombination.[276] This suggests that indirect recombination mechanisms may be dominant, particularly at low temperatures. At higher temperatures, the lifetimes often approach those expected for direct recombination.[8]

The wavelengths from luminescence emission have also been shown to be longer than those expected from conduction to valence band transitions as impurities and other lattice defects are introduced into a material. This is consistent with a shift from direct to indirect recombination processes. In general, as impurities are added to a material, the recombination transitions become dominated by indirect (band-to-center and center-to-center) processes as there is a general increase in recombination centers.[8]

4.2.1.3 Recombination Centers

A recombination center is defined as an electron/hole trap in which the probability of recombination with an opposite sign charge carrier at the site is greater than that of thermal excitation of the trapped

carrier to its respective delocalized band.[12] Though the presence of impurities in general shifts recombination processes from direct to indirect transitions, it is difficult to predict the effect of individual impurities.[277] The role of an impurity as a trap or recombination center is dependent on the base composition of the material, the other impurities present, the concentration of all impurities, and the oxidation state of the impurities. An impurity that acts as a recombination center in one material will not necessarily act as a recombination center in a different material. Also, a recombination center that results in radiative recombination in a material may produce non-radiative recombination in another material.[216, 232, 278-288]

4.2.1.4 Center-to-Center

Center-to-center recombination offers additional pathways for deexcitation. If a trapped electron and hole are situated close to each other in the material, recombination can take place through tunneling (transition (a) in Figure 4-4).[289-290] Alternatively, an electron can be elevated to a higher energy level, then recombination can take place through tunneling (transition (b) followed by transition (c) in Figure 4-4).[291] These pathways can be radiative or non-radiative.[8]

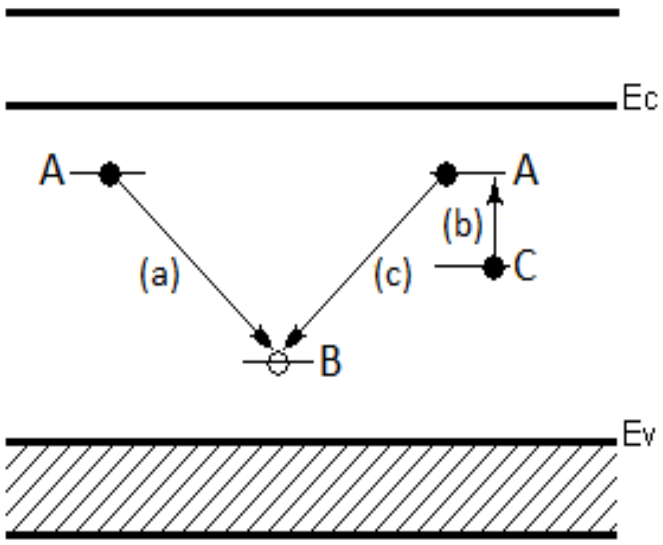

Figure 4-4: Indirect recombination transitions not involving the conduction or valence bands (center-to-center): (a) an electron (solid circle) at level A recombines with a hole (open circle) at level B through tunnelling; (b) an electron at level C is raised to level A, then (c) recombines with a hole at level B through tunnelling. Though not shown, a photon may be released. Adapted from [8].

4.2.2 Instrumentation

The basis of thermoluminescence dosimetry is stimulating electron-hole recombination through thermal treatment and quantifying the resulting light output. By knowing the characteristics of the studied material, the amount of light output can be used to calculate the original dose of radiation that the material received. TL instrumentation can vary from very simple to extremely sophisticated. However, at the core of all TL instrument designs are a sample heater, a temperature control unit, and a light detection system. Instrumentation becomes more sophisticated depending on what capabilities are required. For instance, enhanced designs are needed to measure glow

curves (TL spectra) below room temperature or to simultaneously record thermally stimulated measurements such as the wavelength spectrum in addition to intensity of light emitted.[8, 15]

In this study, TL glow curves were gathered using a Harshaw 3500 TL reader which uses a platinum planchet to heat the sample at a constant heating rate. Glow curves were acquired between 50°C and 400°C at a heating rate of 5°C/s with a 20s hold time at the highest temperature. The Harshaw 3500 uses a 9125B model photomultiplier tube (PMT) from Electron Tubes Inc. for light detection. This PMT is sensitive to light in the 280-630 nm spectral range.[292]

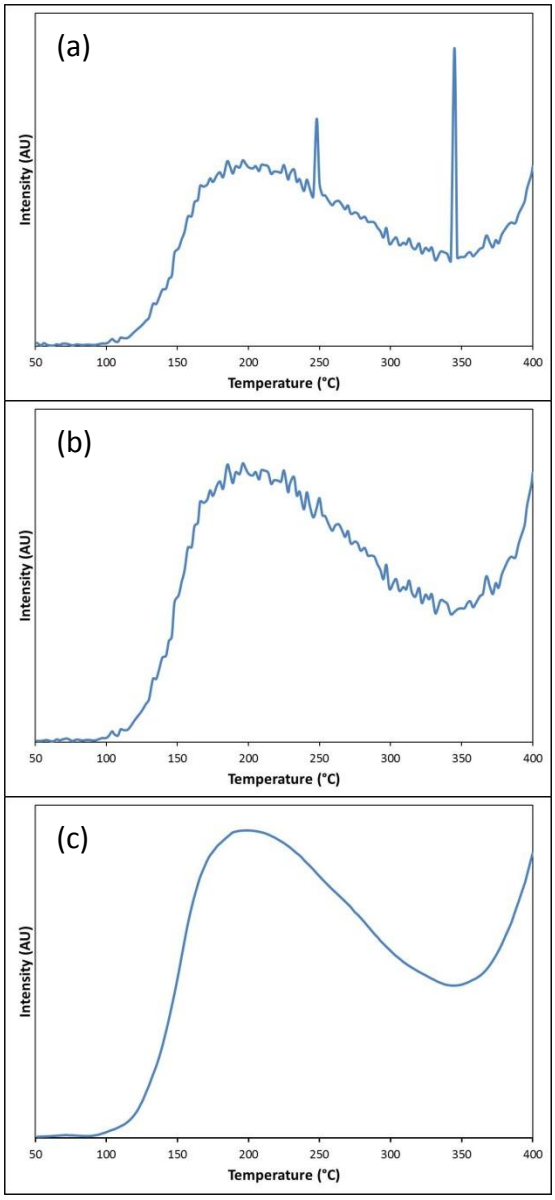

Figure 4-5: Example thermoluminescence glow curves: (a) original glow curve with background spikes; (b) glow curve with background spikes removed; (c) smoothed glow curve.

In some of the TL glow curves, background spikes were observed (Figure 4-5a). These were manually removed by taking the average of the two data points on either side of the spike (Figure 4-5b). Glow curves were smoothed with loess[293-294] local regression smoothing using the Curve Fitting Toolbox[295] for MATLAB[296] (Figure 4-5c).

4.3 Electron Paramagnetic Resonance (EPR)

Electron paramagnetic resonance (EPR) or electron spin resonance (ESR) spectroscopy is an analogous technique to nuclear magnetic resonance (NMR) spectroscopy but excites electron spins rather than nuclear spins. It can be used to study chemical species that have one or more unpaired electrons (paramagnetic).[14] As many of the electron/hole traps result in unpaired electrons (Section 3.5), it is a useful technique for studying radiation effects on solids. EPR spectroscopy can be used to track the formation and ultimate annihilation of the traps. Unlike thermoluminescence, EPR is a direct measurement of the electron/hole centers, and a single sample can be re-evaluated to study the change in the signal.

Like NMR, EPR deals with the interaction between electromagnetic radiation and magnetic moments. In the case of EPR, the magnetic moments arise from electrons rather than nuclei.[297] Each electron possesses an intrinsic magnetic-dipole moment that arises from its spin.[297-298] In the presence of an external magnetic field (B_o in G), the electron's magnetic moment aligns itself either parallel ($m_s = -\frac{1}{2}$) or antiparallel

($m_s = +\frac{1}{2}$) to the field with the separation of the two energy states (ΔE) as follows (Figure 4-6):[298]

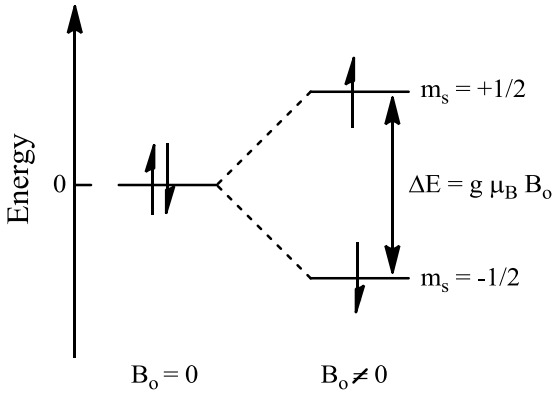

Figure 4-6: Separation of electron spins aligned to either parallel ($m_s = -\frac{1}{2}$) or antiparallel ($m_s = +\frac{1}{2}$) in the presence of an external magnetic field (B_o). Adapted from [298].

$$\Delta E = g\ \mu_B\ B_o \qquad (4.3)$$

where g is the electron's g-factor and μ_B is the Bohr magneton. An unpaired electron can move between the two energy levels (parallel vs. antiparallel) by either absorbing or emitting electromagnetic radiation of energy $h\nu$ such that:[298]

$$h\nu = \Delta E = g\ \mu_B\ B_o \qquad (4.4)$$

where ν is the frequency and h is Planck's constant.

In EPR, a spectrum can be gathered by two methods: (1) the spin system is placed in a constant magnetic field and irradiated with microwave radiation whose frequency is swept; or (2) the spin system is irradiated with a constant microwave radiation and the magnetic field is swept.[298] In both cases, the microwave radiation is absorbed only at the resonance condition given by equation (4.4). When this condition is met, unpaired electrons can move between their two spin states (Figure 4-7). Since there are more electrons in the lower state, there is a net absorption of energy. This absorption is monitored and converted into a spectrum.[14, 297-298]

EPR instruments can collect spectra at various frequencies. Higher frequencies yield better spectral resolution and detection limits, but require diminishingly smaller sample sizes. Most EPR spectra are thus collected at X-band, which offers a reasonable compromise between these conflicting parameters.[14] In the present work, EPR spectra were collected at the Environmental Molecular Sciences Laboratory (EMSL) at Pacific Northwest National Laboratory (PNNL). Continuous wave X-band (9.5 GHz) EPR spectra were collected at room temperature using a Bruker Elexys 580E EPR spectrometer at a fixed frequency of 9.82 GHz.

Once the spectrum is obtained, analysis can obtain further insights into the electron/hole traps formed as follows (Figure 4-8):[299-302]

(a) EPR spectrum obtained.

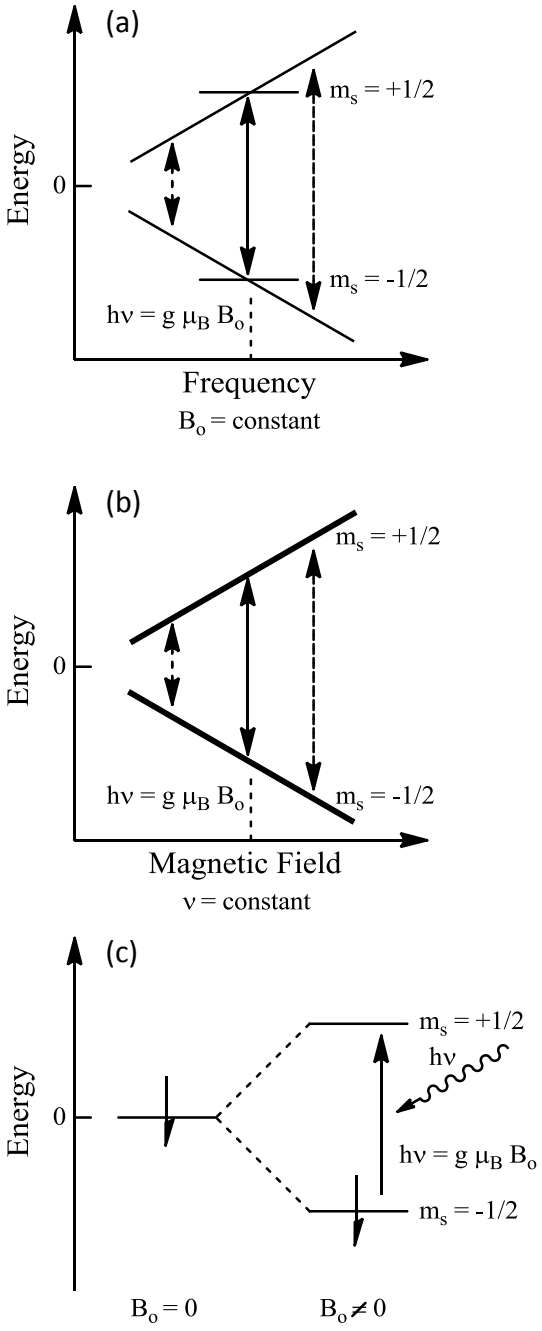

Figure 4-7: Measurements of EPR: (a) the magnetic field (B_o) is held constant, and the frequency (ν) is swept to reach resonance; (b) ν is held and B_o is swept; (c) the electron absorbs energy $h\nu$ to transition between states. Adapted from [298].

(b) Baseline subtracted from the spectrum.

(c) Integration of the spectrum to yield the net absorption of energy (electrons moving from $m_s = -\frac{1}{2}$ to $+\frac{1}{2}$.

(d) A second integration of the EPR line is proportional to the number of unpaired electrons present.

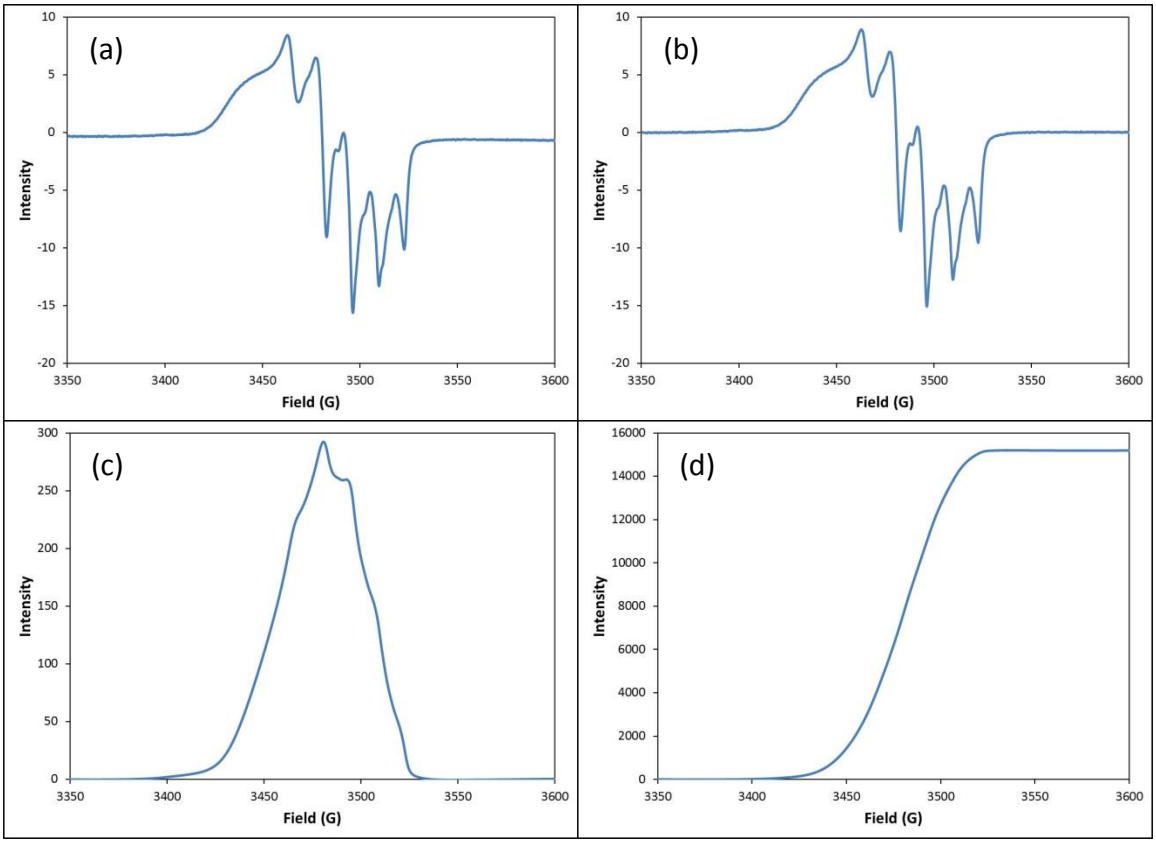

Figure 4-8: Example EPR spectra of: (a) Glass A approximately 20 min after absorbing a total dose of 700 Gy from a ^{60}Co source; (b) baseline corrected spectrum; (c) integration of the spectrum yields the net absorption of energy (i.e. electrons moving from $m_s = -\frac{1}{2}$ to $+\frac{1}{2}$; (d) a second integration of the EPR line is proportional to the number of unpaired electrons present.

4.4 Materials

Several factors were considered when choosing the sample sources for this study. In glass manufacturing, the shape of the final product dictates the forming process. Microscope slides, cut into 5 cm x 5 cm squares, were used in the first intrinsic dosimetry study,[26] as this form provided a commercial source of glass with relatively consistent geometry. However, unlike general laboratory glassware, which is made of borosilicate glass, microscope slides are generally made of soda-lime glass and produced through a "Float Process". This float process floats molten glass onto a mirror-like surface of molten tin.[303] Tin absorbed into the glass from one side can affect the mechanisms of radiation induced defects.[304-306] Follow-on intrinsic dosimetry studies abandoned the use of microscope slides in order to avoid the rather process specific influence of tin on radiation induced defects since the production of container glass does not rely on the "Float Process".

Modern container glass is generally formed through the "Blow Process".[307] In this process, a bubble of the molten glass is put inside a two-piece mold. Air is then forced into the mold, pressing the molten glass against the sides of the mold. The glass cools inside the mold and conforms to the shape.[307-309] Though container glass could be obtained easily, determining the geographical source of the glass and finding a geographical diversity of sources proved difficult as many suppliers of glass containers receive their products from the same manufacturers, or the source of their materials is proprietary.

Glass rods and tubes are made from the same bulk molten glass as container glass, and they are formed through the "Drawing Process". In this process, glass flows from a furnace in the form of a ribbon, which falls on to the upper end of an inclined refractory sleeve, carried on a rotating hollow shaft or blowpipe. The ribbon is wrapped around the sleeve to form a smooth layer of glass, which flows down the sleeve and over the tip of the shaft. Tubing is formed by blowing air through a blowpipe with a hollow tip and rods are made by using a solid tip on the shaft (Figure 4-9).[308-311] As this process takes molten glass directly from the furnace with no additional materials used in forming the rods/tubes, the process should not introduce any additional contaminants.

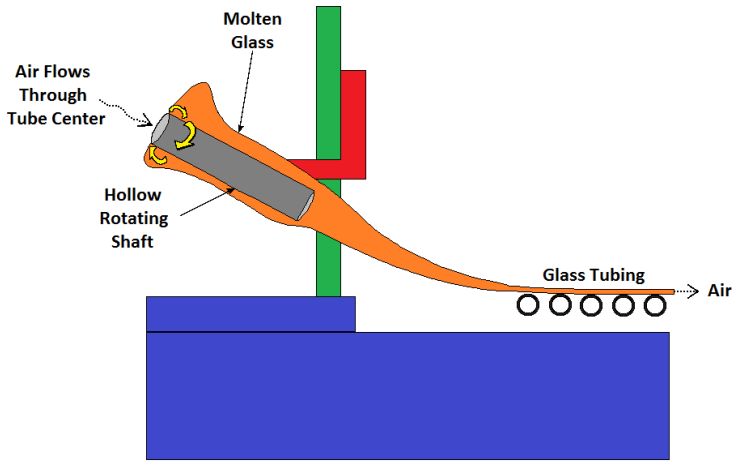

Figure 4-9: Diagram showing the "Drawing Process" for forming glass tubing. To form glass rods, the hollow shaft is replaced with a solid tip and no air is blown through the glass. Adapted from [311].

Manufacturers of borosilicate glass rods from 6 geographical regions were found; to the best of our knowledge, these represent the only commercially available sources of borosilicate glass rods. Of these 6 manufacturers, rods were obtained from 5 of geographical sources (with attempts to obtain rods from the last

source unsuccessful). Hereafter, these five materials are referred to as Glass A-E throughout this study.

Samples for the study were prepared by two methods. Unless otherwise stated, TL samples were prepared by slicing the glass rods (6 mm diameter) into 1 mm thick slices using a saw with a 220 grit metal bonded diamond wheel from DYNACUT. EPR and some TL samples were prepared by grinding the glass to a powder using an IKA® Universalmühle (model M20) high-speed impact mill which utilizes a tungsten carbide blade for grinding. The powder was then sorted using sieves, and material with a particle size of 75-125 μm was used. All samples were stored in and protected from light using LINQSTAT™ black volume conductive bags.

4.5 Irradiations

All gamma-irradiations were performed at the High Exposure Facility at Pacific Northwest National Laboratory (PNNL). The gamma fields produced in this facility are generated by two ^{137}Cs sources (nominal activities of 10 and 100 Ci) and two ^{60}Co sources (nominal activities of 660 and 5890 Ci) using a collimated geometry (30° collimation angle). The calibration dose range of the sources extends to approximately 6 m, with the beam unobstructed until it encounters a concrete wall at a distance of approximately 8.2 m. The radiation fields are standardized using a reference-class, vented, air-equivalent ionization chamber calibrated by the National Institute of Standards and Technology (NIST).[312-313]

Using the High Exposure Facility, a total dose between 0.15 and 20 Gy was delivered to the glass samples using a ^{60}Co source at a dose rate of 4.7 Gy/hr. Samples were protected from light exposure both during and after exposure using LINQSTAT™ black volume conductive bags. X-ray and beta irradiations were performed on samples outside the conductive bags in a darkened room. Samples were transferred to the bags immediately following irradiation. X-ray exposures were to 1.5 Gy at a dose rate of 4.3 Gy/hr using 14 keV x-rays (M20 NIST Technique). X-ray calibrations consist of annual measurements, using a NIST-traceable reference class ionization chamber (secondary or working standard), to establish transmission chamber efficiency (Roentgen/Coulomb).[314-315] Beta irradiations were also to 1.5 Gy at a dose rate of approximately 0.1 Gy/hr using a ^{90}Sr/^{90}Y source. The ^{90}Sr/^{90}Y source was calibrated using a NIST-traceable extrapolation ionization chamber (EIC). The field was assessed and found to be in accordance with the criteria stated in ISO 6980.[316-317] Gamma irradiations to 1.5 Gy using ^{60}Co and ^{137}Cs at dose rates of 4.3 Gy/hr and 0.1 Gy/hr, respectively, were performed for comparison with the x-ray and beta irradiations. All samples were irradiated "in air" rather than mounted on a phantom. The phantom is a slab of tissue mimicking material used to represent a dose rate measurement on a human body.[318]

Bench-top irradiations using a Model UVG-11 Mineralight® Short Wave Ultraviolet (UV) lamp (254 nm – 4.9 eV) were also performed. Samples were irradiated in a darkened room for 30 min with an approximate distance of 2 mm between the

samples and the lamp. Following irradiation, the samples were immediately returned to the conductive bags.

Chapter 5

Thermoluminescence Glow Curves

5.1 Thermoluminescence of Borosilicate Glass

Initial studies of the thermoluminescence of borosilicate glass were performed using glass from source A. In these studies, the glass exhibited a glow curve with a narrow low-temperature peak centered near 120°C and a broad high temperature peak centered near 230°C (Figure 5-1).

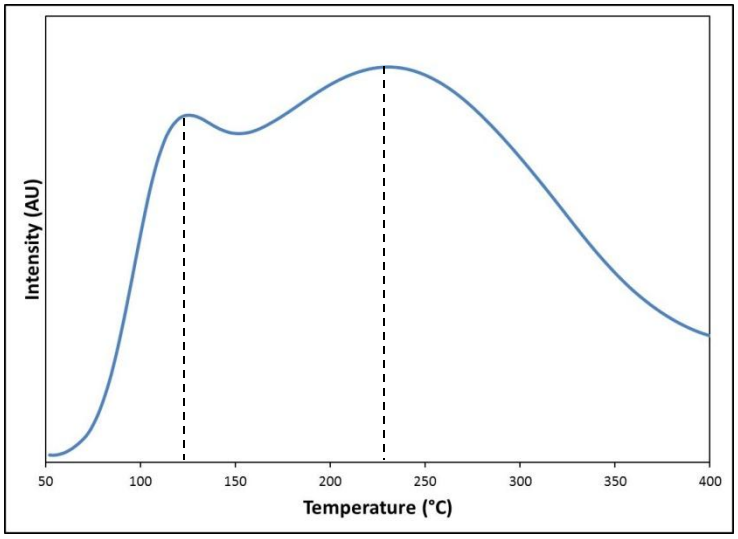

Figure 5-1: Thermoluminescence of borosilicate glass from source A 20 min after receiving a total dose of 20 Gy from ^{60}Co. Glow curves exhibited a narrow peak centered near 120°C and a broad peak centered near 225°C.

Samples were analyzed after receiving a total gamma dose of 0.15-20 Gy from ^{60}Co. Glow curve response (peak intensity) was found to be directly and linearly related to the radiation dose received over the examined range. Figure 5-2 shows TL glow curves for samples receiving 0.15, 1.5, 3, and 20 Gy doses along with results from an unirradiated glass sample, and Figure 5-3 shows the linear correlation of the intensity (nA/mg) of

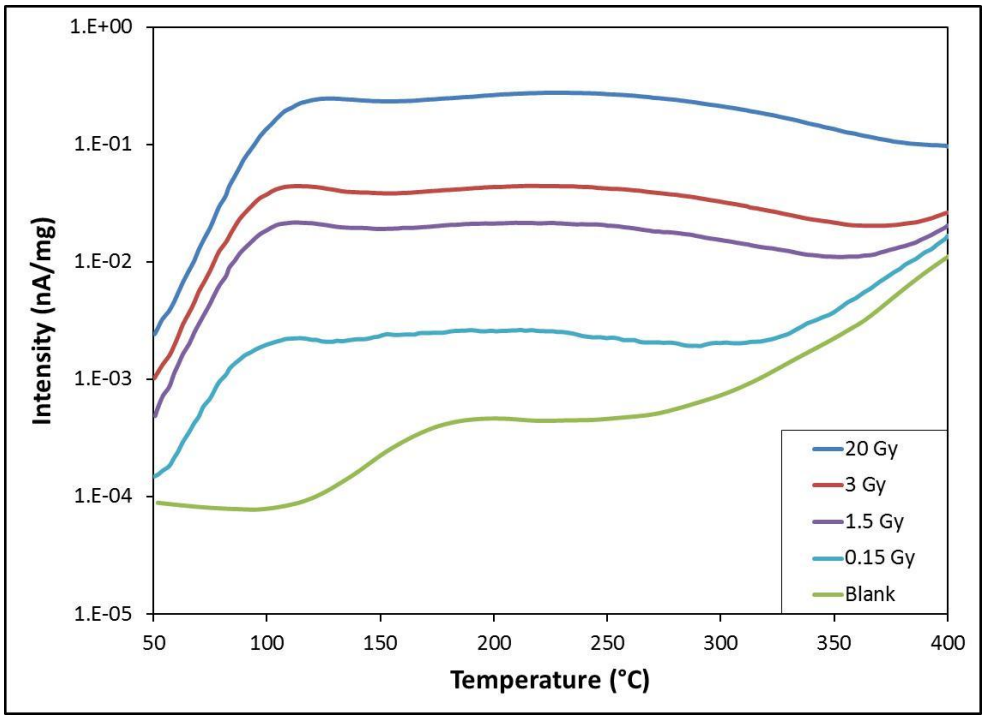

Figure 5-2: Thermoluminescence glow curves for borosilicate samples from source A approximately 20 min after receiving a 0.15, 1.5, 3, and 20 Gy dose from ^{60}Co and an unirradiated sample.

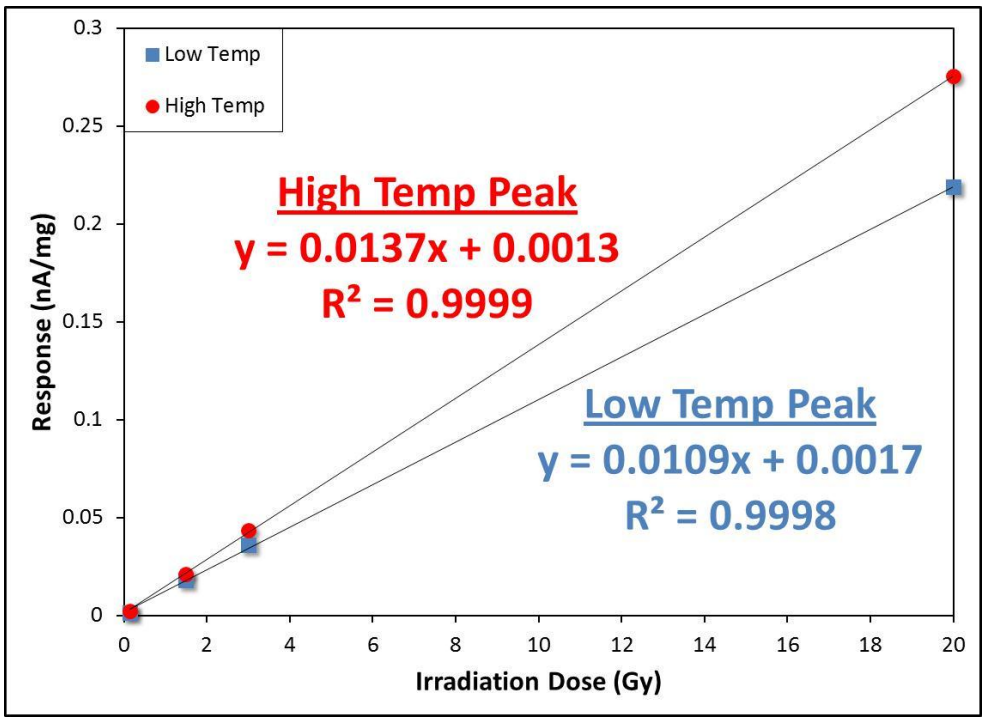

Figure 5-3: Thermoluminescence glow curves were linearly correlated for samples receiving 0.15-20 Gy dose.

both peaks over the studied range. Although the intensity of both peaks was linearly related to the radiation dose received, their sensitivities to radiation varied (seen in their linear divergence at higher doses). This response difference is due to the electron/hole traps that are ultimately responsible for the observed TL forming at different rates and/or due to the instability of the low temperature peak (discussed later) and the increased time it takes to deliver higher doses.

5.2 Source of Borosilicate Glass

Borosilicate samples from different geographical origins were observed to have significant differences in their glow curves following irradiation. Figure 5-4 shows the resulting glow curves for glass samples from the five geographically different sources

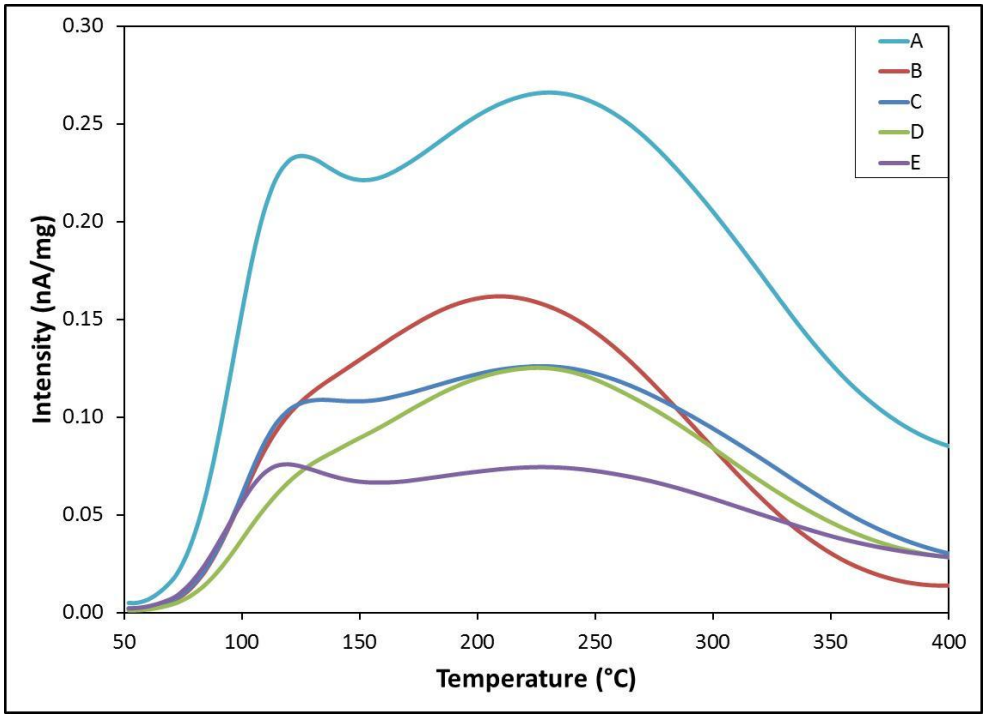

Figure 5-4: Glow curves for glass samples from 5 geographically different sources 20 min after receiving a total dose of 20 Gy from ^{60}Co.

approximately 20 min after receiving a total dose of 20 Gy from a ^{60}Co source. As can be observed, the TL signal differed in both intensity and shape among the various glass sources with Glass A having a significantly higher TL signal than the samples from the other regions.

Upon closer examination, the shapes of the TL glow curves can be sorted into two classifications (Figure 5-5). The first class, which includes glass from regions A, C, and E, are glow curves with two readily distinguished low- and high-temperature peaks located near 120°C and 230°C, respectively (Figure 5-5a). The relative ratio of intensities of the low- to high-temperature peak in this group ranged from 0.85 to 1.05. The second class, which includes glass from region B and D, has a relative intensity ratio of the low- to high-

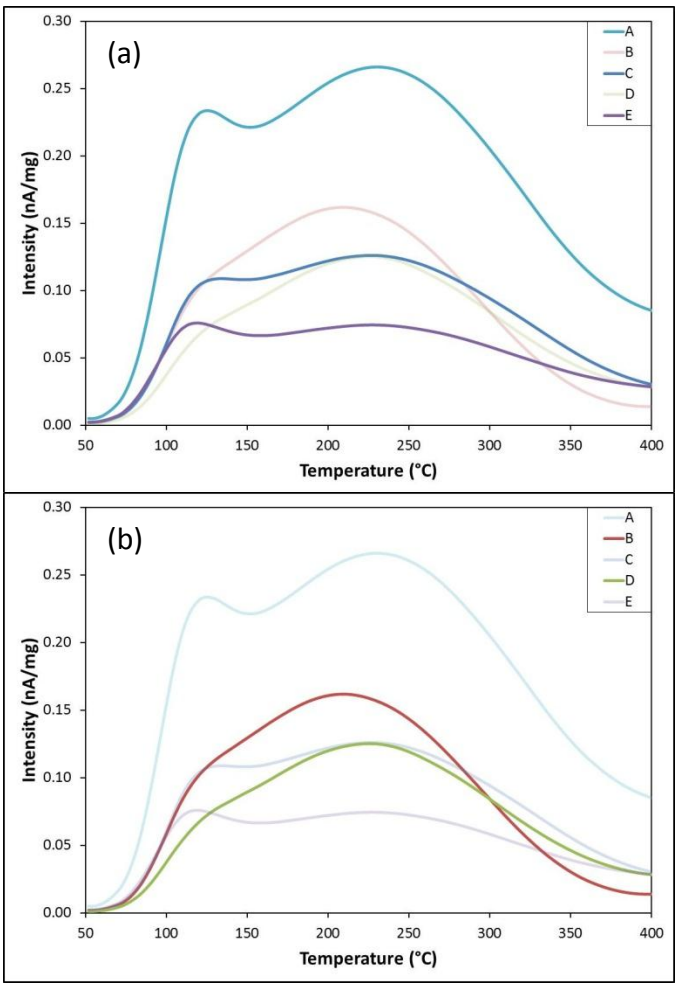

Figure 5-5: Glow curves for glass samples from 5 geographically different sources sorted into two classifications: (a) curves with two readily distinguished peaks, and (b) curves with peaks that are not readily distinguishable.

temperature peak of approximately 0.65. This creates glow curves with low- and high-temperature peaks that are not readily distinguishable (Figure 5-5b), though the peaks still appear to be located near 120°C and 230°C.

5.2.1 Minimum Measurable Dose

The limit of quantification (LOQ) is defined as the lowest level at which a measurement is quantitatively meaningful and is typically defined as a response that is larger than or equal to ten times the standard deviation of the blank signal.[319] To determine the LOQ, 20 blank samples of each glass were analyzed, and the LOQ of thermoluminescence was determined to be 0.002 nA/mg. This equates to an absorbed dose, or Minimum Measurable Dose (MMD), of 0.15 Gy in Glass A, 0.25 Gy in Glass B, 0.3 Gy in Glasses C and D, and 0.5 Gy in Glass E.

As outlined in earlier work,[26-27] it is possible to estimate the exposure accumulated over time ($\dot{X}$) from a specific source:[162]

$$\dot{X} = \frac{\Gamma_\delta \alpha}{d^2} \tag{5.1}$$

where $\dot{X}$ is in R/hr, Γ_δ (R cm^2 h^{-1} mCi^{-1}) is the exposure rate constant for a specific isotope of interest, α is the activity of the source in mCi, and d is the distance from the source in cm. The literature[162] provides values for Γ_δ for three radioactive isotopes (^{60}Co, ^{137}Cs, and ^{226}Ra) which are considered to be high risk precursor materials for the production of radioactive dispersal devices (RDD).[320] A total gamma ray exposure of 100 R (Roentgen) roughly equates to 0.872 Gy.[11] By assuming that the total absorbed dose in air is equivalent to that in glass and

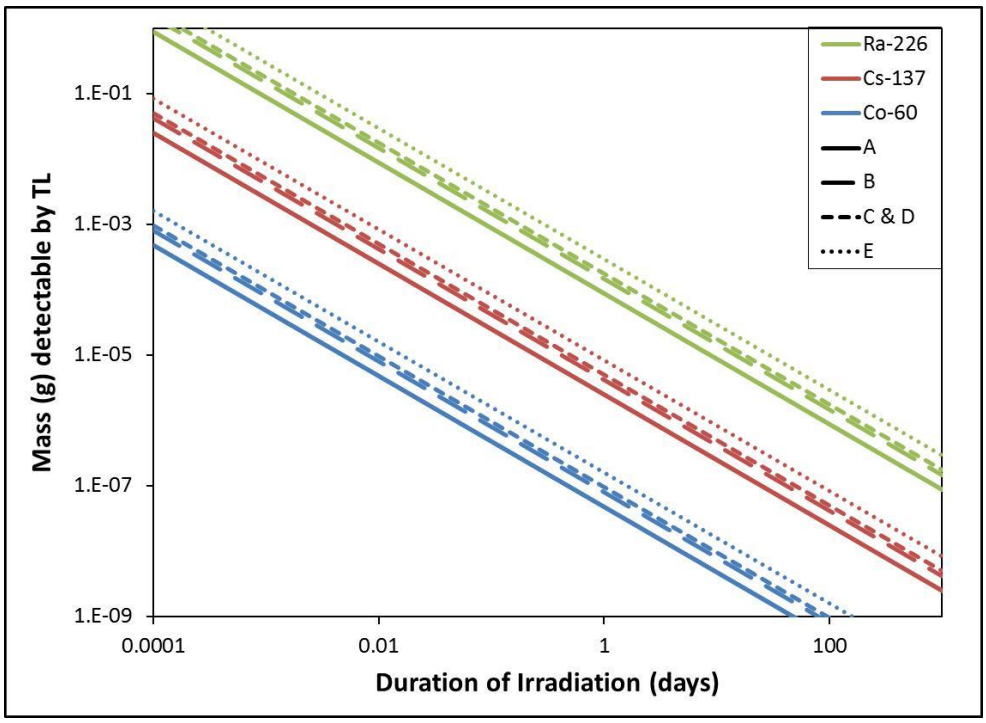

Figure 5-6: The estimated mass and irradiation time required to deliver a measurable dose to the studies borosilicate glass for three radioisotopes (1 cm between the material and container wall).

a distance between the material and container wall of 1 cm, the minimum amount of the three aforementioned radionuclides that would be required to deliver a measurable radiation dose can be estimated. The curves in Figure 5-6 show the mass of ^{60}Co, ^{137}Cs, and ^{226}Ra required to deliver the MMD in each glass sample over a given irradiation time for a sample 1 cm from the radiation source.

5.2.2 Thermoluminescence Fading

The glow curve responses were observed to decrease (fade) as a function of time following irradiation in each glass. Figures 5-7 to 5-11 show results from fade tests of glass samples receiving a total absorbed dose of 20 Gy from a ^{60}Co

source. As can be observed, the 120°C peak rapidly decayed in the first 24 hrs to 7 days. The 230°C peak also appeared to decay to different extents in the various glasses. Through other tests (not shown), decay had mostly stopped by 70 days. All glow curves appear to have a similar shape by 70 days.

As a result of this fading, the 230°C peak of a sample having received the MMD would be detectable (a response that is larger than or equal to three times the standard deviation of the blank signal)[319] for approximately 1 year post-irradiation. However, the signal from a sample that received 10 times the MMD (a 48 ng source of ^{60}Co exposing for 10 days in the case of Glass A) could potentially be detectable and measurable for approximately 6.6 x 10^{12} years; the signal is permanent until the sample is heated.

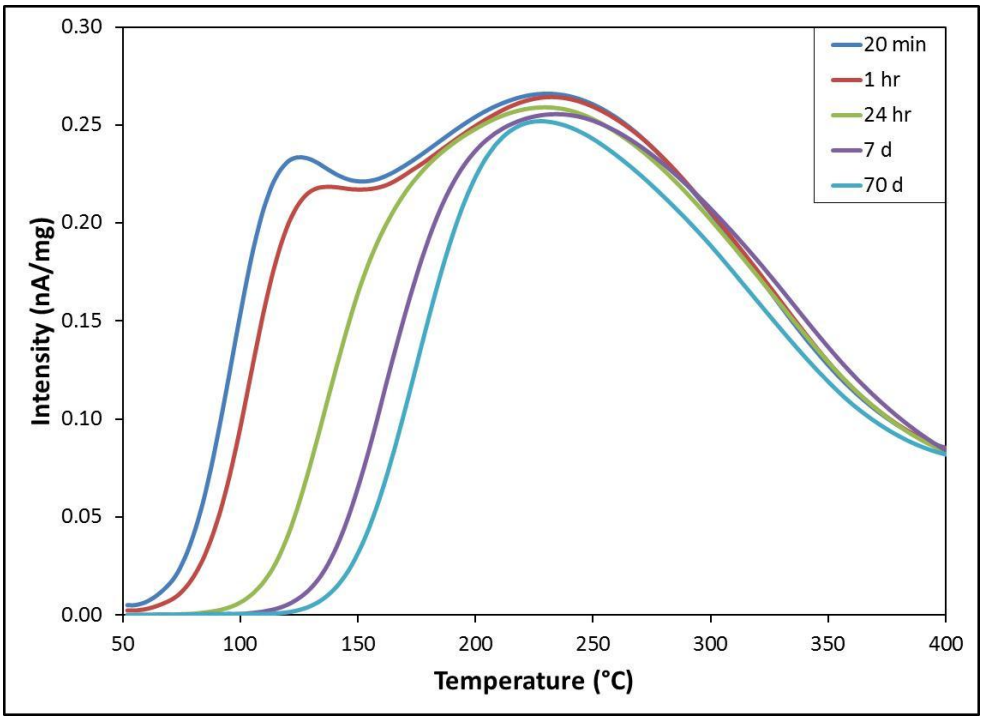

Figure 5-7: Glow curves for Glass A samples at 20 min, 1 hr, 24 hr, 7 d, and 70 d after receiving a total dose of 20 Gy from ^{60}Co.

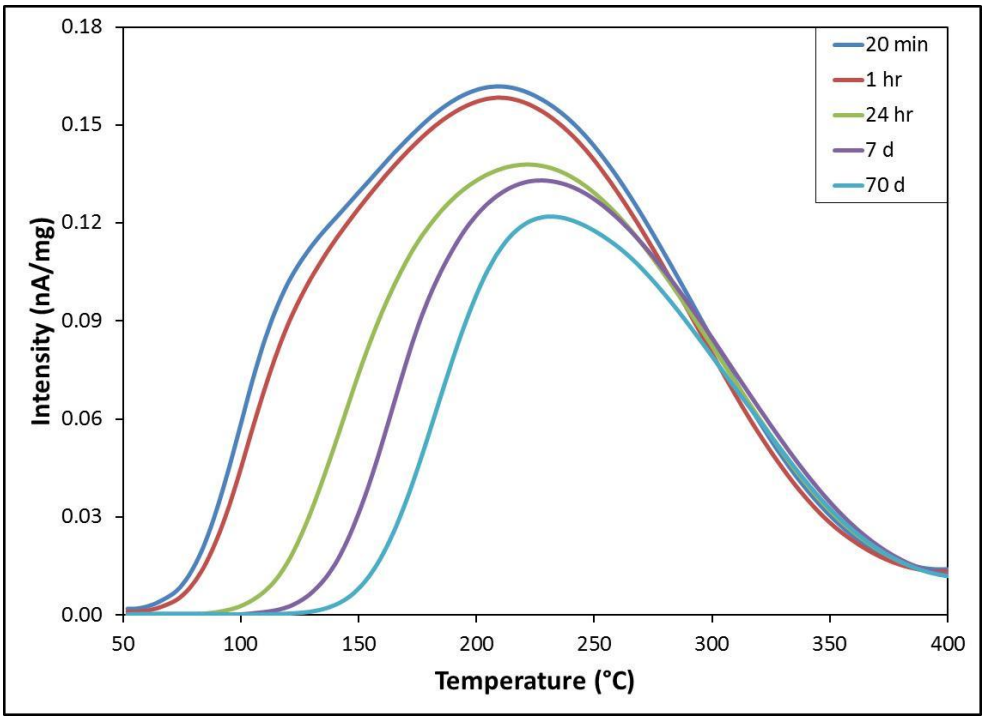

Figure 5-8: Glow curves for Glass B samples at 20 min, 1 hr, 24 hr, 7 d, and 70 d after receiving a total dose of 20 Gy from ^{60}Co.

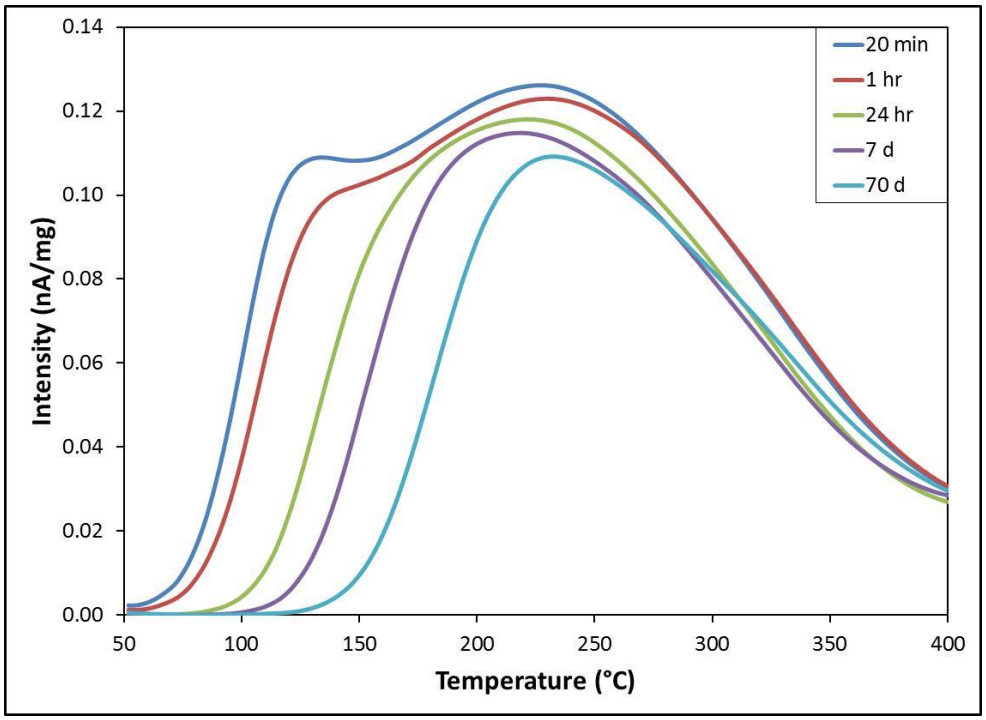

Figure 5-9: Glow curves for Glass C samples at 20 min, 1 hr, 24 hr, 7 d, and 70 d after receiving a total dose of 20 Gy from ^{60}Co.

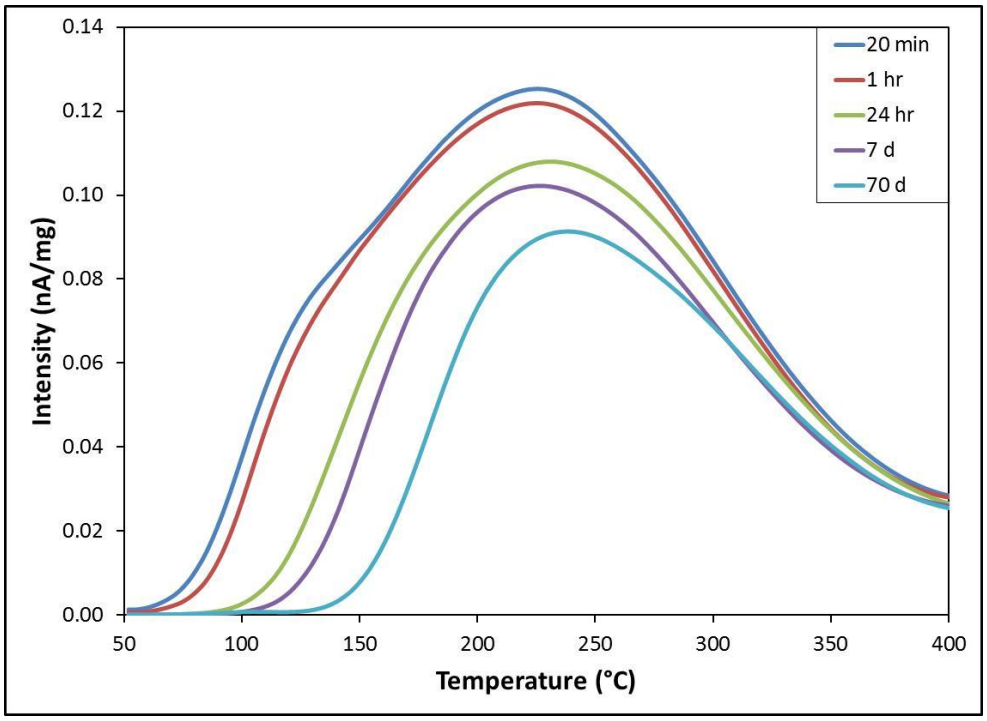

Figure 5-10: Glow curves for Glass D samples at 20 min, 1 hr, 24 hr, 7 d, and 70 d after receiving a total dose of 20 Gy from ^{60}Co.

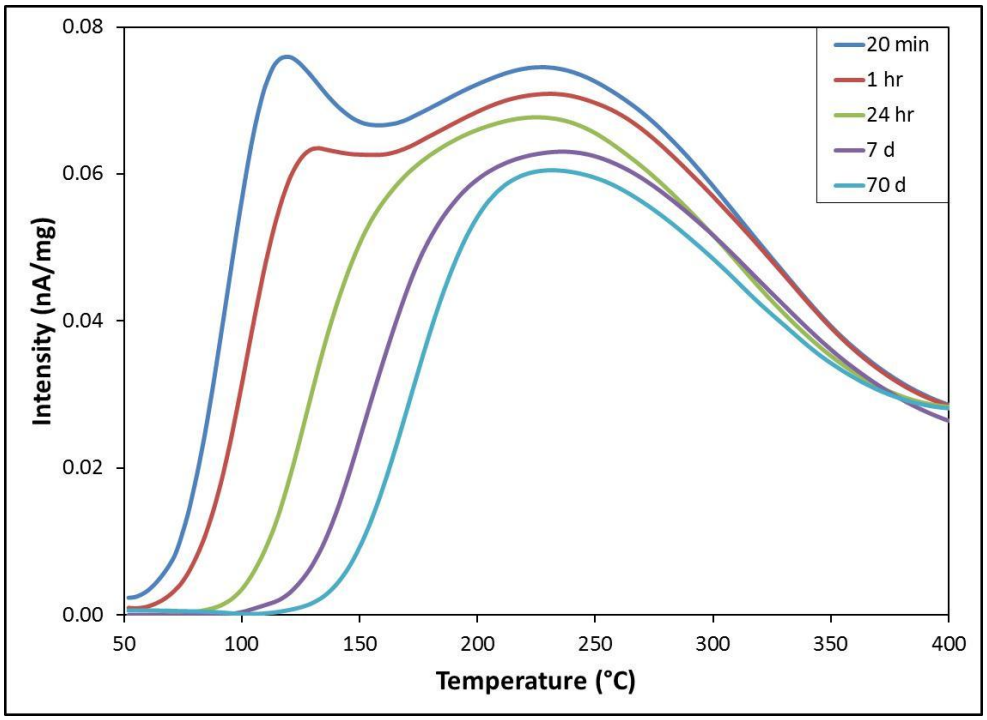

Figure 5-11: Glow curves for Glass E samples at 20 min, 1 hr, 24 hr, 7 d, and 70 d after receiving a total dose of 20 Gy from ^{60}Co.

5.3 Irradiation Source

Glass samples were also irradiated with beta particles (^{90}Sr – maximum 546 keV; ^{90}Y – maximum 2.28 MeV), x-rays (14 keV), and a 245 nm UV-lamp (4.9 eV). The resulting TL glow curves and decay patterns (Appendix) for both beta particles and x-rays were very similar to gamma irradiations (^{60}Co – 1.17 and 1.33 MeV and ^{137}Cs – 0.66 keV) at the same dose rate. When glass samples were irradiated with a 254 nm UV-lamp, differences in the shape and intensity of the resulting TL glow curves were observed between those resulting from a UV irradiation and those resulting from the other forms of ionizing radiation.

After UV irradiations, only one peak was readily observed. Figure 5-12 shows the resulting glow curves approximately 20 min after a 30 min exposure with a 254 nm UV-lamp for the five glass samples. The location and decay of the peak is similar to the unstable low temperature peak (120°C) of the gamma-irradiated glass. Results from fade tests of UV-irradiated glass samples are shown in Figures 5-13 to 5-17.

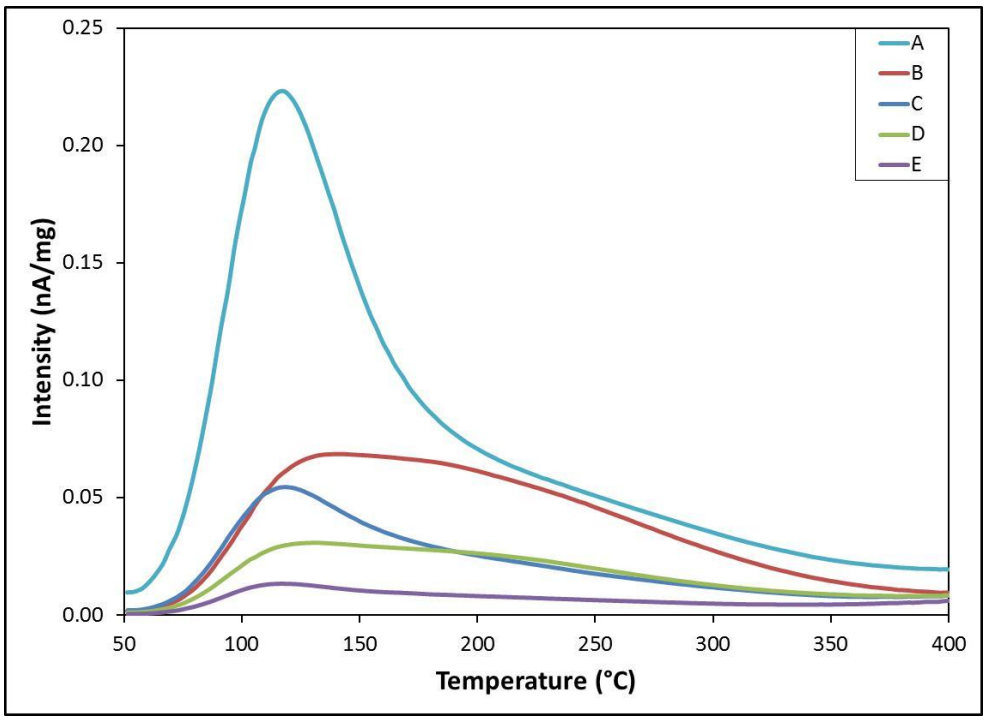

Figure 5-12: Glow curves for glass samples approximately 20 min after being irradiated with a 254nm UV-Lamp for 30 min.

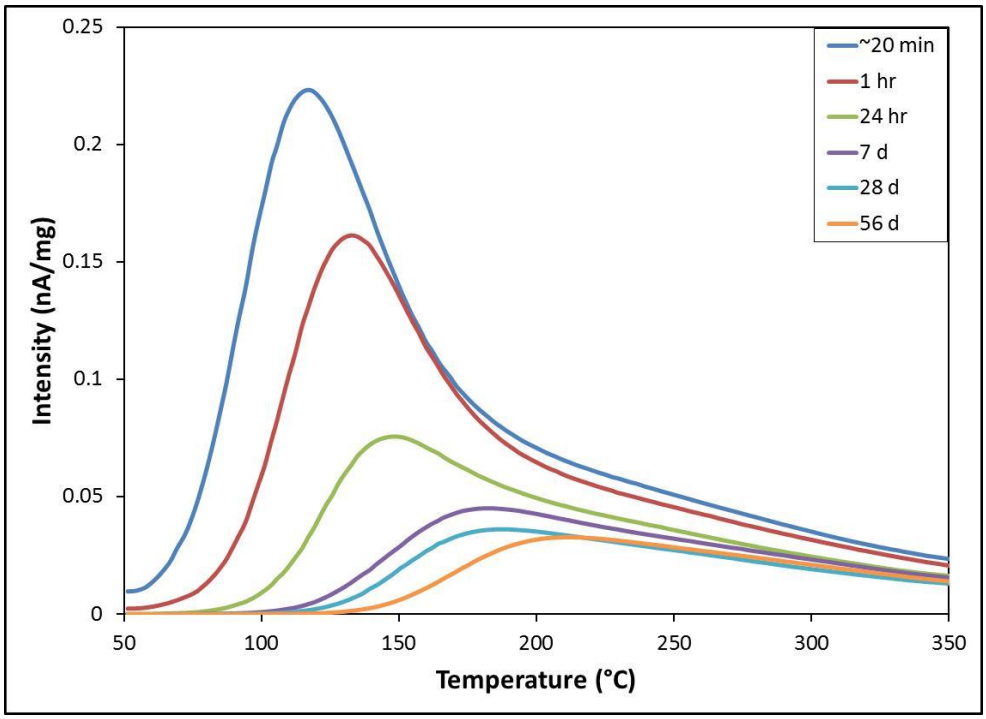

Figure 5-13: Glow curves for Glass A samples at 20 min, 1 hr, 24 hr, 7 d, 28 d, and 56 d after being irradiated with a 254nm UV-Lamp for 30 min.

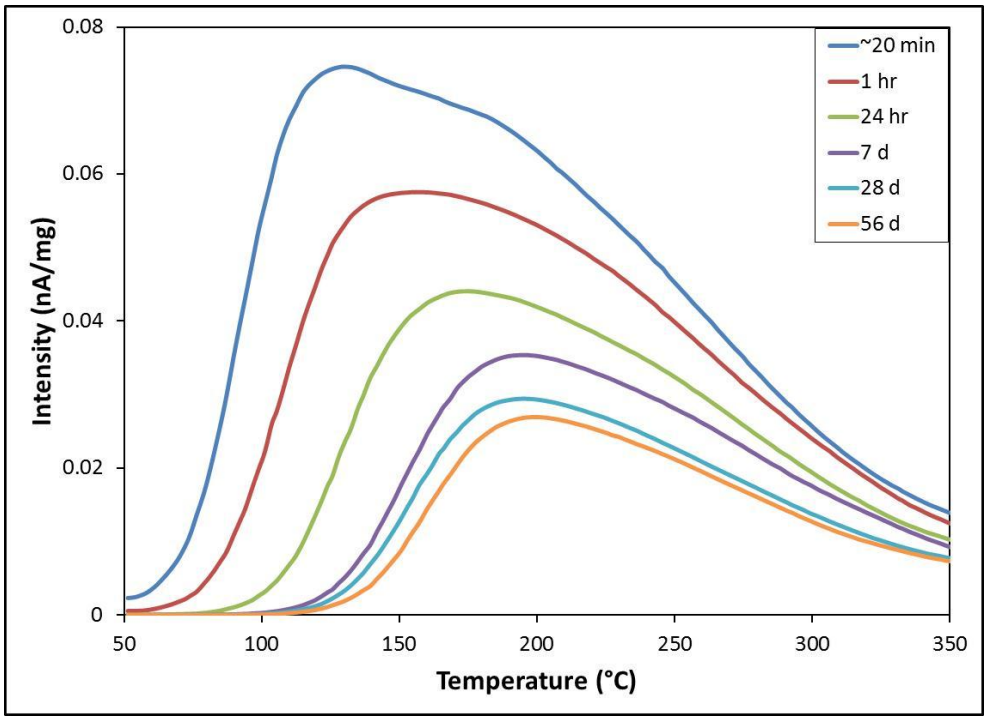

Figure 5-14: Glow curves for Glass B samples at 20 min, 1 hr, 24 hr, 7 d, 28 d, and 56 d after being irradiated with a 254nm UV-Lamp for 30 min.

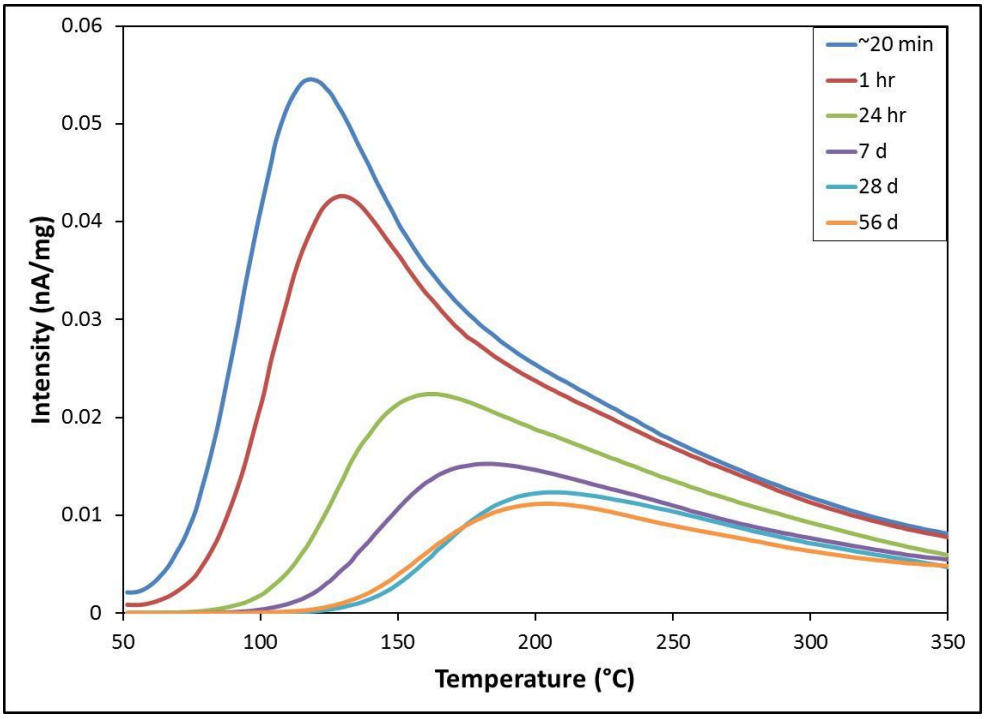

Figure 5-15: Glow curves for Glass C samples at 20 min, 1 hr, 24 hr, 7 d, 28 d, and 56 d after being irradiated with a 254nm UV-Lamp for 30 min.

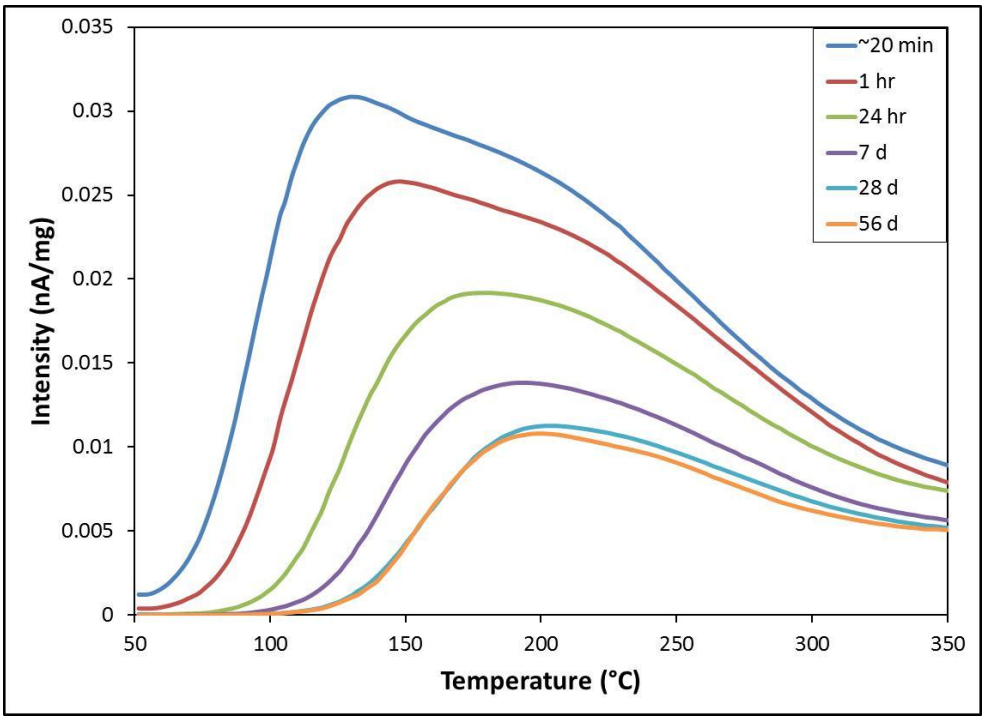

Figure 5-16: Glow curves for Glass D samples at 20 min, 1 hr, 24 hr, 7 d, 28 d, and 56 d after being irradiated with a 254nm UV-Lamp for 30 min.

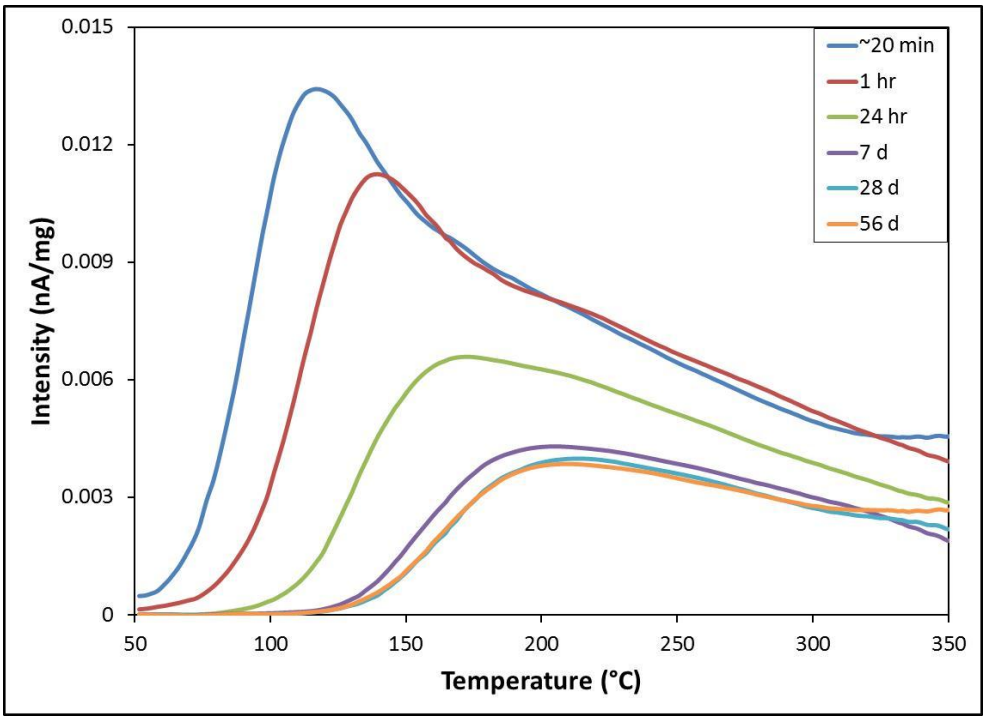

Figure 5-17: Glow curves for Glass E samples at 20 min, 1 hr, 24 hr, 7 d, 28 d, and 56 d after being irradiated with a 254nm UV-Lamp for 30 min.

As stated, a UV irradiation appeared to create only one peak in the glass, and the location of this peak and its subsequent decay corresponded reasonably well with the 120°C peak seen from the other radiation sources. However, a high temperature peak was not initially observed in glass irradiated by UV. This suggested the sources controlling defect formation in the UV and gamma irradiation may be similar with the exception of an energy barrier to mechanisms driving UV-induced defect formation. However, closer inspection of the 20 min and 1 hr glow curves of Glasses B and D (Figure 5-14 and Figure 5-16) revealed evidence of a high temperature peak centered near 200°C. Glasses C and E (Figure 5-15 and Figure 5-17), where the overall intensity of the 120°C peak is not as great, also indicates of a high temperature peak centered near 200°C. Additionally, at 56 day post-irradiation, all of the glass samples showed TL glow curves nearly identical in shape to those exposed to gamma, beta, and x-ray irradiations after similar decay times. This suggests that mechanisms controlling radiation induced defect formation from gamma, beta, x-ray, and UV sources may be similar, but the population of traps differs among the different types of ionizing radiation.

5.4 Thermoluminescence Glow Curve Deconvolution

As seen in Figure 5-4, in the 70 d post-irradiation glow curves the 230°C peak is extremely broad with a peak width at half maximum as large as 150°C in some of the glasses. This is a good indicator that the peak is a combination of closely overlapping or quasi-continuous peaks.[321-323] The T_m-T_{stop} method is a technique that can be used to

estimate both the number and position of individual TL peaks within complex glow curves.[8, 12, 323]

The T_m-T_{stop} method is based on monitoring the position of the peak temperature at the maximum, T_m, of the lowest visible temperature peak. With increasing temperature, the lowest visible temperature peak will shift to a higher temperature as the more unstable recombination processes occur. The process is outlined below, and Figure 5-18 shows a schematic representation of the process.[8, 12]

1. An irradiated sample is heated at a linear heating rate, from room temperature to a temperature T_{stop} which corresponds to a position on the low temperature tail of the first TL peak in the glow curve.
2. Once the sample reaches T_{stop}, the sample is rapidly cooled down to room temperature.
3. The sample is then re-heated at a linear heating rate to record the whole glow curve.
4. The position of the first maximum, T_m of the glow curve is recorded.

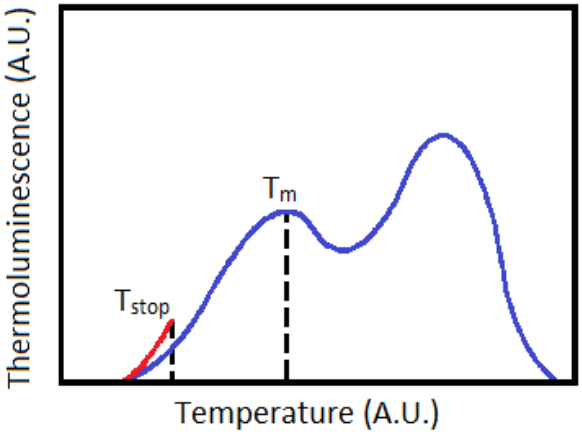

Figure 5-18: Schematic representation of the T_m-T_{stop} method. The sample is heated to a temperature T_{stop} and then rapidly cooled to room temperature. The same sample is then re-heated to record the remaining glow curve. The position of the first maximum, T_m, of the glow curve is recorded. Adapted from [8].

5. A plot of T_m vs. T_{stop} is generated.

As long as there is adequate separation between the TL peaks (not necessarily visibly observable), the number and approximate location of the TL peaks can be gained by plotting T_m vs. T_{stop}. In the plot, the regions where T_m levels out are indicators of a TL peak located near the correlating T_m. The plot can also be used to gain an estimate of the kinetics of the recombination processes (discussed in Chapter 6) with first order kinetics creating a "staircase" function, and second and general order kinetics creating a "wavy" function. A schematic representation the T_m-T_{stop} method is shown in Figure 5-19.

The T_m-T_{stop} method was used to analyze samples of Glass A immediately after receiving a total absorbed dose of 20 Gy from a ^{60}Co source. From this analysis, the glow curve was separated into five peaks centered at

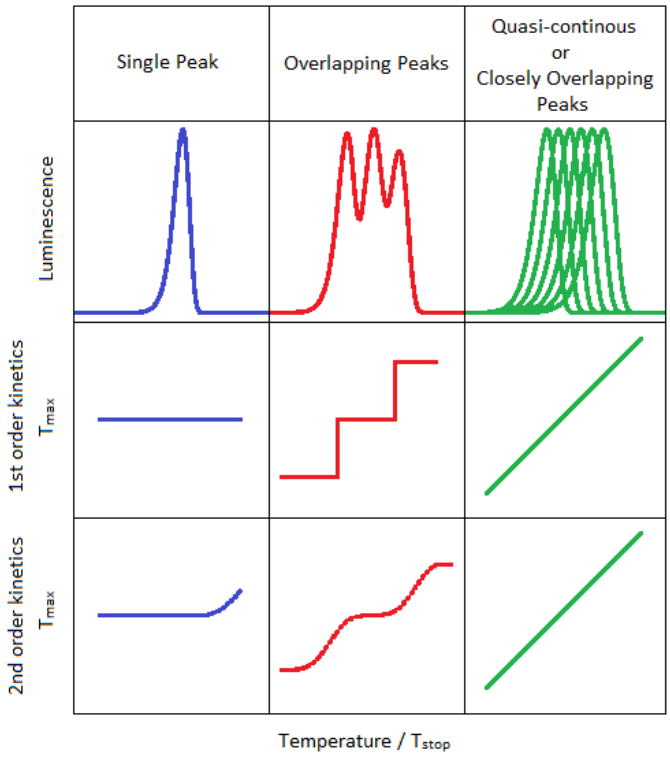

Figure 5-19: Schematic representation of T_m-T_{stop} analyses for a single peak (1st column), overlapping peaks (2nd column), and quasi-continuous or closely overlapping peaks (3rd column). The resulting T_m-T_{stop} functions for 1st order (middle row) and 2nd order (bottom row) kinetics are shown. Adapted from [8].

approximately 120, 160, 225, 300, and 340°C (Figure 5-20). As all the glasses appeared to have peaks around the same locations and the T_m-T_{stop} method only provides evidence of approximate locations of possible peaks, it was assumed that a T_m-T_{stop} analysis of the other glasses would be similar.

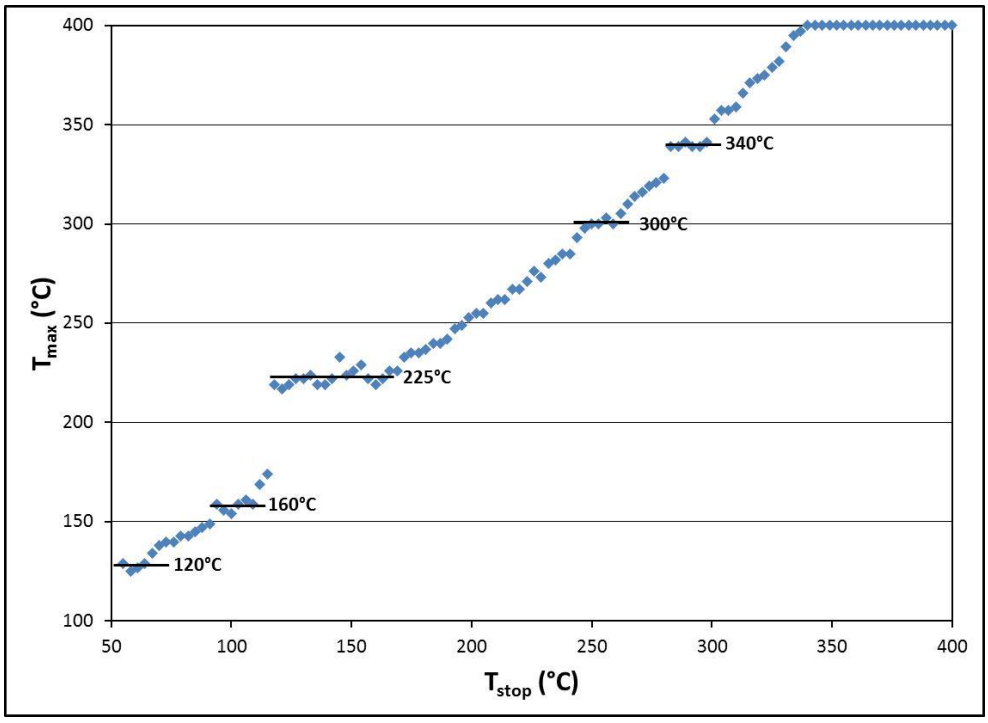

Figure 5-20: The T_m-T_{stop} analysis for irradiated samples of Glass A. The analysis showed evidence of five peaks centered at approximately 120, 160, 225, 300, and 340°C. It was assumed that a T_m-T_{stop} analysis of the other glasses would be similar.

Chapter 6

Peak Modeling

6.1 Thermoluminescence Peak Models

As described in Chapter 4, thermoluminescence is the emission of light from an insulator or semiconductor that is observed when the solid, which has previously been exposed to ionizing radiation, is thermally stimulated. This is the result of trapped electrons and holes recombining in a way that emits light. The nature of thermoluminescence means that the centroid and shape of the resulting peaks of a glow curve can give information about the characteristics of the trap(s) involved in its recombination process. In particular, the measurements yield information on the trapping energy, E (eV), and the frequency factor, s (s^{-1}), which may be simply thought of as how often a trapped charge will attempt to leave a trap (sometimes referred to as the attempt-to-escape factor).[8, 10-12, 260, 269, 324-325]

Mathematical models have been developed that use these factors to describe the centroid, shape, and decay patterns of the observed TL peaks from the glass samples. These models involve some approximations: (1) the concentration of the electrons in the conduction band, n_c (m^{-3}), is always very much less than the number of trapped electrons, n (m^{-3}),

$$n_c \ll n \tag{6.1}$$

and (2) the rate of change of the electrons entering or leaving the conduction band is small compared to the rate of change of the concentration of trapped electrons.

$$\frac{\mathrm{d}n_c}{\mathrm{d}t} \ll \frac{\mathrm{d}n}{\mathrm{d}t} \tag{6.2}$$

Taken together, these equations imply that the lifetime of electrons in the conduction band is much less than the lifetime of electrons in a trap.[8] For simplicity, only electron transitions were considered; similar equations could be given for hole transitions.

Through heating, the trapped electrons can be stimulated to the conduction band. These electrons will either be retrapped or recombine with trapped holes, possibly accompanied with light output. By comparing the rate, or probability, of retrapping, A_n, with the rate, or probability, of recombination, A_m, the glow curves are classified into different kinetic types.

If the rate of recombination is much greater than the rate of retrapping, the glow peak follows first-order kinetics.[260, 326-327]

$$A_m \gg A_n \tag{6.3}$$

Under this criterion, the expected intensity of a recombination process (TL glow peak), $I(t)$, can be written as:[10, 260, 325-328]

$$I(t) = -\frac{\mathrm{d}n}{\mathrm{d}t} = s\, n \exp\left(-\frac{E}{kT}\right) \tag{6.4}$$

where k is Boltzmann's constant (eV K^{-1}) and T is the absolute temperature (K). Integrating from $t = 0$ to t, using a constant heating rate $\beta = dT/dt$ (K s^{-1}) yields the first-order expression for a TL peak

$$I(t) = n_o\, s \exp\left(-\frac{E}{kT}\right) \exp\left\{-\left(\frac{s}{\beta}\right)\int_{T_o}^{T} \exp\left(-\frac{E}{kT'}\right)\, dT'\right\} \tag{6.5}$$

where n_o (m^{-3}) is the initial value of n at time $t = 0$, T_o (K) is the initial temperature at time $t = 0$, and T' is a dummy variable used for integration that represents temperature. Simulated first-order glow curves with arbitrary but representative parameters are given in Figure 6-1. From these glow curves, it can be seen that as a first-order glow peak decays away, the temperature of the peak max (T_{max} or T_m) remains constant. This can also be viewed as the T_{max} of the glow curve will always be at the same temperature as the dose delivered to a material increases if the TL peak follows first-order kinetics. It should also be noted that the peaks are relatively narrow, and the tail appears on the lower temperature end of the curve in the case of first-order TL kinetics.

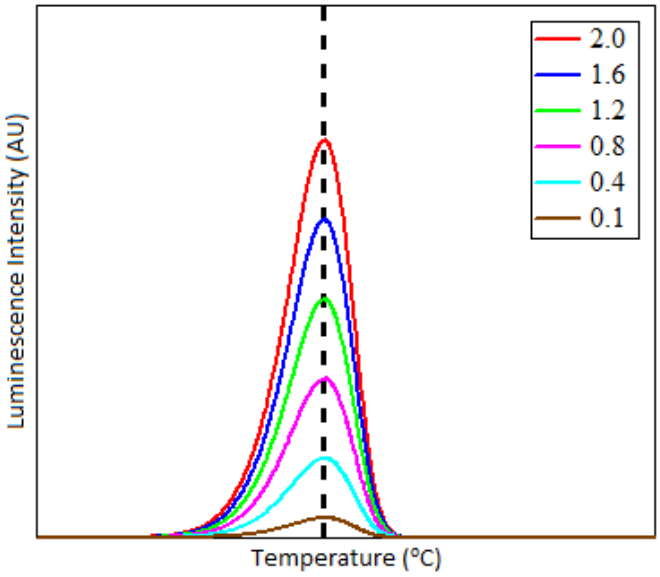

Figure 6-1: Simulated first-order glow curves computed at various values of n_o and with $E = 1.0$ eV, $s = 10^{10}$ s^{-1}, and $\beta = 10$ K/s. Adapted from [8].

In the situation where rate of recombination and the rate of retrapping are equal, the glow peak would follow second-order kinetics.[260, 326-327]

$$A_m = A_n \tag{6.6}$$

Under this criterion, the expected intensity of a recombination process can be written as:[8, 12]

$$I(t) = -\frac{\mathrm{d}n}{\mathrm{d}t} = s'\, n^2 \exp\left(-\frac{E}{kT}\right) \tag{6.7}$$

with

$$s' = s/N \tag{6.8}$$

where N is the total trap concentration (m^{-3}). Again, integrating from $t = 0$ to t, using a constant heating rate β yields the second-order expression for a TL peak.[8, 10, 268-269, 325-327]

$$I(t) = \frac{n_o^2}{N}\, s \exp\left(-\frac{E}{kT}\right) \left[1 + \left(\frac{n_o\, s}{\beta\, N}\right) \int_{T_o}^{T} \exp\left(-\frac{E}{kT'}\right) dT'\right]^{-2} \tag{6.9}$$

Some simulated second-order glow curves with arbitrary but representative parameters are shown in Figure 6-2. From these glow curves, it can be seen that as a glow peak that follows second-order kinetics decays away, the location of T_{max} shifts to a higher temperature. Unlike the first-order case, TL peaks following second-order kinetics have a tail that appears on the higher temperature end of the curve. Second-order peaks are also broader than first-order peaks (Figure 6-3). If all parameters are equal (i.e. E, s, β, N, and n_o), the overall intensity at T_{max} will also be greater for a first-order peak.

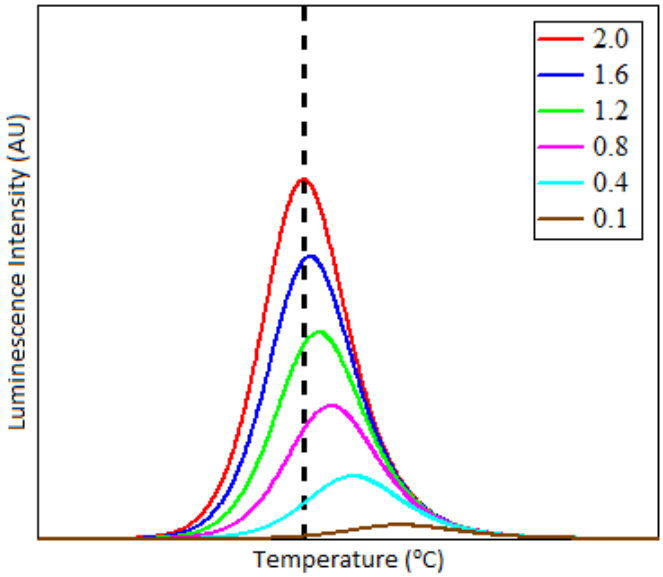

Figure 6-2: Simulated second-order glow curves computed at various values of n_o and with $E = 1.0$ eV, $s = 10^{10}$ s^{-1}, and $\beta = 10$ K/s. Adapted from [8].

If neither the criteria for first-order kinetics (rate of recombination is much higher than rate of retrapping) or second-order kinetics (rate of recombination and retrapping are equal) are met, general-order kinetics may be applied to the glow peak.[328-330] Using general-order kinetics the expected intensity of a recombination process can be written as:[10, 327]

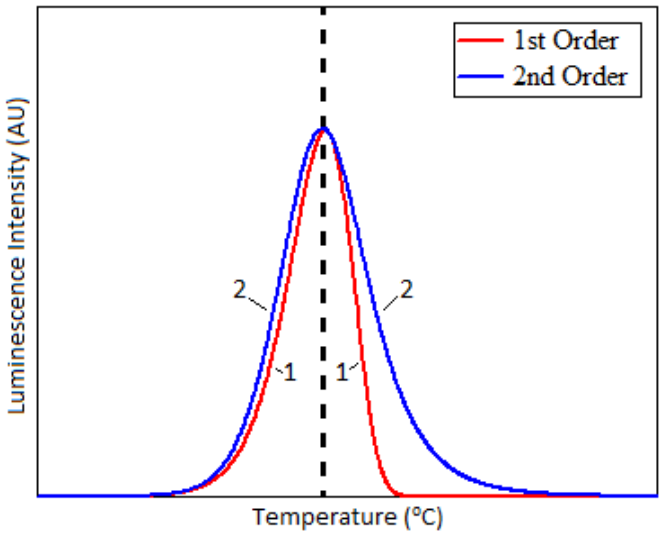

Figure 6-3: Comparison of TL glow peaks that follow first- and second-order kinetics with $E = 1.0$ eV, $s = 10^{10}$ s^{-1}, $\beta = 10$ K/s, and $n_o = 2.0$ m^{-3}. Overall intensities were shifted for comparison. Adapted from [8].

$$I(t) = -\frac{\mathrm{d}n}{\mathrm{d}t} = \left(\frac{n^b}{N^{b-1}}\right) s \exp\left(-\frac{E}{kT}\right) \tag{6.10}$$

where b is defined as the general-order parameter. At $b = 1$ or 2, the above intensity expression reduces to that of first- and second-order kinetics, respectively. Integration now gives:

$$I(t) = n_o^b \, s \, N^{(1-b)} \exp\left(-\frac{E}{kT}\right) \left[1 + \left(\frac{s\,(b-1)\,(n_o/N)^{(b-1)}}{\beta}\right) \int_{T_o}^{T} \exp\left(-\frac{E}{kT'}\right) dT'\right]^{-\frac{b}{b-1}} \tag{6.11}$$

The shape of a glow peak following general-order kinetics would fall between a first- and second-order peak when b is between 1 and 2 with all other parameters equal, or

broader with a longer tail than a second-order peak when b is greater than 2 (Figure 6-4).

Unlike the first-order kinetics where T_{max} does not change with increasing dose or peak decay, the second- and general-order kinetic equations predict that by increasing n_o (i.e. increasing the dose), T_{max} would shift towards a lower temperature.

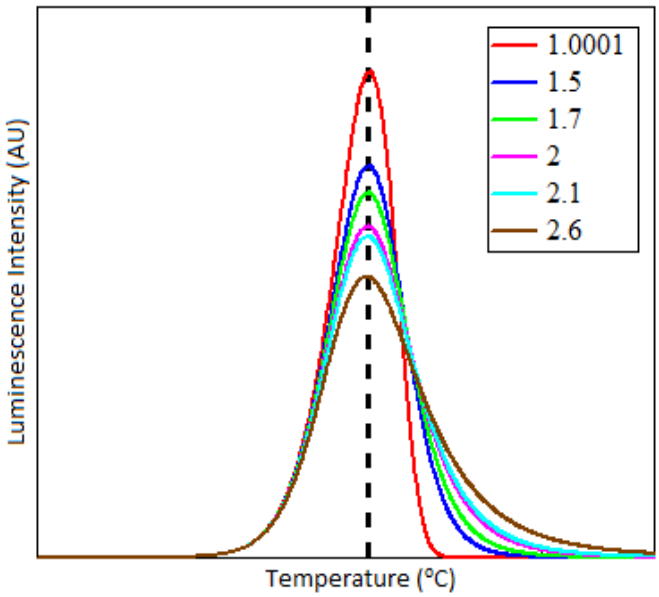

Figure 6-4: Simulated general-order glow curves computed at various values of b and with $E = 1.0$ eV, $s = 10^{10}$ s^{-1}, $\frac{n_o}{N} = 1$, and $\beta = 10$ K/s. Adapted from [10].

However, these predictions are in disagreement with the experimental behavior of many dosimetric materials.[331-333] This can be accounted for by linking N to the number of initially filled traps (traps filled immediately following irradiation) rather than the total number of available traps. The ratio of n_o to N then becomes the parameter that influences how much decay has taken place, and their overall intensity only affects the overall peak intensity observed in a glow curve.[334]

6.2 Parameter Acquisition

Several analyses have been developed to determine the corresponding parameters of the glow peaks in a TL glow curve.[8, 12, 267, 333] In general, the analysis becomes easier when each glow peak is isolated, or mostly isolated from the other

peaks in the overall glow curve. With an isolated peak, the Kirsh method[334-335] can be applied to determine the parameters E, s, and b. As the parameters E and s measure values with the most physical meaning (trap depth and attempt-to-escape factor, respectively),[333] this method is of particular interest.

The Kirsh method analyzes the shape of an isolated glow peak by taking the difference of TL intensity and remaining area under the glow curve (area under curve from point T to $T = \infty$) between a reference point and multiple other points along the curve. It then uses the mathematical relationships in the general-order kinetics equation to determine E, s, and b. It was shown that:[334-335]

$$\Delta \ln I / \Delta \ln \left(\frac{n}{n_o}\right) = b - \left(\frac{E}{k}\right)\left[\Delta \ln \left(\frac{1}{T}\right) / \Delta \ln \left(\frac{n}{n_o}\right)\right] \tag{6.12}$$

where Δ represents the difference between any two points along the glow curve. The value n/n_o is given by the area of the TL glow peak from the given point (T, I) of the peak to the end of the peak, namely

$$\frac{n}{n_o} = \frac{1}{\beta}\int_T^{T_f} I(T')dT' \tag{6.13}$$

where T_f is the end point temperature of the glow peak (ideally $T_f = \infty$).[334]

As can be seen from equation (6.12), plotting $\Delta \ln I / \Delta \ln \left(\frac{n}{n_o}\right)$ against $\Delta \ln \left(\frac{1}{T}\right) / \Delta \ln \left(\frac{n}{n_o}\right)$ will create a line with slope $(-E/k)$ and intercept b. By knowing the activation energy, or trap depth, (E), the order of kinetics (b), the peak temperature (T_m), and the heating rate used (β), the frequency factor (s) can be calculated as follows:[334-336]

$$s = \frac{\beta\, E}{k\, T_m^2} \exp \frac{E}{k\, T_m} \;\mid\; b = 1 \tag{6.14}$$

$$s = \beta \Big/ \left[\frac{b\, k\, T_m^2}{E} \exp\left(-\frac{E}{k\, T_m}\right) - (b-1) \int_{T_o}^{T_m} \exp\left(-\frac{E}{k\, T'}\right) dT' \right] \;\mid\; b \neq 1 \tag{6.15}$$

The integral $\int_{T_o}^{T_m} \exp\left(-\frac{E}{k\, T'}\right) dT'$ can be expressed in terms of a second exponential integral as:[334, 337]

$$\int_{T_o}^{T_m} \exp\left(-\frac{E}{k\, T'}\right) dT' = T_m\, E_2(u_m) - T_o\, E_2(u_o) \tag{6.16}$$

where

$$E_2(u) = u \int_u^{\infty} \frac{\exp(-z)}{z^2} dz \tag{6.17}$$

with

$$u_m = \frac{E}{k\, T_m} \text{ and } u_o = \frac{E}{k\, T_o} \tag{6.18}$$

6.2.1 Peak Separation

In order to apply the Kirsh method, a glow peak needs to be isolated from the other peaks. From observation of the TL fading seen in the gamma-irradiated glass samples (Figures 5-7 to 5-11), it appears that the majority of the fading occurs in the low-temperature region. Upon examination of the TL fading curves from UV-irradiated glass samples (Figures 5-13 to 5-17), it appears that the intensity of the low-temperature region is much greater than the high-temperature region. It also appears that the fading stops between 7 and 28 days post-irradiation, and all further fading appears to follow first-order kinetics. If several assumptions are made, then it becomes possible to separate a low- and

high-temperature peak for evaluation with the Kirsh method for the peak parameters.

1. The glow peaks have the same parameters regardless of the source of irradiation, but only their relative intensities differ.
2. The low-temperature peak is completely faded by 28 days post-irradiation.
3. The fading that occurs in the high-temperature region can be modeled by first-order kinetics.
4. The low-temperature region fades at the same rate in UV- and gamma-irradiated samples.

Using these assumptions, low- and high-temperature glow peaks can be extracted for each of the studied glasses as follows (Figure 6-5):

1. Using the UV-irradiated data, multiples of the 56 day post-irradiation glow curve are subtracted from the other glow curves resulting in an isolated low-temperature peak (Figure 6-5c).
2. The isolated low-temperature peak is subtracted from corresponding gamma-irradiated glow curves resulting in an isolated high-temperature peak (Figure 6-5e).

These resulting TL curves then form the basis for evaluation using the Kirsh method, and provide a starting point for estimating the true peak parameters that control the occurring recombination processes.

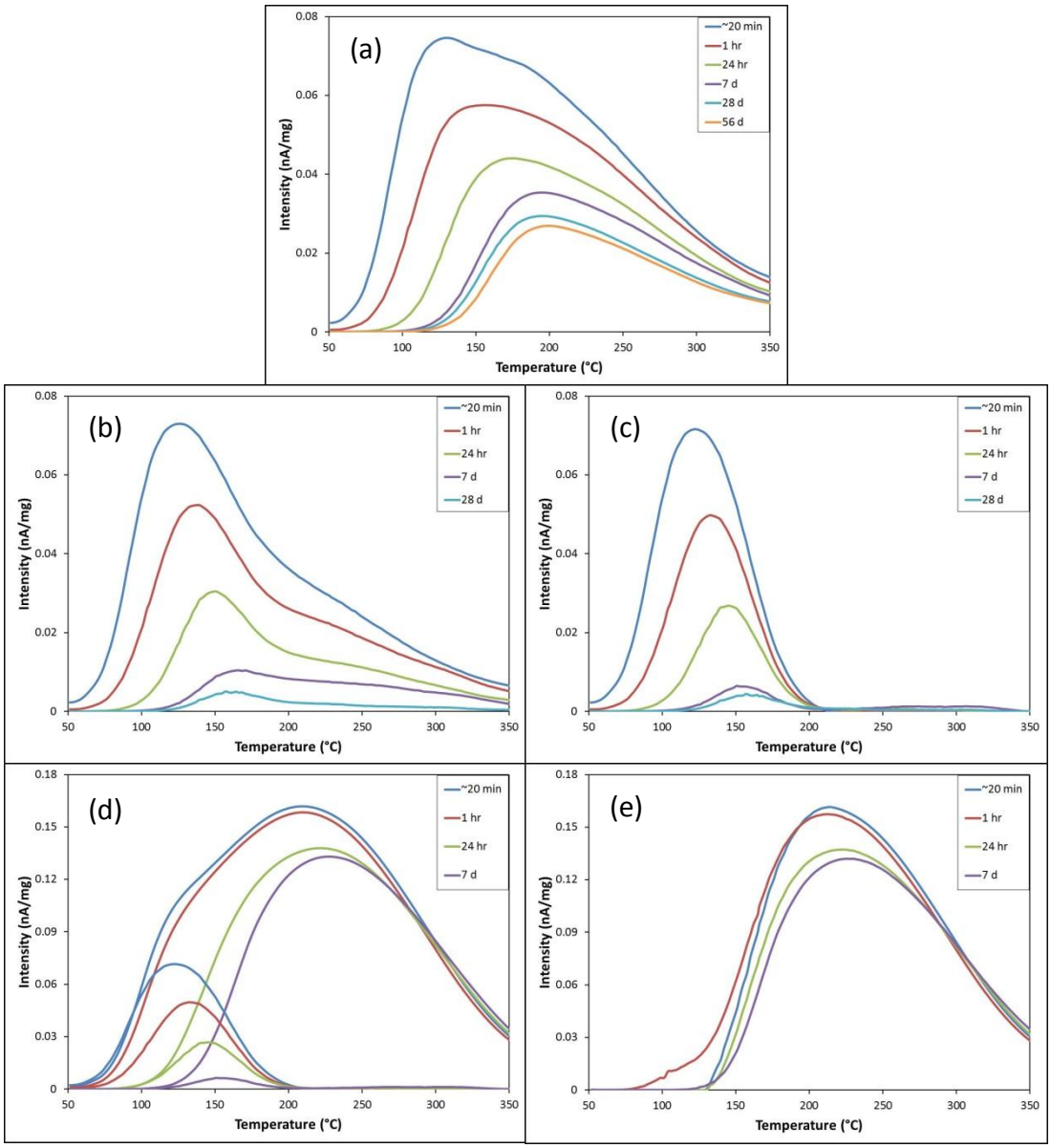

Figure 6-5: Example separation of low- and high-temperature region of TL glow curve using Glass B: (a) TL glow curves of UV-irradiated samples at various times post-irradiation; (b) Subtraction of 56 d glow curve resulting in curves of the faded signal; (c) Removal of the tail by subtracting multiples of the 56 d glow curve; (d) The isolated peak is compared to gamma-irradiated glow curves; (e) The low-temperature region is subtracted to isolate a high-temperature region.

6.2.2 Peak Parameters

Using the Kirsh method to analyze the peaks isolated through the aforementioned method resulted in the parameter values reported in Table 6-1 for the low temperature peak. The values of b, E, s, and T_{max} were roughly the same regardless of the glass and in line with literature values of these parameters.[338] A linear correlation was not observed for the high-temperature peak using the Kirsh method; therefore, the acceptable parameter values could not be achieved. This is likely due to the high-temperature peak being a combination of closely overlapping peaks as determined through the T_m-T_{stop} analysis (Figure 5-20). It is also possible that the isolated low-temperature peak has some overlap with the peak observed through T_m-T_{stop} centered near 160°C.

Table 6-1: TL peak parameters for isolated low- and high-temperature glow peaks using the Kirsh method.

	Low Temperature Peak			
Glass	b	E (eV)	s (s^{-1})	T_{max} (°C)
A	2.38 ± 0.23	0.837 ± 0.037	(1.88E ± 1.28) x 10^{10}	117 ± 7
B	2.38 ± 0.28	0.870 ± 0.039	(3.67 ± 2.55) x 10^{10}	122 ± 4
C	2.39 ± 0.25	0.864 ± 0.038	(4.21 ± 2.89) x 10^{10}	117 ± 6
D	2.37 ± 0.26	0.837 ± 0.037	(1.34 ± 0.91) x 10^{10}	122 ± 6
E	2.39 ± 0.25	0.859 ± 0.038	(3.74 ± 2.57) x 10^{10}	117 ± 7
Avg.	2.38 ± 0.25	0.853 ± 0.038	(3.09 ± 2.04) x 10^{10}	119 ± 6

6.3 Computerized Thermoluminescence Glow Curve Deconvolution

For the Kirsh method to be applied, individual peaks are needed for analysis. In many cases, a complete separation is not possible.[8] As such, many techniques have been developed to determine peak parameters without separation.[8, 12, 267] However,

the majority of these techniques requires some degree of peak separation and cannot be applied to closely overlapping peaks, as is present in the TL curves of the studied glasses (Figure 5-20). One technique that could potentially determine the trap depth (E) of overlapping peaks was developed by Gobrecht and Hofmann and is known as the 'fractional glow technique',[339] discussed in Section 9.2.1.

An alternative method is to use computerized glow curve deconvolution software to fit the experimental glow curves with peak models. These programs optimize estimated parameters to give the best fit to the experimental data. In this study, TL Glow Curve Analyzer, a glow curve deconvolution software developed by Chung et al.,[340-345] was used. This software offers the advantage of utilizing several different peak models, and can simultaneously optimize a set of peaks to multiple experimental glow curves. This assists in modeling the fading that has been observed by allowing individual peaks to decay while holding others constant.

Though the TL Glow Curve Analyzer has first-, second-, and general-order kinetic models, in order to optimize peaks to simultaneously model the observed fading, the general approximation (GA), also known as the generalized approach,[333] was used. In the general approximation, the kinetic order parameter (b) is ignored, and the ratio of the rate of retrapping (A_n) to the rate of recombination (A_m) is used.

$$R = \frac{A_n}{A_m} \tag{6.19}$$

Using this relationship, Halperin and Braner were able to show:[8, 333, 341-343, 346]

$$I(t) = -\frac{\mathrm{d}n}{\mathrm{d}t} = \frac{s\, n^2 \exp(-E/kT)}{n + R\,(N - n)} \tag{6.20}$$

Unlike the first-, second-, and general-order kinetic models, the general approximation must be solved numerically rather than symbolically.[333, 340-343]

Using the TL Glow Curve Analyzer, the glow curves of each of the five geographically diverse glass samples were deconvoluted as shown in Figures 6-6 to 6-10. A figure-of-merit (FOM)[340, 347-348] was calculated with each deconvolution (Table 6-2). A FOM less than 2.5% is considered a good fit.[347] As can be observed, a good fit for the glow curves of each of the glasses was deconvoluted using the same set of glow peaks (parameters displayed in Table 6-3).

Table 6-2: Figure-of-merit values for deconvolution.

	Figure-of-merit (FOM)
A	1.34%
B	1.18%
C	1.14%
D	0.80%
E	1.11%

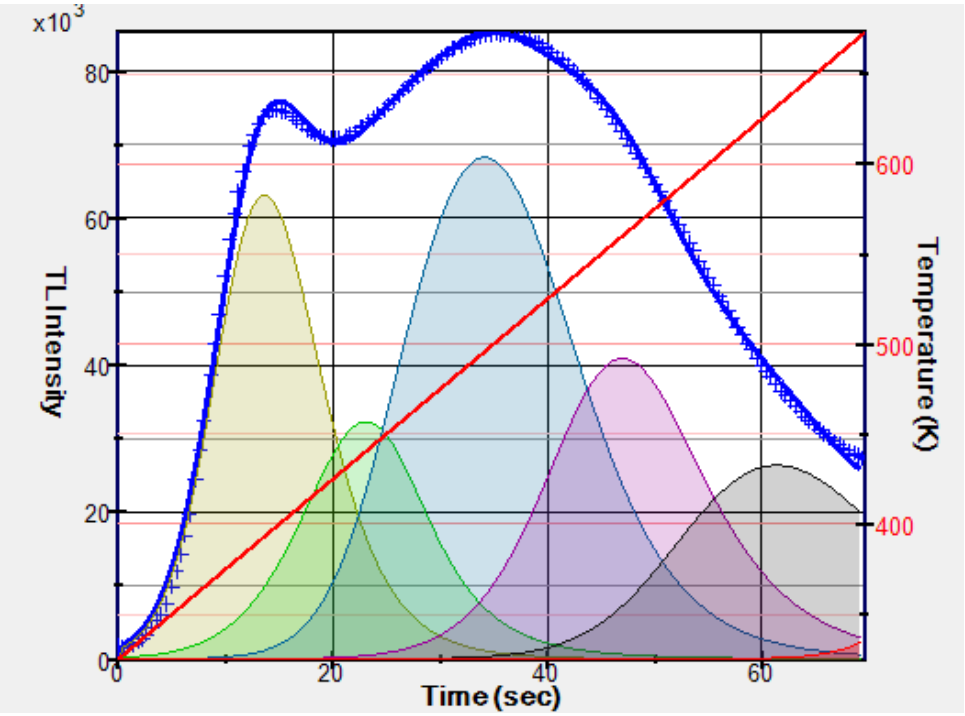

Figure 6-6: Deconvoluted glow curve for Glass A samples approximately 20 min after receiving a total dose of 20 Gy from ^{60}Co.

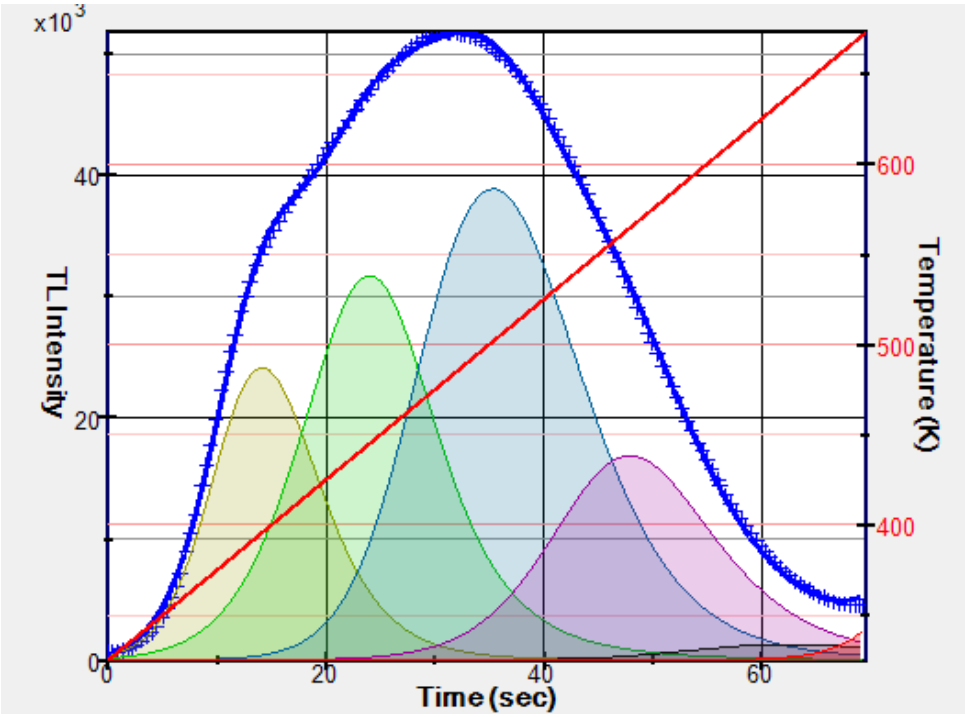

Figure 6-7: Deconvoluted glow curve for Glass B samples approximately 20 min after receiving a total dose of 20 Gy from ^{60}Co.

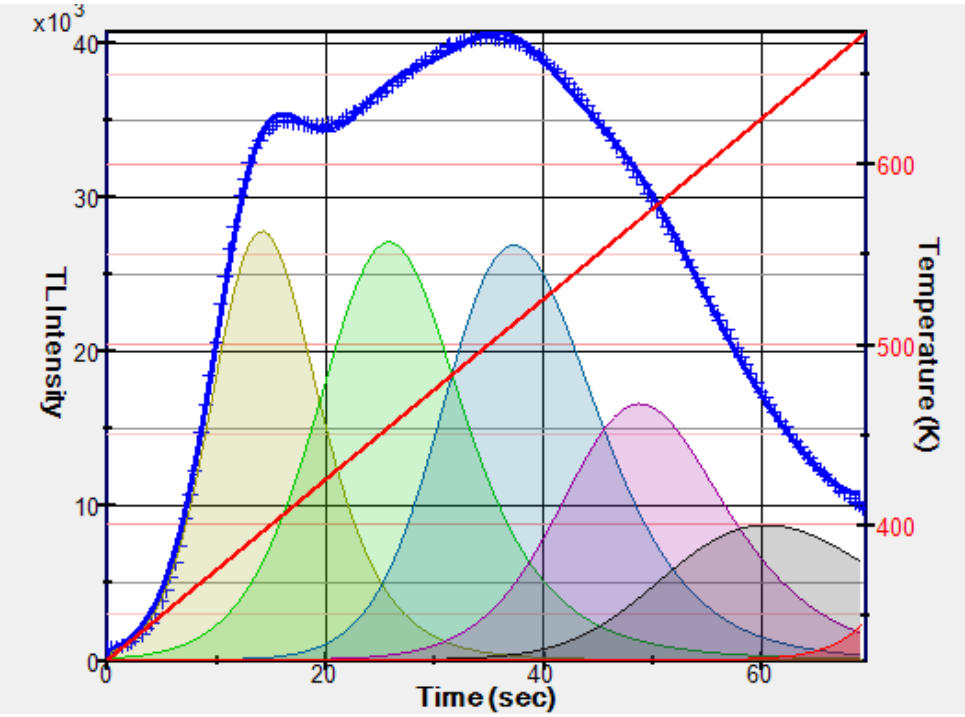

Figure 6-8: Deconvoluted glow curve for Glass C samples approximately 20 min after receiving a total dose of 20 Gy from ^{60}Co.

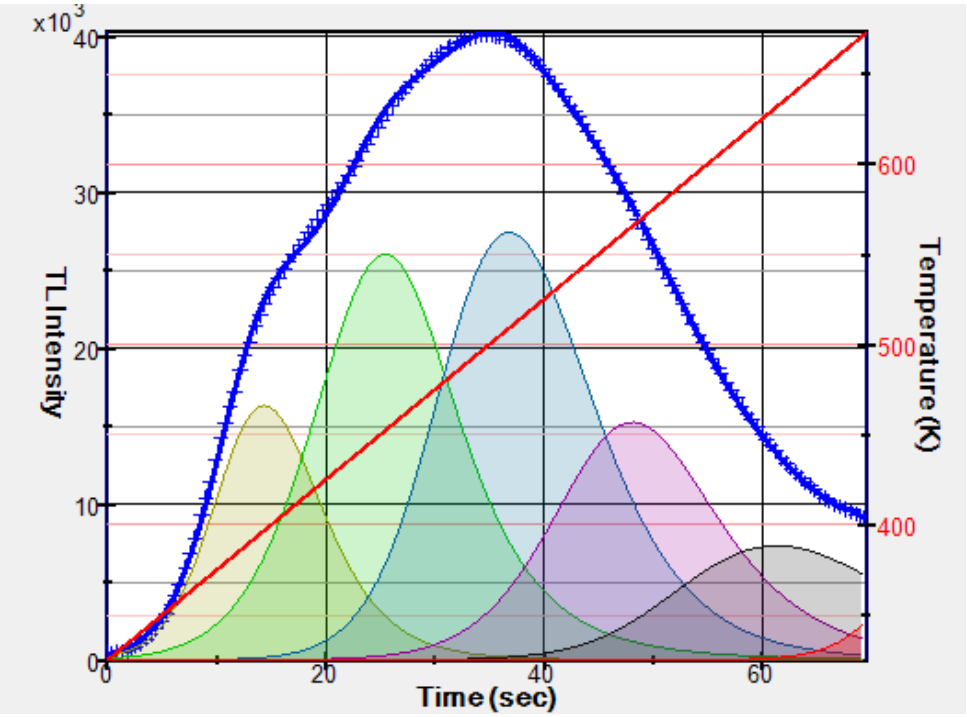

Figure 6-9: Deconvoluted glow curve for Glass D samples approximately 20 min after receiving a total dose of 20 Gy from ^{60}Co.

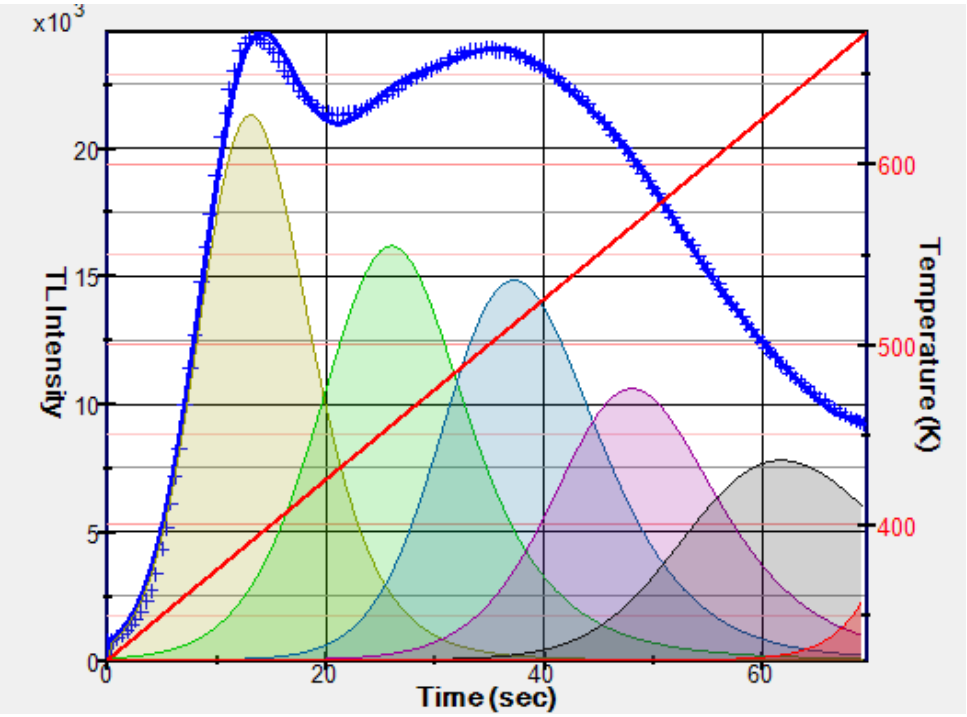

Figure 6-10: Deconvoluted glow curve for Glass E samples approximately 20 min after receiving a total dose of 20 Gy from ^{60}Co.

Table 6-3: Peak parameters obtained using TL Glow Curve Analyzer. Peak locations using the T_m-T_{stop} method are provided for comparison.

	E (eV)	s (s^{-1})	R	T_{max} (°C)	T_m-T_{stop} (°C)
Peak 1	0.877 ± 0.066	(1.12 ± 0.63) x 10^{11}	2.96 ± 0.32	120 ± 3	120
Peak 2	0.656 ± 0.155	(3.32 ± 0.36) x 10^{6}	0.660 ± 0.165	165 ± 7	160
Peak 3	1.042 ± 0.072	(1.06 ± 0.32) x 10^{10}	3.49 ± 0.73	225 ± 10	225
Peak 4	1.005 ± 0.029	(8.00 ± 1.03) x 10^{10}	(6.80 ± 1.65) x 10^{-04}	285 ± 8	300
Peak 5	1.237 ± 0.189	(1.67 ± 0.49) x 10^{11}	(2.07 ± 0.33) x 10^{2}	360 ± 13	340

In this generalized analysis, the same set of peaks could be used to fit the glow curves with good agreement regardless of the glass source. The peak locations were also in good agreement with those found through the T_m-T_{stop} method. The most variation was seen in Peaks 4 and 5 which could be an indication of unidentified peaks. In addition to glass source, these same peaks could fit glow curves regardless of irradiation source (example of a fit for a UV irradiation is seen in Figure 6-11) or time post-irradiation (examples seen in Figures 6-12 to 6-15) by only changing the peak intensities. This supports the hypothesis that the mechanisms involved in the production of the TL curves are the same for all the glasses studied, but the relative intensity of each mechanism varies between the glasses and the type of ionizing radiation. These mechanisms are not currently well understood, but are thought to be related to differences in composition, manufacturing process, or both. By observing the electron/hole traps and following their decay, these can be compared to the observed TL decay to gain insights into the mechanisms of the TL peak formation (Chapter 7). Understanding can also be gained by correlating the glass composition to changes in the observed TL peak intensities (Chapter 8).

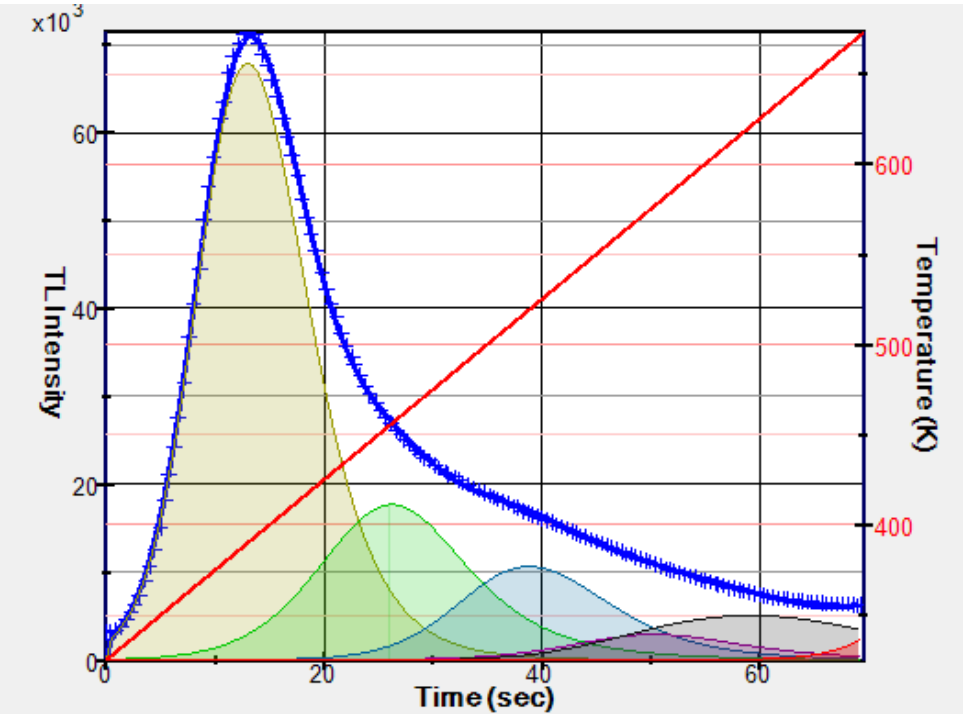

Figure 6-11: Deconvoluted glow curve for Glass A samples approximately 20 min after being irradiated with a 254nm UV-Lamp for 30 min.

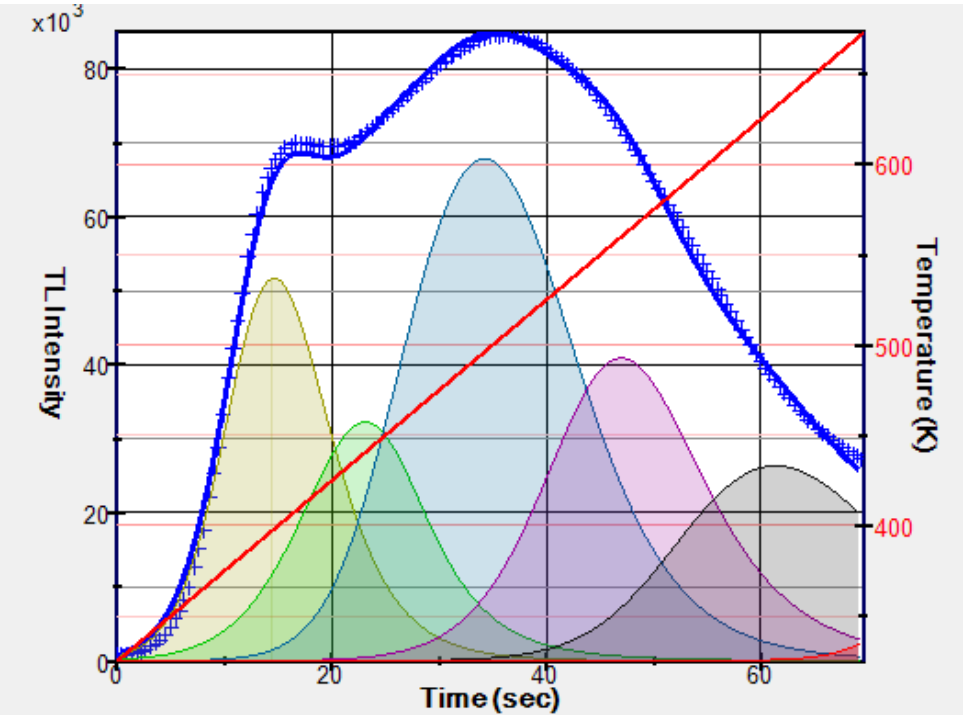

Figure 6-12: Deconvoluted glow curve for Glass A samples at 1 hr after receiving a total dose of 20 Gy from ^{60}Co.

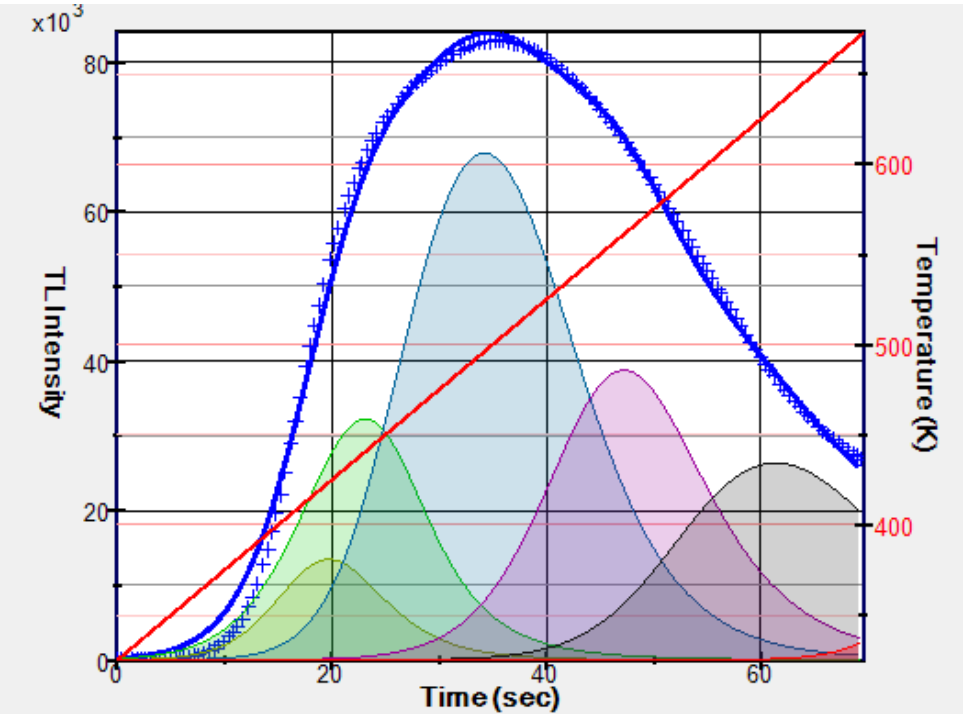

Figure 6-13: Deconvoluted glow curve for Glass A samples at 24 hr after receiving a total dose of 20 Gy from ^{60}Co.

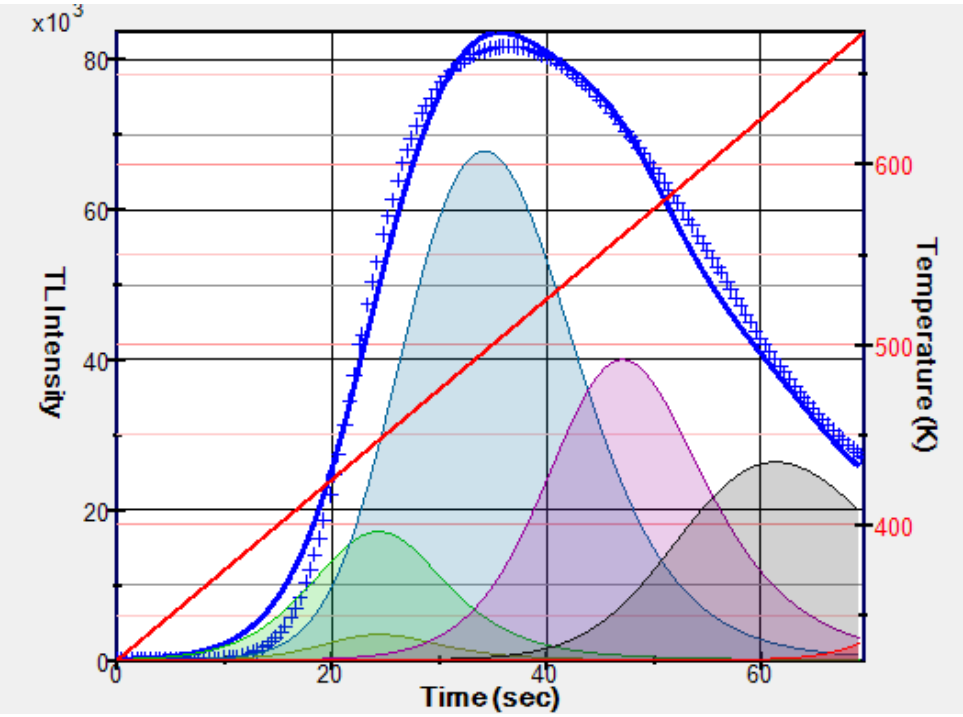

Figure 6-14: Deconvoluted glow curve for Glass A samples at 7 d after receiving a total dose of 20 Gy from ^{60}Co.

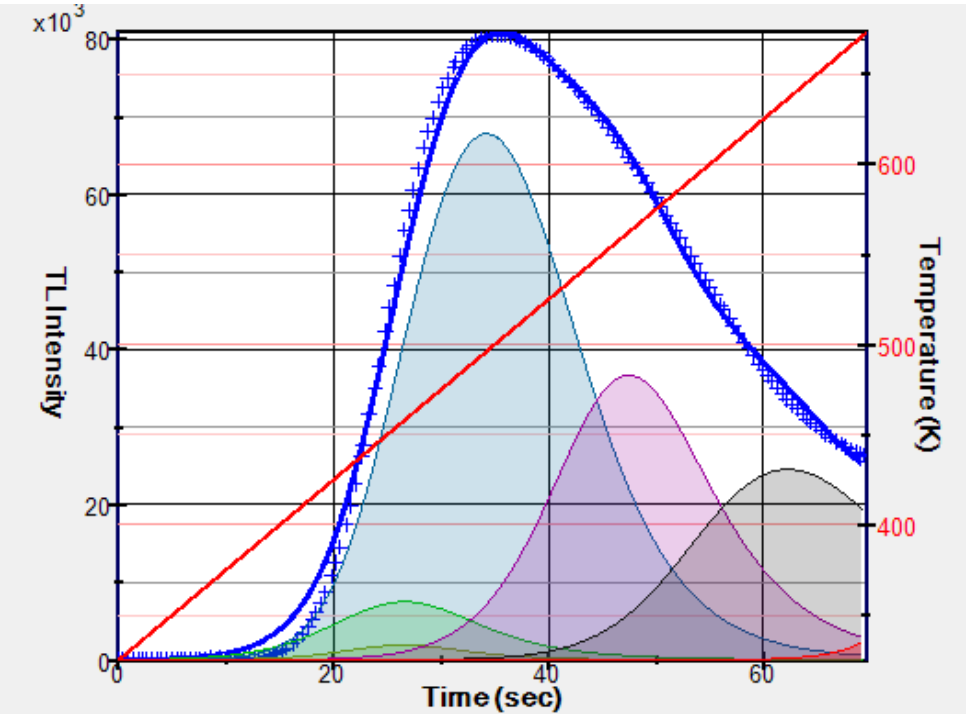

Figure 6-15: Deconvoluted glow curve for Glass A samples at 70 d after receiving a total dose of 20 Gy from ^{60}Co.

Chapter 7

Electron Paramagnetic Resonance (EPR)

7.1 Introduction

As described in Chapter 4, electron paramagnetic resonance (EPR) spectroscopy can be used to study chemical species that have one or more unpaired electrons.[14] As many of the electron/hole traps result in unpaired electrons (Section 3.5), it is a useful technique for studying radiation effects on solids. For this study, continuous wave EPR spectra were collected at room temperature using a Bruker Elexys 580E EPR spectrometer at a fixed frequency of 9.82 GHz.

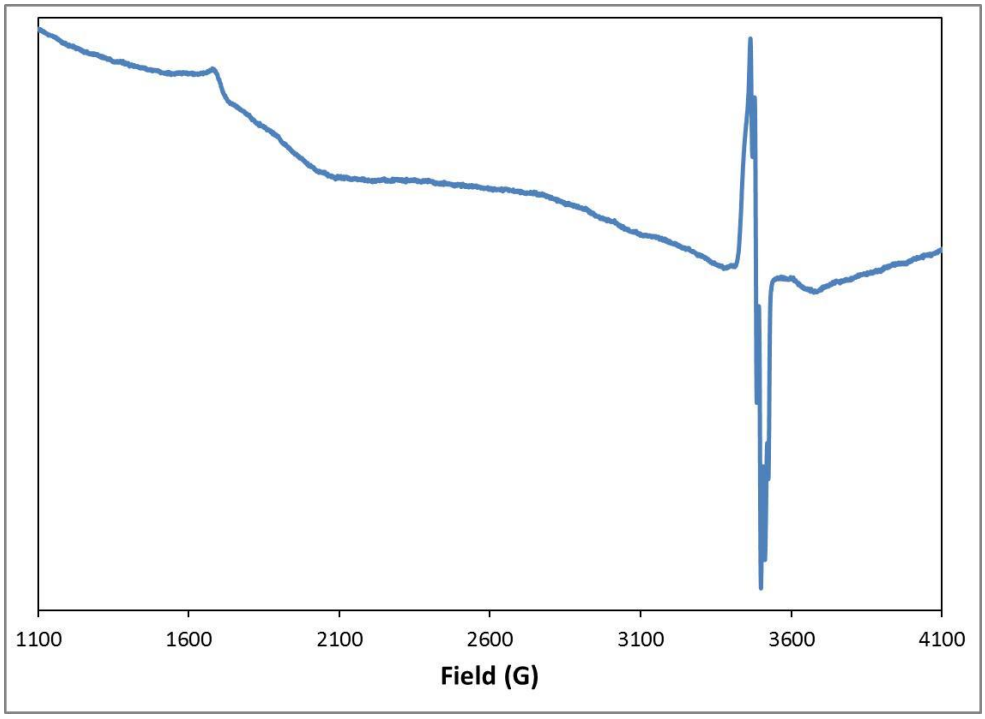

Figure 7-1: EPR spectrum of Glass A at 1 hr after receiving a total dose of approximately 700 Gy from ^{60}Co. Spectrum was collected at a fixed frequency of 9.82 GHz.

Initial studies using EPR were performed using Glass A. Figure 7-1 shows an EPR spectrum from 950-3950 Gauss of Glass A 20 min after receiving a total dose of approximately 700 Gy from ^{60}Co. Two areas of interest were observed from the spectrum: (1) a single peak near 1650 G, and (2) a group of peaks from 3400-3550 G. The single peak near 1650 G is connected with Fe^{3+} ions in glass.[174, 190, 349-352] At the irradiation doses used in this study, no significant change was observed in this signal as a result of ionizing radiation or time post-irradiation.

7.2 Boron Oxygen Hole Center (BOHC)

A closer look at the group of peaks from 3250-3400 G revealed five peaks and a shoulder structure (Figure 7-2) in all the glasses studied. This signal (the five peaks plus a shoulder) has been connected with the creation of boron oxygen hole centers (BOHC's).[146-147, 230, 255, 353-358] This signal was also observed to decay with time yielding a constant signal around 14 days post irradiation. Figure 7-3 shows the EPR signal at 1 hr and 21 d post-irradiation for comparison.

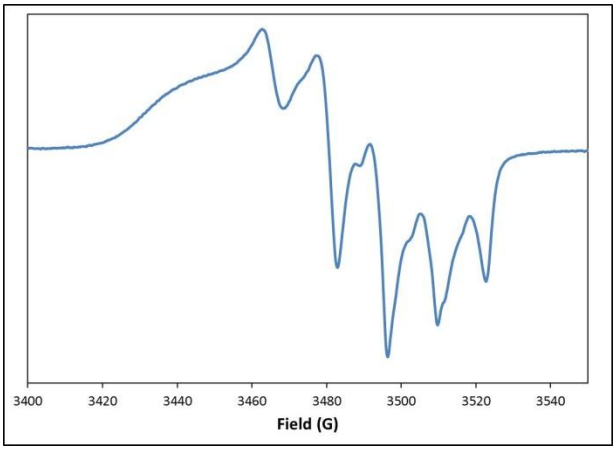

Figure 7-2: EPR signal created in Glasses A-E after receiving a total dose of approximately 700 Gy from ^{60}Co. Spectrum was collected at a fixed frequency of 9.82 GHz.

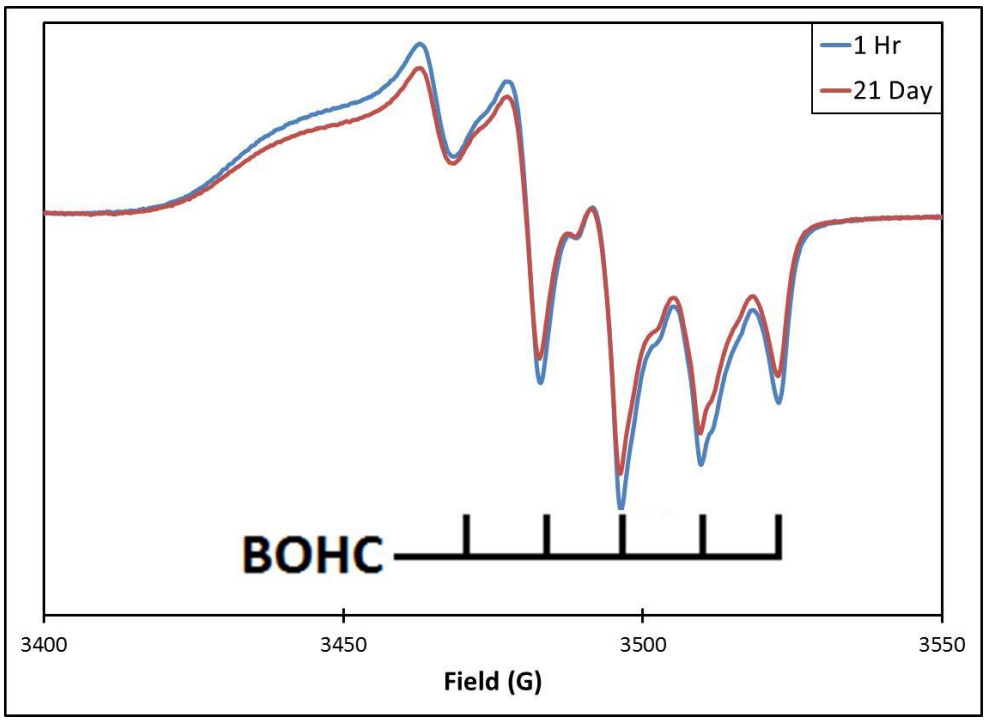

Figure 7-3: EPR signal from Glass A at 1 hr and 21 d after receiving a total dose of approximately 700 Gy from ^{60}Co. Signal decay virtually ceased by 14 d post-irradiation. Spectrum was collected at a fixed frequency of 9.82 GHz.

By integrating the EPR lines twice (Section 4.3), the relative amount of trap centers was calculated and followed with time. The decay of the EPR signal appeared to have a short-lived component that followed a logarithmic decay, and a long-lived component that followed a very slow linear decay. By subtracting off the linear component, a decay rate for the BOHC EPR signal was calculated for each of the 5 glasses. This was compared to the logarithmic decay fit to each of the 5 deconvoluted TL peaks found in Chapter 6. Results of this analysis are presented in Table 7-1. As can be seen, there is a strong correlation between the TL Peak 1 (120°C) and the BOHC observed in EPR. This would suggest that the BOHC is involved in the recombination

process occurring during TL Peak 1. However since the decay of the BOHC EPR signal ceases after approximately two weeks, Peak 1 is likely due to a trapped electron that is recombining with a trapped BOHC. If the BOHC were recombining with a trapped electron, natural recombination involving the BOHC would be expected to continue beyond two weeks. At approximately 14 days post-irradiation, this trapped electron species has "completely" recombined.

Table 7-1: Logarithmic decay rates for each of the deconvoluted TL peaks and the short-lived component of the EPR signal for each of the 5 studied glasses.

	Thermoluminescence					Short-lived
y=m*ln(x)+b	Peak 1	Peak 2	Peak 3	Peak 4	Peak 5	EPR
A	-0.1209	-0.08397	-0.00099	-0.00991	-0.01002	-0.1224
B	-0.1249	-0.07843	-0.02387	-0.01326	-0.02417	-0.1250
C	-0.1202	-0.04921	-0.00616	-0.02134	-0.04514	-0.1240
D	-0.1234	-0.06193	-0.01879	-0.03776	-0.02851	-0.1287
E	-0.1181	-0.04155	-0.01277	-0.02613	-0.01964	-0.1237

EPR results for the different glasses also showed that approximately the same number of BOHCs is created per dose regardless of the glass source. This means that the formation of BOHCs alone cannot explain the different response in the overall intensity of the TL glow curves in borosilicate glass from different regions.

7.3 E'-Defect Center (Network Defect)

After receiving a 700 Gy dose, some samples were heated to 400°C at 5°C/sec followed by rapid cooling. Heated samples showed a much reduced EPR signal as well as almost complete destruction of the valley near 3510 G (Figure 7-4). Malchukova and Boizot have linked this part of the EPR spectrum to the E'-defect center (network

defect).[230, 358] Following the decay of this peak could potentially give further insights into the TL recombination processes that are occurring.

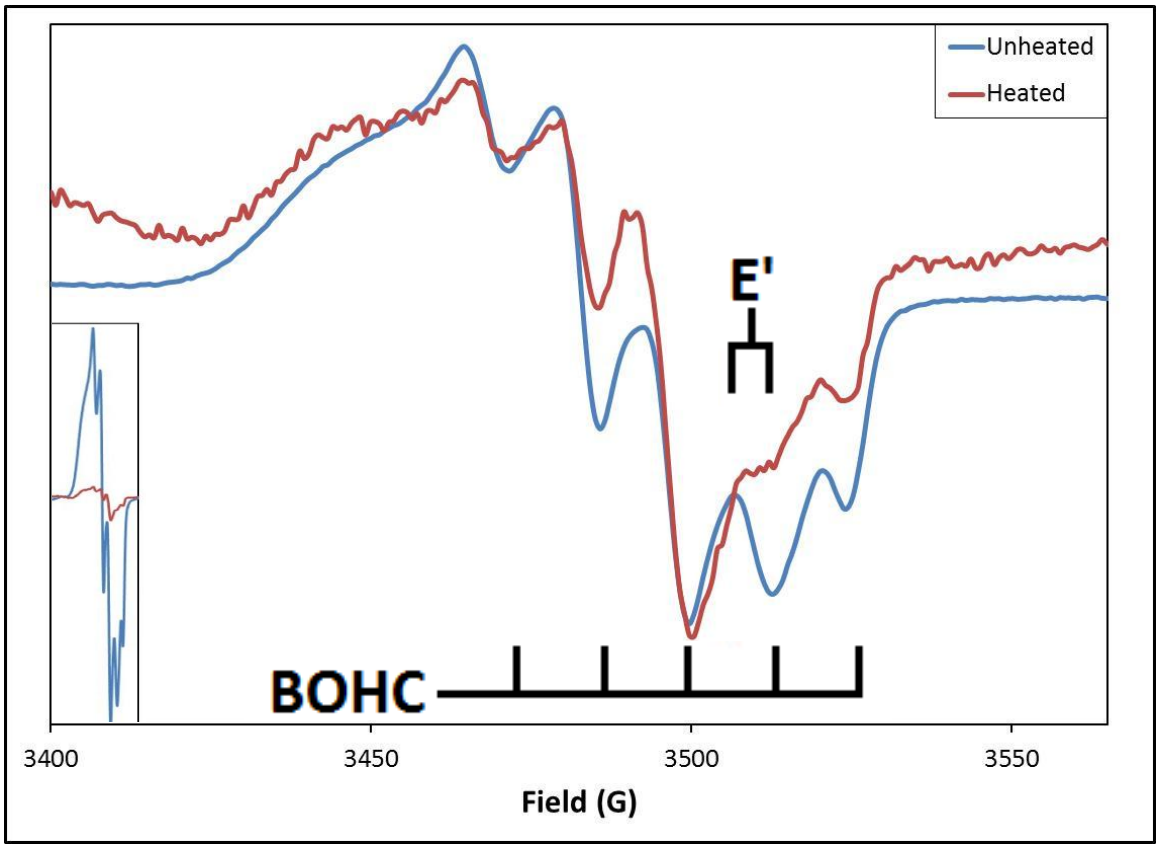

Figure 7-4: EPR signal from Glass A that received a total dose of approximately 700 Gy from ^{60}Co before and after being heated to 400°C followed by rapid cooling to room temperature. The observed quintet in the unheated sample is attributed to the creation of Boron Oxygen Hole Centers (BOHC), and the loss of signal near 3510 G in the heated sample is associated with the destruction of E'-defects. Spectrum was collected at a fixed frequency of 9.82 GHz. (Inset compares signal intensity)

Chapter 8

Multivariate Analysis (MVA)

8.1 Glass Composition

The elemental composition of the glass from each of the five regions was determined by Southwest Research Institute (SWRI; San Antonio, TX). Samples were digested by two techniques. The first technique was a closed vessel digestion using concentrated nitric, hydrochloric, and hydrofluoric acids. The second technique was performed using concentrated nitric, perchloric, hydrofluoric, and hydrochloric acids in an open vessel. The first digestion technique was used to determine boron, chromium, and silicon as these elements are known to yield volatile fluoride species during digestion. The remaining elements were determined using the second digestion technique. Elemental composition was determined using Inductively Coupled Plasma-Mass Spectroscopy (ICP-MS) and Inductively Coupled Plasma-Atomic Emission Spectroscopy (ICP-AES).

Six aliquots of each glass sample were analyzed. Table 8-1 shows the determined composition of each glass by major oxide component (in weight percent). The average composition of each minor and trace analyte is shown in Table 8-2 (values in ppm). A “U” indicates that a value was “undetected”, or that the analyte was not present in the sample at a level above the method reporting limit (quantification limit–Section 5.2.1), and the average reporting limit at the time of analysis is given.

Table 8-1: Average (n = 6) composition (weight percent) of glasses by major oxide component and standard deviation.

	A	B	C	D	E
Al_2O_3	2.19 ± 0.02	2.42 ± 0.04	2.12 ± 0.02	2.63 ± 0.02	2.14 ± 0.03
B_2O_3	12.9 ± 0.2	13.1 ± 0.3	12.5 ± 0.1	12.2 ± 0.2	12.2 ± 0.1
K_2O	0.883 ± 0.011	0.542 ± 0.004	0.0524 ± 0.0010	0.0884 ± 0.0012	0.00590 **(U)**
SiO_2	80.5 ± 1.0	80.5 ± 1.6	79.0 ± 0.7	79.5 ± 0.7	80.8 ± 0.9
Na_2O	3.42 ± 0.03	3.47 ± 0.05	4.33 ± 0.04	4.18 ± 0.04	3.84 ± 0.06

Table 8-2: Average (n = 6) elemental composition of glasses and standard deviation. Values in ppm.

	A	B	C	D	E
Aluminum (Al)	11600 ± 120	12800 ± 230	11200 ± 100	13900 ± 140	11300 ± 150
Antimony (Sb)	19.6 **(U)**	19.4 **(U)**	19.4 **(U)**	19.4 **(U)**	19.6 **(U)**
Arsenic (As)	0.978 **(U)**	0.971 **(U)**	0.969 **(U)**	0.970 **(U)**	0.979 **(U)**
Barium (Ba)	19.5 ± 0.2	19.5 ± 0.2	6.91 ± 0.05	21.4 ± 0.4	1.59 ± 0.02
Beryllium (Be)	0.978 **(U)**	0.971 **(U)**	0.969 **(U)**	0.970 **(U)**	0.979 **(U)**
Bismuth (Bi)	2.935 **(U)**	2.91 **(U)**	2.91 **(U)**	2.91 **(U)**	2.94 **(U)**
Boron (B)	39900 ± 780	40600 ± 810	38700 ± 400	38000 ± 710	37900 ± 330
Cadmium (Cd)	0.978 **(U)**	0.971 **(U)**	0.969 **(U)**	0.970 **(U)**	0.979 **(U)**
Calcium (Ca)	103 ± 6	236 ± 5	172 ± 15	262 ± 9	90.5 ± 12.3
Cerium (Ce)	19.6 ± 0.3	1.90 ± 0.03	6.37 ± 0.11	2.45 ± 0.09	0.700 ± 0.018
Chromium (Cr)	46.7 **(U)**	44.0 **(U)**	43.1 **(U)**	46.1 **(U)**	46.0 **(U)**
Cobalt (Co)	0.978 **(U)**	0.971 **(U)**	0.969 **(U)**	0.970 **(U)**	1.08 ± 0.11
Copper (Cu)	1.16 **(U)**	1.47 ± 0.25	1.28 ± 0.25	0.970 **(U)**	0.979 **(U)**
Dysprosium (Dy)	0.263 ± 0.002	0.225 ± 0.003	0.377 ± 0.007	0.192 ± 0.008	0.126 ± 0.003
Erbium (Er)	0.194 ± 0.003	0.230 ± 0.004	0.320 ± 0.003	0.180 ± 0.008	0.148 ± 0.002
Europium (Eu)	0.0520 ± 0.0013	0.0486 **(U)**	0.0946 ± 0.0014	0.0485 **(U)**	0.0490 **(U)**
Gadolinium (Gd)	0.369 ± 0.015	0.170 ± 0.003	0.456 ± 0.006	0.168 ± 0.005	0.0629 ± 0.0023
Holmium (Ho)	0.0539 ± 0.0010	0.0555 ± 0.0011	0.0778 ± 0.0010	0.0485 **(U)**	0.0490 **(U)**
Iron (Fe)	171 ± 41	300 ± 39	250 ± 14	299 ± 25	177 ± 16
Lanthanum (La)	1.65 ± 0.28	1.06 **(U)**	2.87 ± 0.16	1.12 ± 0.13	0.979 **(U)**
Lead (Pb)	1.20 ± 0.20	1.30 ± 0.21	2.79 ± 0.26	0.970 **(U)**	1.01 **(U)**
Lithium (Li)	9.68 ± 0.10	6.29 ± 0.09	13.9 ± 2.2	8.84 ± 1.55	5.12 ± 0.13
Lutetium (Lu)	0.0489 **(U)**	0.0603 ± 0.0008	0.0485 **(U)**	0.0485 **(U)**	0.0490 **(U)**
Magnesium (Mg)	30.8 ± 4.1	45.1 ± 3.3	105 ± 4	120 ± 6	19.1 ± 2.0
Manganese (Mn)	2.18 ± 0.22	2.73 ± 0.64	2.63 ± 0.10	3.53 ± 0.14	2.33 ± 0.07
Molybdenum (Mo)	2.11 ± 0.18	2.63 ± 0.12	1.45 **(U)**	1.90 ± 0.09	4.18 ± 0.17
Neodymium (Nd)	1.61 ± 0.03	0.795 ± 0.011	2.70 ± 0.03	0.911 ± 0.028	0.265 ± 0.007
Nickel (Ni)	1.04 **(U)**	1.36 ± 0.62	0.969 **(U)**	0.970 **(U)**	0.979 **(U)**
Potassium (K)	7330 ± 93	4500 ± 31	435 ± 8	734 ± 10	49.0 **(U)**

Table 8-2 (continued): Average (n = 6) elemental composition of glasses and standard deviation. Values in ppm.

	A	B	C	D	E
Praseodymium (Pr)	0.434 ± 0.007	0.208 ± 0.003	0.712 ± 0.011	0.236 ± 0.015	0.0595 ± 0.0017
Samarium (Sm)	0.324 ± 0.006	0.163 ± 0.003	0.489 ± 0.009	0.181 ± 0.014	0.0490 **(U)**
Silicon (Si)	376000 ± 4900	376000 ± 7500	369000 ± 3200	372000 ± 3400	378000 ± 3900
Silver (Ag)	0.978 **(U)**	1.39 ± 0.71	0.969 **(U)**	0.970 **(U)**	0.979 **(U)**
Sodium (Na)	25400 ± 230	25700 ± 380	32100 ± 300	31100 ± 270	28500 ± 440
Strontium (Sr)	4.80 ± 0.05	3.67 ± 0.03	11.9 ± 0.1	3.87 ± 0.04	1.08 ± 0.02
Terbium (Tb)	0.049 **(U)**	0.0486 **(U)**	0.0688 ± 0.0008	0.0485 **(U)**	0.049 **(U)**
Thulium (Tm)	0.0489 **(U)**	0.0486 **(U)**	0.0484 **(U)**	0.0485 **(U)**	0.049 **(U)**
Tin (Sn)	9.78 **(U)**	9.71 **(U)**	9.69 **(U)**	9.70 **(U)**	9.79 **(U)**
Titanium (Ti)	122 ± 2	114 ± 1	95.5 ± 0.7	114 ± 2	97.8 ± 0.9
Tungsten (W)	29.3 **(U)**	29.1 **(U)**	29.1 **(U)**	29.1 **(U)**	29.4 **(U)**
Vanadium (V)	0.978 **(U)**	0.971 **(U)**	0.969 **(U)**	1.42 ± 0.14	0.979 **(U)**
Ytterbium (Yb)	0.214 ± 0.006	0.313 ± 0.007	0.275 ± 0.004	0.249 ± 0.005	0.236 ± 0.005
Zinc (Zn)	7.83 **(U)**	7.77 **(U)**	7.75 **(U)**	7.76 **(U)**	7.84 **(U)**
Zirconium (Zr)	127 ± 1	396 ± 7	149 ± 3	273 ± 4	305 ± 5

8.2 Multivariate Analysis (MVA)

Multivariate statistical methods are used to cluster samples into distinct groups based on the variations within the different variables of the measured data set. This clustering is accomplished by finding combinations of variables called principal components (PCs) that describe major trends in the data. In effect, these methods take large data sets and look for common variances and combine these variations into single principal components.[359-361] Also, essential information often lies not in any individual variable but in how the variables change with respect to one another (covariance).[362]

8.2.1 Principal Component Analysis (PCA)

Principal component analysis (PCA) is a chemometric tool that describes the common variance observed among differing datasets through PCs. If **X** is a

data matrix with m rows and n columns, with each variable being a column and each sample a row, PCA decomposes **X** as the sum of $\mathbf{t}_i$ and $\mathbf{p}_i$:[361-362]

$$\mathbf{X} = \mathbf{t}_1\mathbf{p}_1^{\mathsf{T}} + \mathbf{t}_2\mathbf{p}_2^{\mathsf{T}} + \ \ldots\ + \mathbf{t}_k\mathbf{p}_k^{\mathsf{T}} + \ \ldots\ + \mathbf{t}_r\mathbf{p}_r^{\mathsf{T}} \tag{8.1}$$

where the $\mathbf{t}_i$ vectors are known as scores and contain information on how the samples relate to each other, the $\mathbf{p}_i$ vectors are known as loadings and contain information on how the variables relate to each other, r is the mathematical rank of the data matrix, and the superscript T denotes transpose. The scores and loading pairs in equation (8.1) represent the principal components, and their total number equals the mathematical rank (r) of the data matrix.[362] The $\mathbf{t}_i\mathbf{p}_i^{\mathsf{T}}$ pairs are ordered according to the amount of variance captured. The PCA model is generally truncated after the number (k) of meaningful scores and loadings is discovered.[361] Following truncation, the remaining PCs are consolidated into a residual matrix (**E**):[362]

$$\mathbf{X} = \mathbf{t}_1\mathbf{p}_1^{\mathsf{T}} + \mathbf{t}_2\mathbf{p}_2^{\mathsf{T}} + \ \ldots\ + \mathbf{t}_k\mathbf{p}_k^{\mathsf{T}} + \mathbf{E} \tag{8.2}$$

PCA uses an eigenvector decomposition of the covariance (or correlation matrix) of the variables of the data set. Provided that the columns of a given data matrix **X** with m rows and n columns have been mean-centered by subtracting off the original mean of each column, the correlation matrix of **X** can be defined as:[362]

$$\text{cov}(\mathbf{X}) = \frac{\mathbf{X}^{\mathsf{T}}\mathbf{X}}{m-1} \tag{8.3}$$

The correlation matrix of **X** can also be given by equation (8.1) if the columns (variables) of **X** have been autoscaled (adjusted to zero mean and unit variance by dividing each column by its standard deviation). In the PCA decomposition, the loadings ($\mathbf{p}_i$) are eigenvectors of the correlation matrix:[362]

$$\text{cov}(\mathbf{X})\mathbf{p}_i = \lambda_i \mathbf{p}_i \tag{8.4}$$

where λ_i is the eigenvalue associated with the eigenvector $\mathbf{p}_i$. The scores ($\mathbf{t}_i$) form an orthogonal set ($\mathbf{t}_i^{\mathsf{T}}\mathbf{t}_j = 0$ for $i \neq j$), while the loadings are orthonormal ($\mathbf{p}_i^{\mathsf{T}}\mathbf{p}_j = 0$ for $i \neq j$ and $\mathbf{p}_i^{\mathsf{T}}\mathbf{p}_j = 1$ for $i = j$).[362]

Through this process, PCA finds the maximum variance among the samples in one direction, and then looks for the maximum variance remaining in a direction orthogonal to the first. The process is repeated until all of the variance is accounted. In general, in PCA analysis the data can be adequately described using far fewer factors than original variables. PCA also often finds combinations of variables that are useful descriptions, or even predictors, of particular events or phenomena. These combinations of variables are often strong indicators of laboratory sample or process conditions than individual variables due to the signal averaging aspects of PCA.[360, 362]

8.2.2 Partial Least Squares (PLS)

Partial least squares (PLS) regression is a multivariate calibration method that utilizes an approach analogous to PCA, and is based on inverse least squares

(ILS) methods.[360-363] It assumes that a regression vector $\mathbf{b}$ can be used to determine a property of the system (y) from the measured variables $\mathbf{x}$:[360-362]

$$y = \mathbf{x}\,\mathbf{b} \tag{8.5}$$

The regression vector ($\mathbf{b}$) is determined using a collection of measurements $\mathbf{C}$, or calibration matrix, and a vector $\mathbf{y}$ containing the respective values of the quantity of interest for each measurement in $\mathbf{C}$. PLS uses $\mathbf{C}$ and $\mathbf{y}$ to find factors called latent variables that capture variance in $\mathbf{C}$ while also achieving a correlation with $\mathbf{y}$. Ultimately, it tries to maximize the covariance between $\mathbf{C}$ and $\mathbf{y}$.[361-362] The PLS parameters can be calculated in several ways. One such method is known as SIMPLS,[362, 364] which was used in this work. SIMPLS uses both $\mathbf{C}$ and $\mathbf{y}$ to calculate the scores ($\mathbf{T}$) and loadings ($\mathbf{P}$) which are similar to the scores and loadings from PCA. It also calculates an additional set of vectors known as weights, $\mathbf{W}$. The addition of the weights is needed to keep the scores orthogonal. Using these, SIMPLS can estimate the regression vector $\mathbf{b}$ as:[360-362]

$$\mathbf{b} = \mathbf{C}^{+}\,\mathbf{y} \tag{8.6}$$

where $\mathbf{C}^{+}$ is the pseudo-inverse of $\mathbf{C}$. This pseudo-inverse ($\mathbf{C}^{+}$) is estimated by replacing the original variables in the calibration matrix $\mathbf{C}$ with linear combinations of the variables.[361] It can then be estimated as:[361-362]

$$\mathbf{C}^{+} = \mathbf{W}(\mathbf{P}^{\mathrm{T}}\mathbf{W})^{-1}(\mathbf{T}^{\mathrm{T}}\mathbf{T})^{-1}\mathbf{T}^{\mathrm{T}} \tag{8.7}$$

The scores and loadings calculated in PLS are not the same as those calculated in PCA. However, they can be thought of as PCA scores and loadings that have been rotated to be more relevant for predicting $\mathbf{y}$.[361-362]

8.2.3 Preprocessing

Preprocessing is the modification of data done before building a model or analyzing the data. The purposes of preprocessing are to linearize the response of the measured variables and to remove extraneous sources of variation which are not of interest in the analysis.[362] In Section 8.2.1, some preprocessing methods were mentioned as criteria for the correlation matrix. As these (mean-center and autoscale) were used in this work, they require further explanation.

8.2.3.1 Mean-Center

A common preprocessing method is mean-centering. In this method, the mean of each variable (in this case concentration) is calculated and subtracted from the column. After mean-centering, each row of the mean-centered data effectively only includes how that row differs from the average sample in the original data matrix.[362]

8.2.3.2 Autoscale

Autoscaling is a preprocessing method that uses mean-centering followed by dividing each variable by the standard deviation of that variable. This results in each column having a mean of zero and a standard deviation of one. This is a valid approach to correct for different

variable scaling and units as long as the predominant source of variance in each variable is signal rather than noise. Under these conditions, each variable is scaled such that its useful signal has an equal footing with the signal of the other variables.[362] In this study, all the data was autoscaled prior to applying PCA and PLS.

8.3 Potential Elements of Importance

PCA was applied to the elemental composition of the individual measurements for the glass samples for the 5 geographical regions using the PLS Toolbox[365] for MATLAB.[296] The compositional data was limited to the elements of largest structural importance to glass (*network formers*, *network modifiers*–alkali and alkaline earth metals, and *network intermediates*–transition metals). The data was also limited to those elements where the element was observed above the reporting limit in at least 3 of the 5 glasses. Using PCA, the data was separated into groups using 3 PCs. Plots of

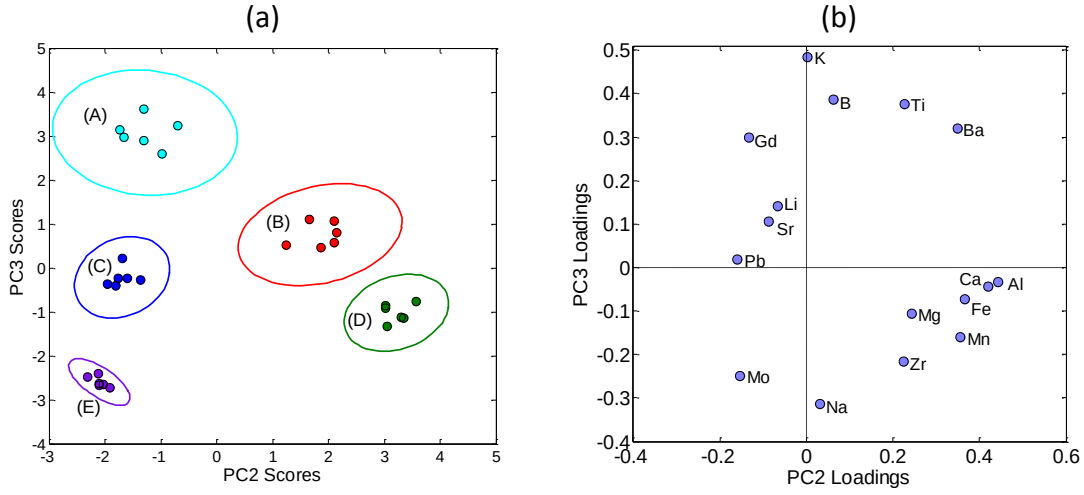

Figure 8-1: PCA analysis of borosilicate glass: (a) plot of the scores of PC3 vs. PC2 showing separation of the 5 glasses; (b) plot of the loadings of PC3 vs. PC2.

the scores and loadings of PC3 vs. PC2 are shown in Figure 8-1. The separation of the glasses described in PC2 and PC3 had similarities to the classification of the glasses TL shape and the TL intensity of the glasses, respectively, and warrants further examination.

As can be seen in Figure 8-2a, the scores of PC2 separated the 5 glasses according to their TL shape. The loadings (Figure 8-2b) reveal the elements that contribute to the separation. Of those that appear to have a significant contribution (±0.2) were the alkaline earths (affect the number of non-bridging oxygens; Section 2.4) and several *network intermediates*, including Al (affects the coordination of boron in glass; Section 2.6.2), Fe (a multivalent ion center; Section 3.5.4), and Zr (an electron trap; Section 3.5.4). In general, both Glasses B and D have elevated concentration of all the elements that contribute to PC2 (Table 8-3).

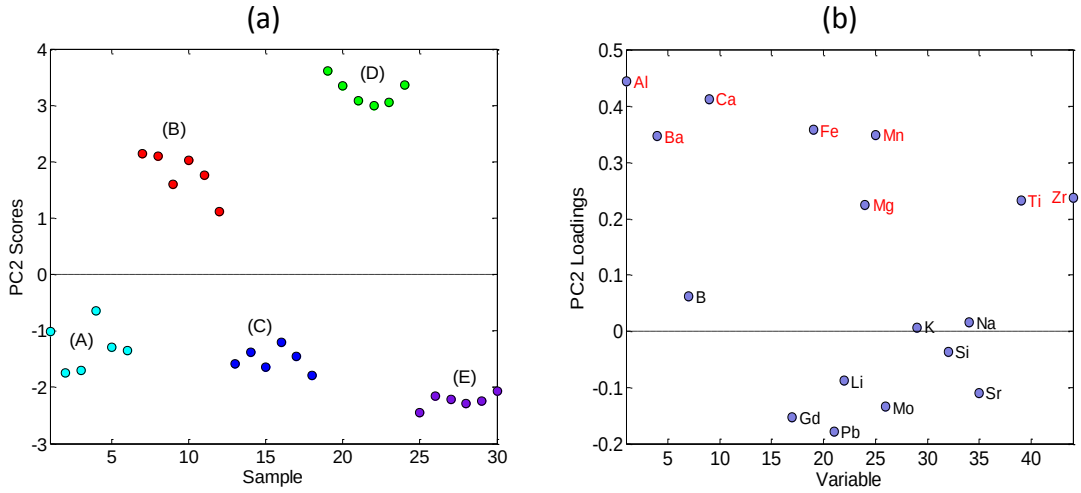

Figure 8-2: PCA analysis of borosilicate glass: (a) scores for PC2 showing separation of the 5 sources according to their TL shape; (b) plot of the loadings of PC2 with those elements with a loading above ±0.2 highlighted.

Table 8-3: Average (n = 6) elemental composition of glasses and standard deviation of those elements with loadings above ±0.2 for PC2. Values in ppm.

	A	B	C	D	E
Aluminum (Al)	11600 ± 120	12800 ± 230	11200 ± 100	13900 ± 140	11300 ± 150
Barium (Ba)	19.5 ± 0.2	19.5 ± 0.2	6.91 ± 0.05	21.4 ± 0.4	1.59 ± 0.02
Calcium (Ca)	103 ± 6	236 ± 5	172 ± 15	262 ± 9	90.5 ± 12.3
Iron (Fe)	171 ± 41	300 ± 39	250 ± 14	299 ± 25	177 ± 16
Magnesium (Mg)	30.8 ± 4.1	45.1 ± 3.3	105 ± 4	120 ± 6	19.1 ± 2.0
Manganese (Mn)	2.18 ± 0.22	2.73 ± 0.64	2.63 ± 0.10	3.53 ± 0.14	2.33 ± 0.07
Titanium (Ti)	122 ± 1.7	114 ± 1.2	95.5 ± 0.7	114 ± 2.1	97.8 ± 0.9
Zirconium (Zr)	127 ± 1	396 ± 7	149 ± 3	273 ± 4	305 ± 5

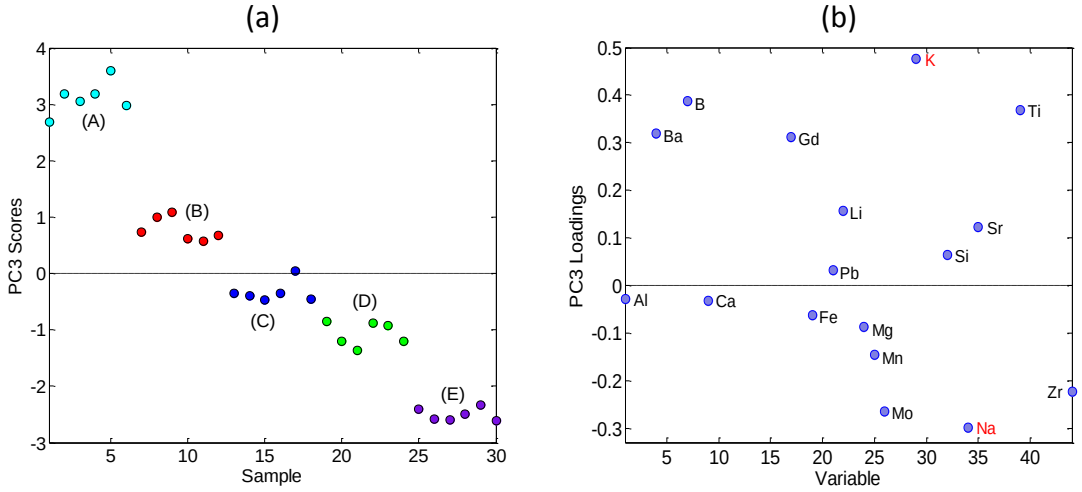

Figure 8-3: PCA analysis of borosilicate glass: (a) scores for PC3 showing separation of the 5 sources according overall TL intensity trend; (b) plot of the loadings of PC3 with two elements of particular interest (Na and K) highlighted.

Where PC2 separated the glasses according to their TL shape, the scores of PC3 showed separation that followed the general trend of overall TL intensity (Figure 8-3a). Of particular interest from the loadings (Figure 8-3b) is the separation and importance of potassium and sodium. Boizot et al. have suggested that the total number of holes trapped on non-bridging oxygens can be linked to the ratio of sodium to the total

amount of alkali metal present $\left(\frac{[Na]}{[Li+Na+K]}\right)$.[174, 356] Though a correlation between the total amount of defects and the sodium : alkali ratio was not observed in this study using EPR, a similar trend to Boizot et al. was observed with the total overall TL intensity and TL intensity of the 225°C peak increasing as the sodium : alkali ratio decreases (Table 8-4).

Table 8-4: Average (n = 6) elemental composition of glasses and standard deviation of alkali metals (in ppm) and percent Na of alkali content. The normalized overall TL intensity and the normalized TL intensity of the 225°C peak are also given.

	A	B	C	D	E
Lithium (Li)	9.68 ± 0.10	6.29 ± 0.09	13.9 ± 2.2	8.84 ± 1.55	5.12 ± 0.13
Potassium (K)	7330 ± 93	4500 ± 31	435 ± 8	734 ± 10	49.0 (U)
Sodium (Na)	25400 ± 230	25700 ± 380	32100 ± 300	31100 ± 270	28500 ± 440
Pct. Na of Modifier	77.6	85.1	98.6	97.7	99.8
Overall TL Intensity	1.00	0.48	0.46	0.40	0.30
225°C TL Intensity	1.00	0.61	0.47	0.47	0.28

8.4 Thermoluminescence Intensity

Following PCA, PLS was applied to the data set to find the minimum number of elements needed to adequately describe the observed thermoluminescence. For these analyses, the elemental composition remained the input ($\mathbf{x}$), and TL properties were used as the output (y). As different samples of each glass were used to determine the elemental composition than those used in studying TL, the average (n=5) of the TL signal for each glass was used as the y for each sample for the corresponding glass.

Using PLS, a model using one latent variable (LV) was created to predict the overall TL intensity of the glass by using all the elements with concentration levels above the reporting limit set by SWRI. Variable Importance in Projection (VIP) scores estimate

the importance of each variable in the projection used in a PLS model. Variables with low VIP scores are less important and might be good candidates for exclusion from the model.[366] Variables with low VIP scores were systematically removed to form a PLS model with the fewest variables that resulted in a coefficient of determination (R^2) above 0.95. Using this approach, a model was created that fit the overall TL intensity using only potassium and cerium (Figure 8-4). Both potassium and cerium positively influenced the intensity (increasing the concentration increased the TL intensity). The fit was improved by moving to two LVs (Figure 8-4b) which suggests that both variables are needed to predict the TL intensity, and the concentration of one element is independent of the other. This suggests that cerium and potassium influence the probability that a recombination process is radiative.

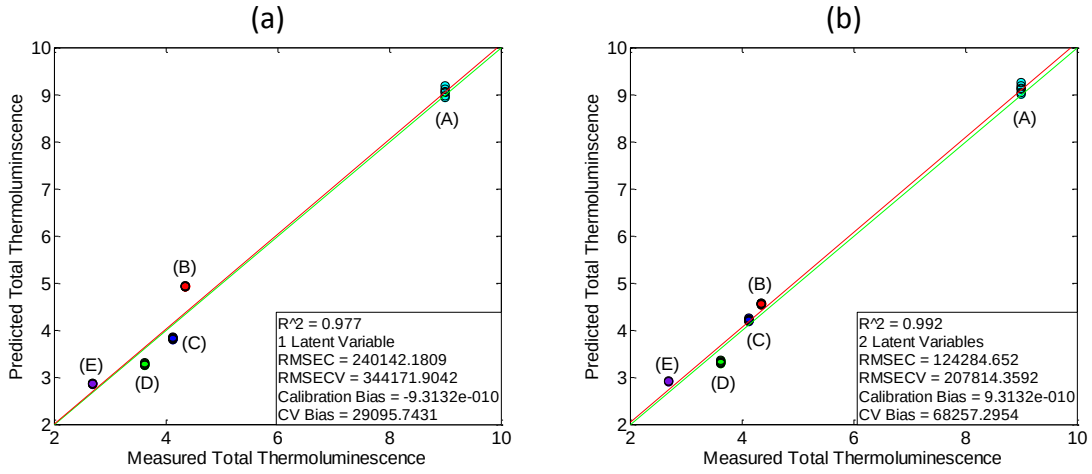

Figure 8-4: PLS models to predict the overall TL intensity using potassium and cerium with: (a) 1 LV; and (b) 2 LVs.

8.5 Correlation of Elements to TL Glow Peaks

PLS was also used to investigate the core influences of the individual TL peaks. In order to do this, the factors that influence the overall TL intensity need to be marginalized. This was done by normalizing the TL glow curves in two manners:

(1) the individual glow peaks were normalized to Peak 3 (225°C) in their own glow curve (intensity of Peak 3 equals 1), and the ratios of the individual peaks to Peak 3 were modeled.

(2) the entire glow curve was normalized to the high temperature region (intensity of the unseparated high temperature region equals 1), the ratios of the individual peaks to Peak 3 of Glass A were modeled.

The resulting normalized glow curves can be observed in Figure 8-5, and the resulting peak ratios in Table 8-5.

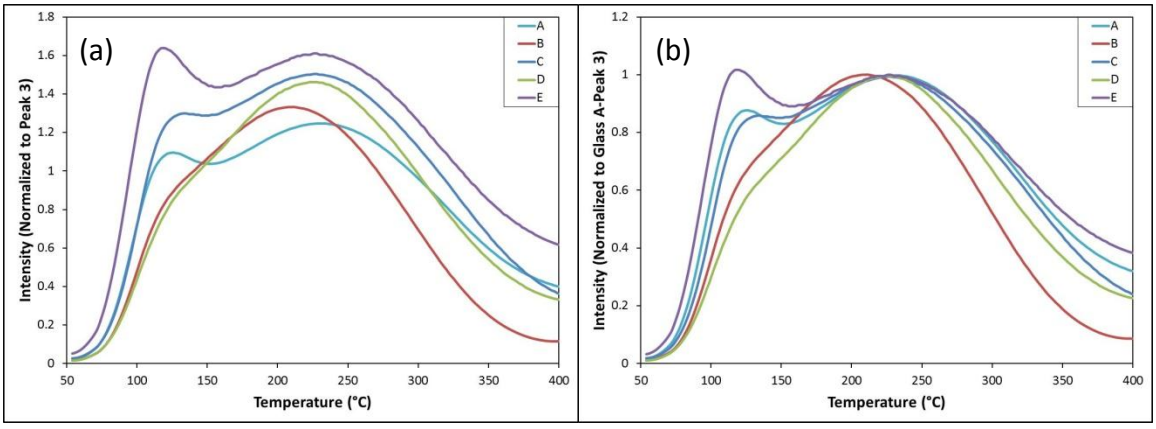

Figure 8-5: Resulting TL glow curves after normalizing the individual TL glow peaks to: (a) intensity of the deconvoluted Peak 3; and (b) intensity of the unseparated high temperature region.

Table 8-5: Peak ratios of the individual peaks after being normalized.

	Ratio to Peak 3					Ratio to Glass A Peak 3				
	Peak 1	Peak 2	Peak 3	Peak 4	Peak 5	Peak 1	Peak 2	Peak 3	Peak 4	Peak 5
A	0.589	0.360	1	0.557	0.356	0.589	0.360	1	0.557	0.356
B	0.416	0.696	1	0.433	0.031	0.368	0.614	0.883	0.382	0.027
C	0.727	0.976	1	0.653	0.351	0.539	0.724	0.742	0.484	0.260
D	0.413	0.901	1	0.579	0.271	0.319	0.694	0.771	0.446	0.209
E	1.031	1.066	1	0.749	0.526	0.719	0.743	0.697	0.522	0.367

8.5.1 Peak 1 (120°C)

With the calculated ratios, PLS was used to find elements that influenced the relative peak intensity of Peak 1 in the TL spectrum. The same method using VIP scores to systematically remove variables was again utilized. Models were created (Figure 8-6) that fit the peak ratios using barium, calcium, and magnesium (alkaline earth metals). A good fit (R^2 above 0.95) was not achieved with just 1 LV using method (1) of normalizing; however, a good fit was achieved with method (2). Both normalizing methods had good fits when 2 LVs were used. In these PLS models, the alkaline earths negatively influenced the peak ratio (increasing the concentration decreased the relative TL intensity of Peak 1). Combining this result with the PCA, the alkaline earths are good candidates to explain the difference in the shape of the observed TL glow curves.

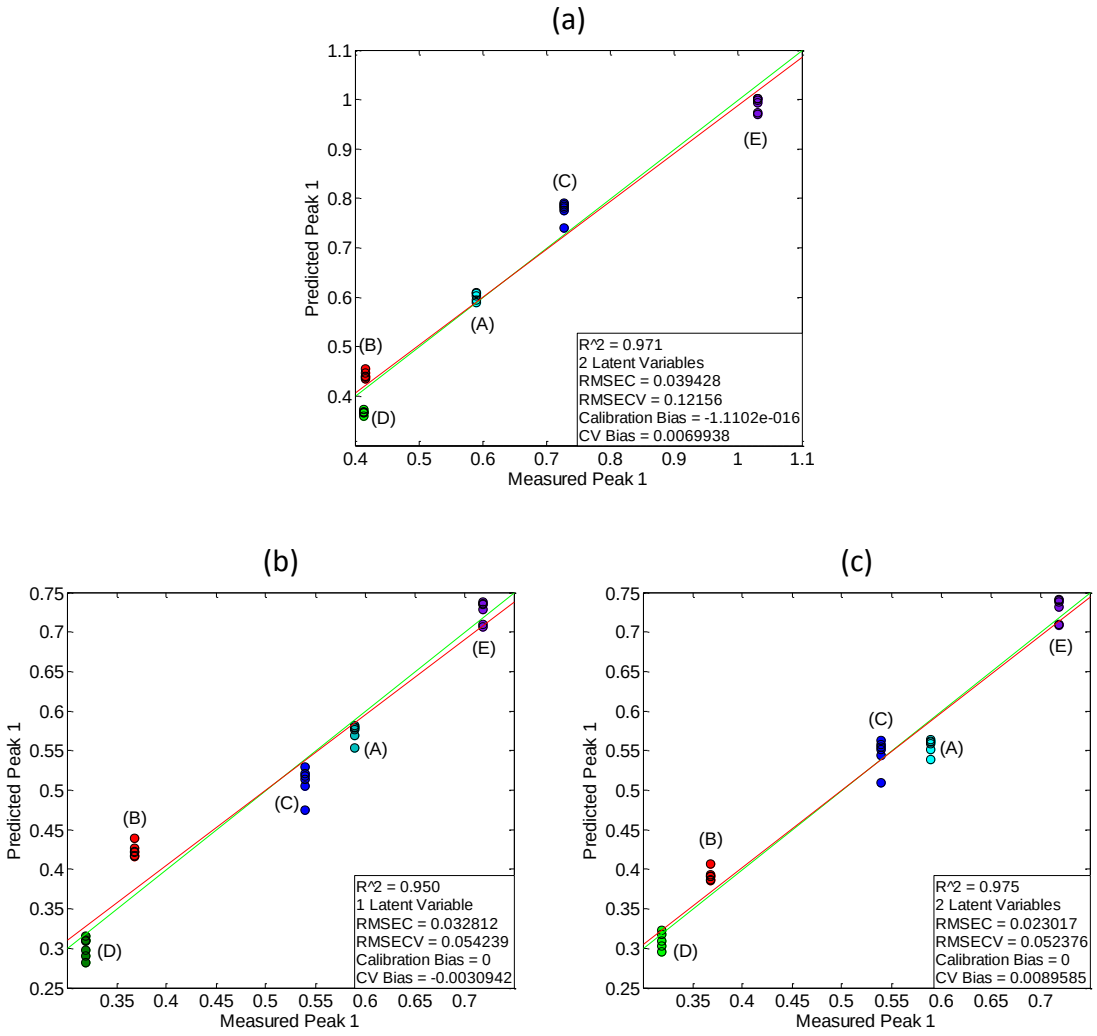

Figure 8-6: PLS models to predict the relative intensity of Peak 1 (120°C) using barium, calcium, and magnesium with: (a) 2 LVs normalized through method (1); (b) 1 LV normalized through method (2); and (c) 2 LVs normalized through method (2).

8.5.2 Peak 2 (160°C)

PLS was also used to find elements that influenced relative peak intensity of Peak 2 (160°C). As before, VIP scores were used to systematically remove variables. Models were created using 1 LV through both normalizing techniques (Figure 8-7). It was found that only cerium, potassium, and titanium were

needed to construct the model, and all of these variables had a negative influence on the peak ratio.

Though attempts were made at correlating the other peak ratios to elemental variables, efforts, thus far, have been unsuccessful (a fit with a R^2 above 0.95 and using less than 10 elements in the model).

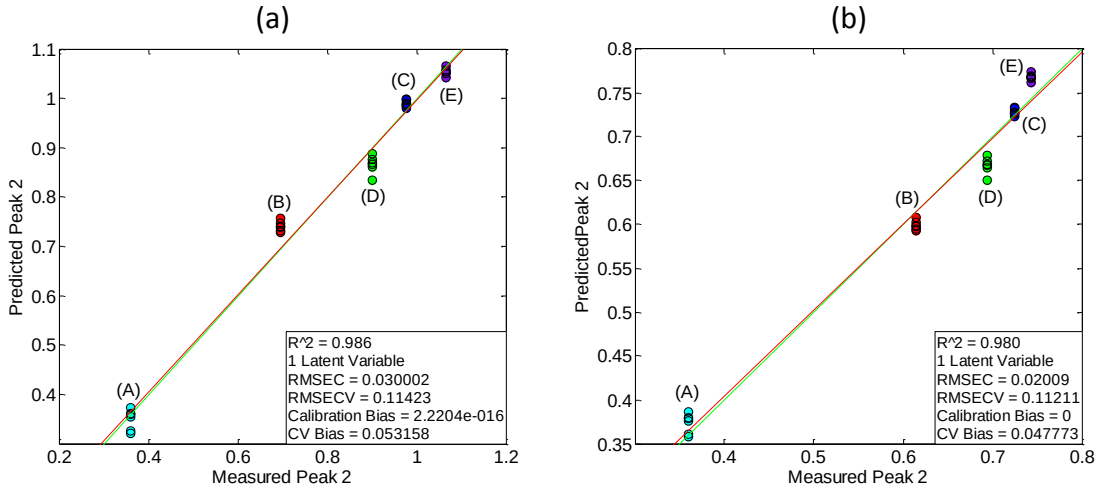

Figure 8-7: PLS models to predict the relative intensity of Peak 2 (160°C) using cerium, potassium, and titanium with 1 LV. Data was normalized through: (a) method (1); and (b) method (2).

Chapter 9

Conclusion and Suggestions for Future Work

9.1 Conclusion

In this work, the thermoluminescence (TL) properties and the processes that govern the TL properties of commercial borosilicate glass were explored. When irradiated with a gamma source (^{60}Co), all TL glow curves of borosilicate glass from the 5 studied geographical sources revealed a narrow, unstable low-temperature peak centered near 120°C and a broad, stable high temperature peak centered near 230°C. The TL glow curves of the different glasses could be separated into two classifications (Figure 5-5): (a) TL glow curve with two readily distinguished low- and high-temperature peaks, and (b) TL glow curve with low- and high-temperature peaks that are not resolved. These classifications could also be viewed as: (a) TL glow curve with a relative ratio of the low- to high-temperature peak approximately equal to 1, and (b) TL glow curve with a relative ratio of the low- to high-temperature peak equal to approximately 0.65. Irradiations using beta and x-ray sources revealed similar TL properties when normalized for dose rate. When compared with these irradiation sources (gamma, beta, and x-ray), UV irradiations showed TL glow curves with only one readily observable peak due to a much more intense low-temperature peak. This suggests that mechanisms controlling radiation induced defect formation from gamma, beta, x-ray, and UV sources

may be similar, but the population of specific electron/hole traps differs based upon type of ionizing radiation.

Further analysis revealed that all of the glow curves could be separated into the same TL peaks centered at 120, 165, 225, 285, and 360°C with parameters as reported in Table 6-3. These five peaks could be used to reproduce the observed glow curves regardless of geographical source, irradiation source, or time post-irradiation by only changing the peak intensities. This supports the hypothesis that the mechanisms involved in the production of the TL curves are the same for all the glasses studied, but the relative intensity of each mechanism varies between the glasses.

The limit of quantification (LOQ) of the thermoluminescence signal was determined to be 0.002 nA/mg. This equates to an absorbed dose, or Minimum Measurable Dose (MMD), of 0.15-0.5 Gy depending on the borosilicate glass source. The MMD is roughly equivalent to the dose that a 48-160 ng source of ^{60}Co would deliver to a borosilicate sample in 24 hr if it was placed 1 cm from the sample.

Electron paramagnetic resonance (EPR) results showed production of boron oxygen hole centers (BOHCs) and E'-defect centers (network defects). Following the decay of the EPR signal of the BOHC revealed initial decay rates that were approximately equal to the observed 120°C TL peak (Peak 1) decay rate (Table 7-1) in all the studied glasses. This suggests that the BOHC is involved in the recombination process occurring during TL measurement of Peak 1. However, since the BOHC signal decay nearly ceases, it is likely a trapped electron that is recombining with a trapped BOHC. At

approximately 14 days post-irradiation, this trapped electron species has "completely" recombined. EPR results for the different glasses also showed that approximately the same number of BOHC is created per dose regardless of the glass source. This means that the formation of BOHC alone cannot explain the different response in the overall intensity of the TL glow curves in borosilicate glass from different regions.

Using partial least squares (PLS) regression, a positive correlation was found between the overall TL glow curve intensity and the concentration of potassium and cerium in the glass. To remove the overall intensity factor, TL glow curves were normalized, and the ratio of individual peaks to Peak 3 (225°C) were examined. After being normalized, analysis of the glasses using PLS revealed a negative correlation between the relative intensity of Peak 1 (120°C) and the concentration of the alkaline earth metals (magnesium, calcium, and barium) present in the glass. Analysis using PLS also revealed a negative correlation between the relative intensity of Peak 2 (165°C) and the concentration of potassium, cerium, and titanium present in the glass.

Overall, this work showed that the studied ionizing radiation (gamma, beta, x-ray, and UV) imparted a stable, measureable TL signal to all the studied commercial borosilicate glasses. This signal would be sufficient for calculations of residence time. The ionizing radiation also imparted an unstable TL signal which could potentially be beneficial for intrinsic dosimetry calculations of residence time, sample splitting, and amount of material that once resided in an empty container. Hypothetical scenarios of some of these calculations are described below.[26-27] The study also increased the

understanding of the mechanisms driving the TL processes by correlating a specific trap to a TL glow peak. Correlations were also found between the TL properties (signal shape and intensity) and composition. Additional probing of these relationships could provide additional understanding of the underlying TL mechanisms.

9.1.1 Residence Time

A 5 cm^3 borosilicate vial containing 550 mg of ^{137}Cs oxide solid has been discovered by cleanup crews at a disposal site. A small section of the vial was interrogated by TL dosimetry. The 225°C glow peak indicated the glass wall had received a total dose of 1.6E7 R. Based upon the amount of ^{137}Cs found in the container, the dose rate to the small section of the container wall was estimated to be 1.5E5 R h^{-1}. At this rate, the time required for accumulating the measured absorbed dose on the interrogated section of glass, or the time the material was assumed to reside in the glass prior to discovery, was estimated to be approximately 100 days.

9.1.2 Sample Splitting

Assuming the same container of Cs in scenario 1 was interdicted by investigators and all other aspects of scenario 1 are constant, except only 250 μg, instead of 550 mg, of ^{137}Cs oxide from the container was recovered, the time since the material was placed in the vial would have been estimated to be approximately 600 years. In this case, the extreme length of time would indicate a large portion of the material was removed at some point during transit.

9.2 Suggestions for Future Work

This research has probed the TL properties of commercial borosilicate glass with similar composition to commercial borosilicate containers. Analysis has focused on evaluating the properties of the observed TL glow peaks and the recombination processes that control them. To further the understanding of the recombination mechanisms of each TL glow peak and the factors that control the relative intensity of each peak as well as the overall TL intensity, several additional investigations are proposed.

9.2.1 Fractional Glow Technique

Using computerized glow curve deconvolution software, an estimate of each of the separated TL glow peak parameters was found (Table 6-3). These parameters should only be taken as initial estimates as the software undergoes iterations to find the best fit to the experimental glow curve within given restraints. When TL glow peaks are well separated, many techniques can be employed to experimentally determine the peak parameters.[8, 12, 267] However, when the peaks are closely overlapping, methods are limited.[8] One technique that could potentially determine the trap depth (E) of overlapping peaks was developed by Gobrecht and Hofmann and is known as the 'fractional glow technique'.[339]

In the fractional glow technique, the thermoluminescence glow curve of a sample is analyzed by repeated heating and cooling cycles where each heating

cycle is increased by only a few degrees. This process is similar to the T_m-T_{stop} method (Section 5.4), but without analysis of the entire TL glow curve and the same sample is used throughout the analysis. If the temperature is raised by only a few degrees there will be very little change in the number of trapped electrons (n) during heating. Thus, if the TL intensity is monitored during the cooling and heating cycles, there will be little difference in intensity between the two cycles. By repeatedly heating and cooling the sample in small cycles, the average trap depth (E) being emptied during each temperature cycle may be determined from the slope of the heating and cooling curves.[8, 339]

The main problems with this technique are experimental. For the best results, the heating rate should be quite high to give a short cycle interval in order to ensure that only a few traps are affected. This requires there to be excellent thermal contact between the sample and the heating strip. The form of the sample also needs to be considered as a thermal gradient may be induced across the sample at higher heating rates.[8] The technique also generates enormous amounts of data which would require computerized handling procedures.[8, 339, 367] Additionally, the software controlling the Harshaw 3500 TL Reader has limited control of heating and does not have the option to monitor the thermoluminescence output during the cooling cycle. To employ this method, alterations to the instrument/software would need to be made.

9.2.2 Analysis of Thermoluminescence Wavelength

The Harshaw 3500 TL Reader uses a photomultiplier tube (PMT) sensitive to light output in the 280-630 nm spectral range.[292] However, in the recorded TL glow curve, there is no distinguishing between the emitted wavelengths. As suggested by Levy et al.[368] and Mattern et al.,[369] simultaneous analysis of the spectrum of the wavelength emitted and the total thermoluminescence could provide information of the traps involved in the recombination processes. To perform this analysis, alterations to the Harshaw 3500 TL Reader would need to be made, or a new TL reader would need to be built. The analysis would involve insertion of an additional instrument (such as a spectrometer) between the sample and the PMT.[370-371]

9.2.3 Investigation of Multivalent Traps

In studies using electron paramagnetic resonance (EPR) spectroscopy to study the electron/hole traps created in the glass, a single EPR peak near 1650 G was observed (Figure 7-1). This EPR peak has been connected with Fe^{3+} ions in glass.[174, 190, 349-352] At the radiation doses used in this study, no significant change was observed in this signal as a result of ionizing radiation or time post-irradiation. A more detailed study focused solely on this signal could connect the iron multivalent traps to the observed TL peaks.

9.2.4 EPR Investigations Following Successive Heating Cycles

The T_m-T_{stop} method (Section 5.4) is a technique that can estimate both the number and position of individual TL glow peaks within a complex glow curve.[8, 12, 323] This idea could be applied to EPR to connect individual electron/hole traps to the TL glow peaks. In Section 7.3, it was shown that the EPR signal from 3250-3400 G was greatly reduced after samples were heated to 400°C at 5°C/sec followed by rapid cooling. In addition, there was almost complete destruction of the valley near 3510 G (Figure 7-4) which has been connected to the E'-defect center (network defect).[230, 358] By monitoring the EPR signal after incremental heating and cooling cycles, the decay of these peaks in relation to each other could potentially give further insights into the TL recombination processes that are occurring.

9.2.5 Glass Composition

In Chapter 8, multivariate statistical methods were used to find correlations between elemental concentrations and overall TL glow curve intensity and TL glow peak ratios. The analysis was limited by the compositional variation from the commercial borosilicate glasses. Though some variation existed and potential connections were found, competing compositional changes make it difficult to identify TL response due to individual elemental variation. To better understand the effect on TL response due to compositional changes, control over the glass manufacturing processes would be needed. Future

experimentation should include synthesizing glass in the laboratory and analyzing the effects on TL response by changing the concentration of individual elements. The important elements identified through principal component analysis (PCA) and partial least squares (PLS) regression should be used as starting point of this experimentation.

9.2.6 Manufacturing Conditions

In addition to the suggested future work above involving glass composition, analysis of the effects on TL response due to manufacturing conditions should also be explored. The ratio of the oxidative states of multivalent ions is controlled by the manufacturing procedure (reductive vs. oxidative environment).[148-152] As these are potential electron/hole traps, the manufacturing procedure could have an impact on the observed TL.

In addition to the manufacturing conditions, other manufacturing processes could have an impact on the TL signal and need to be explored. After a glass bottle (or other product) is formed, it is generally reheated to a specified temperature (annealed) and cooled down at controlled temperatures.[308, 372-374] This process is used to eliminate areas of stress in the glass to strengthen it.[374-375] Depending on the procedure used, the amount of intrinsic defects, and available electron/hole traps, in the glass could be altered.

LIST OF APPENDIX FIGURES

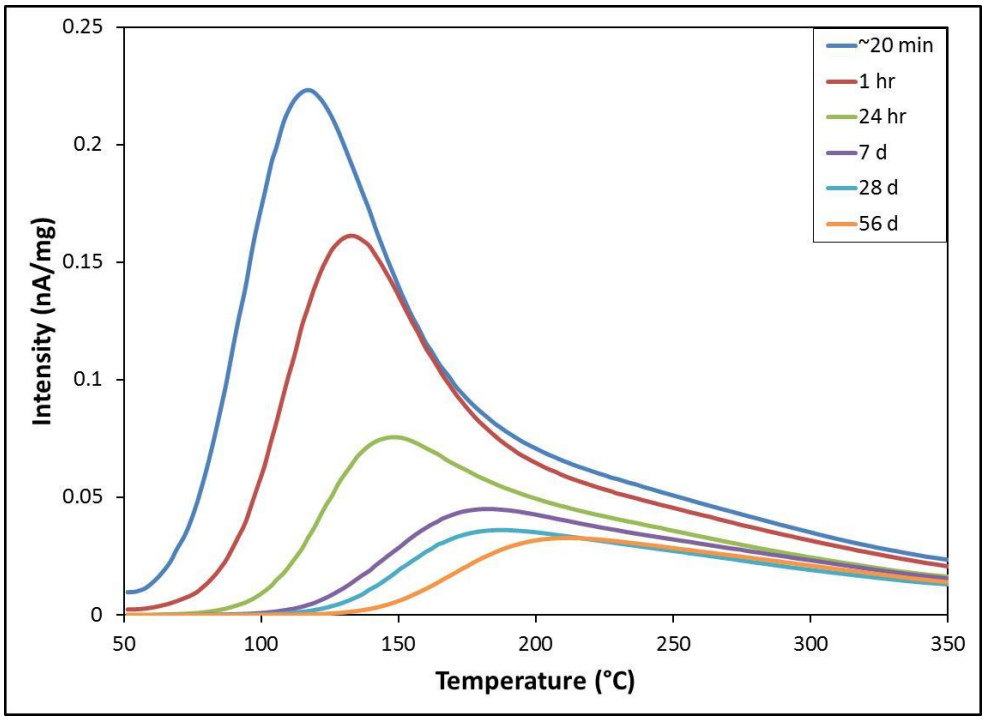

Figure A-1: Glow curves for Glass A samples at 20 min, 1 hr, 24 hr, 7 d, 28 d, and 56 d after being irradiated with a 254nm UV-Lamp for 30 min.

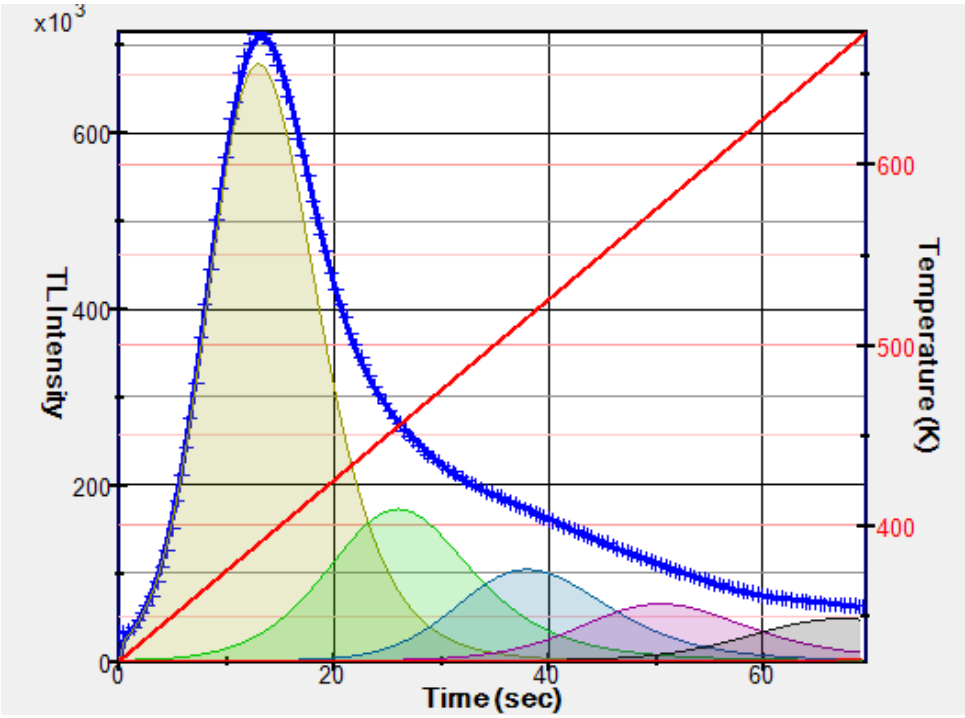

Figure A-2: Deconvoluted glow curve for Glass A samples approximately 20 min after being irradiated with a 254nm UV-Lamp for 30 min.

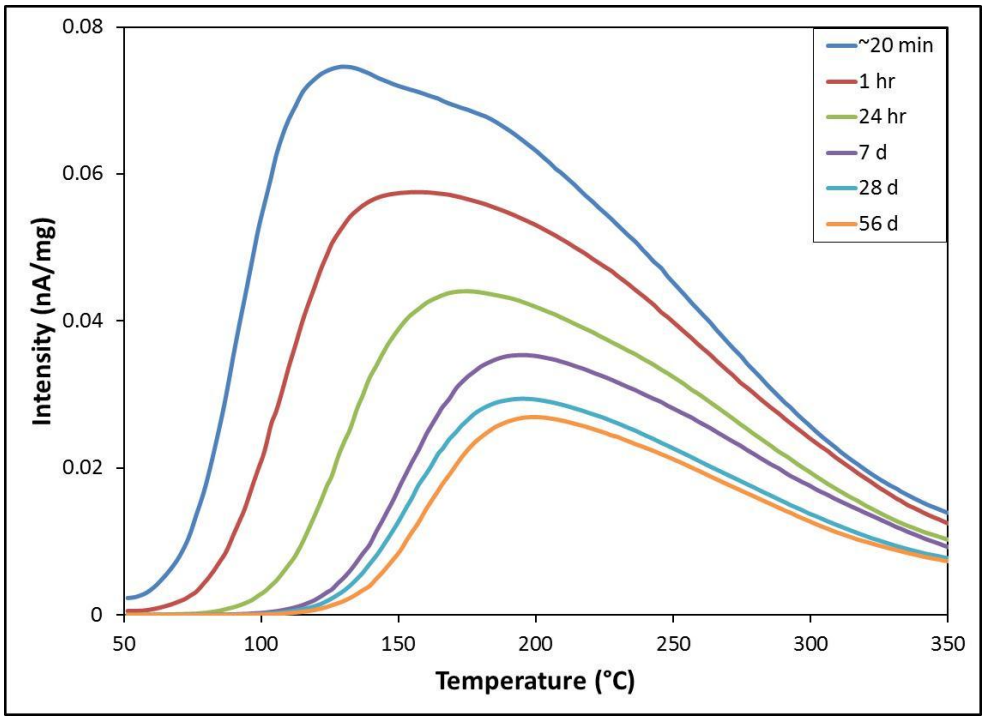

Figure A-3: Glow curves for Glass B samples at 20 min, 1 hr, 24 hr, 7 d, 28 d, and 56 d after being irradiated with a 254nm UV-Lamp for 30 min.

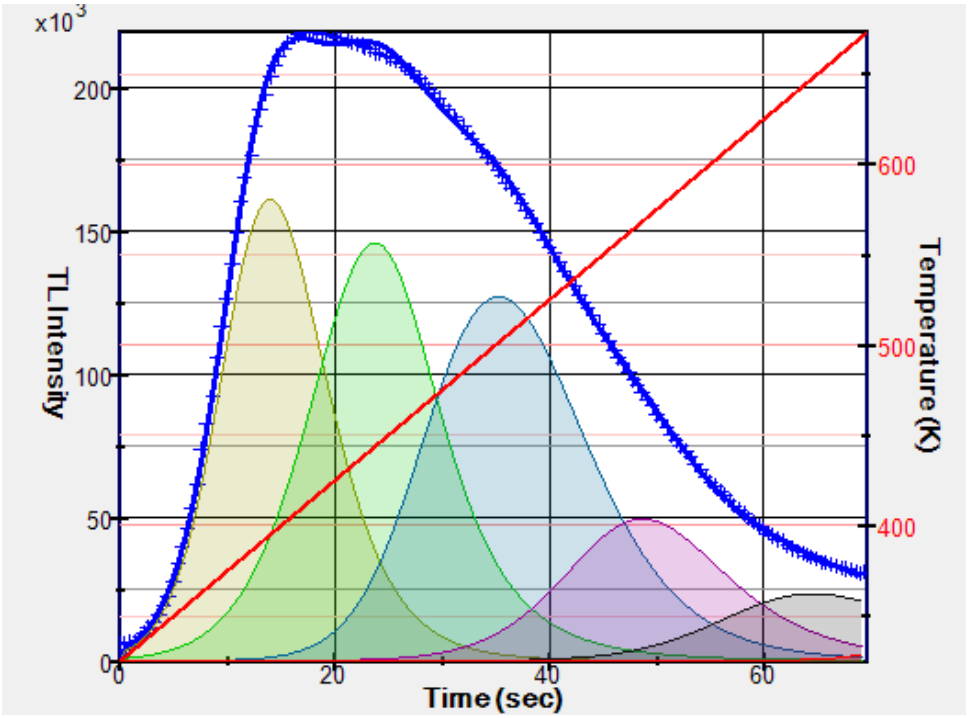

Figure A-4: Deconvoluted glow curve for Glass B samples approximately 20 min after being irradiated with a 254nm UV-Lamp for 30 min.

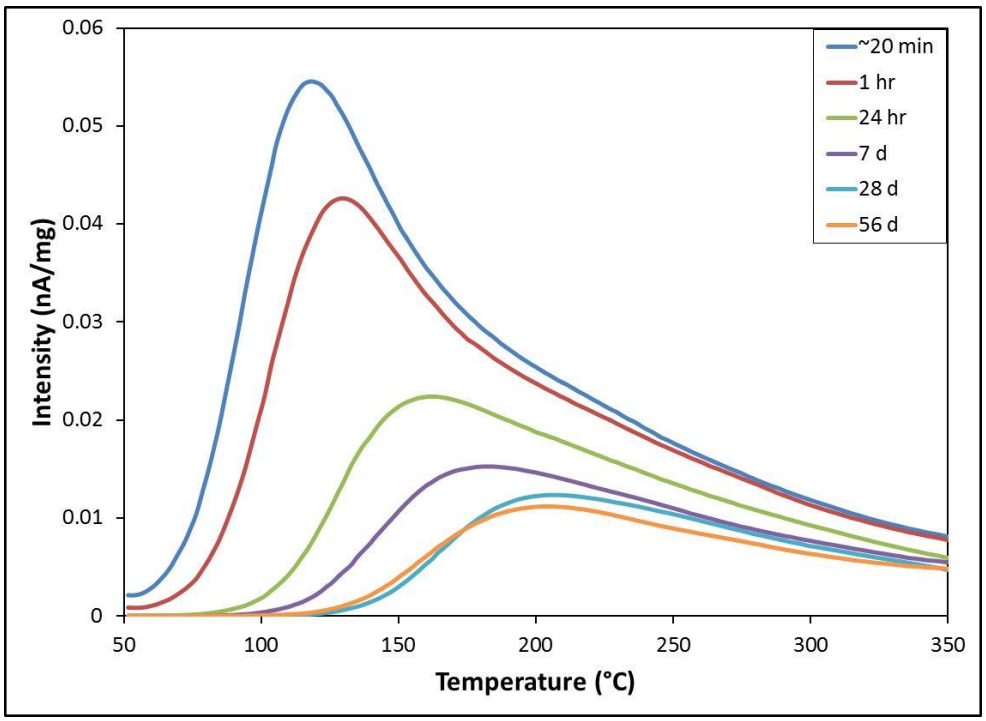

Figure A-5: Glow curves for Glass C samples at 20 min, 1 hr, 24 hr, 7 d, 28 d, and 56 d after being irradiated with a 254nm UV-Lamp for 30 min.

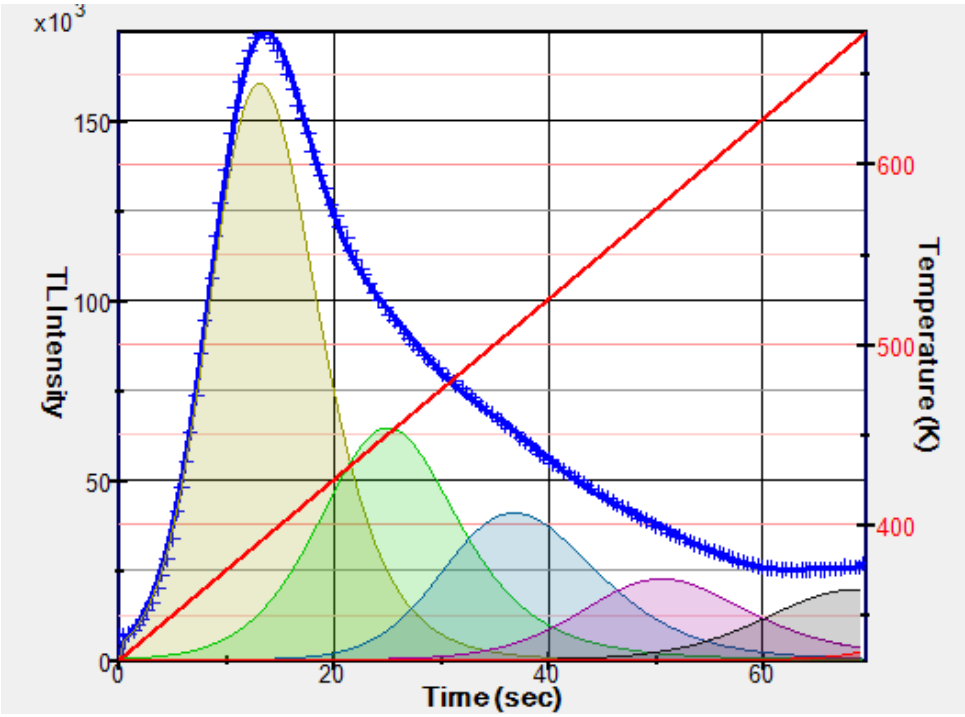

Figure A-6: Deconvoluted glow curve for Glass C samples approximately 20 min after being irradiated with a 254nm UV-Lamp for 30 min.

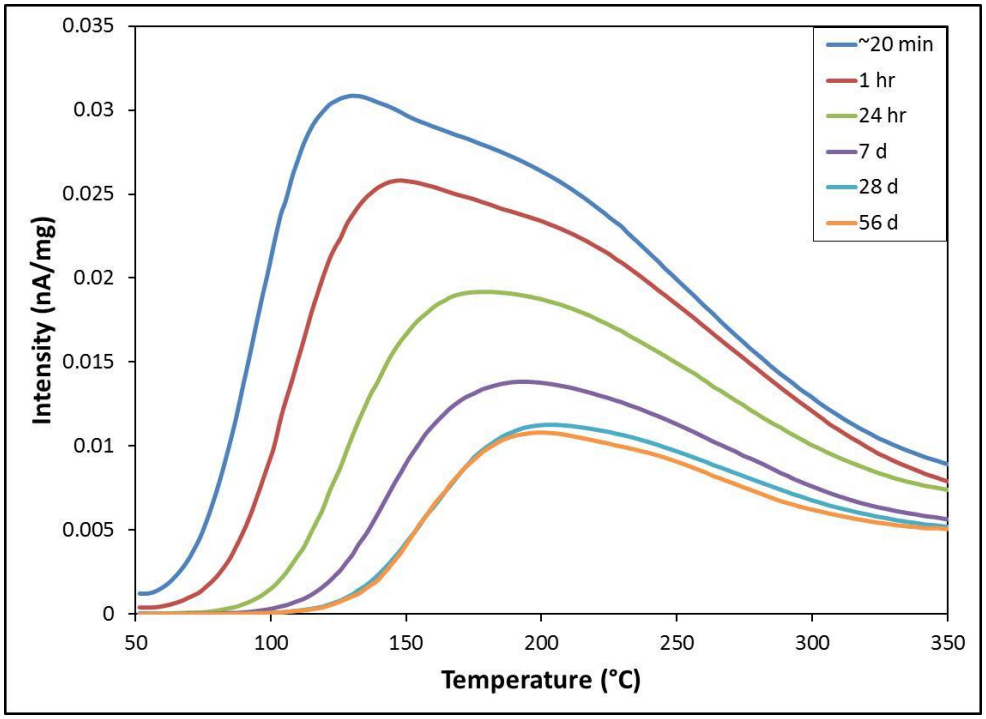

Figure A-7: Glow curves for Glass D samples at 20 min, 1 hr, 24 hr, 7 d, 28 d, and 56 d after being irradiated with a 254nm UV-Lamp for 30 min.

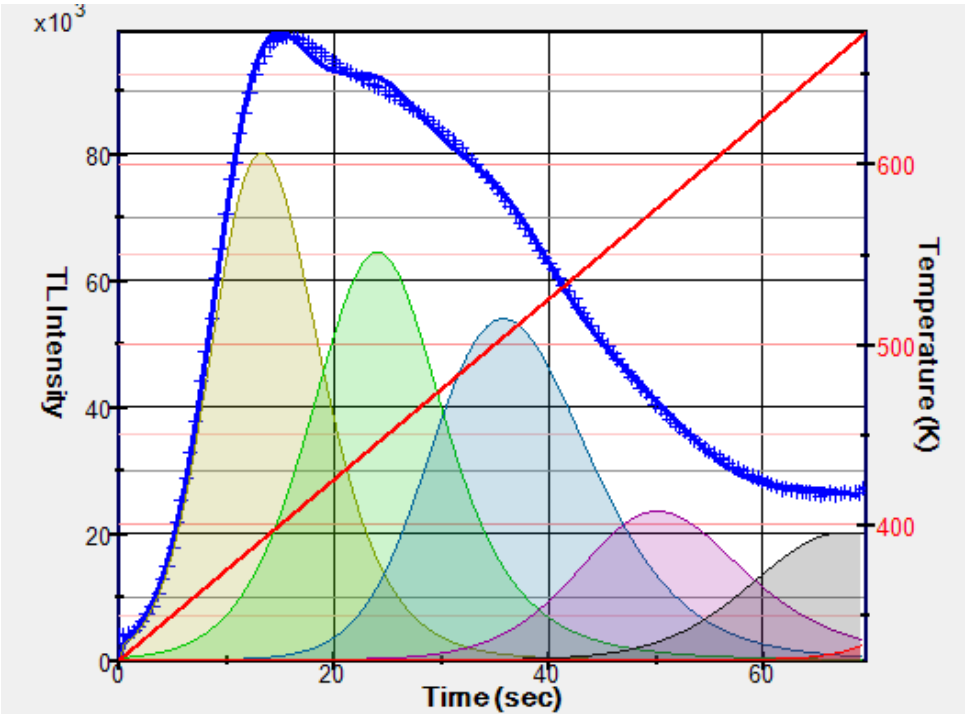

Figure A-8: Deconvoluted glow curve for Glass D samples approximately 20 min after being irradiated with a 254nm UV-Lamp for 30 min.

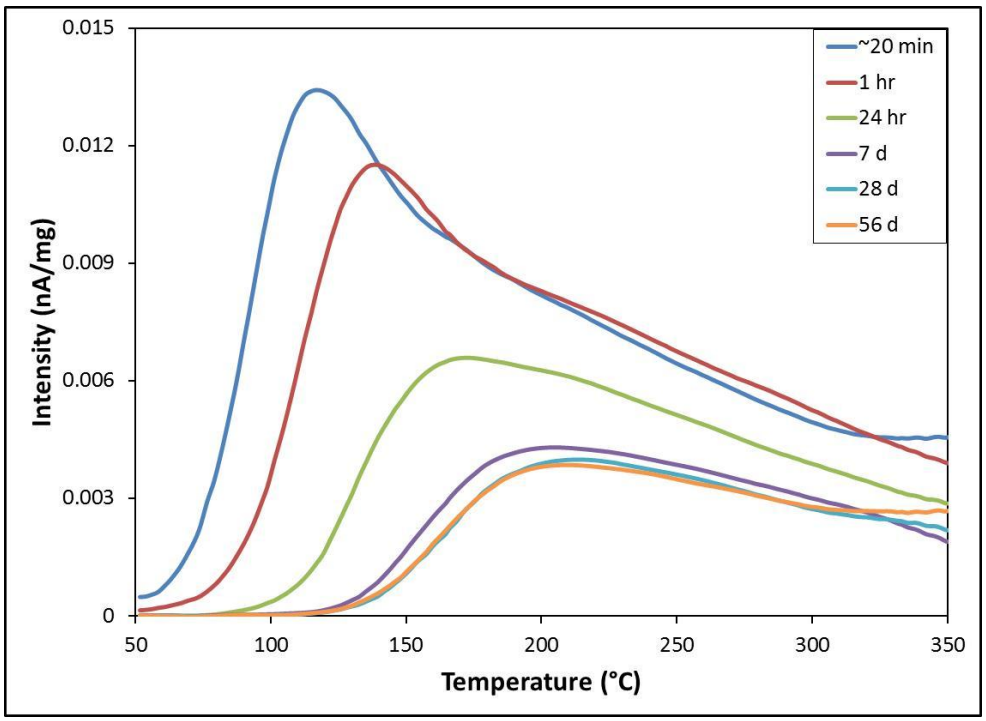

Figure A-9: Glow curves for Glass E samples at 20 min, 1 hr, 24 hr, 7 d, 28 d, and 56 d after being irradiated with a 254nm UV-Lamp for 30 min.

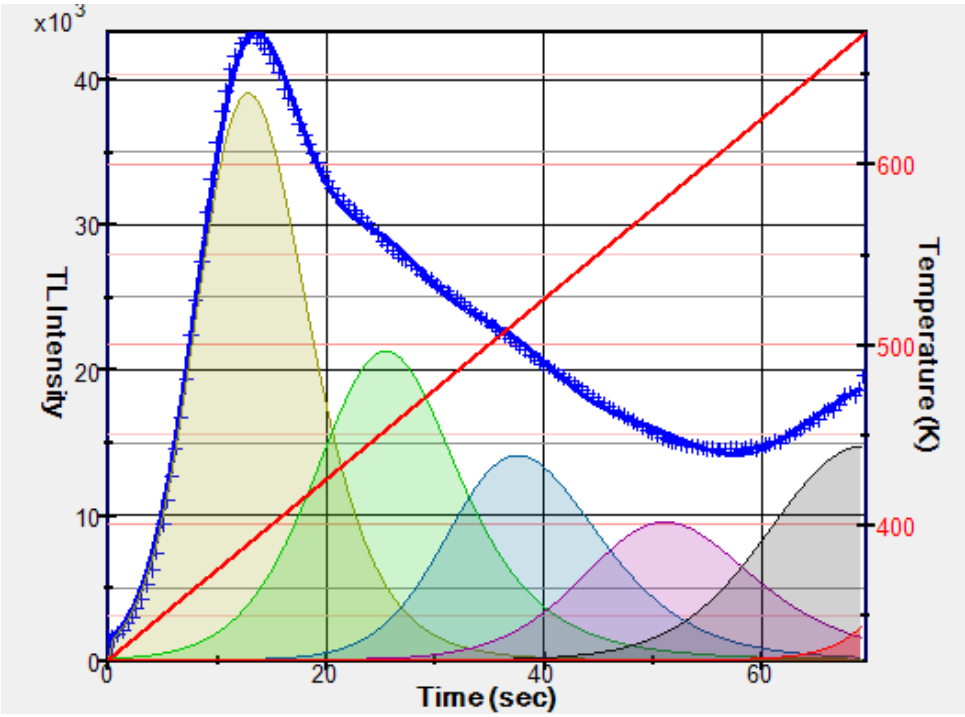

Figure A-10: Deconvoluted glow curve for Glass E samples approximately 20 min after being irradiated with a 254nm UV-Lamp for 30 min.

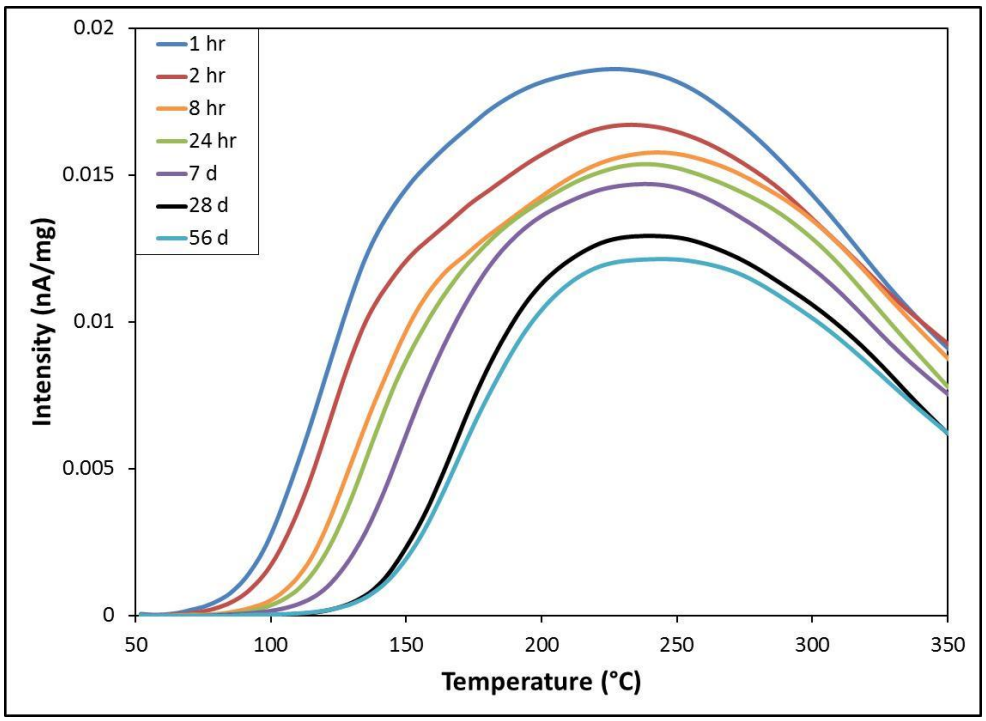

Figure A-11: Glow curves for Glass A samples at 1 hr, 2 hr, 8 hr, 24 hr, 7 d, 28 d, and 56 d after receiving a total dose of 1.5 Gy from a ^{137}Cs source at 0.1 Gy/hr.

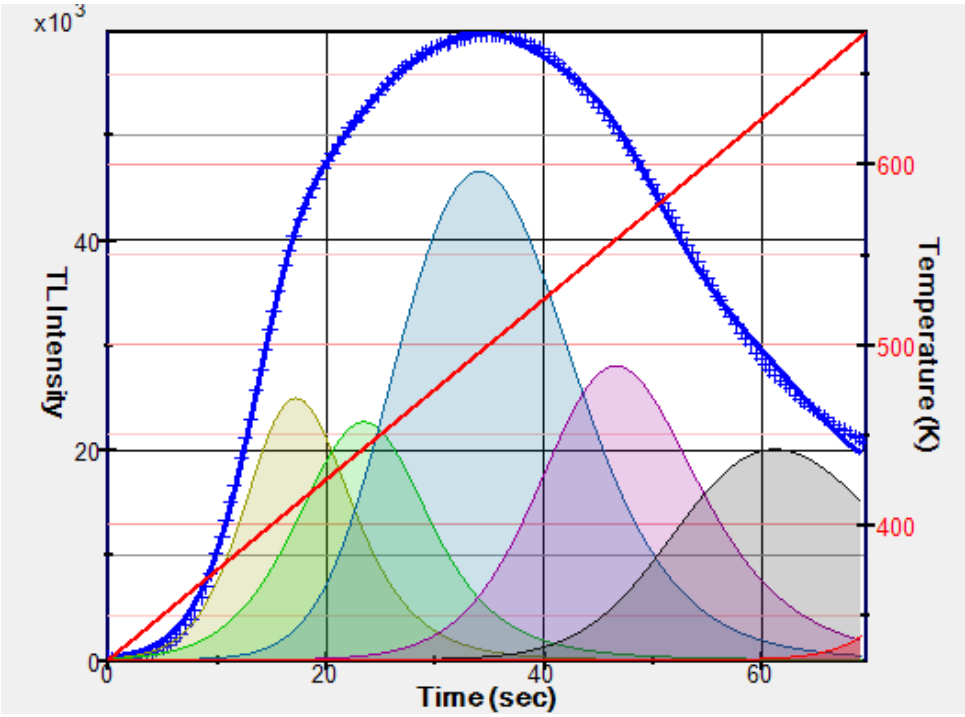

Figure A-12: Deconvoluted glow curve for Glass A samples at 1 hr after receiving a total dose of 1.5 Gy from a ^{137}Cs source at 0.1 Gy/hr.

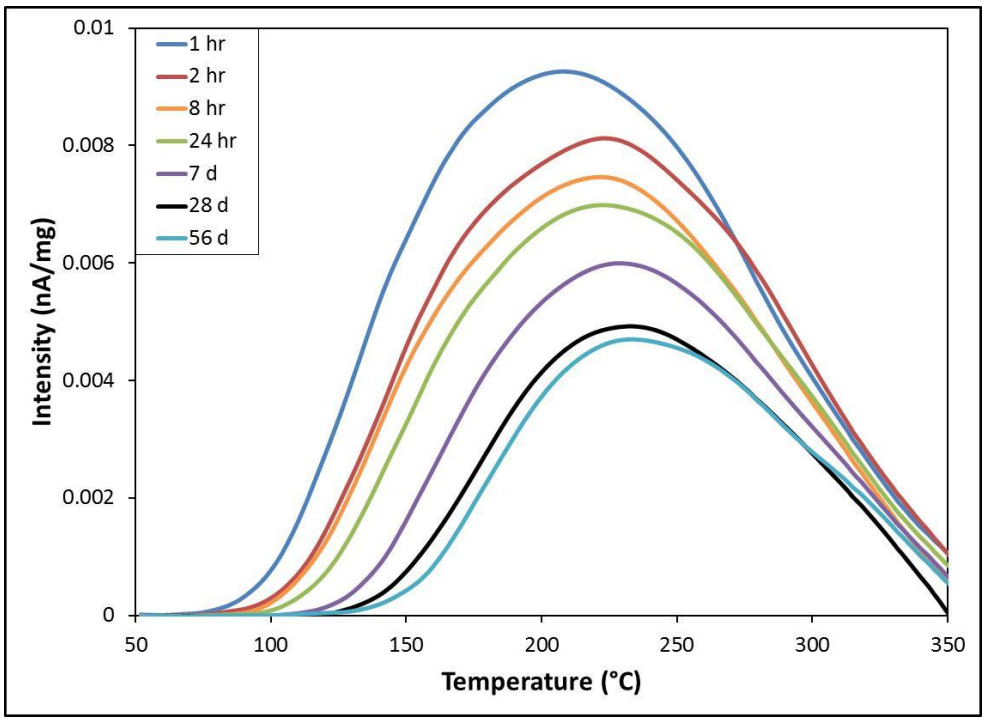

Figure A-13: Glow curves for Glass B samples at 1 hr, 2 hr, 8 hr, 24 hr, 7 d, 28 d, and 56 d after receiving a total dose of 1.5 Gy from a ^{137}Cs source at 0.1 Gy/hr.

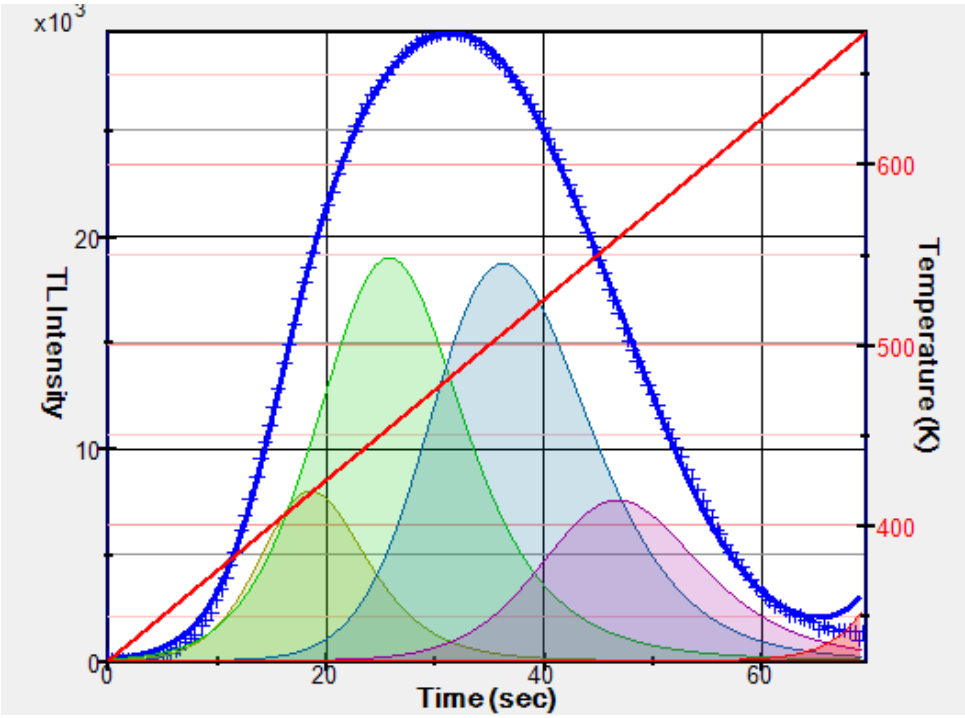

Figure A-14: Deconvoluted glow curve for Glass B samples at 1 hr after receiving a total dose of 1.5 Gy from a ^{137}Cs source at 0.1 Gy/hr.

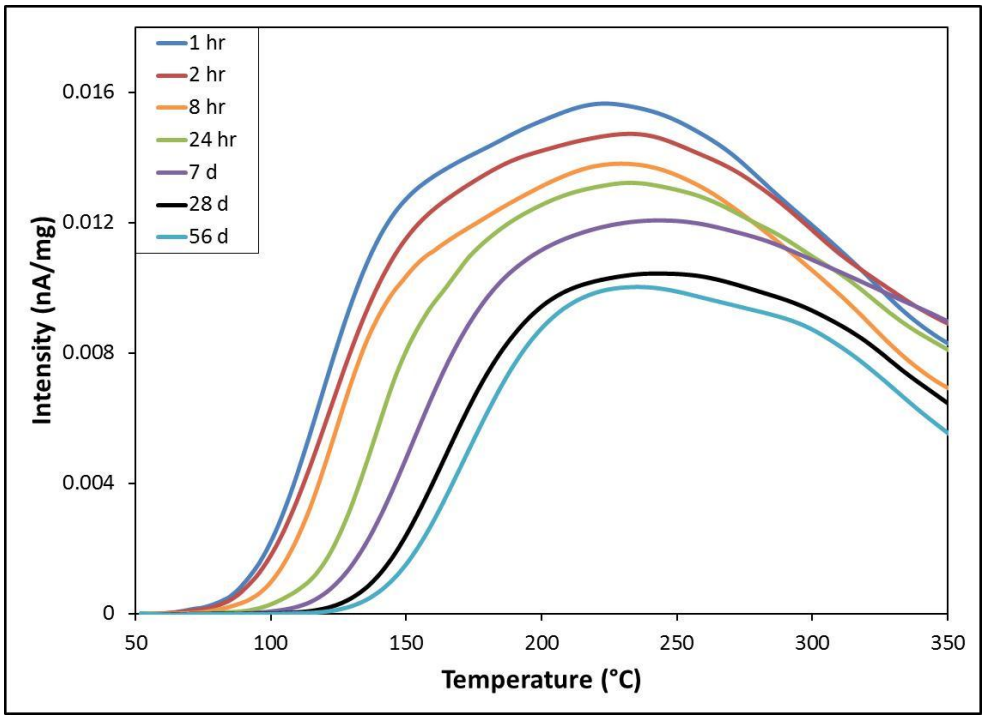

Figure A-15: Glow curves for Glass A samples at 1 hr, 2 hr, 8 hr, 24 hr, 7 d, 28 d, and 56 d after receiving a total dose of 1.5 Gy from a $^{90}Sr/^{90}Y$ source at 0.1 Gy/hr.

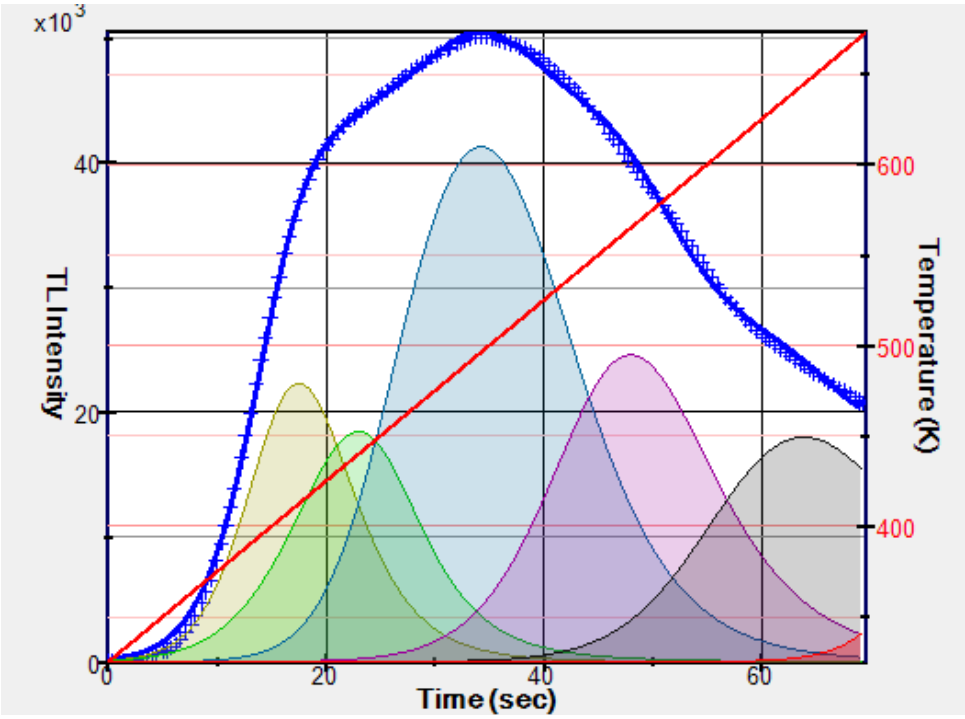

Figure A-16: Deconvoluted glow curve for Glass A samples at 1 hr after receiving a total dose of 1.5 Gy from a $^{90}Sr/^{90}Y$ source at 0.1 Gy/hr.

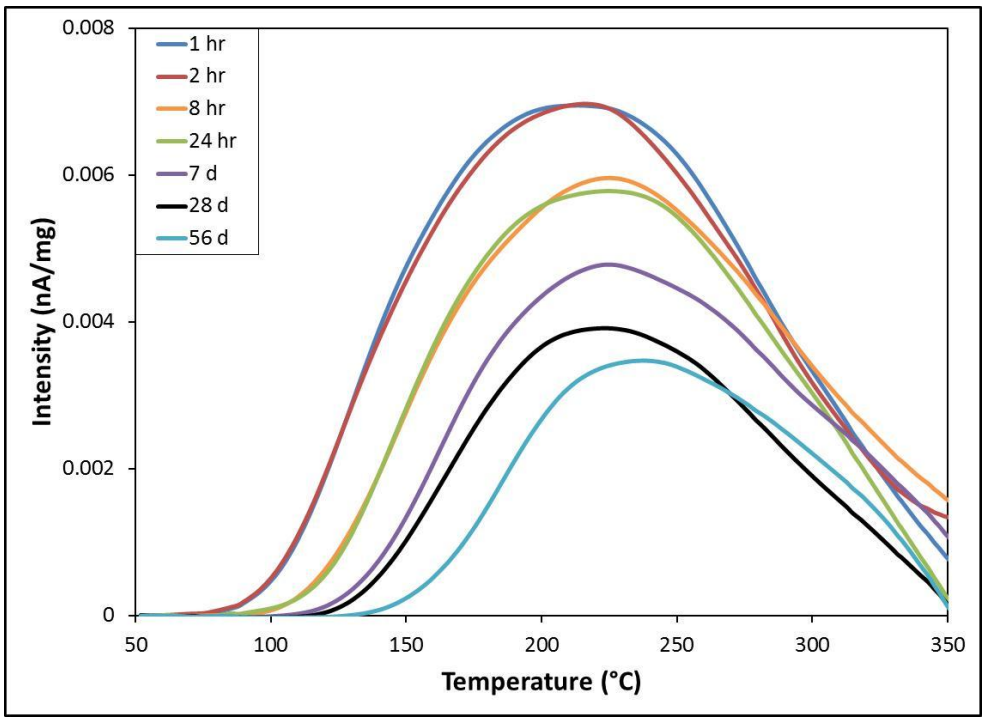

Figure A-17: Glow curves for Glass B samples at 1 hr, 2 hr, 8 hr, 24 hr, 7 d, 28 d, and 56 d after receiving a total dose of 1.5 Gy from a $^{90}Sr/^{90}Y$ source at 0.1 Gy/hr.

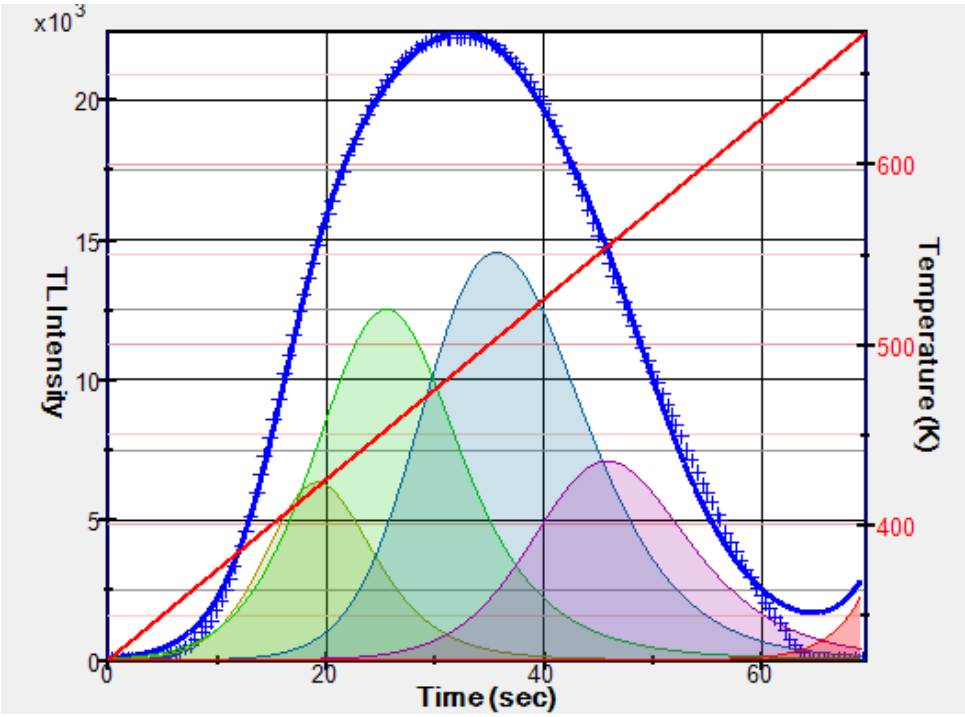

Figure A-18: Deconvoluted glow curve for Glass B samples at 1 hr after receiving a total dose of 1.5 Gy from a $^{90}Sr/^{90}Y$ source at 0.1 Gy/hr.

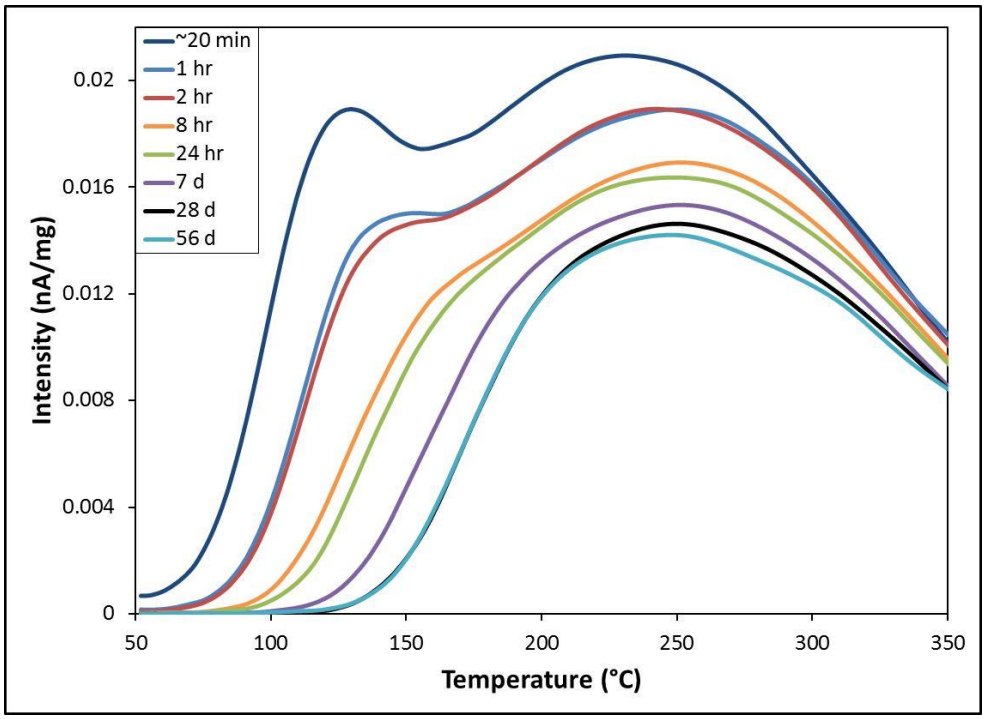

Figure A-19: Glow curves for Glass A samples at 20 min, 1 hr, 2 hr, 8 hr, 24 hr, 7 d, 28 d, and 56 d after receiving a total dose of 1.5 Gy from 14 keV x-rays at 4.3 Gy/hr.

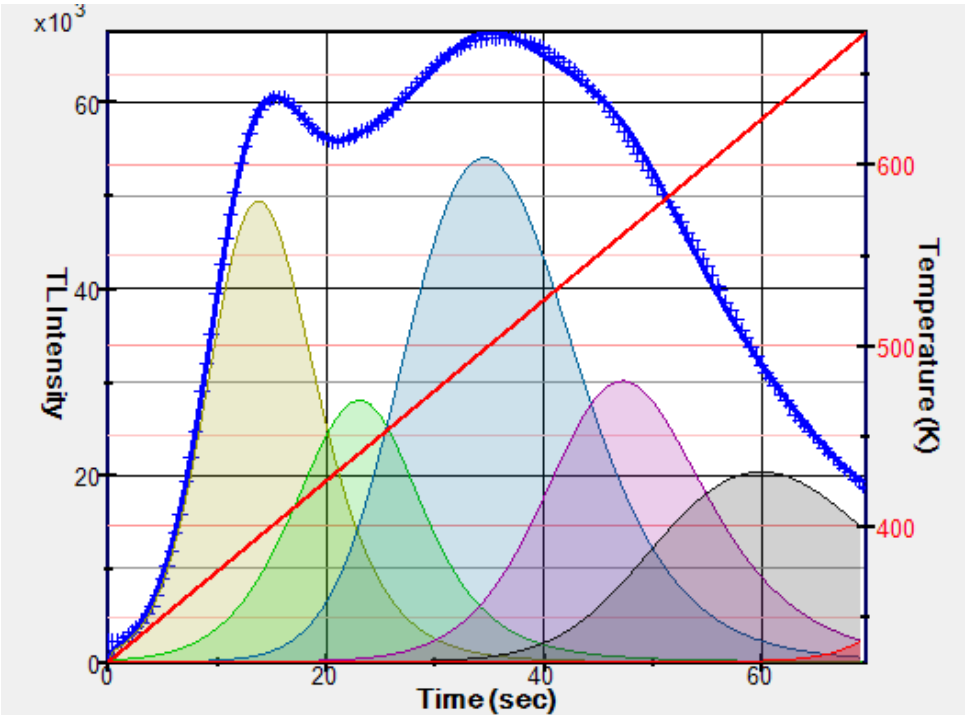

Figure A-20: Deconvoluted glow curve for Glass A samples approximately 20 min after receiving a total dose of 1.5 Gy from 14 keV x-rays at 4.3 Gy/hr.

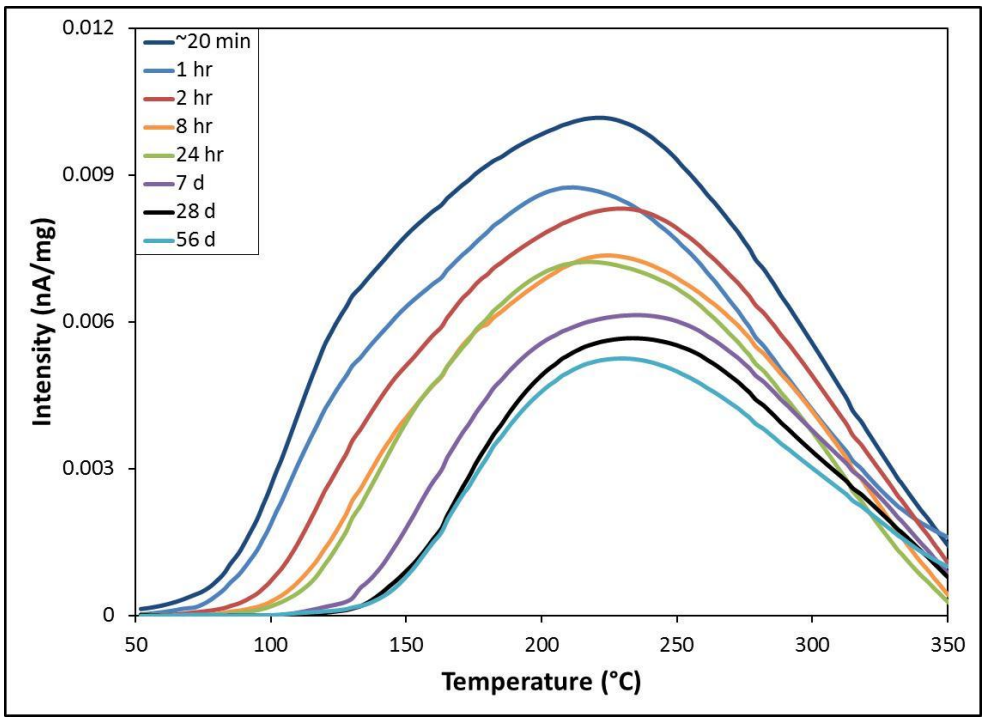

Figure A-21: Glow curves for Glass B samples at 20 min, 1 hr, 2 hr, 8 hr, 24 hr, 7 d, 28 d, and 56 d after receiving a total dose of 1.5 Gy from 14 keV x-rays at 4.3 Gy/hr.

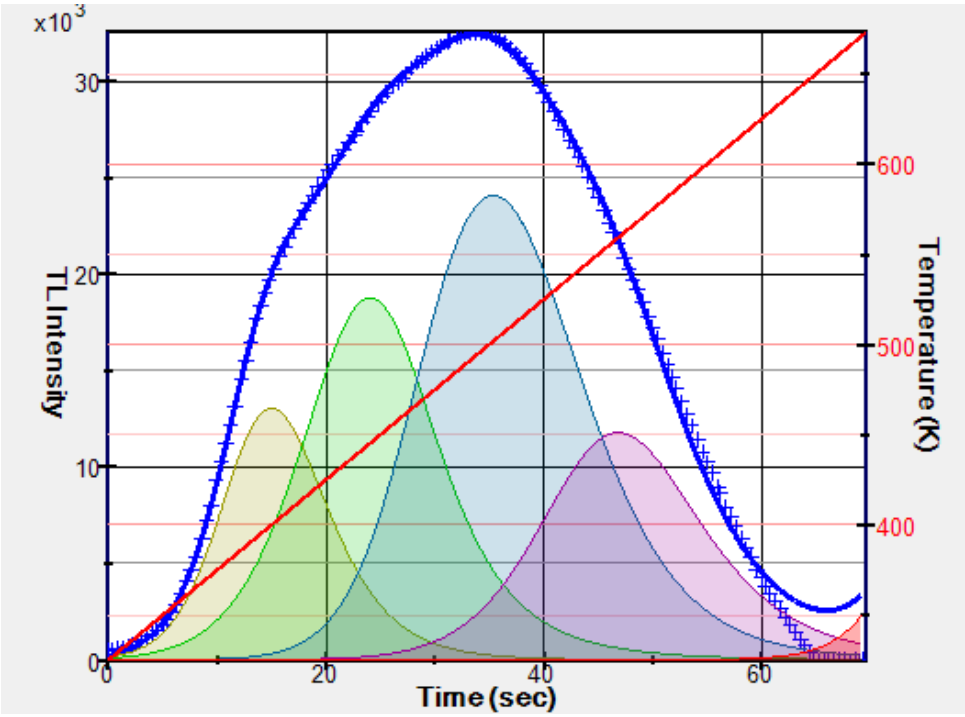

Figure A-22: Deconvoluted glow curve for Glass B samples approximately 20 min after receiving a total dose of 1.5 Gy from 14 keV x-rays at 4.3 Gy/hr.

BIBLIOGRAPHY

1. MacNeill, K. R., *Recycling waste streams using glass making activities*, In Proceeding of Contaminated Land: Policy, Regulation, and Technology, London, UK, IBC Technical Services: 1991.

2. Moody, K. J.; Hutcheon, I. D.; Grant, P. M., *Nuclear Forensic Analysis*. Taylor and Francis: New York, 2005.

3. Schwantes, J. M.; Douglas, M.; Bonde, S. E.; Briggs, J. D.; Farmer, O. T.; Greenwood, L. R.; Lepel, E. A.; Orton, C. R.; Wacker, J. F.; Luksic, A. T., Nuclear archeology in a bottle: Evidence of pre-trinity U.S. weapons activities from a waste burial site. *Analytical Chemistry* **2009,** *81*, 1297-1306.

4. Schmid, A. P.; Spencer-Smith, C., Illicit radiologival and nuclear trafficking, smuggling and security incidents in the black sea region since the fall of the iron curtain - an open source inventory. *Perspectives on Terrorism* **2012,** *6*, 117-157.

5. Lutze, W.; Ewing, R. C., *Radioactive Waste Forms for the Future*. Elsevier: New York, 1988.

6. Lohmann, W.; Kesternich, W., *On the possibility of using amorphous metals in high radiation environments*, In Effects of Radiation on Materials: Eleventh Conference, Brager, H. R.; Ferrin, J. S., Eds. 1982; pp 779-798.

7. Mott, N. F.; Davies, E. A., *Electronic Processes in Non-crystalline Materials*. Clarendon Press: Oxford, 1979.

8. McKeever, S. W. S., *Thermoluminescence of Solids*. Cambridge University Press: Cambridge, 1985.

9. Zarzycki, J., *Glasses and the Vitreous State*. Cambridge University Press: Cambridge, 1991.

10. Chen, R.; McKeever, S. W. S., *Theory of Thermoluminescence and Related Phenomena*. World Scientific Publishing Co. Pte. Ltd.: River Edge, New Jersey, 1997.

11. Horowitz, Y. S., *Thermoluminescence and Thermoluminescent Dosimetry*. CRC Press: Boca Raton, 1984; Vol. 1.

12. Furetta, C., *Handbook of Thermoluninescence*. World Scientific Publishing Co. Pte. Ltd.: River Edge, New Jersey, 2003.

13. Huntley, D. J.; Godfrey-Smith, D. I.; Thewalt, M. L. W., Optical dating of sediments. *Nature* **1985,** *313*, 105-107.

14. Wertz, J. E.; Bolton, J. R., *Electron Spin Resonance: Elementary Theory and Practical Applications*. Chapman and Hall: New York, 1972.

15. Aitken, M. J., *Thermoluminescence Dating*. Academic Press: New York, 1985.

16. Bøtter-Jensen, L.; Murray, A. S., Optically stimulated luminescence techniques in retrospective dosimetry. *Radiation Physics and Chemistry* **2001,** *61*, 181-190.

17. Göksu, H. Y., Telephone chip-cards as individual dosimeters. *Radiation Measurements* **2003,** *37*, 617-620.

18. Larsson, C.; Koslowsky, V.; Gao, H.; Khanna, S.; Estan, D., Optically stimulated luminescence in forensics. *Applied Radiation and Isotopes* **2005,** *63*, 689-695.

19. Inrig, E. L.; Godfrey-Smith, D. I.; Khanna, S., Optically stimulated luminescence of electronic components for forensic, retrospective, and accident dosimetry. *Radiation Measurements* **2008,** *43*, 726-730.

20. Woda, C.; Bassinet, C.; Trompier, F.; Bortolin, E.; Monaca, S.; Fattibene, P., Radiation-induced damage analysed by luminescence methods in retrospective dosimetry and emergency response. *Annali dell'Istituto superiore di sanita* **2009,** *45*, 297-306.

21. Campos, S. S.; Sasaki, J. M.; Gennari, R. F.; Souza, S. O., Proposal for a new method to extract quartz from materials used for retrospective dosimetry and dating. *Radiation Measurements* **2011,** *46* (12), 1509-1513.

22. Spooner, N. A.; Smith, B. W.; Williams, O. M.; Creighton, D. F.; McCulloch, I.; Hunter, P. G.; Questiaux, D. G.; Prescott, J. R., Analysis of luminescence from common salt (NaCl) for application to retrospective dosimetry. *Radiation Measurements* **2011,** *46*, 1856-1861.

23. Fiedler, I.; Woda, C., Thermoluminescence of chip inductors from mobile phones for retrospective and accident dosimetry. *Radiation Measurements* **2011,** *46* (12), 1862-1865.

24. Oks, H.; Spooner, N. A.; Smith, B. W.; Prescott, J. R.; Creighton, D. F.; McCulloch, I.; Adamiec, G., Assessment of thermoluminescence peaks in porcelain for use in retrospective dosimetry. *Radiation Measurements* **2011,** *46* (12), 1873-1877.

25. Mesterházy, D.; Osvay, M.; Kovács, A.; Kelemen, A., Accidental and retrospective dosimetry using TL method. *Radiation Physics and Chemistry* **2011**.

26. Schwantes, J. M.; Miller, S. D.; Piper, M. K.; Amonette, J. E.; Bonde, S.; Duckworth, D. C., Intrinsic dosimetry of glass containers used to transport nuclear materials: Potential implications to the fields of waste management and nuclear forensics. *Radiation Measurements* **2009,** *44*, 405-408.

27. Clark, R. A.; Miller, S. D.; Robertson, J. D.; Gregg, R. A.; Murphy, M. K.; Schwantes, J. M., *Intrinsic dosimetry: A potential new tool for nuclear forensics investigations*, In Proceedings of the 51st Annual Institute of Nuclear Materials Management Conference, Baltimore, MD, July 11-15; 2010.

28. Clark, R. A.; Robertson, J. D.; Walter, E. D.; Miller, S. D.; Schwantes, J. M. Intrinsic dosimetry of glass containers: A potential interrogation tool for nuclear forensics and waste management, **2012**, 1-6, doi:10.1007/s10967-012-2051-0.

29. Britton, M. G., Glass as an engineering material. I. The nature of glass. *Physics in Technology* **1981,** *12*, 187-195.

30. Bach, H.; Krause, D., *Analysis of the Composition and Structure of Glass and Glass Ceramics*. Springer-Verlag: Berlin, 1999.

31. Scholze, H., *Glass: Nature, Structure, and Properties*. Springer-Verlag: New York, 1990.

32. Rao, K. J., *Structural Chemistry of Glasses*. Elsevier Science Ltd.: Oxford, 2002.

33. Shelby, J. E., *Introduction to Glass Science and Technology*. The Royal Society of Chemistry: Cambridge, 2005.

34. Glascock, M. D.; Braswell, G. E.; Cobean, R. H., A systematic approach to obsidian source characterization. In *Archaeological Obsidian Studies: Method and Theory*, Shackley, M. S., Ed. Plenum Press: New York, 1998; pp 15-65.

35. Douglas, R. W.; Frank, S. A., *A History of Glassmaking*. Foulis: London, 1972.

36. Prasad, S.; Clark, T. M.; Sefzik, T. H.; Kwak, H. T.; Gan, Z.; Grandinetti, P. J., Solid-state multinuclear magnetic resonance investigation of Pyrex *Journal of Non-Crystalline Solids* **2006,** *352*, 2834-2840.

37. Tammann, G., *The States of Aggregation*. Van Nostrand, New York, 1925.

38. Le Bourhis, E., *Glass: Mechanics and Technology*. Wiley-VCH: Weinheim, Germany, 2008.

39. Weyl, W. A., *Coloured Glass*. The Society of Glass Technology: Sheffield, England, 1951.

40. Cooper, A. R., W.H. Zachariasen - the melody lingers on. *Journal of Non-Crystalline Solids* **1982,** *49*, 1-17.

41. Zachariasen, W. H., The atomic arrangement in glass. *Journal of the American Chemical Society* **1932,** *54*, 3841-3851.

42. Warren, B. E.; Biscob, J., Fourier analysis of x-ray patterns of soda-silica glass. *Journal of the American Ceramic Society* **1938,** *21*, 259-265.

43. Wright, A. C., Neutron and x-ray amorphography. In *Experimental Techniques of Glass Science*, Simmons, C. J.; El-Bayoumi, O. H., Eds. The American Ceramic Society: Westerville, Ohio, 1993.

44. Jantzen, C. M., Thermodynamic approach to glass corrosion. In *Corrosion of Glass, Cermaics and Ceramic Superconductors: Principles, Testing, Characterization and Applications*, Clark, D. E.; Zoitos, B. K., Eds. Noyes Publications: New Jersey, 1992.

45. IARC, *IARC Monographs on the Evaluation of Carcinogenic Risks to Humans, Vol. 81, Man-made Vitreous Fibres*. IARC Press: Lyon, France, 2002.

46. de Mestral, F.; Drew, R. A. L., Calcium phosphate glasses and glass-ceramics for medical applications. *Journal of the European Ceramic Society* **1989,** *5*, 47-53.

47. Mekki, A.; Holland, D.; Ziq, K. A.; McConville, C. F., Structural and magnetic properties of sodium iron germanate glasses. *Journal of Non-Crystalline Solids* **2000,** *272*, 179-190.

48. Pinakidou, F.; Katsikini, M.; Paloura, E. C.; Kavaouras, P.; Kehagias, T.; Komninou, P.; Karakostas, T.; Erko, A., On the distribution and bonding environment of Zn and Fe in glasses containing electric arc furnace dust: A μ-XAFS and μ-XRF study. *Journal of Hazardous materials* **2007,** *142*, 297-304.

49. Chawla, S. L.; Gupta, R. K., *Materials Selection for Corrosion Control*. ASM International: Materials Park, OH, 1993.

50. Hoppe, U.; Kranold, R.; Ghosh, A.; Landron, C.; Neuefeind, J.; Jóvári, P., Environments of lead cations in oxide glasses probed by x-ray diffration. *Journal of Non-Crystalline Solids* **2003,** *328*, 146-156.

51. Moreno, M. S.; Punte, G.; Rigotti, G.; Mercader, R. C.; Weisz, A. D.; Blesa, M. A., Kinetic study of the disproportionation of tin monoxide. *Solid State Ionics* **2001**, 81-86.

52. Chirikure, S.; Heimann, R. B.; Killick, D., The technology of tin smelting in the Rooiberg Valley, Limpopo Province, South Africa, ca. 1650–1850 CE. *Journal of Archaeological Science* **2010,** *37*, 1656-1669.

53. Caferra, D.; Grassi, A.; Saiello, S.; Buri, A.; Marotta, A., The role of TiO_2 and ZrO_2 in Na_2O-MO_2-SiO_2 glasses. *Materials Letters* **1983,** *2*, 53-55.

54. Shaim, A.; Et-tabirou, M.; Montagne, L.; Palavit, G., Role of bismuth and titanium in Na_2O-Bi_2O_3-TiO_2-P_2O_5 glasses and a model of structural units. *Materials Research Bulletin* **2002,** *37*, 2459-2466.

55. Boyd, D.; Towler, M. R., The processing, mechanical properties and bioactivity of zinc based glass ionomer cements. *Journal of Materials Science Materials in Medicine* **2005,** *16*, 843-50.

56. Barbieri, L.; Corradi, A.; Lancellotti, I.; Leonelli, C.; Siligardi, C., The effect of ZrO_2 in $30K_2O$-$70SiO_2$ glass: a comparison with $30Li_2O$-$70SiO_2$. *Journal of Materials Science* **2003,** *38*, 2627-2631.

57. Connelly, A. J.; Travis, K. P.; Hand, R. J.; Hyatt, N. C., Composition-structure relationships in simplified nuclear waste glasses: 2. The effect of ZrO_2 additions. *Journal of the American Ceramic Society* **2011,** *94*, 137-144.

58. Waseda, Y.; Matsubara, E.; Shinoda, K., *X-Ray Diffraction Crystallography: Introduction, Examples and Solved Problems*. Springer-Verlag: Berlin, 2011.

59. Sayers, D. E.; Stern, E. A.; Lytle, F. W., New techique for investigating noncrystalline structures: Fourier analysis of the extended X-Ray–Absorption Fine Structure. *Physical Review Letters* **1971,** *27*, 1204-1207.

60. Bacon, G. E., *Neutron Diffraction*. Clarendon Press: Oxford, 1962.

61. Wright, A. C., Glass structure by scattering methods and spectroscopy: x-ray and neutron diffraction. In *Insulating and Semiconducting Glasses*, Boolchand, P., Ed. World Scientific Publishing Co. Pte. Ltd.: Singapore, 2000.

62. Luo, Z.; Huang, Y.; Chen, X., *Spectroscopy of Solid-State Laser and Luminescenct Materials*. Nova Science Publishers, Inc.: New York, 2007.

63. Greaves, G. N.; Vaills, Y.; Sen, S.; Winter, R., Density fluctuations, phase separation and microsegregation in silicate glasses. *Journal of Optoelectronics and Advanced Materials* **2000,** *2*, 299-316.

64. Henderson, G. S., The structure of silicate melts: A glass perspective. *Canadian Mineralogist* **2005,** *43*, 1921-1958.

65. Greaves, G. N., EXAFS and the structure of glass. *Journal of Non-Crystalline Solids* **1985,** *71*, 203-217.

66. Huang, L.; Cormack, A. N., The structure of sodium silicate glass. *Journal of Chemical Physics* **1990,** *93*, 8180-8186.

67. Huang, L.; Cormack, A. N., Structural differences and phase separation in alkali silicate glasses. *Journal of Chemical Physics* **1991,** *95*, 3634-3642.

68. Smith, W.; Greaves, G. N.; Gillan, M. J., The structure and dynamics of sodium disilicate glass by molecular simulation. *Journal of Non-Crystalline Solids* **1995,** *192-193*, 267-271.

69. Vessal, B.; Wright, A. C.; Hannon, A. C., Alkali silicate glasses: Interpreting neutron diffraction results using the molecular simulation technique. *Journal of Non-Crystalline Solids* **1996,** *196*, 233-238.

70. Greaves, G. N.; Sen, S., Inorganic glasses, glass-forming liquids and amorphizing solids. *Advances in Physics* **2007,** *56*, 1-166.

71. Brückner, R., Properties and structure of vitreous silica. *Journal of Non-Crystalline Solids* **1970,** *5*, 123-175.

72. Bando, Y.; Ishizuka, K., Study of the structure of silica glass by high-resolution electron microscopy. *Journal of Non-Crystalline Solids* **1979,** *33*, 375-382.

73. Wright, A. C.; Connell, G. A. N.; Allen, J. W., Amorphography and the modelling of amorphous solid structures by geometric transformations. *Journal of Non-Crystalline Solids* **1980,** *42*, 69-86.

74. Gerber, T.; Himmel, B., The structure of silica glass. *Journal of Non-Crystalline Solids* **1986,** *83*, 324-334.

75. Wright, A. C.; Clare, A. G.; Grimley, D. I., Neutron scattering studies of network glasses. *Journal of Non-Crystalline Solids* **1989,** *112*, 33-47.

76. Hobbs, L. W.; Jesurum, C. E.; Berger, B., The topology of silica networks. In *Structure and Imperfections in Amorphous and Crystalline Silicon Dioxide*, Devine, R. A. B.; Duraud, J.-P.; Dooryhée, E., Eds. John Wiley & Sons Ltd.: England, 2000.

77. Salmon, P. S., Amorphous materials: Order within disorder. *Nature Materials* **2002,** *1*, 87-88.

78. Zarzycki, J., Glass structure. *Journal of Non-Crystalline Solids* **1982,** *52*, 31-43.

79. Wright, A. C., Neutron scattering from vitreous silica. V. The structure of vitreous silica: What have we learned from 60 years of diffraction studies? *Journal of Non-Crystalline Solids* **1994,** *179*, 84-115.

80. Sitarz, M.; Mozgawa, W.; Handke, M., Rings in the structure of silicate glasses. *Journal of Molecular Structure* **1999,** *511-512*, 281-285.

81. Clark, T. M.; Grandinetti, P. J.; Florian, P.; Stebbins, J. F., Correlated structural distributions in silica glass. *Physical Review B* **2004,** *70*, 064202/1-8.

82. Matson, D. W.; Sharma, S. K.; Philpotts, J. A., The structure of high-silica alkali-silicate glasses, a Raman spectroscopic investigation. *Journal of Non-Crystalline Solids* **1983,** *58*, 323-352.

83. McMillan, P., Structural studies of silicate glasses and melts–applications and limitations of Raman spectroscopy. *American Mineralogist* **1984,** *69*, 622-644.

84. Henderson, G. S.; Calas, G.; Stebbins, J. F., The structure of slicate glasses and melts. *Elements* **2006,** *2*, 269-273.

85. Tilocca, A.; de Leeuw, N. H., Structural and electronic properties of modified sodium and soda-lime silicate glasses by Car–Parrinello molecular dynamics. *Journal of Materials Chemistry* **2006,** *16*, 1950-1955.

86. Varshneya, A. K., *Fundamentals of Inorganic Glasses*. Academic Press, Inc.: San Diego, CA, 1994.

87. Doweidar, H., Regractive index–structure correlations in silicate glasses. *Journal of Non-Crystalline Solids* **2000,** *277*, 98-105.

88. Utegulov, Z. N.; Eastman, M. A.; Prabakar, S.; Mueller, K. T.; Hamad, A. Y.; Wicksted, J. P.; Dixon, G. S., Structural characterization of Eu_2O_3–MgO–Na_2O–Al_2O_3–SiO_2 glasses with varying Eu_2O_3 content: Raman and NMR studies. *Journal of Non-Crystalline Solids* **2003,** *315*, 43-53.

89. Gatterer, K., Alkali silicate glasses. In *The Structure of Glasses*, http://www.ptc.tugraz.at/specmag/struct/ss.htm (accessed 1 March 2012).

90. Isard, J. O., The mixed alkali effect in glass. *Journal of Non-Crystalline Solids* **1969,** *1*, 235-261.

91. Day, D. E., Mixed alkali glasses – Their properties and uses *Journal of Non-Crystalline Solids* **1976,** *21*, 343-372.

92. Eckert, H., Structural characterization of noncrystalline solids and glasses using solid state NMR. *Progress in Nuclear Magnetic Resonance Spectroscopy* **1992,** *24*, 159-293.

93. Maekawa, H.; Maekawa, T.; Kawamura, K.; Yokokawa, T., The structural groups of alkali silicate glasses determined from ^{29}Si MAS-NMR. *Journal of Non-Crystalline Solids* **1991,** *127*, 53-64.

94. Kloss, T.; Lautenschläger, G.; Schneider, K., Advances in the process of floating borosilicate glasses and some recent applications for specialty borosilicate float glasses. *Glass Technology* **2000,** *41*, 177-181.

95. Konijnendijk, W. L.; Stevels, J. M., The structure of borate glasses studied by Raman scattering. *Journal of Non-Crystalline Solids* **1975,** *18*, 307-331.

96. Minakova, N. A.; Zaichuk, A. V.; Belyi, Y. I., The structure of borate glass. *Glass and Ceramics* **2008,** *65*, 70-73.

97. Windisch Jr, C. F.; Risen Jr, W. M., Vibrational spectra of oxygen- and boron-isotopically substituted B_2O_3 glasses. *Journal of Non-Crystalline Solids* **1982,** *48*, 307-323.

98. Krogh-Moe, J., The structure of vitreous and liquid boron oxide. *Journal of Non-Crystalline Solids* **1969,** *1*, 269-284.

99. Mozzi, R. L.; Warren, B. E., The structure of vitreous boron oxide. *Journal of Applied Crystallography* **1970,** *3*, 251-257.

100. Jellison Jr, G. E.; Panek, L. W.; Bray, P. J.; Rouse, G. B., Determinations of structure and bonding in vitreous B_2O_3 by means of B^{10}, B^{11}, and O^{17} NMR. *Journal of Chemical Physics* **1977,** *66*, 802-812.

101. Walrafen, G. E.; Samanta, S. R.; Krishnan, P. N., Raman investigation of vitreous and molten boric oxide. *Journal of Chemical Physics* **1980,** *72*, 113-120.

102. Hannon, A. C.; Wright, A. C.; Blackman, J. A.; Sinclair, R. N., The vibrational modes of vitreous B2O3: inelastic neutron scattering and modelling studies. *Journal of Non-Crystalline Solids* **1995,** *182*, 78-89.

103. Youngman, R. E.; Zwanziger, J. W., Multiple boron sites in borate glass detected with dynamic angle spinning nuclear magnetic resonance. *Journal of Non-Crystalline Solids* **1994,** *168*, 293-297.

104. Takada, A.; Catlow, C. R. A.; Price, G. D., 'Computer synthesis' of B_2O_3 polymorphs. *Physics and Chemistry of Glasses* **2003,** *44*, 147-149.

105. Verhoef, A. H.; den Hartog, H. W., Structure and dynamics of alkali borate glasses: A molecular dynamics study. *Journal of Non-Crystalline Solids* **1995,** *182*, 235-247.

106. Bray, P. J.; O'Keefe, J. G., Nuclear magnetic resonance investigations of the structure of alkali borate glasses. *Physics and Chemistry of Glasses* **1963,** *4*, 37-46.

107. Greenblatt, S.; Bray, P. J., Nuclear magnetic resonance investigations of the system $BaO\text{-}B_2O_3$. *Physics and Chemistry of Glasses* **1967,** *8*, 190-193.

108. Greenblatt, S.; Bray, P. J., A discussion of the fraction of four-co-ordinated boron atoms present in borate glasses. *Physics and Chemistry of Glasses* **1967,** *8*, 213-216.

109. Kriz, H. M.; Park, M. J.; Bray, P. J., New interpretations of ^{11}B NMR spectra from glassy borates. *Physics and Chemistry of Glasses* **1971,** *12*, 45-49.

110. Park, M. J.; Kim, K. S.; Bray, P. J., The determination of the structures of compounds and glasses in the system $MgO\text{-}B_2O_3$ using B^{11} NMR. *Physics and Chemistry of Glasses* **1979,** *20*, 31-34.

111. Clarida, W. J.; Berryman, J. R.; Affatigato, M.; Feller, S. A.; Kroeker, S. C.; Ash, J.; Zwanziger, J. W.; Meyer, B.; Borsa, F.; Martin, S. W., Dependence of N_4 upon alkali modifier in binary borate glasses. *Physics and Chemistry of Glasses* **2003,** *44*, 215-217.

112. Kamitsos, E. I.; Chryssikos, G. D., Borate glass structure by Raman and infrared spectroscopies. *Journal of Molecular Structure* **1991,** *247*, 1-16.

113. Yun, Y. H.; Bray, P. J., Nuclear magnetic resonance studies of the glasses in the system $Na_2O\text{-}B_2O_3\text{-}SiO_2$. *Journal of Non-Crystalline Solids* **1978,** *27*, 363-380.

114. Yun, Y. H.; Feller, S. A.; Bray, P. J., Correction and addendum to "Nuclear Magnetic Resonance Studies of the Glasses in the System Na_2O-B_2O_3-SiO_2". *Journal of Non-Crystalline Solids* **1979,** *33*, 273-277.

115. Dell, W. J.; Bray, P. J.; Xiao, S. Z., ^{11}B NMR studies and structural modeling of Na_2O-B_2O_3-SiO_2 glasses of high soda content. *Journal of Non-Crystalline Solids* **1983,** *58*, 1-16.

116. Kamitsos, E. I.; Karakassides, M. A.; Chryssikos, G. D., A vibrational study of lithium sulfate based fast ionic conducting borate glasses. *Journal of Physical Chemistry* **1986,** *90*, 4528-4533.

117. Shiraishi, Y.; Gra'na'sy, L.; Waseda, Y.; Matsubara, E., Viscosity of glassy Na_2O-B_2O_2-SiO_2 system. *Journal of Non-Crystalline Solids* **1987,** *95-96*, 1031-1038.

118. Bunker, B. C.; Tallant, D. R.; Kirkpatrick, R. J.; Turner, G. L., Multinuclear nuclear magnetic resonance and Raman investigation of sodium borosilicate glass structures. *Physics and Chemistry of Glasses* **1990,** *31*, 30-41.

119. Konijnendijk, W. L.; Stevels, J. M., The structure of borosilicate glasses studied by Raman scattering. *Journal of Non-Crystalline Solids* **1976,** *20*, 193-224.

120. Manara, D.; Grandjean, A.; Neuville, D. R., Structure of borosilicate glasses and melts: A revision of the Yun, Bray and Dell model. *Journal of Non-Crystalline Solids* **2009,** *355*, 2528-2531.

121. Gatterer, K., The Bray model. In *The Structure of Glasses*, http://www.ptc.tugraz.at/specmag/struct/braytab.htm (accessed 1 March 2012).

122. Galoisy, L.; Cormier, L.; Rossano, S.; Ramos, A.; Calas, G.; Gaskell, P.; Le Grand, M., Cationic ordering in oxide glasses: the example of transition elements. *Mineralogical Magazine* **2000,** *64*, 409-424.

123. Dulski, T. R., *A Manual for the Chemical Analysis of Metals*. American Society for Testing and Materials: Ann Arbor, MI, 1996.

124. Merzbacher, C. I.; White, W. B., The structure of alkaline earth aluminosilicate glasses as determined by vibrational spectroscopy. *Journal of Non-Crystalline Solids* **1991,** *130*, 18-34.

125. Darwish, H.; Gomaa, M. M., Effect of compositional changes on the structure and properites of alkali-alumino borosilicate glasses. *Journal of Materials Science - Materials in Electronics* **2006,** *17*, 35-42.

126. Alexander, M. N.; Onorato, P. I. K.; Struck, C. W.; Rozen, J. R.; Tasker, G. W.; Uhlmann, D. R., Structure of alkali (alumino)silicate glasses: 1. Tl^{+} luminescence and the nonbridging oxygen issue. *Journal of Non-Crystalline Solids* **1986,** *79*, 137-154.

127. Siwadamrongpong, S.; Koide, M.; Matusita, K., Structure of ternary alumino-silicate glasses. *Journal of the Ceramic Society of Japan* **2004,** *112*, 590-593.

128. Schaller, T.; Stebbins, J. F., The structural role of lanthanum and yttrium in aluminosilicate glasses: A ^{27}Al and ^{17}O MAS NMR study. *Journal of Physical Chemistry B* **1998,** *102*, 10690-10697.

129. Engelhardt, G.; Nofz, M.; Forkel, K.; Wihsmann, F. G.; Magi, M.; Samoson, A.; Lippmaa, E., Structural studies of calcium aluminosilicate glasses by high resolution solid state ^{29}Si and ^{27}Al magic angle spinning nuclear magnetic resonance. *Physics and Chemistry of Glasses* **1985,** *26*, 157-165.

130. Sato, R. K.; McMillan, P. F.; Dennison, P.; Dupree, R., High-resolution aluminum-27 and silicon-29 MAS NMR investigation of silica-alumina glasses. *Journal of Physical Chemistry* **1991,** *95*, 4483-4489.

131. Dupree, R.; Holland, D.; Williams, D. S., The structure of binary alkali silicate glasses. *Journal of Non-Crystalline Solids* **1986,** *81*, 185-200.

132. Stebbins, J. F., Effects of temperature and composition on silicate glass structure and dynamics: Si-29 NMR results. *Journal of Non-Crystalline Solids* **1988,** *106*, 359-369.

133. Du, L.-S.; Stebbins, J. F., Network connectivity in aluminoborosilicate glasses: A high-resolution ^{11}B, ^{27}Al and ^{17}O NMR study. *Journal of Non-Crystalline Solids* **2005,** *351*, 3508-3520.

134. Bishop, S. G.; Bray, P. J., Nuclear magnetic resonance studies of calcium boroaluminate glasses. *Physics and Chemistry of Glasses* **1966,** *7*, 73-81.

135. Nassar, A. M.; Adawi, M. A., The role of Al^{3+} ions in alumino borate glasses as revealed by molar volume, refractive index and microhardness. *Journal of Non-Crystalline Solids* **1982,** *50*, 155-161.

136. Bunker, B. C.; Kirkpatrick, R. J.; Brow, R. K.; Turner, G. L.; Nelson, C., Local structure of alkaline-earth boroaluminate crystals and glasses: II. ^{11}B and ^{27}Al MAS NMR spectroscopy of alkaline-earth boroaluminate glasses. *Journal of the American Ceramic Society* **1991,** *74*, 1430-1438.

137. Baltisberger, J. H.; Xu, Z.; Stebbins, J. F.; Wang, S. H.; Pines, A., Triple-quantum two-dimensional ^{27}Al magic-angle spinning nuclear magnetic resonance spectroscopic study of aluminosilicate and aluminate crystals and glasses. *Journal of the American Chemical Society* **1996,** *118*, 7209-7214.

138. Pires, R. A.; Abrahams, I.; Nunes, T. G.; Hawkes, G. E., The role of alumina in aluminoborosilicate glasses for use in glass–isonomer cements. *Journal of Materials Chemistry* **2009,** *19*, 3652-3660.

139. Züchner, L.; Chan, J. C. C.; Müller-Warmuth, W.; Eckert, H., Short-range order and site connectivities in sodium aluminoborate glasses: I. Quantification of local environments by high-resolution ^{11}B, ^{23}Na, and ^{27}Al solid-state NMR. *Journal of Physical Chemistry B* **1998,** *102*, 4495-4506.

140. Bertmer, M.; Züchner, L.; Chan, J. C. C.; Eckert, H., Short and medium range order in sodium aluminoborate glasses. 2. Site connectivities and cation distributions studied by rotational echo double resonance NMR spectroscopy. *Journal of Physical Chemistry B* **2000,** *104*, 6541-6553.

141. Ramkumar, J.; Sudarsan, V.; Chandramouleeswaran, S.; Shrikhande, V. K.; Kothiyal, G. P.; Ravindran, P. V.; Kulshreshtha, S. K.; Mukherjee, T., Structural studies on boroaluminosilicate glasses. *Journal of Non-Crystalline Solids* **2008,** *354*, 1591-1597.

142. Rasmussen, S. C., *How Glass Changed the World: The History and Chemistry of Glass from Antiquity to the 13th Century*. Springer: Berlin, 2012.

143. Lambert, J. B., *Traces of the Past: Unraveling the Secrets of Archaeology through Chemistry*. Perseus Publishing: Reading, MA, 1997.

144. Williams, J. P.; Su, Y.; Wise, W. M. *Trace chemical analysis of high-purity glass*; Research and Development Laboratory, Corning Glass Works: New York, 1977.

145. De Souza, J. J. V.; Gupta, B. K.; Gupta, S., Analysis of pharmaceutical glass containers manufactured in India. *Indian Journal of Pharmacy* **1971,** *33*, 72-73.

146. Möncke, D.; Ehrt, D., Irradiation induced defects in glasses resulting in the photoionization of polyvalent dopants. *Optical Materials* **2004,** *25*, 425-437.

147. Möncke, D.; Ehrt, D., *Photoionization of Polyvalent Ions*. Nova Science Publishers, Inc.: New York, 2010.

148. Spurný, Z.; Novotný, J., Effect of ionizing radiation on glasses: The relation between optical absorption and thermoluminescence of borate glasses. *Journal of Physics and Chemistry of Solids* **1965,** *26*, 1107-1110.

149. Fenstermacher, J. E., Optical absorption due to tetrahedral and octahedral ferric iron in silicate glasses. *Journal of Non-Crystalline Solids* **1980,** *38-39*, 239-244.

150. Galoisy, L., Structure–property relationships in industrial and natural glasses. *Elements* **2006,** *2*, 293-297.

151. Magnien, V.; Neuville, D. R.; Cormier, L.; Roux, J.; Hazemann, J. L.; de Ligny, D.; Pascarelli, S.; Vickridge, I.; Pinet, O.; Richet, P., Kinetics and mechanisms of iron redox reactions in silicate melts: The effects of temperature and alkali cations. *Geochimica et Cosmochimica Acta* **2008,** *72*, 2157-2168.

152. Mirhadi, B.; Mehdikhani, B., Effect of batch melting temperature and raw material on iron redox state in sodium silicate glasses. *Journal of the Korean Chemical Society* **2011,** *48*, 117-120.

153. Taragin, M. F.; Eisenstein, J. C., Mössbauer effect in some complex borosilicate glasses. *Journal of Non-Crystalline Solids* **1970,** *3*, 311-316.

154. Galimov, D. G.; Yudin, D. M.; Yafaev, N. R., The coordination of iron in glasses. *Journal of Applied Spectroscopy* **1973,** *19* (2), 1097-1099.

155. Brown, G., The ESR behavior of iron in gamma-irradiated Pyrex. *Journal of Materials Science* **1975,** *10*, 1481-1486.

156. Magini, M.; Sedda, A. F., On the coordination of iron ions in sodium borosilicate glasses. *Journal of Non-Crystalline Solids* **1984,** *65*, 145-159.

157. Bilan, O. N.; Gorbachev, S. M.; Cherenda, N. G.; Voropai, Y. S.; Yudin, D. M., Iron coordination in silicate glasses. *Radiation Effects and Defects in Solids* **1991,** *115*, 285-287.

158. Cochain, B.; Neuville, D. R.; Henderson, G. S.; McCammon, C. A.; Pinet, O.; Richet, P., Effects of the iron content and redox state on the structure of sodium borosilicate glasses: A Raman, Mössbauer and boron K-edge XANES spectroscopy study. *Journal of the American Ceramic Society* **2012,** *95*, 962-971.

159. Dooryhée, E.; Duraud, J.-P.; Devine, R. A. B., Radiation-induced defects and structural modifications. In *Structure and Imperfections in Amorphous and Crystalline Silicon Dioxide*, Devine, R. A. B.; Duraud, J.-P.; Dooryhée, E., Eds. John Wiley & Sons Ltd.: England, 2000.

160. Holmes-Siedle, A.; Adams, L., *Handbook of Radiation Effects*. Second ed.; Oxford University Press: Oxford, 2002.

161. Ehman, W. D.; Vance, D. E., *Radiochemistry and Nuclear Methods of Analysis*. John Wiley & Sons Ltd.: New York, 1991.

162. Knoll, G. F., *Radiation Detection and Measurement*. John Wiley & Sons, Inc.: Hoboken, New Jersey, 1999.

163. Choppin, G.; Jan-Olov, L.; Rydberg, J., *Radiochemistry and Nuclear Chemistry*. Third ed.; Butterworth–Heinemann: Woburn, MA, 2002.

164. Loveland, W.; Morrissey, D. J.; Seaborg, G. T., *Modern Nuclear Chemistry*. John Wiley & Sons, Inc.: Hoboken, New Jersey, 2006.

165. Bos, A. J. J.; De Jong, R. W.; Meijvogel, K., Effects of type of radiation on glow curve and thermoluminescence emission spectrum of CaF_2:Tm. *Radiation Measurements* **1995,** *24*, 401-405.

166. Vandenverghe, D.; De Corte, F.; Van den haute, P., Observations on the thermoluminescence signal induced by alpha radiation. *Radiation Measurements* **2000,** *32*, 813-817.

167. Weber, W. J.; Ewing, R. C.; Angell, C. A.; Arnold, G. W.; Cormack, A. N.; Delaye, J. M.; Griscom, D. L.; Hobbs, L. W.; Navrotsky, A.; Price, D. L.; Stoneham, A. M.; Weinberg, M. C., Radiation effects in glasses used for immobilization of high-level waste and plutonium disposition. *Journal of Materials Research* **1997,** *12*, 1946-1978.

168. *DOE Fundamentals Handbook: Material Science*. U.S. Department of Energy: Springfield, VA, 1993; Vol. 2.

169. Driscoll, C. M. H., Studies of the effect of LET on the thermoluminescent properties of thin lithium fluoride layers. *Physics in Medicine and Biology* **1978,** *23*, 777-781.

170. Kopeliovich, D., Imperfections of crystal structure. http://www.substech.com/dokuwiki/doku.php?id=imperfections_of_crystal_structure (accessed 1 February 2010).

171. Shelby, J. E., Effect of radiation on the physical properties of borosilicate glasses. *Journal of Applied Physics* **1980,** *51*, 2561-2565.

172. Fischer, H.; Götz, G.; Karge, H., Radiation damage in ion-implanted quartz crystals. II. Annealing behaviour. *Physica Status Solidi A - Applications and Materials Science* **1983,** *76*, 493-498.

173. Amossov, A. V.; Rybaltovsky, A. O., Radiation color center formation in silica glasses: a review of photo- and thermo-chemical aspects of the problem. *Journal of Non-Crystalline Solids* **1994,** *179*, 226-234.

174. Boizot, B.; Ollier, N.; Olivier, F.; Petite, G.; Ghaleb, D.; Malchukova, E., Irradiation effects in simplified nuclear waste glasses. *Nuclear Instruments and Methods in Physics Research B* **2005,** *240*, 146-151.

175. Perez-Mendez, V.; Mulera, T.; Kaplan, S. N.; Wiedenbeck, P., *Large-area non-crystalline semiconductor detectors*, In American Physical Society Division of Particles and Fields Workshop on Hadron Collider Detectors, Lawrence Berkeley Laboratory, Berkeley, CA, 28 February - 4 March, 1983.

176. Perez-Mendez, V.; Cho, G.; Drewery, J.; Jing, T.; Kaplan, S. N.; Qureshi, S.; Wildermuth, D.; Fujieda, I.; Street, R. A., Amorphous silicon based radiation detectors. *Journal of Non-Crystalline Solids* **1991,** *137&138*, 1291-1296.

177. del Cueto, M. E.; Cabal, A. E., Medical applications of amorphous silicon detectors. *AIP Conference Proceedings* **1998,** *440*, 179-186.

178. Stiegler, J. O.; Mansur, L. K., Radiation effects in structural materials. *Annual Review of Materials Science* **1979,** *9*, 405-454.

179. Roorda, S.; Poate, J. M.; Jacobson, D. C.; Eaglesham, D. J.; Dennis, B. S.; Dierker, S., Point defect populations in amorphous and crystalline silicon. *Solid State Communications* **1990,** *75*, 197-200.

180. Liang, Z. N.; Niesen, L.; van den Hoven, G. N.; Custer, J. S., Similar point defects in crystalline and amorphous silicon. *Physical Review B* **1994,** *49*, 16331-16337.

181. Maroudas, D.; Pantelides, S. T., Point defects in crystalline silicon, their migration and their relation to the amorphous phase. *Chemical Engineering Science* **1994,** *49*, 3001-3014.

182. Wagner, D., Point defects in crystalline and amorphous silicon. *Journal of Optoelectronics and Advanced Materials* **2004,** *6*, 345-347.

183. Ojovan, M. I.; Lee, W. E., Topologically disordered systems at the glass transition. *Journal of Physics: Condensed Matter* **2006,** *18*, 11507-11520.

184. Holmes-Siedle, A.; Adams, L., *Handbook of Radiation Effects*. First ed.; Oxford University Press: Oxford, 1993.

185. Johns, H. E.; Cunningham, J. R., *The Physics of Radiology*. Fourth ed.; Charles C. Thomas Pub. Ltd.: Springfield, IL, 1983.

186. Hobbs, L. W.; Clinard Jr., F. W.; Zinkle, S. J.; Ewing, R. C., Radiation effects in ceramics. *Journal of Nuclear Materials* **1994,** *216*, 291-321.

187. Souquet, J. L., Ionic transport in amorphous solid electrolytes. *Annual Review of Materials Science* **1981,** *11*, 211-231.

188. Silins, A. R., Defects in glasses. *Radiation Effects and Defects in Solids* **1995,** *134*, 7-10.

189. Griscom, D. L., Defects in amorphous insulators. *Journal of Non-Crystalline Solids* **1978,** *31*, 241-266.

190. Griscom, D. L., Electron spin resonance in glasses. *Journal of Non-Crystalline Solids* **1980,** *40*, 211-272.

191. Vignaud, G.; Berger, R.; Haddad, M., Review of ESR centers induced by x-ray irradiation in both vitreous and crystalline borates or hologenoborates. *Journal of Non-Crystalline Solids* **1986,** *86*, 6-12.

192. Kordas, G.; Camara, B.; Oel, H. J., Electron spin resonance studies of radiation damage in silicate glasses. *Journal of Non-Crystalline Solids* **1982,** *50*, 79-95.

193. Cases, R.; Griscom, D. L., On the structure of defect centers in γ-irradiated alkali silicate glasses. *Nuclear Instruments and Methods in Physics Research B* **1984,** *1*, 503-510.

194. Griscom, D. L., Characterization of three E'-center variants in x- and γ-irradiated high purity a-SiO_2. *Nuclear Instruments and Methods in Physics Research B* **1984,** *1*, 481-488.

195. Griscom, D. L.; Friebele, E. J., Fundamental radiation-induced defect centers in synthetic fused silicas: Atomic chlorine, delocalized E' centers, and a triplet state. *Physical Review B* **1986,** *34*, 7524-7533.

196. Imai, H.; Hirashima, H., Intrinsic- and extrinsic-defect formation in silica glasses by radiation. *Journal of Non-Crystalline Solids* **1994,** *179*, 202-213.

197. Shkrob, I. A.; Tadjikov, B. M.; Trifanac, A. D., Magnetic resonance studies on radiation-induced point defects in mixed oxide glasses. II. Spin centers in alkali silicate glasses. *Journal of Non-Crystalline Solids* **2000,** *262*, 35-65.

198. Weeks, R. A., The many varieties of E' centers: A review. *Journal of Non-Crystalline Solids* **1994,** *179*, 1-9.

199. Weeks, R. A.; Nelson, C. M., Trapped electrons in irradiated quartz and silica: II. Electron spic resonance. *Journal of the American Ceramic Society* **1960,** *43*, 399-404.

200. Nelson, C. M.; Weeks, R. A., Trapped electrons in irradiated quartz and silica: I. Optical absorption. *Journal of the American Ceramic Society* **1960,** *43*, 396-399.

201. Weeks, R. A.; Nelson, C. M., Irradiation effects and short-range order in fused silica and quartz. *Journal of Applied Physics* **1960,** *31*, 1555-1558.

202. Kerwin, D. B.; Galeener, F. L., Creation of E' defects in vitreous SiO_2 by energetic electrons produced by x irradiation. *Applied Physics Letters* **1991,** *59*, 2959-2961.

203. Agnello, S.; Gelardi, F. M.; Boscaino, R.; Cannas, M.; Boizot, B.; Petite, G., Intrinsic defects induced by β-irradiation in silica. *Nuclear Instruments and Methods in Physics Research B* **2002,** *191*, 387-391.

204. Stesmans, A.; Clémer, K.; Afanas'ev, V. V., Primary ^{29}Si hyperfine structure of E' centers in nm-sized silica: Probing the microscopic network structure. *Physical Review B* **2008,** *77*, 094130/1-12.

205. Griscom, D. L., Trapped-electron centers in pure and doped glassy silica: A review and synthesis. *Journal of Non-Crystalline Solids* **2011,** *357*, 1945-1962.

206. Griscom, D. L., The nature of point defects in amophous silicon dioxide. In *Defects in SiO_2 and Related Dialectrics: Science and Technology*, Pacchioni, G.; Skuja, L.; Griscom, D. L., Eds. Kluwer Academic Publishers: Netherlands, 2000.

207. Warren, W. L., Paramagnetic point defects in amorphous silicon dioxide and amorphous silicon nitride thin films. *Journal of the Electrochemical Society* **1992,** *139*, 872-880.

208. Katz, A., Hydrogen in quartz. *Philips Research Reports* **1962,** *17*, 133-279.

209. Griscom, D. L.; Sigel, G. H.; Ginther, R. J., Defect centers in a puresilicacore borosilicateclad optical fiber: ESR studies. *Journal of Applied Physics* **1976,** *47*, 960-967.

210. Shkrob, I. A.; Tadjikov, B. M.; Trifanac, A. D., Magnetic resonance studies on radiation-induced point defects in mixed oxide glasses. I. Spin centers in B_2O_2 and alkali borate glasses. *Journal of Non-Crystalline Solids* **2000,** *262*, 6-34.

211. Jivanescu, M.; Stesmans, A.; Afanas'ev, V. V., Multifrequency ESR analysis of the E'_δ defect in α-SiO_2. *Physical Review B* **2011,** *83*, 094118/1-16.

212. Griscom, D. L., ESR studies of an intrinsic trapped-electron center in x-irradiated alkali borate glasses. *Journal of Chemical Physics* **1971,** *55*, 1113-1122.

213. Griscom, D. L., ESR and optical studies of alkai-associated trapped-electron centers in alkali borate glasses irradiated at 77°K. *Journal of Non-Crystalline Solids* **1971,** *6*, 275-282.

214. Pontuschka, W. M.; Isotani, S.; Piccini, A., Optical and thermal bleaching of x-irradiated barium aluminoborate glasses. *Journal of the American Ceramic Society* **1987,** *70*, 59-64.

215. Del Nery, S. M.; Pontuschka, W. M.; Isotani, S.; Rouse, C. G., Luminescence quenching by iron in barium aluminoborate glasses. *Physical Review B* **1994,** *49*, 3760-3765.

216. Pascoal, H. B.; Pontuschka, W. M.; Rechenberg, H., Luminescence quenching by iron in calcium aluminoborate glasses. *Journal of Non-Crystalline Solids* **1999,** *258*, 92-97.

217. Pontuschka, W. M.; Kanashiro, L. S.; Courrol, L. C., Luminescence mechanisms for borate glasses: The role of local structural units. *Glass Physics and Chemistry* **2001,** *17*, 37-47.

218. da Rocha, M. S. F.; Pontuschka, W. M.; Blak, A. R., Radiation induced capacitance in barium alumionborate glasses. *Journal of Non-Crystalline Solids* **2003,** *321*, 29-36.

219. Giehl, J. M.; Miranda, A. R.; Pontuschka, W. M.; Navarro, M.; Da Costa, Z. M., EPR study of MnO and MnO_2 doped barium aluminoborate glasses. *Journal of Superconductivity and Novel Magnetism* **2012**, 1-4.

220. Wang, Q.; Geng, H.; Sun, C.; Zhang, Z.; He, S., Evolution of defects in a multicomponent glass irradiated by 1 MeV electrons. *Nuclear Instruments and Methods in Physics Research B* **2010,** *268*, 1478-1481.

221. Boizot, B.; Petite, G.; Ghaleb, D.; Pellerin, N.; Fayon, F.; Reynard, B.; Calas, G., Migration and segregation of sodium under β-irradiation in nuclear glasses. *Nuclear Instruments and Methods in Physics Research B* **2000,** *166-167*, 500-504.

222. Brown, G., An ESR study of electron and hole trapping in gamma-irradiated Pyrex. *Journal of Materials Science* **1975,** *10*, 1841-1848.

223. El Batal, F. H.; Selim, M. S.; Marzouk, S. Y.; Azooz, M. A., UV-Vis absorption of the transition metal-doped SiO_2–B_2O_3–Na_2O glasses. *Physica B* **2007,** *398*, 126-134.

224. Bishay, A., Radiation induced color centers in multicomponent glasses. *Journal of Non-Crystalline Solids* **1970,** *3*, 54-114.

225. Tsai, T. E.; Friebele, E. J.; Griscom, D. L.; Pannhorst, W., Radiation-induced defect centers in glass ceramics. *Journal of Applied Physics* **1989,** *65*, 507-514.

226. Rädlein, E.; Frischat, G. H.; Speit, B., Paramagnetic centers in glasses and glass-ceramics induced by simulated space radiation. *Journal of Non-Crystalline Solids* **1993,** *162*, 101-106.

227. Qiu, J.; Makishima, A., Ultraviolet-radiation-induced structure and long-lasting phophorescence in Sn^{2+}–Cu^{2+} co-doped silicate glass. *Science and Technology of Advanced Materials* **2003,** *4*, 35-38.

228. Möncke, D.; Ehrt, D., Photoinduced redox-ractions and transmission changes in glasses doped with 4d- and 5d-ions. *Journal of Non-Crystalline Solids* **2006,** *352*, 2631-2636.

229. Kadona, K.; Itakura, N.; Akai, T.; Yamashita, M.; Yazawa, T., Effect of additive ions on the optical density and stability of the color centers induced by x-ray irradiation in soda-lime silicate glass. *Nuclear Instruments and Methods in Physics Research B* **2009,** *267*, 2411-2415.

230. Malchukova, E.; Boizot, B., Reduction of Eu^{3+} to Eu^{2+} in aluminoborosilicate glasses under ionizing radiation. *Materials Research Bulletin* **2010,** *45*, 1299-1303.

231. Pankratov, V.; Millers, D.; Grigorjeva, L.; Matkovskii, A. O.; Potera, P.; Pracka, I.; Łukasiewicz, T., The role of Fe and Cu dopants in electron–hole trapping and relaxation process in congruent $LiNbO_3$. *Optical Materials* **2003,** *22*, 257-262.

232. Ghosh, A. K., Color centers in aluminoborate glass. *Journal of Chemical Physics* **1966,** *44*, 541-546.

233. Boizot, B.; Petite, G.; Ghaleb, D.; Calas, G., Radiation induced paramagnetic centres in nuclear glasses by EPR spectroscopy. *Nuclear Instruments and Methods in Physics Research B* **1998,** *141*, 580-584.

234. Kikuchi, T., The thermoluminescence of glasses. *Journal of the Physical Society of Japan* **1958,** *13*, 526-531.

235. Kotomin, E. A.; Popov, A. I., Radiation-induced point defects in simple oxides. *Nuclear Instruments and Methods in Physics Research B* **1998,** *141*, 1-15.

236. Shkrob, I. A.; Tarasov, V. F., On the structure of trapped holes in borosilicate. *Journal of Chemical Physics* **2000,** *113*, 10723-10732.

237. Trifanac, A. D.; Shkrob, I. A.; Werst, D. W. *Radiation effects on transport and bubble formation in silicate glasses*; Argonne National Laboratory: Argonne, IL, 2000.

238. Griscom, D. L., E.S.R. studies of radiation damage and structure in oxide glasses not containing transition group ions: a contemporary overview with illustrations from the alkali borate system. *Journal of Non-Crystalline Solids* **1973/74,** *13*, 251-285.

239. Griscom, D. L., Electron spin resonance studies of trapped hole centers in irradiated alkali silicate glasses: A critical comment on current models for HC_1 and HC_2. *Journal of Non-Crystalline Solids* **1984,** *64*, 229-247.

240. Chan, S. L.; Gladden, L. F.; Elliot, S. R., Magnetic resonance studies on neutron irradiated quartz and amorphous silica. *Journal of Non-Crystalline Solids* **1988,** *106*, 413-416.

241. Dutt, D. A.; Higby, P. L.; Merzbacher, C. I.; Griscom, D. L., Compositional dependence of trapped hole centers in gamma-irradiated calcium aluminosilicate glasses. *Journal of Non-Crystalline Solids* **1991,** *135*, 122-130.

242. Ikeya, M., *New Applications of Electron Spin Resonance: Dating, Dosimetry and Microscopy*. World Scientific Publishing Co. Pte. Ltd.: Singapore, 1993.

243. Kumar, M.; Seshagiri, T. K.; Kadam, R. M.; Godbole, S. V., Photoluminescence, thermally stimulated luminescence and electron paramagnetic resonance investigations of Tb^{3+} doped $SrBPO_5$. *Materials Research Bulletin* **2011,** *46*, 1359-1365.

244. Kordas, G., On the structure of the BOHC in borosilicate and borophosphosilicate glasses. *Journal of Non-Crystalline Solids* **2005,** *351*, 2358-2360.

245. Deligiannakis, Y.; Astrakas, L.; Kordas, G.; Smith, R. A., Electronic structure of B_2O_3 glass studied by one- and two-dimensional electron-spin-echo envelope modulation spectroscopy. *Physical Review B* **1998,** *58*, 11420-11434.

246. Kordas, G., CW-EPR, 1D-ESEEM, HYSCORE, pulsed ENDOR and SCF-HF calculations for the interpretation of defects in borate systems. *Physics and Chemistry of Glasses* **2000,** *41*, 325-329.

247. Kordas, G., Complementary use of cw-EPR, HYSCORE and pulsed ENDOR spectroscopies for scanning the environment of unpaired states in a- and c-B_2O_3. *Journal of Non-Crystalline Solids* **1999,** *260*, 75-82.

248. Pacchioni, G.; Vezzoli, M.; Fanciulli, M., Electronic structure of the paramagnetic boron oxygen hole center in B-doped SiO_2. *Physical Review B* **2001,** *64*, 155201/1-7.

249. Carboni, R.; Pacchioni, G.; Fanciulli, M.; Giglia, A.; Mahne, N.; Pedio, M.; Nannarone, S.; Boscherini, F., Coordination of boron and phosphorous in Borophosphosilicate glasses. *Applied Physics Letters* **2003,** *83*, 4312-4314.

250. Shelby, J. E., Chemical annealing of the aluminum-oxygen hole center in vitreous silica. *Journal of Applied Physics* **1986,** *60*, 4325-4327.

251. Dutt, D. A.; Higby, P. L.; Griscom, D. L., An electron spin resonance study of x-irradiated calcium aluminosilicate glasses. *Journal of Non-Crystalline Solids* **1991,** *130*, 41-51.

252. Hosono, H.; Kawazoe, H., Radiation-induced coloring and paramagnetic centers in synthetic SiO_2 : Al glasses. *Nuclear Instruments and Methods in Physics Research B* **1994,** *91*, 395-399.

253. Wang, Q.; Zhang, Z.; Geng, H.; Sun, C.; Yang, D.; He, S.; Hu, Z., Radiation-induced damage and recovery effects in GG17 glass irradiated by 1 MeV electrons. *Nuclear Instruments and Methods in Physics Research B* **2012,** *281*, 1-7.

254. Chah, K.; Boizot, B.; Reynard, B.; Ghaleb, D.; Petite, G., Micro-Raman and EPR studies of β-radiation damages in aluminosilicate glass. *Nuclear Instruments and Methods in Physics Research B* **2002,** *191*, 337-341.

255. Boizot, B.; Petite, G.; Ghaleb, D.; Calas, G., Dose, dose rate and irradiation temperature effects in β-irradiated simplified nuclear waste glasses by EPR spectroscopy. *Journal of Non-Crystalline Solids* **2001,** *283*, 179-185.

256. Attix, F. H., *Introduction to Radiological Physics and Radiation Dosimetry*. Wiley-VCH: Weinheim, Germany, 2004.

257. Yacobi, B. G.; Holt, D. B., *Cathodoluminescence Microscopy of Inorganic Solids*. Plenum Press: New York, 1990.

258. Ozawa, L., *Cathodoluminescence and Photoluminescence: Theories and Practical Applications*. Taylor & Francis Group, LLC: Boca Raton, FL, 2007.

259. Furetta, C., *Questions and Answers on Thermoluminescence (TL) and Optically Stimulated Luminescence (OSL)*. World Scientific Publishing Co. Pte. Ltd.: Singapore, 2008.

260. Bos, A. J. J., Theory of thermoluminescence. *Radiation Measurements* **2007,** *41*, S45-S56.

261. Tipler, P. A.; Mosca, G., *Physics for Scientists and Engineers. Volume 2: Electricity and Magnetism, Light, Modern Physics*. Fifth ed.; W.H. Freeman and Company: New York, 2003.

262. Ahmed, S. N., *Physics & Engineering of Radiation Detection*. Academic Press Inc.: San Diego, CA, 2007.

263. Takeno, S.; Goda, M., A theory of phonon-like excitations in non-crstalline solids and liquids. *Progress of Theoretical Physics* **1972,** *47*, 790-806.

264. Böttger, H., On the theory of phonon-like excitations in noncrystalline solids. *Physica Status Solidi B* **1973,** *59*, 517-523.

265. Zaitlin, M. P.; Anderson, A. C., Phonon thermal transport in noncrystalline materials. *Physical Review B* **1975,** *12*, 4475-4486.

266. Thakore, B. Y.; Khambholja, S. G.; Joshi, M.; Jani, A. R., Phonon modes in non-crystalline lithium, sodium and their binary alloys. *Journal of Optoelectronics and Advanced Materials* **2011,** *13*, 293-301.

267. Shalgaonkar, C. S.; Narlikar, A. V., Review: A review of the recent methods for determining trap depth from glow curves. *Journal of Materials Science* **1972,** *7*, 1465-1471.

268. Levy, P. W., Thermoluminescence systems with two or more glow peaks described by anomalous kinetic parameters. *Nuclear Instruments and Methods in Physics Research B* **1984,** *1*, 436-444.

269. McKeever, S. W. S.; Chen, R., Luminescence models. *Radiation Measurements* **1997,** *27*, 625-661.

270. Furetta, C.; Weng, P.-S., *Operational Thermoluminescence Dosimetry*. World Scientific Publishing Co. Pte. Ltd.: Singapore, 1998.

271. van Roosbroeck, W.; Shockley, W., Photon-radiative recombination of electrons and holes in germanium. *Physical Review* **1954,** *94*, 1558-1560.

272. van Roosbroeck, W.; Casey Jr., H. C., Transport in relaxation semiconductors. *Physical Review B* **1972,** *5*, 2154-2175.

273. van Roosbroeck, W., Principles of electrical behavior of amorphous semiconductor alloys. *Journal of Non-Crystalline Solids* **1973,** *12*, 232-262.

274. Bube, R. H., *Photoconductivity of Solids*. Wiley & Sons: New York, 1960.

275. Williams, E. W.; Hall, R., *Luminescence and the Light Emitting Diode*. Pergamon Press: Oxford, 1978.

276. Kao, J. C.; Hwang, W., *Electrical Transport in Solids*. Pergamon Press: Oxford, 1981.

277. Pagonis, V.; Chen, R.; Lawless, J. L., Nonmonotonic dose dependence of OSL intensity due to competition during irradiation and readout. *Radiation Measurements* **2006,** *41*, 903-909.

278. Cohn, B. E.; Harkins, W. D., Thermoluminescence in glasses which contain two activators. *Journal of the American Chemical Society* **1930,** *52*, 5146-5154.

279. Nyswander, R. E.; Nyswander, B. E., Measurements of thermoluminescence of glass exposed to light. *Journal of the Optical Society of America* **1930,** *20*, 131-136.

280. Hampel, C., The use of cerium dioxide in the glass industry. *Glass and Ceramics* **1961,** *18*, 212-213.

281. Bishop, S. G.; Taylor, P. C., Iron impurities as non-radiative recombination centres in chalcogenide glasses. *Philosophical Magazine B* **1979,** *40*, 483-495.

282. Nasipuri, R.; Banerjee, H. D.; Paul, A., Energy storage behaviour of some binary alkali borate glasses by thermoluminescence studies. *Journal of Materials Science* **1980,** *15*, 557-562.

283. Chen, R.; Leung, P. L.; Stokes, M. J., Apparent anomalous fading of thermoluminescence associated with competition with radiationless transitions. *Radiation Measurements* **2000,** *32*, 505-511.

284. Rao, G. V.; Reddy, P. Y.; Veeraiah, N., Thermoluminescence studies on $Li_2O–CaF_2–B_2O_3$ glasses doped with manganese ions. *Materials Letters* **2002,** *57*, 403-408.

285. Rao, G. V.; Veeraiah, N.; Reddy, P. Y., Luminescence quenching by manganese ions in $MO–CaF_2–B_2O_3$ glasses. *Optical Materials* **2003,** *22*, 295-302.

286. Raghavaiah, B. V.; Rao, R. N.; Reddy, P. Y.; Veeraiah, N., Thermoluminescence studies on PbO–Sb2O3–As2O3 glasses doped with iron ions. *Optical Materials* **2007,** *29*, 566-572.

287. Deshpande, V. K.; Taikar, R. N., Effect of cerium oxide addition on electrical and physical properties of alkali borosilicate glasses. *Materials Science and Engineering B* **2010,** *172*, 6-8.

288. Ayta, W. E. F.; Silva, V. A.; Cano, N. F.; Silva, M. A. P.; Dantas, N. O., Thermoluminescence, structural and magnetic properties of a $Li_2O–B_2O_3–Al_2O_3$ glass system doped with LiF and TiO_2. *Journal of Luminescence* **2011,** *131*, 1002-1006.

289. Charlesby, A., Field enhanced luminescence of irradiated organics due to electron tunnelling. *Radiation Physics and Chemistry* **1981,** *17*, 399-411.

290. Visocekas, R.; Ceva, T.; Marti, C.; Lefaucheux, F.; Robert, M. C., Tunneling processes in afterglow of calcite. *Physica Status Solidi A* **1976,** *35*, 315-327.

291. Johnson, P. D.; Williams, F. E., Energy levels and rate processes in the thallium activated potassium chloride phosphor *Journal of Chemical Physics* **1952,** *20*, 124-128.

292. Electron Tubes Inc. 30 mm (1 1/8") photomultiplier 9125B series data sheet.

293. Curve Fitting Toolbox User's™ Guide, Manual. The MathWorks, Inc.: Natick, MA, 2012.

294. SAS/STAT® 9.1 User's Guide, Manual. SAS Institute Inc.: Cary, NC, 2004.

295. Curve Fitting Toolbox, Version 2.2, The MathWorks, Inc., Natick, MA, 2010.

296. MATLAB, Version 7.10.0 (R2010a), The MathWorks, Inc., Natick, MA, 2010.

297. Weil, J. A.; Bolton, J. R., *Electron Paramagnetic Resonance: Elementary Theory and Practical Applications*. John Wiley & Sons, Inc.: Hoboken, New Jersey, 2007.

298. Corvaja, C., Introduction to electron paramagnetic resonance. In *Electron Paramagnetic Resonance: A Practitioner's Toolkit*, Brustolon, M.; Giamello, E., Eds. John Wiley & Sons, Inc.: Hoboken, New Jersey, 2009.

299. Wyard, S. J., Double integration of electron spin resonance spectra. *Journal of Scientific Instruments* **1965,** *42*, 769-770.

300. Sun, A. S.; Calvin, M., Stabilization of electron spin resonance probes for photosynthesis studies. *Proceedings of the National Acadamy of Sciences of the United States of America* **1975,** *72*, 3107-3110.

301. McManus, H. J. D.; Kang, Y. S.; Kevan, L., Electron paramagnetic resonance and proton matrix electron nuclear double resonance studies of *N*,*N*,*N'*,*N'*-tetramethylbenzidine photoionization in sodium dodecyl sulfate micelles: structural effects of added alcohols. *Journal of the Chemical Society, Faraday Transactions* **1993,** *89*, 4085-4089.

302. Ćirić, L.; Djokić, D. M.; Jaćimović, J.; Sienkiewicz, A.; Magrez, A.; Forró, L.; Šljivančanin, Ž.; Lotya, M.; Coleman, J. N., Magnetism in nanoscale graphite flakes as seen via electron spin resonance. *Physical Review B* **2012,** *85*, 205437/1-6.

303. British Glass, Making Flat Glass by the Float Process. http://www.britglass.org.uk/sites/all/themes/britishglass/files/form2float_process.pdf (accessed 1 March 2012).

304. Colombin, L.; Jelli, A., Penetration depth of tin in float glass. *Journal of Non-Crystalline Solids* **1977,** *24*, 253-258.

305. Townsend, P. D.; Can, N.; Chandler, P. J.; Farmery, B. W.; Lopez-Heredero, R.; Peto, A.; Salvin, L.; Underdown, D.; Yang, B., Comparisons of tin depth profile analyses in float glass. *Journal of Non-Crystalline Solids* **1998,** *223*, 73-85.

306. Frischat, G. H., Tin ions in float glass cause anomalies. *Comptes Rendus Chimie* **2002,** *5*, 759-763.

307. British Glass, Making Glass Containers by Automatic Process. http://www.britglass.org.uk/sites/all/themes/britishglass/files/form1auto_container_process.pdf (accessed 1 March 2012).

308. Corning, Modern machine forming. In *The Corning Museum of Glass*.

309. Romanowski, P., Pyrex. In *How Products are Made: Volume 7*, http://www.madehow.com/Volume-7/Pyrex.html (accessed 1 April 2012).

310. British Glass, Manufacture of Tubing. http://www.britglass.org.uk/sites/all/themes/britishglass/files/form5tubing_prodn.pdf (accessed 1 March 2012).

311. Pellegrino, J. L. *Energy and environmental profile of the U.S. glass industry*; Energetics, Inc.: Columbia, MD, 2002.

312. National Bureau of Standards, Report of Calibration. http://cra.pnnl.gov/docs/pdfs/cal_reports/DG8165-83.pdf (accessed 1 July 2012).

313. National Institute of Standards and Technology, Report of Calibration. http://cra.pnnl.gov/docs/pdfs/cal_reports/DG9495-92.pdf (accessed 1 July 2012).

314. National Bureau of Standards, Report of Calibration. http://cra.pnnl.gov/docs/pdfs/cal_reports/415a_149.pdf (accessed 1 May 2011).

315. National Institute of Standards and Technology, Report of Air-Kerma Calibration. http://cra.pnnl.gov/docs/pdfs/cal_reports/DG12143-05.pdf (accessed 1 July 2012).

316. International Organization for Standardization (ISO), *Reference Beta Radiations for Calibrating Dosimeters and Doseratemeters and for Determining Their Response as a Function of Beta Radiation Energy*. ISO 6980: 1984.

317. National Bureau of Standards, Report of Calibration. http://cra.pnnl.gov/docs/pdfs/cal_reports/DG8783-87.pdf (accessed 1 July 2012).

318. Izewska, J.; Rajan, G., Radiation dosimeters. In *Radiation Oncology Physics: A Handbook for Teachers and Students*, Podgorsak, E. B., Ed. International Atomic Energy Agency: Vienna, 2005.

319. Kebbekus, B. B.; Mitra, S., *Environmental Chemical Analysis*. Chapman & Hall/CRC: Boca Raton, FL, 1998.

320. Furgusen, C. D.; Kazi, T.; Perera, J. *Commercial radioactive sources: Surveying the security risks*; Report, Monterey Institute for International Studies, Occasional paper no. 11: 2003.

321. Srivastava, J. K.; Supe, S. J., Trap distribution analysis for thermoluminescence of $CaSO_4$:Dy. *Journal of Physics D: Applied Physics* **1983,** *16*, 1813-1818.

322. Justus, B. L.; Johnson, T. L.; Huston, A. L., Radiation dosimetry using thermoluminescence of semiconducter-doped Vycor glass. *Nuclear Instruments and Methods in Physics Research B* **1995,** *95*, 533-536.

323. Kitis, G.; Pagonis, V.; Carty, H.; Tatsis, E., Detailed kinetic study of the thermoluminescence glow curve of synthetic quartz. *Radiation Protection Dosimetry* **2002,** *100*, 225-228.

324. Whitley, V. H.; Agersnap, L. N.; McKeever, S. W. S., Determination of ionisation energies and attempt-to-escape factors using thermally stimulated conductivity. *Radiation Protection Dosimetry* **2002,** *100*, 147-152.

325. Pagonis, V.; Kitis, G.; Furetta, C., *Numerical and Practical Exercises in Thermoluminescence*. Springer: New York, 2006.

326. Prakash, J.; Rai, S. K.; Singh, P. K.; Gupta, H. O., Mechanisms inherent in the thermoluminescence processes. *Indian Journal of Pure and Applied Physics* **2004,** *42*, 565-571.

327. Rasheedy, M. S., On the general-order kinetics of the thermoluminescence glow peak. *Journal of Physics: Condensed Matter* **1993,** *5*, 633-636.

328. Kitis, G.; Gomez-Ros, J. M.; Tuyn, J. W. N., Thermoluminescence glow-curve deconvolution functions for first, second and general orders of kinetics. *Journal of Physics D: Applied Physics* **1998,** *31*, 2636-2641.

329. Sunta, C. M.; Kulkarni, R. N.; Piters, T. M.; Ayta, W. E. F.; Watanabe, S., General order kinetics of thermoluminescence–A comparison with physical models. *Journal of Physics D: Applied Physics* **1998,** *31*, 2074-2081.

330. Sunta, C. M.; Ayta, W. E. F.; Chubaci, J. F. D.; Watanabe, S., General order and mixed order fits of thermoluminescence glow curves–A comparison. *Radiation Measurements* **2002,** *35*, 47-57.

331. Sunta, C. M.; Ayta, W. E. F.; Chubaci, J. F. D.; Watanabe, S., A critical look at the kinetic models of thermoluminescence–II. Non-first order kinetics. *Journal of Physics D: Applied Physics* **2005,** *38*, 95-102.

332. Pagonis, V.; Kitis, G., Prevalence of first-order kinetics in thermoluminescence materials: An explanation based on multiple competition processes. *Physica Status Solidi B* **2012,** *249*, 1590-1601.

333. Sunta, C. M.; Ayta, W. E. F.; Kulkarni, R. N.; Piters, T. M.; Watanabe, S., General-order kinetics of thermoluminescence and its physical meaning. *Journal of Physics D: Applied Physics* **1997,** *30*, 1234-1242.

334. Singh, S. D.; Mazumdar, P. S.; Gartia, R. K.; Deb, N. C., The determination of the trapping parameters of a thermoluminescence peak by using the Kirsh method. *Journal of Physics D: Applied Physics* **1998,** *31*, 231-234.

335. Kirsh, Y., Kinetic analysis of thermoluminescence. *Physica Status Solidi A* **1992,** *129*, 15-48.

336. Chen, R.; Kirsh, Y., *Analysis of Thermally Stimulated Processes*. Pergamon: Oxford, 1981.

337. Gartia, R. K.; Singh, S. D.; Mazumdar, P. S., Computerized glow curve deconvolution: the case of LiF TLD-100. *Journal of Physics D: Applied Physics* **1993,** *26*, 858-861.

338. Pagonis, V.; Mian, S.; Mellinger, R.; Chapman, K., Thermoluminescence kinetic study of binary lead-silicate glasses. *Journal of Luminescence* **2009,** *129*, 570-577.

339. Gobrecht, H.; Hofmann, D., Spectroscopy of traps by fractional glow technique. *Journal of Physics and Chemistry of Solids* **1966,** *27*, 509-522.

340. Chung, K. S.; Choe, H. S.; Lee, J. I.; Kim, J. L.; Chang, S. Y., A computer program for the deconvolution of thermoluminescence glow curves. *Radiation Protection Dosimetry* **2005,** *115*, 345-349.

341. Chung, K. S.; Choe, H. S.; Lee, J. I.; Kim, J. L., A new method for the numerical analysis of thermoluminescence glow curve. *Radiation Measurements* **2007,** *42*, 731-734.

342. Chung, K. S.; Park, C. Y.; Lee, J. D.; Choe, H. S.; Chang, I. S.; Lee, J. I.; Kim, J. L., A new computer program for thermoluminescence glow curve deconvolution by the general approximation. [Poster]. LED2008, Beijing, September 18-22, **2008**.

343. Chung, K. S.; Park, C. Y.; Lee, J. I.; Kim, J. L., Development of a new curve deconvolution algorithm for optically stimulated luminescence. *Radiation Measurements* **2010,** *45*, 320-322.

344. Chung, K. S.; Choe, H. S.; Lee, J. I.; Kim, J. L., An algorithm for the deconvolution of the optically stimulated luminescence glow curves involving the mutual interactions among the electron traps. *Radiation Measurements* **2011,** *46*, 1598-1601.

345. Chung, K. S.; Lee, J. I.; Kim, J. L., A computer program for the deconvolution of the thermoluminescence glow curves by employing the interactive trap model. *Radiation Measurements* **2012,** *47*, 766-769.

346. Halperin, A.; Braner, A. A., Evaluation of thermal activation energies from glow curves. *Physical Review* **1960,** *117*, 408-415.

347. Balian, H. G.; Eddy, N. W., Figure-of-merit (FOM), an improved criterion over the normalized chi-squared test for assessing goodness-of-fit of gamma-ray spectral peaks. *Nuclear Instruments and Methods* **1977,** *145*, 389-395.

348. Misra, S. K.; Eddy, N. W., IFOM, a formula for universal assessment of goodness-of-fit of gamma ray spectra. *Nuclear Instruments and Methods* **1979,** *166*, 537-540.

349. Peteanu, M.; Cociu, L.; Ardelean, I., EPR study of borax–glasses with addition of Fe^{3+} ions. *Journal of Materials Science and Technology* **1994,** *10*, 97-106.

350. Stefanovskii, S. V., EPR of ion, manganese, and copper ions and radiation centers in multicomponent glasses and glass ceramic materials. *Journal of Applied Spectroscopy* **1995,** *62*, 1110-1115.

351. Radchenko, Y. S.; Levitskii, I. A.; Ugolev, I. I., Investigation of glasses and glaze coats of composition R_2O–RO–Fe_2O_3(FeO)–Al_2O_3–B_2O_3–SiO_2 by the EPR method. *Journal of Applied Spectroscopy* **2003,** *70*, 821-826.

352. Ardelean, I.; Lungu, R.; Pascuta, P., EPR and magnetic susceptibility studies of iron ions in $3B_2O_3$·SrO glass matrix. *Journal of Optoelectronics and Advanced Materials* **2008,** *10*, 1306-1310.

353. Takeuchi, N.; Miyanaga, T.; Inabe, K.; Fukuda, Y., A hole trapped centre responsible for high temperature thermoluminescence in sodium borate glass. *Journal of Materials Science Letters* **1985,** *4*, 247-248.

354. Nechaev, A. F.; Aloi, A. S.; Suvarov, O. A.; Fadeev, I. S., An ESR study of gamma-irradiated borosilicate glass containing cesium and strontium oxides. *Atomnaya Énergiya* **1993,** *75*, 800-804.

355. Griscom, D. L.; Merzbacher, C. I.; Weeks, R. A.; Zuhr, R. A., Electron spin resonance studies of defect centers induced in a high-level nuclear waste glass simulant by gamma-irradiation and ion-implantation. *Journal of Non-Crystalline Solids* **1999,** *258*, 34-47.

356. Ollier, N.; Boizot, B.; Reynard, B.; Ghaleb, D.; Petite, G., β irradiation in borosilicate glasses: The role of the mixed alkali effect. *Nuclear Instruments and Methods in Physics Research B* **2004,** *218*, 176-182.

357. Mohapatra, M.; Kadam, R. M.; Mishra, R. K.; Dutta, D.; Pujari, P. K.; Kaushik, C. P.; Kshirsagar, R. J.; Tomar, B. S.; Godbole, S. V., Electron beam irradiation effects in Trombay nuclear waste glass. *Nuclear Instruments and Methods in Physics Research B* **2011,** *269*, 2057-2062.

358. Ollier, N.; Pukhkaya, V., Point defect stability in gamma irradiated aluminoborosilicate glasses: Influence of Yb^{3+} doping ions. *Nuclear Instruments and Methods in Physics Research B* **2012,** *277*, 121-125.

359. Malinowski, E., *Factor Analysis in Chemistry*. John Wiley & Sons, Inc.: New York, 2008.

360. Beebe, K. R.; Pell, R. J.; Seasholtz, M. B., *Chemometrics: A Practical Guide*. John Wiley & Sons, Inc.: New York, 1998.

361. Orton, C. R.; Fraga, C. G.; Christensen, R. N.; Schwantes, J. M., Proof of concept simulations of the Multi-Isotope Process monitor: An online, nondestructive, near-real-time safeguards monitor for nuclear fuel reprocessing facilities. *Nuclear Instruments and Methods in Physical Research A* **2011,** *629*, 209-219.

362. Wise, B. M.; Gallagher, N. B.; Bro, R.; Shaver, J. M.; Windig, W.; Koch, R. S., PLS_Toolbox 4.0 for use with MATLAB™, Manual. Eigenvector Research, Inc.: Wenatchee, WA, 2006.

363. Martens, H.; Naes, T., *Multivariate Calibration*. John Wiley & Sons, Ltd.: Chichester, 1989.

364. de Jong, S., SIMPLS: An alternative approach to partial least squares regression. *Chemometrics and Intelligent Laboratory Systems* **1993,** *18*, 251-263.

365. PLS_Toolbox, Version 6.7.1, Eigenvector Research, Inc., Wenatchee, WA, 2012.

366. Chong, I.-G.; Jun, C.-H., Performance of some variable selection methods when multicollinearity is present. *Chemometrics and Intelligent Laboratory Systems* **2005,** *78*, 103-112.

367. Rudlof, G.; Becherer, J.; Glaefeke, H., A remark on determining activation energies by fractional glow technique (FGT) in case of complex glow spectra – a procedure of improving this method *Physical Status Solidi A* **1979,** *52*, K137-K141.

368. Levy, P. W.; Mattern, P. L.; Lengweiler, K., Three dimensional thermoluminscent analysis of minerals. *Modern Geology* **1971,** *2*, 295-297.

369. Mattern, P. L.; Lengweiler, K.; Levy, P. W.; Esser, P. D., Thermoluminescence of KCl:Tl between 30 and 400°C determined by simultaneous intensity and spectral distribution measurements. *Physical Review Letters* **1970,** *24*, 1287-1291.

370. Mattern, P. L.; Lengweiler, K.; Levy, P. W., Apparatus for the simulaneous determination of thermoluminescent intensity and spectral distribution. *Modern Geology* **1971,** *2*, 293-294.

371. Prescott, J. R.; Fox, P. J.; Akber, R. A.; Jensen, H. E., Thermoluminescence emission spectrometer. *Applied Optics* **1988,** *27*, 2496-3502.

372. Corning, Annealing. In *The Corning Museum of Glass*.

373. Bottle Making Manufacturing. http://www.nearsoft.eu/ind_glass.htm (accessed 1 March 2012).

374. How Glass Is Made. http://www.glasstopsdirect.com/how-glass-made.php (accessed 1 March 2012).

375. Corning, Prince rupert's drop and glass stress. In *The Corning Museum of Glass*.

VITA

Richard Aaron Clark was born to Bradley D. and Janette R. Clark on 1 October 1982 in Austin, TX. From an early age, he showed interest in and an aptitude for mathematics and the sciences. Through his elementary and high school education, he enrolled in every mathematical based and physical science class available. He graduated as the salutatorian from Sugar-Salem High School located in Sugar City, ID in 2001.

Following his high school graduation, Richard took time off from his formal education to give full-time service to his religious faith. He was called and served a two-year proselyting mission in England for the Church of Jesus Christ of Latter-day Saints starting in Dec. 2001.

During his final year of high school, Richard found the opportunity to work in the Research and Development department of Caisson Laboratories, Inc., a plant and animal tissue culture media production facility, which increased his interest in science. After returning from his mission, he was again hired by Caisson Laboratories, Inc., this time as the Production Manager where he would remain employed until the company's relocation to Logan, UT. Also following his return, he met and became acquainted with Alisha Faye Rosencrantz in Jan 2004. They were married on 21 May 2005, and thus far have one child, Caleb, who was born in November 2009.

In the fall of 2004, Richard enrolled at Brigham Young University–Idaho where he earned his B.S. in Chemistry with minors in Mathematics and Physics in 2008. While attending BYU–Idaho, he was awarded the 2005 CRC Press Freshman Chemistry Achievement Award and BYU-Idaho Award of Excellence (2004-2007). During the course of his studies, he became interested in and familiar with radiochemistry. He was able to attend the ACS Nuclear and Radiochemistry Summer School at San José State University in 2007 and returned to be a Teaching Assistant in 2008. During these times, his interest in radiochemistry increased and he became familiar with the work of Dr. J. David Robertson at the University of Missouri–Columbia.

In Aug 2008, Richard enrolled in the doctoral program of the Department of Chemistry at the University of Missouri–Columbia and joined Dr. Robertson's research group. While at the University of Missouri–Columbia, Richard received the ANS Vogt Radiochemistry Scholarship (2009) and was named the 2010-11 David E. Troutner Fellow. In 2009, he became a recipient of the Nuclear Forensics Graduate Fellowship Program. Starting in January 2010 and following completion of his coursework, he became a visiting scientist at PNNL and, working closely with Dr. Jon M. Schwantes, he performed the bulk of the research-to-date (August 2012) on Intrinsic Dosimetry.